The adult hindgut as a model to study left-right morphogenesis in Drosophila : coupling of myosin ID and planar cell polarity for left/right morphogenesis in Drosophila

Nicanor González Morales

Université de Nice Sophia Antipolis – UFR Sciences

École doctorale des sciences de la vie et de la santé

Thèse

pour obtenir le titre de

Docteur en Sciences de l'Université de Nice Sophia Antipolis

Discipline: sciences de la vie (aspects moléculaires et cellulaires de la biologie)
Présentée et soutenue par

Nicanor González Morales

L'intestin adulte comme modèle d'étude de l'asymétrie droite-gauche chez la Drosophile:

Couplage entre la myosine ID et la polarité planaire dans l'asymétrie droite-gauche chez la Drosophile

Thèse dirigée par Stéphane Noselli

Soutenue publiquement le 3 octobre 2014 devant le jury composé de:

Lepage Thierry	**Directeur de Recherche**	**Examinateur**
Noselli Stéphane	**Directeur de Recherche**	**Directeur**
Blader Patrick	**Directeur de Recherche**	**Rapporteur**
Bellaïche Yohanns	**Directeur de Recherche**	**Rapporteur**

Université de Nice Sophia Antipolis – UFR Sciences

École doctorale des sciences de la vie et de la santé

Thèse

pour obtenir le titre de

Docteur en Sciences de l'Université de Nice Sophia Antipolis

Discipline: sciences de la vie (aspects moléculaires et cellulaires de la biologie)
Présentée et soutenue par

Nicanor González Morales

The Adult Hindgut as a model to study Left-Right morphogenesis in Drosophila:

Coupling of Myosin ID and Planar Cell Polarity for Left/Right morphogenesis in Drosophila

Thèse dirigée par Stéphane Noselli

Soutenue publiquement le 3 octobre 2014 devant le jury composé de:

Lepage Thierry	**Directeur de Recherche**	**Examinateur**
Noselli Stéphane	**Directeur de Recherche**	**Directeur**
Blader Patrick	**Directeur de Recherche**	**Rapporteur**
Bellaïche Yohanns	**Directeur de Recherche**	**Rapporteur**

Index

Thesis abstract 7
Résumé de la Thèse 9
I Introduction 12
L/R asymmetry and chirality 16
L/R axis interaction with other body axes 18
L/R asymmetry in the Animal kingdom 19
1 L/R asymmetry is a conserved feature of the animal kingdom 19
2 Diversity and convergence of mechanisms establishing L/R asymmetry in metazoan (Review article) 26
L/R asymmetry in Drosophila 27
1 Drosophila as a genetic model 27
2 The Myosin ID Pathway and Left–Right Asymmetry in Drosophila (Review article) 32
Planar cell polarity (PCP) 33
1 Definition 33
2 The core planar cell polarity pathway 35
3 The global planar cell polarity pathway 37
4 Interaction between Global and Core PCP pathways 43
5 L/R asymmetry and PCP 47
The adult hindgut 49
General Experimental procedures 53
1 Fly strains 53
2 UAS/GAl4 system 53
3 Gal80TS and temperature dependent expression 54
4 RNAi silencing 54
5 FLP/FRT mitotic clones 55
6 Visualization of terminallia rotation 56
7 Visualization of adult hindgut looping 56
Blue Erioglaucine staining 57
Wholemount for confocal microscopy 57
8 Standard procedures 57

DNA preparation from single fly 58

Fosmid/BAC modification 58
Co-immunoprecipitation and Western Blott 59

9 Antibodies and staining reagents 60
10 Hobo mediated deficiency generation 61
11 CRISPR/CAS9 mutagenesis 62
Aims 64
II Aims 65
III Results 67
The Atypical Cadherin Dachsous and Planar Cell Polarity control Left-Right Asymmetry in Drosophila 69
Evolution of the Adult Hindgut loop 71
1 Summary 71

2 Adult hindgut looping is an evolutionary novelty of Sophophora flies 71

3 Putative AHG Cis-Regulatory Module revealed by conservation scores 74

4 Abd-B expression/function in the AHG organizer 76

5 CRISPR/Cas9 mutants induce tissue specific phenotypes 78

Regional division and development of the Adult Hindgut in Drosophila 80
1 Introduction 80

2 Selective screen for Gal4 lines differentially expressed in the AHG 82

3 AHG subdivision revealed by Gal4 expression patterns 83

4 Lineage tracing experiment confirms progenitors of all the AHG 85

5 The progenitors of the rectal junction 87

6 The progenitors of the anterior ileum 88

7 The progenitors of the Adult stem cells 89

8 Discussion 90

The AHG insights 93
1 The growth and looping 93

2 Abd-B in hindgut looping and hindgut morphogenesis 96

3 Imaginal ring culture 98

4 L/R patterning and the Centrosomes 101

Genome wide screen and the identification of Profilin homolog 103
1 Genome wide deficiency based interaction screen 103

2 The role of chikadee in LR patterning 107
Deficiency based screen identified chic locus 107

Over expression of *chickadee* rescues *myoID* loss of function phenotype 108

Chickadee-RNAi depletion leads to a No-rotation phenotype 109

Chic in the A8 is efficiently depleted 110

Chic RNAi phenotype cannot be rescued by Chic over expression 110

Temporal requirement 112

Chic and DE-Cadherin 112

Chic and DE-Cadherin function in H1 cells to control Adult Hindgut looping 114

IV General Discussion 117
The AHG as a model to study L/R patterning 117
Ft/Ds in L/R patterning 121
Chic and the underlying actin cytoskeleton 123
The sinistral factor 125
The evolution of L/R asymmetry 128
V Figure index 132
VI General References 135
VII Acknoledgements 161
VIII Supplementary Material 162

Thesis abstract

Stereotyped left right (L/R) asymmetry ensures proper looping of internal organs. In Drosophila, the adult hindgut (AHG) has a clear stereotypical dextral loop and, like all LR asymmetric organs, require Myosin ID (MyoID) for correct orientation. MyoID is an unconventional type I myosin that binds to DE-Cadherin, this association being required for proper LR establishment; however, the mechanism that translates MyoID chirality into proper morphogenesis remains unknown.

The AHG is a long tube coiled dextrally and located in the middle of the abdominal region. It develops from a cluster of progenitors containing two different populations of cells, H1 and H2. Here, we show that MyoID controls the AHG dextral loop by binding to the atypical cadherin Dachsous (Ds) in H1 cells. Further, Ds-Fat signaling propagates towards the H2 cells which in turn become polarized towards the right and consequently loop. H1 is a transient population of cells that wear off in the first hours of metamorphosis; nevertheless, the dextral information generated in H1 is maintained in H2 cells due to the cooperative action of PCP components. We demonstrate that the molecular basis of the LR establishment downstream of MyoID action lies in the PCP system, which has a double role transmitting and maintaining a dextral signal in the AHG. Thus, we provide for the first time a link in L/R morphogenesis between Drosophila and vertebrates in which PCP mutants result in L/R defects.

Furthermore, in our attempts to better understand the evolution of L/R morphogenesis

we found the recently co-appearance of a *myoID* cis-regulatory element and the AHG dextral loop, during Drosophilidae evolution, suggesting that changes in myoID expression pattern induced the evolution of asymmetric structures.

In summary, we present in this study a recently appeared regulatory network of L/R asymmetric morphogenesis, where MyoID appears to be upstream of the Dachsous/Fat and the canonical PCP pathway, through direct binding and regulation of Dachsous protein.

Résumé de la Thèse

L'asymétrie Droite-Gauche (DG) est responsable de l'empaquetage et l'enroulement stéréotypé des organes internes au cours du développement. Chez la Drosophile, l'intestin postérieur adulte (AHG) se développe asymétriquement selon l'axe DG en formant une boucle dextrale. Comme pour tous les organes asymétriques DG de la Drosophile, la mise en place de l'axe DG nécessite l'expression de la myosine non conventionnelle de type I : MyoID. Cette myosine se lie à la DE-Cadherine au niveau des jonctions adhérentes (AJ) pour mettre en place l'axe DG, mais le mécanisme moléculaire qui transforme la chiralité de MyoID en une morphogenèse asymétrique DG est totalement inconnu.

L'AHG est un long tube situé au milieu de l'abdomen, qui présente une boucle dextrale dans sa partie proximale. Il se développe à partir d'un groupe de progéniteurs formés de deux populations de cellules : H1 et H2. Dans cette étude, nous avons mis en évidence que MyoID contrôle la formation de la boucle dextrale du AHG grâce à son interaction avec la cadhérine atypique Dachsous dans les cellules H1. De plus, nous avons pu mettre en évidence que la signalisation Dachsous-Fat est activée à travers les cellules H2 entrainant leur polarisation du coté droit, et ainsi formant l'enroulement du AHG. Les cellules H1 sont transitoires, elles disparaissent lors des premières heures de la métamorphose. Cependant, l'information dextrale générée dans les cellules H1 perdure dans les cellules H2 grâce à l'action coordonnée des composants de la polarité planaire.

Nous montrons que la polarité planaire contrôle l'établissement de l'asymétrie DG en aval de MyoID, en transmettant et en maintenant l'information DG dans le AHG. Ainsi, nous proposons pour la première fois, qu'il existe un lien entre la morphogenèse asymétrique DG de la Drosophile et des vertébrés chez lesquels des mutants des composants de la polarité planaire entrainent des défauts d'asymétrie DG. De plus, nous montrons que la boucle dextrale de l'AHG est apparue récemment au cours de l'évolution de la Drosophile de manière concomitante à un élément régulateur du gène codant pour MyoID.

Cette étude propose un nouveau réseau de régulation de la morphogenèse asymétrique DG, dans lequel MyoID agît sur la signalisation Dachsous-Fat et la voie canonique de polarité planaire, grâce à son interaction directe avec Dachsous, pour transmettre l'information asymétrique à l'ensemble du tissu.

Introduction

I Introduction

L/R asymmetries are common to all animals and they can be separated into subtle asymmetries and conspicuous asymmetries. Subtle asymmetries are best represented by fluctuating asymmetries which are all the small perturbations that deviate from a perfect bilateral symmetry. These asymmetries are present at an individual level and are not shared among members of the same species (i.e. the human face thus originally symmetric displays some small L/R defects that make it overall asymmetric). Fluctuating asymmetries are a consequence of developmental noise coupled to environmental effects and as so are used as a measure of developmental stability. During development, small random perturbations or environmental conditions cause the development to deviate from its expected path. As these processes act locally, therefore likely affecting only one body part, their effects will become apparent on the left or the right side separately, leading to asymmetric phenotypes or fluctuating asymmetries (Dongen, 2006).

The other types of asymmetries, the conspicuous are not random accumulation of defects but are generally shared among most individuals from a species. This type of L/R asymmetries can be further subdivided into random asymmetries (or anti-symmetries) and fixed (or stereotyped) asymmetries. Anti-symmetries are L/R asymmetries present in all the members of a given species but in which the right and the left sides are randomized (for example: many crab species develop one bigger claw than the other),

however this is not stereotyped or fixed as the number of big-right claw individuals are equal to the number of big-left claw individuals. It has been proposed based on its random characteristic, that anti-symmetries are generated by an external environmental cue that forces the developmental program to break symmetry thus choosing randomly either left or right side.

On the other hand, stereotyped or fixed asymmetries, only right or left handed members in a species, are thought to be genetically controlled. A good example for stereotyped L/R asymmetries in the positioning of the heart in the human body, normally located to the left side, the stereotypic looping of the human intestine going from right to left or the differential size of the left lugh in relationship to the right one. There are many examples of stereotypic L/R asymmetries in animals that go from the fixed direction of toad vomit to the coiled direction in the shell of snails (Pohl, 2011; Asami et al., 2008; Grande, 2010; a very detailed list of asymmetries fount in animals has been gathered by Richard Palmer http://www.biology.ualberta.ca/palmer.hp/asym/Curiosities/Curiosities.htm)

Stereotyped left right (L/R) asymmetry is important in animals for the proper packing and function of internal organs. For example, complete L/R axis inversions in humans are not common and though people with this condition are relatively healthy, randomization in the L/R positioning of internal organs is more common (estimated around 1/5000-10000 in humans) and results in early miscarriage, heart defects and misrotation of the intestine. It has even been proposed that the main cause of miscarriage in

humans is due to this type of L/R defects (Reviewed in Coutelis et al., 2014). Therefore the accurate establishment of stereotypical L/R asymmetry is under strong genetic control as is crucial for the organism fitness. But also it represents an important biological question: how are fixed asymmetries generated from a symmetric and thus naïve state?

The study of the establishment of L/R asymmetry has aided by several animal models mainly vertebrates. Over the years a huge amount of data has been recovered however most of the mechanism that have been described have turned out to be downstream of an early L/R asymmetry breaking event (for details see L/R asymmetry in the animal kingdom section). Thus, the main question of how stereotypical L/R asymmetry is generated from an original symmetry break event has remained elusive.

Recently, the addition of invertebrate genetic models in the study of L/R asymmetry development has proved to be useful for the understanding of common and divergent mechanism that govern L/R axis throughout development. While the genetic bases of L/R patterning in insects have only been recently exploited as a genetic model, it is now clear that the *Drosophila* fruit flies offer several advantages as a genetic model for L/R studies. In *Drosophila* L/R asymmetric patterning is controlled by the unconventional type 1 myosin, MyosinID (MyoID), if this protein is missing the whole fly develops with a completely inverted L/R axis (for details see L/R asymmetry in *Drosophila* chapter). However, neither the mechanisms that translate MyoID activity into proper asymmetric organ nor the mechanism in which MyoID activity is able to break symmetry have yet

been revealed.

L/R asymmetry and chirality

Chirality is an accessible synonym for handedness and for L/R asymmetry. The term chirality as a property of handedness was first introduced by Sir William Thomson (later Lord Kelvin) in 1893 (Gerlach, 2013). The overly confusing exact words were:

«I call any geometrical figure or group of points chiral and say it has chirality, if its image in a plane mirror, ideally realized, cannot be brought to coincide with itself. Two equal and similar right hands are homochirally similar. Equal and similar right and left hands are heterochirally similar. They are also called enantiomorphs as introduced by German writers I believe. Any chiral object and its image in a plane mirror are heterochirally similar.»

Any chiral object and its mirror image are isometric, which means that the corresponding points have the same distance. The two objects cannot be distinguished, if we take only their metric into account. But chiral objects can be related pairwise either by translation or by reflection. These pairs then have equal or opposite chiral sense, homochiral or heterochiral respectively (Gerlach, 2013). Similar definitions are “An object is chiral if it cannot be brought to congruence with its mirror image by translation or rotation” (Prelog, 1982) and “An object is chiral if it is not superposable on its mirror image” (Mislow, 1999).

Chirality is an important geometrical feature in animals as it is present in many

steotyped L/R asymmetric features. For example the directional coiling of snails is a chiral structure (Pohl, 2011; Asami et al., 2008; Grande, 2010); most importantly, the direction of the coiling can be found to be right handed in some species or left handed in others; therefore a chiral geometry is an important evolving trait.

At the level of an individual organism, two types of asymmetries have to be distinguished. First the fixed L/R asymmetry which arises during early development, is genetically determined and controls the L/R asymmetry of internal organs, for example the coiling of gut, the shape and position of the heart and the laterality of the nervous system. And second, the stochastic fluctuating L/R asymmetry which is not necessarily genetically controlled and forms independently of the internal L/R body axis. A good example is the random yet dramatic difference in claw size of fiddler crabs or the stochastic L/R asymmetries in human faces (Géminard et al., 2014; Okumura et al., 2008; Pohl, 2011 ; Wood, 1998).

The decision on an organism's primary L/R asymmetry can be thought of as a critical point early in development at which the system's chiral fate is determined by choosing either dextral or sinistral fate. The current paradigm for L/R patterning is that, after the initial critical point, fields of asymmetric gene expression are established. Asymmetric cellular behaviors emerge that eventually lead to asymmetric morphogenesis. Reversal experiments in many species indicate that in order to develop consistent directional L/R asymmetry, the initial chirality decision has to be propagated effectively (Géminard et al., 2014; Okumura et al., 2008; Pohl, 2011; Wood, 1998).

L/R axis interaction with other body axes

All animals have three body axes: the antero-posterior (A/P) axis, the dorso-ventral (D/V) axis and of course the L/R axis. The L/R axis is particular in respect to the other two axes in the sense that it appears after the other two axes during development and because the L/R axis should be oriented in relation to the other axes. Of course the mechanism that aligns the L/R axis to the other axes is not known and it likely lies at the very core of the original symmetry breaking event. However, a very simple hypothesis that explains this alignment has been proposed by Brown and Wolpbert called the “F-molecule” hypothesis. This hypothesis states the existence of a chiral molecule called “F-molecule” that is able to read and align to both the A/P and the D/V axis, then given the chiral nature of this hypothetical molecule the L/R axis would be generated automatically (Brown and Wolpert, 1990).

L/R asymmetry in the Animal kingdom

1 L/R asymmetry is a conserved feature of the animal kingdom

L/R asymmetry is a conserved feature of the animal kingdom as it has been reported in the majority of phylogenetic groups, from protozoa to mammals (Ludwig, 1932; Neville, 1976). Despite L/R being a conserved trait, the specific organs that exhibit L/R asymmetry are not all so conserved, the exception of the intestine or gut, which is looped in a stereotypic L/R fashion in most animals. Some general examples include: the heart, an asymmetrically localized structure in humans that in insects is dorsally located in a symmetric fashion and the coiled shell of snails, only present in mollusks (Figure 1). L/R axis is arguably one of the most diverse axis in terms of asymmetric organs and patterns in the animal kingdom, from coiled shells in snails to asymmetric positioning of the heart in humans and asymmetric neurons in nematodes. All animals studied so far have a common logic in L/R establishment (Reviewed in Coutelis et al., 2014). The process can be break-down into two processes: first an early asymmetry break in which the organism passes from a completely symmetric shape into early asymmetric cues (expression patterns, cila movements, ion gradients, for detailed description of these see Figure 1 of next Chapter) and a second phase in which these early asymmetries are transformed into proper morphogenetic processes (For extensive reviews on L/R asymmetry establishment see: Aw and Levin, 2009; Nakamura and Hamada, 2012; Vandenberg and Levin, 2013; Namigai et al., 2014; Géminard et al., 2014; Grande, 2010;

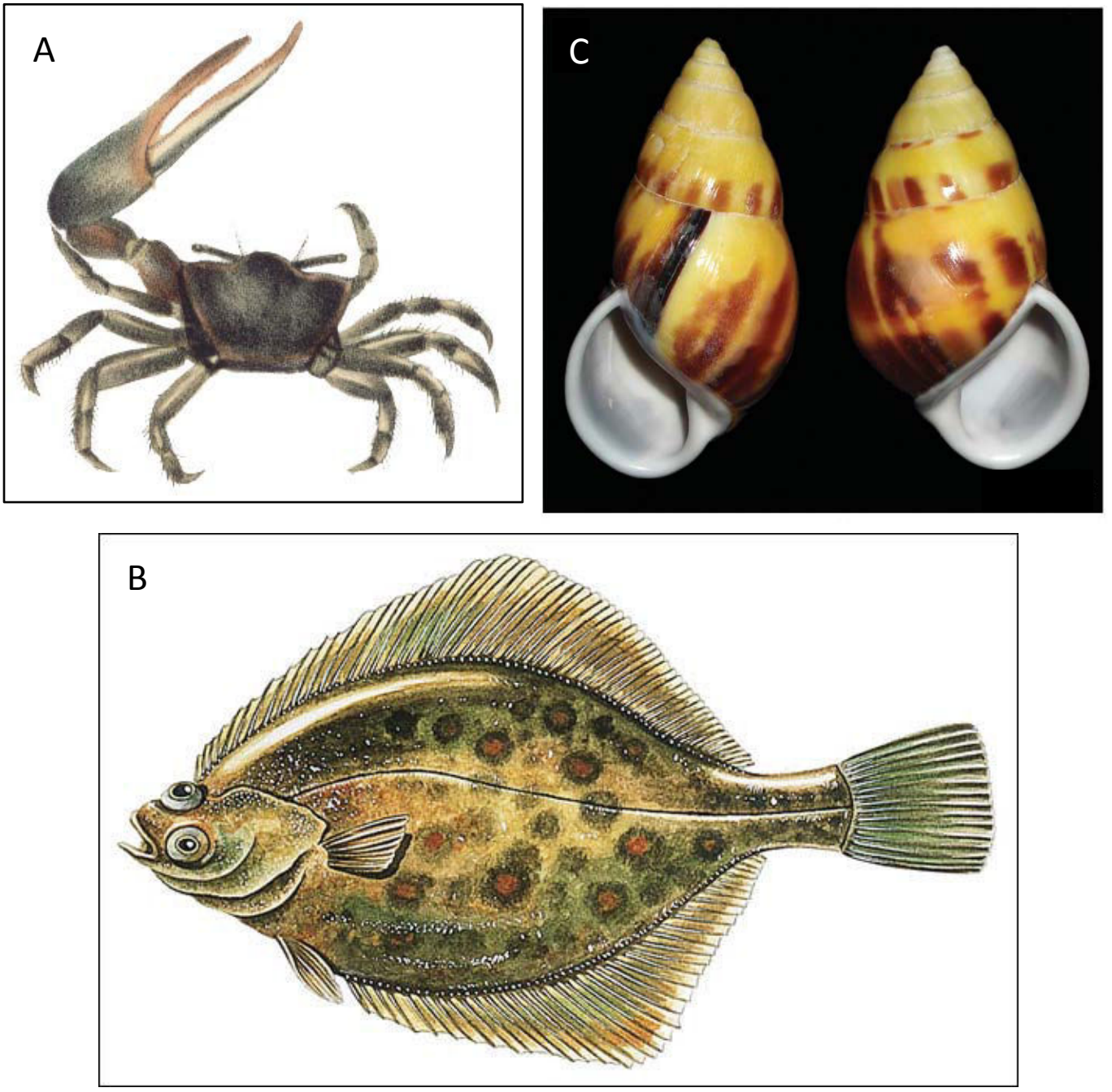

Figure 1. Examples of L/R asymmetric traits in the animal kingdom.
(A) Fiddler crab with heterochelie (*Uca pugnax,* drawing is from De Kay (1844).*). (B) Flatfish with two eyes placed on one body half (Pleuronectiformes from* http://www.gofishing.co.uk/Sea-Angler*). (C))* Sinistral (left) and dextral (right) shells of Amphidromus perversus, a species with chiral dimorphism (Grande, 2009).

Okumura et al., 2008; Pohl, 2011; Coutelis et al., 2014). Common to most animals studied is the fact that these two crucial events happen only once during embryogenesis. The most classic example is the embryonic mouse node (the Nodal Model), a structure containing small cilia that rotate in one chiral direction, thus breaking the system symmetry, the chiral movement of these cilia controls an asymmetric movement of fluid inside this node that leads to the specific deposit of Nodal-containing vesicles in the left side of the Node (Hirokawa et al., 2006; Coutelis et al., 2014; Vandenberg and Levin, 2013). Finally, these vesicles induce a transcriptional activation cascade that initially leads to higher expression of *Nodal*, *Pitx2* and the TGF-Beta homolog *Lefty* (see Figure 1 in next section review article).

However there are some clear evidences showing that the Nodal-cilia pathway is not all inclusive nor it is representative of all vertebrates studied; it has coined the term L/R organizer: a transient structure whose activity is needed to control later L/R asymmetryc developmental events. Of course one property of a L/R organizer is that when disrupted L/R organs will no longer be able to distinguish right from left and in consequence will become either symmetrical or randomly asymmetrical.

As stated above, the vertebrate embryonic node is a crucial structure controlling L/R patterning. In mouse, where it is best described, the node forms at stage E8.5/6, while the flow happens during late gastrulation. Similar structures have been identified in other animals: the Kupffer's Vesicle in *Zebrafish*, the Gastrocoel Roof Plate in *Xenopus,* and the Hensen's Node in chicken (Vandenberg and Levin, 2013). In mouse the node is a

monociliated epithelium transient structure that forms a cavity at the ventral side of the embryo just at the end of the notochrord (Lee and Anderson, 2008). The cilia present in the Node are crucial players in the early phases of L/R asymmetry (Hashimoto et al., 2010; Yoshiba and Hamada, 2014). If their motility is disrupted (by mutating the *Dynein* homolog) or if the cilia are absent L/R defects arise later in development (Supp et al., 1997; Babu and Roy, 2013; Hirokawa et al., 2006). These cilia have a particular characteristic that they rotate in a chiral fashion, turning in a repetitive way clockwise; this rotation is also crucial for L/R establishment (Hashimoto et al., 2010). It has been proposed that the movement of these cilia generate a small current in the inside of the Node that goes from the right-sided wall towards the left-sided wall (Hashimoto et al., 2010). The seminal experiments demonstrating the link between the flow and L/R patterning were conducted by artificially altering the flow movement by means of modifying its viscosity, leading to L/R randomization or directly changing its direction, leading to the imposed expression of Pitx2 and Lefty on the right side (Nonaka et al., 2002; Hashimoto et al., 2010). Strangely, while the node contains around 200 cilia, some mutant conditions in which only two “normally-rotating” cilia are present in the Node, the resulting animals do not exhibit obvious L/R defects, indicating that very small and subtle asymmetries generated in this system are able to stereotypically break symmetry and efficiently propagate the L/R signal to the overall embryo (Shinohara et al., 2012). Another interpretation of these results is that despite the induction of a huge damage in the beating-cilia present in the Node, leaving only two of them functional, L/R defects are barely noticeable, thus questioning the importance of cilia in L/R

establishment/propagation.

The second step in the Nodal model of L/R patterning comprised the specific transcriptional activation of specific genes on one side of the embryo, the left side. Nodal, a member of the Transforming growth factor beta (TGF-B) family originally expressed in a symmetric fashion is rapidly restricted to the left side of the Lateral Plate mesoderm, where it reinforces its own expression along with *Lefty* and *Pitx2* expressions (Nakamura et al., 2006; Brennan et al., 2002). Finally, regulatory loops between these three components refine the final expression domains (Nakamura et al., 2006). Though the link between Nodal expression and the rotating cilia is not completely resolved it has been proposed the existence of a specific type of vesicle, termed Nodal Vesicle Parcels which are released into the Node and which are systematically transported by the flow (Tanaka et al., 2005). Alternatively another hypothesis has been raised based on the presence of another type of cilia, sensory cilia present in the perinodal crown cells. This alternative mechanism postulates that the signal present in the nodal flow is a mechanical one felt by the sensory cilia. Consistently, two Ca^{2+} channel encoding genes *Pkd2* and *Pkd11* are required specifically in crown cells to translate the signal coming from the nodal flow (Field et al., 2011; Pennekamp et al., 2002; McGrath et al., 2003).

While the Nodal flow model is particularly useful in explaining the two steps needed for L/R patterning (Symmetry breaking and propagation) evidence in other animal models suggest that additional mechanisms are also involved in L/R patterning in vertebrate models (For review see: Aw and Levin, 2009; Vandenberg and Levin, 2013;

Okumura et al., 2008; Pohl, 2011; Coutelis et al., 2014). The key set of experiments questioning the validity of the Nodal-Flow simplicity are i) the evidence of early asymmetries present in different vertebrate animals (Zebrafish, Xenopus and Chicken, though not yet in the mouse) before the appearance of the Nodal Flow, like the H+/K+ ATPase activity leading to asymmetric cellular movements in chicken and ii) the apparent Nodal/Cilia-independent structures, like the heart looping in *Zebrafish* or the chicken Node which has immotile cilia (Stephen et al., 2014). In chicken the homologous region to the Node does not develop from mesodermal tissue, like the mouse one, but from endodermal tissue; yet the most striking difference between this region from chicken and the mouse's Node is that the chicken Node has either short and non-motile cilia (Stephen et al., 2014). Therefore the chicken must rely in a different mechanism for establishing L/R asymmetry. One mechanism that has been revealed is that the node itself becomes asymmetric through cellular rearrangements and migration (Gros et al., 2009). This mechanism contributes to the later in developmental asymmetries. This mechanism seems to contradict the importance of cilia-driven establishment of L/R patterning at least in the chicken. On the other hand, even in species with proper cilia-containing Nodes (*Xenopus laevis*), some evidence points to the existence of a previous asymmetric event taking place before the Node is formed (Levin et al., 2002). The clearest example of this is the presence of a graded L/R asymmetric expression/activity of the H+/K+ ATPase (Levin et al., 2002). Though the exact mechanism that links this early asymmetries to later events has not been extensively studied, the proposed mechanism involves the generation of an asymmetric signal based

on a differential pH formed through graded activity of the H+/K+ ATPase pump (Adams et al., 2006). Finally, even in mouse, where the cilia Nodal-flow model is most solid, there is one particular mutation (*inversin*) able to completely inverse the L/R axis, including the chiral cilia titling, thus suggesting an underlying mechanism controlling cilia mediated flow (Morgan et al., 1998).

Far from resolved, the L/R asymmetry field has encountered many open questions that have still to be clarified. What has become evident is that the Nodal flow in not a completely conserved feature in the animal kingdom and that several mechanism can influence L/R patterning (For review see: Vandenberg and Levin, 2013). Nodal signaling cascade on the other hand is much more conserved, being present in all studied animals from mouse to snails and ascidia *Ciona intestinalis*, and only absent in some invertebrates, including *Drosophila* and *C.elegans*. However the upstream mechanisms that control this cascade are not conserved, since not all rely in the flow happening in the nodal and/or in cilia, most of these mechanisms remain to be identified. Therefore, the critical questions are, as they have been from the very beginning of the L/R field: How is L/R symmetry initially broken, where does this rupture happen and what are the underlying mechanisms? One approach to identifying the very early conserved events/mechanisms that generate L/R asymmetries is based on the hypothesis that the initial L/R symmetry breaking mechanism is conserved among all animals and that what is not conserved in the downstream effectors (such as Nodal signaling pathway. Thus, through the study of the underlying mechanisms that establish L/R asymmetry in animals that lack both Node-like structures and Nodal signaling

pathway (for example some invertebrates) it is possible to identify the most early steps in L/R asymmetric patterning in higher vertebrates.

One particularly good example of invertebrate that despite lacking Nodal canonical pathway relies on one single L/R asymmetry breaking event to control all the asymmetric positioning of organs and structures is the nematode *C. elegans.* This genetically easy to manipulate model has recently become a good model for studying this initial rupture (Pohl and Bao, 2010; Pohl et al., 2012). In the very early embryo (with already a settled A/P axis), during the transition from 4 to 6 cells, the mitotic spindle rapidly shifts its polarity from being aligned to the A/P axis towards being slightly tilted in a L/R asymmetric manner (Pohl and Bao, 2010 and Figure 2 of next chapter). This shift has been placed under the control of the underlying actin cytoskeleton. Depletion of the WAVE-Arp3 complex or the formin homolog disrupts the L/R mitotic spindle shift, thus revealing an actin imposing role in L/R asymmetry (Pohl and Bao, 2010; Pohl et al., 2012). While some links are missing it has become clear that later asymmetries in the nematode body plan can all be traced back to this early event (Pohl, 2011; Singh and Pohl, 2014; see also Figure 2 in next section review article).

We have very recently published a review on L/R asymmetry in Metazoa with more details about particular experiments, detailed references and controversies in the field; this review is presented in the next chapter as a support for what has been stated here.

2 Diversity and convergence of mechanisms establishing L/R asymmetry in metazoan (Review article)

Review

EMBO reports

Diversity and convergence in the mechanisms establishing L/R asymmetry in metazoa

Jean-Baptiste Coutelis[1,2,3], Nicanor González-Morales[1,2,3], Charles Géminard[1,2,3] & Stéphane Noselli[1,2,3,*]

Abstract

Differentiating left and right hand sides during embryogenesis represents a major event in body patterning. Left–Right (L/R) asymmetry in bilateria is essential for handed positioning, morphogenesis and ultimately the function of organs (including the brain), with defective L/R asymmetry leading to severe pathologies in human. How and when symmetry is initially broken during embryogenesis remains debated and is a major focus in the field. Work done over the past 20 years, in both vertebrate and invertebrate models, has revealed a number of distinct pathways and mechanisms important for establishing L/R asymmetry and for spreading it to tissues and organs. In this review, we summarize our current knowledge and discuss the diversity of L/R patterning from cells to organs during evolution.

Keywords L/R asymmetry; symmetry breaking; directional morphogenesis; evolution, invertebrates; vertebrates

DOI 10.15252/embr.201438972 | Received 28 April 2014 | Revised 3 July 2014 | Accepted 16 July 2014

EMBO Reports (2014) 15: 926–937

Introduction

The first mutation affecting the whole body plan was isolated a century ago and was shown to invert shell coiling in a small aquatic snail (*Lymnaea peregra*) [1,2]. Despite this early finding and important work describing genetic and cellular aspects of L/R asymmetry [3–11], the first molecular study of L/R asymmetry was described only recently, showing for the first time asymmetric expression of the *nodal* gene in vertebrates [12]. A possible reason for this lag is the fact that in contrast to A/P and D/V asymmetries, laterality is not obvious at first sight, when looking at the external body shape, with snail shell coiling being an exception. Indeed, despite looking mostly bilaterally symmetrical, metazoa also differentiate along the "invisible" L/R axis, leading to asymmetric positioning of unique organs, such as the heart, liver and stomach, and asymmetrical morphogenesis of bilateral ones, as for example the lung and brain. In addition, L/R asymmetry controls the looping of tubular organs (heart tube, gut, and other ducts) toward one direction. Laterality is thus essential for the correct arrangement of visceral organs in the abdomen and thorax, but is also essential for the asymmetric morphogenesis, hence the function, of the heart and brain, for example. Clinical studies led to an estimation of 1/5,000–1/10,000 humans suffering from L/R defects (*situs inversus*, heterotaxia, and isomerism), being responsible for a number of complex congenital heart defects, misrotation of the intestine, and spontaneous miscarriage. Furthermore, L/R asymmetry defects, which often originate from ciliopathies, are associated with polycystic renal disease, Kartagener and Ivemark syndromes, and others.

L/R asymmetry is therefore essential, and outstanding questions remain to be addressed to understand how body shape and function are established during evolution. What is, or what are, the origin(s) of L/R asymmetry? Where and when does it take place in the embryo? Are there any conserved features among metazoa and how did L/R asymmetry establishment evolve in metazoa (Sidebar A)?

A specificity of L/R asymmetry is the fact that it has to be coordinated with the other two—A/P and D/V—body axes and thus is established relative to and after them as a "secondary" axis. This important notion was summarized by Brown and Wolpert in their elegant F-molecule model [13]. The incremental/two-step establishment of body patterning is particularly interesting, as it implies that L/R asymmetry establishment depends on mechanisms that integrate existing 2D positional information. Over the last few years, several studies using different model organisms helped to identify unique mechanisms at play during the establishment of L/R asymmetry. Although a variety of mechanisms have been discovered, fascinating similarities between quite distant phyla are emerging. On the following pages, we will discuss the various mechanisms and synthesize common principles of L/R asymmetry establishment in vertebrates and invertebrates.

Vertebrate embryonic node and Nodal flow in L/R patterning

A well-established model for the determination of the body situs in several vertebrate species is that of the Nodal flow occurring at the

1 Institut de Biologie Valrose, University of Nice Sophia Antipolis, Nice, France
2 CNRS, Institut de Biologie Valrose, UMR 7277, Nice, France
3 INSERM, Institut de Biologie Valrose, U1091, Nice, France
*Corresponding author. Tel: +33 4 9207 6433; E-mail: noselli@unice.fr

Glossary

A/P	anterior/posterior
Abd-B	abdominal-B
ASEL, ASER	left–right asymmetric bilateral sensory neurons in *C. elegans*
D/V	dorsal/ventral
dvl	*dishevelled-like*
FGF	fibroblast growth factor
GSK3	glycogen synthase kinase 3
Heterotaxia	also *situs ambiguus*, uncoordinated placing of the internal organs
Isomerism	situation in which both sides of the body adopt the same fate
iv	*inversus viscerum*
L/R	left–right
LPM	lateral plate mesoderm
myoID	*myosin ID*
PCP	planar cell polarity
PH	Pleckstrin Homology
Pitx2	*paired-like homeodomain transcription factor 2*
Pkd1l1	*polycystic kidney disease-like 1*
Pkd2	*polycystic kidney disease 2*
Shh	sonic hedgehog
situs inversus	inverted placing of the internal organs
situs solitus	normal placing of the internal organs
TGF-β	transforming growth factor beta
vangl	*Van Gogh-like*

late-gastrulation-neurulation stage in the mouse node and node-like structures of other animals (Posterior Notochordal Plate in rabbit, Kupffer's Vesicle in zebrafish, Gastrocoel Roof Plate in Xenopus) [14–16].

The Nodal flow model is best described in mouse, which serves as the model paradigm; hence, we focus in the following on the description of the data obtained in mouse. The node is a transitory structure located on the ventral side of the embryo at the end of the developing notochord (Fig 1A). The node is a cavity covered by a monociliated epithelium-like monolayer of cells, which appears decisive for proper lateralization [17]. Indeed, when the node cilia are missing, mice show abnormal L/R patterning with random lateralization, that is, both the normal *situs solitus* and the inverted *situs inversus* are observed. This is for instance the case in mice mutant for the Kif3A or Kif3B subunits of the kinesin-II complex, a microtubule motor essential for proper ciliogenesis and maintenance of the cilium. In these mutants, cilia fail to assemble [18,19].

However, it is not merely the presence of these cilia that is important, but rather their motility. Indeed, *inversus viscerum* (*iv*) mutant mice, in which the cilia are present but immotile, show similar randomized lateralization phenotypes [20,21]. *iv* encodes the L/R dynein, another microtubule motor essential for node cilia motility [20]. Node cilia rotate clockwise, thereby producing a leftward flow of extra-embryonic fluid, which appears to determine the directionality of embryo lateralization [18,19,22,23]. Cilia have been known for some time to be important for lateralization [24], but their role in the production of the Nodal flow was only recently described [18] (Fig 1A). Impairing the flow genetically (with mutant mice) or experimentally (by increasing the viscosity of the medium) leads to L/R patterning defects [25]. When the node cilia are missing or immotile, the Nodal flow is abolished

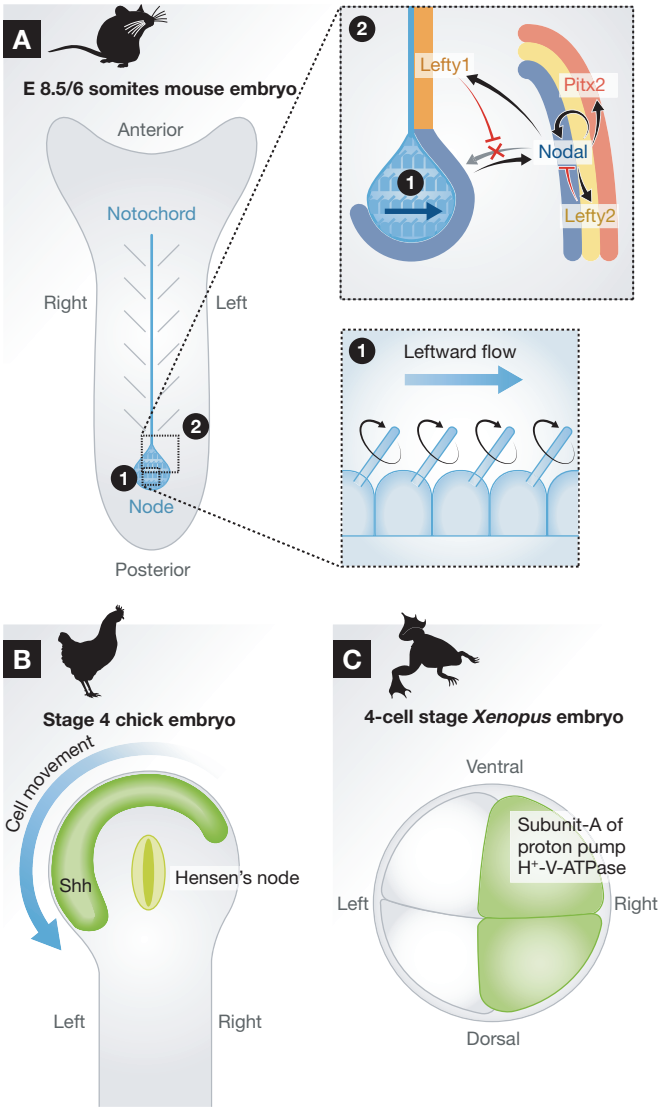

Figure 1. Left/Right determination in vertebrates.
(A) Schematic depiction of a E8.5 mouse embryo. Nodal is expressed around the node. Nodal flow (i) leads to stronger expression of Nodal on the left side (ii) and in the Lateral Plate Mesoderm (LPM) where it positively regulates its own expression by a positive feedback loop. Nodal also activates expression of the homeobox transcription factor Pitx2 and of the TGF-β homologues Lefty2 and Lefty1 in the LPM near the notochord. Lefty1/2 antagonize Nodal diffusion to the right side of the embryo and ultimately shut down Nodal signaling. Pitx2 expression is self-maintained and induces left-sided morphogenesis of the LPM. (B) Schematic depiction of a stage 4 chick embryo's primitive streak and Hensen's node. The leftward movement of cells from the right of Hensen's node induces the asymmetric remodffieling of the node's morphology as well as asymmetric gene expression patterns (e.g. Shh, green) due to the intermingling of cells with different genetic programs [57,58]. (C) *Xenopus* embryo at the 4-cell stage shows right-sided enrichment in subunit-A of the proton pump H^+-V-ATPase, whose activity is necessary for proper lateralization of the animal. Interestingly, this early L/R asymmetric localization appears to be sensitive to actin but not microtubule depolymerization [60].

and the L/R *situs* is consequently randomized. Interestingly, the restoration of an artificially generated leftward Nodal flow is sufficient to reinstate normal L/R patterning of mutant mice [25]. Conversely, in wild-type mice, superimposition of an artificial

rightward Nodal flow is able to override normal patterning and leads to inversion of the axis, demonstrating the importance of the flow in this process [25].

The normal mouse node is thought to comprise between 200 and 300 motile cilia, nevertheless only a couple of them seem to be required for normal lateralization [26]. This precision was achieved through thorough analysis of the phenotype of mutant mice, in which ciliogenesis was strongly impaired but that nevertheless retain some cilia at the node. This is for instance the case in mice mutant for the Rfx3 transcription factor necessary for ciliogenesis. The discovery that only two motile cilia—but not one—wherever their position in the node, were sufficient to trigger normal L/R patterning questions the sensitivity of the Nodal flow signal or the existence of a on/off effect of the flow [26]. Remarkably, the generation of a small difference or initial bias between the left and right sides by the Nodal flow appears to be sufficient to be turned into robust asymmetry [27]. Similar analyses of flow dynamics in various genetic conditions showed that in zebrafish, the flow generated by thirty motile cilia or more reliably predicts the future laterality of the animal [28]. Interestingly, the authors revealed distinct sensitivities of different organs to the flow. These observations could account for heterotaxia in conditions in which the flow is compromised but not abolished.

How is the information provided by the Nodal flow implemented for asymmetric morphogenesis, and how does the Nodal-signaling cascade initiate left-sided morphogenesis? Originally detected on both sides of the node, Nodal expression is reinforced on the left side by the Nodal flow. Nodal, a TGF-β family member, diffuses to the LPM surrounding the node where it activates a positive feedback loop inducing its own expression, as well as those of Lefty2 and Pitx2 in the LPM and that of Lefty1 around the midline [29] (Fig 1A). Lefty1 and Lefty2 molecules are monomeric TGF-β family members that compete with Nodal signaling in the extracellular medium. The expression of Lefty1 at the midline antagonizes the Nodal produced on the left side of the embryo LPM, thus preventing the diffusion of Nodal activity to the right side and subsequent ectopic left-sided development [30,31]. Consistently, *nodal* mutants display right-sided characteristics on both sides (right isomerism), whereas both sides of *Lefty1* mutants show left-sided characteristics [27,29,30]. Downstream of Nodal signaling is the homeodomain-bearing transcription factor Pitx2. *Pitx2* expression once activated by Nodal remains expressed in the LPM. Its expression dictates left-sided morphogenesis of the asymmetric organs, thus presaging the development of morphological asymmetries of the body [32–35].

These data show the importance of the flow generated by the node cilia in locking the directionality of the L/R axis. However, cilia rotating around their axis (from their base to their tip) should produce a vortex without any clear directionality and not the laminar flow that is observed experimentally. How can the clockwise rotation of the cilia produce a leftward flow? The answer is twofold. First, the apical surface of the node cells forming the embryonic cavity appears to be convex, and second, their basal body (that anchors the cilium in the cell) is asymmetrically positioned. In the node epithelium, the cilia basal bodies are not positioned in the middle of the apical side but at the posterior end [36,37]. These two factors lead to a posterior tilt of the cilia, which in turn leads to an effective stroke toward the left side and an ineffective recovery stroke toward the right side, thereby creating the observed leftward flow [36–38].

How is this coordinated localization of the node cell basal bodies from their initial central apical location to the posterior attained across the node epithelium? A well-known example of the uniform orientation of all cells in the plane of an epithelium is that of PCP. PCP was first described in *Drosophila* ommatidia and wing bristles, whose coordinated orientation was shown to genetically depend on so-called PCP genes [39]. Proper L/R axis establishment is also impaired in mice mutant for the PCP genes *dvl* and *vangl,* due to the randomization of the cilia position at the surface of the node pit cells. Thanks to PCP signaling, all node cells have their cilium basal body located similarly at the posterior end of their apical domain and can thus participate in the generation of the coordinated Nodal flow [40–43]. Interestingly, the positioning of the cilia basal bodies also depends on actin cytoskeleton remodeling, as the cooperation of the PCP core protein Vangl2 and the actin-severing protein Cofilin1 appears to be important in this process [44]. In *vangl2;cofilin1* double mutant mice, the basal body fails to migrate posteriorly and remains centrally located leading to L/R patterning randomization [44]. Taken together, these data link the generation of the extra-embryonic Nodal flow to the intracellular cell cytoskeleton organization and A/P axis.

Several questions remain, as for example, how does the Nodal flow induce organism lateralization and subsequent asymmetric morphogenesis? How is the Nodal flow sensed? It is now clear that in addition to the node pit cell cilia, a second population of cilia located on the crown cells around the node is crucial for sensing the flow. To date, two not mutually exclusive hypotheses are debated, the first chemical and the other mechanical (for review see [36,45]). The former asserts that a morphogen gradient is established by the Nodal flow and sensed by the perinodal crown cells. Nodal Vesicular Parcels are membrane-sheathed vesicles originating from the node cell that are released in an FGF-dependent fashion [46]. These Nodal Vesicular Parcels are suggested to be transported by the Nodal flow and to produce a putative gradient of molecules, such as Shh and retinoic acid [18]. This hypothesis needs to gather firmer experimental confirmation in order to be corroborated. The latter hypothesis, the mechanical one, claims that the signal carried by the Nodal flow is actually the pressure that is sensed by the sensory cilia of the perinodal crown cells [21].

Whichever the mechanism, it has been shown that the perception of the Nodal flow requires the Ca^{2+} channel encoded by the *Pkd2* and *Pkd1l1* genes [47,48]. Interestingly, this complex appears to be required solely in the perinodal crown cells for proper L/R establishment. In *Pkd2* null-mutant mice, Pkd2 expression was reintroduced by transgenesis in the perinodal crown cells but not in the node pit cells. This localized expression was sufficient to restore normal L/R patterning [49]. Consistently, mice with normal *Pkd2* expression, in which cilia are absent from node pit cells and only present in the perinodal crown cells, are able to respond to an artificial flow and trigger proper left-sided morphogenesis [19]. This suggests that the Pkd2 and Pkd1l1 complex could be responsible for the detection of the Nodal flow and possibly for the resultant Ca^{2+} signal observed on the left side of the node [47,48,50]. However, how this Ca^{2+} signal impacts on Nodal expression and the subsequent signaling cascade remains to be resolved.

The Nodal flow model is very popular as it provides a comfortable mental frame to link cell polarity to structural chirality and

ultimately to organism lateralization, but additional mechanisms could be at play during vertebrate L/R axis establishment. Although no early L/R asymmetry has yet been described in mouse, one study found that blastomere repositioning at the 4- and 8-cell stages affects the stereotypical embryonic axial rotation occurring days later [51]. Furthermore, the left–right dynein encoded by the *iv* locus and known for its role in L/R asymmetry (as mentioned above) has recently been implicated in the process of chromatid segregation [52], thus opening the way for a "chromatid segregation" model hypothesizing a L/R asymmetric imprinting of the chromatin from the zygote first cell division on [53]. In addition, recent investigations suggest that a Nodal-independent mechanism, relying on actin polymerization and myosin II activity, could control heart-looping lateralization in zebrafish [54]. Other Nodal flow independent mechanisms of L/R patterning in vertebrates and invertebrates are discussed in more detail below.

Ion flux and left–right determination in vertebrates

Several vertebrate species with a node-like structure do not seem to rely on the Nodal flow for their L/R axis determination. In chick for instance, the homologous structure, the Hensen's node, differs from the mouse node. The mouse or rabbit node is formed of mesodermal pit cells whose motile cilia produce a flow [36,55]. In the chick, on the other hand, Hensen's node cells are endodermal cells with shorter and immotile cilia [56]. Interestingly, the chick node itself becomes morphologically asymmetric and adopts a leftward tilt due to cellular rearrangements, cell migration, and interactions with the surrounding tissues (Fig 1B) [57,58]. This observation does not seem to be a peculiarity of the chick, or of non-mammalian vertebrates, as it was also reported in the pig embryo [58]. Remarkably, these cell migration properties, which precede asymmetric Nodal expression by several hours, directly depend on the L/R program and are downstream of the earlier H^+/K^+ ATPase activity [58].

A whole body of work has shown the involvement of ion pumps of various kinds in L/R patterning at the earliest stages of development. Initially identified through pharmacological screening for the effect of drugs on lateralization, ion pumps and ion channels such as H^+/K^+-ATPase, H^+-V-ATPase, or Na^+/K^+-ATPase, were found to possess asymmetric localizations and activities at developmental stages prior to the "Node" and as early as the first cleavages in several vertebrate species (Fig 1C) [59–61]. The asymmetric expression of these pumps and channels on one side of the embryo is thought to generate a localized ion flow creating steady differences in pH and transmembrane voltage between left and right sides of the embryo. These pH or electrical gradients are thought to orient lateralization or to mediate the local concentration of small signaling molecules (for review see [14,16]). Indeed, when the ion pump or channel activity is missing, the resultant phenotype is often heterotaxia, that is, an uncoordinated L/R axis [59–61]. Interestingly, some data indicate that the initial asymmetry of these ion pumps during early development depends on the correct organization of the cell cytoskeleton [60]. To our knowledge, no data on whether ion pumps, channels or other mechanisms preceding the Nodal flow stage could be at play in mouse L/R asymmetry establishment are yet available. Taken together, it appears that in several vertebrate species, L/R asymmetry is established at different times of development and via different mechanisms.

Left–right asymmetry determination in non-vertebrate deuterostomes

Several of the actors and mechanisms found in vertebrate L/R determination appear to be conserved in non-vertebrate deuterostomes without Node-like structures, such as the ascidian *Ciona intestinalis* and *Halocynthia roretzi* or the echinodermata sea urchin. The *C. intestinalis* larva possesses two asymmetrically located sensory pigment spots near the brain as well as an asymmetric gut [62]. Similarly to the aforementioned vertebrates, Nodal signaling is detected on the left side of *C. intestinalis* and leads to the expression of the Pitx2 homologue, which in turn directs left-sided morphogenesis [62]. Interestingly, H^+/K^+ ATPase activity also appears to act shortly before Nodal expression in *C. intestinalis* and its perturbation affects the left-sided expression of the *Pitx2* homologue, indicating the requirement for the ion channel in *C. intestinalis* L/R patterning as well [62]. In *H. roretzi*, another ascidian, Nodal signaling is also detected on the left side of the embryo for L/R morphogenesis. However, in *H. roretzi*, Nodal expression depends on embryo-wide movements that bring the embryo epidermis and the vitelline membrane in contact. Indeed, a recent study shows that Nodal expression originates from this contact [63]. Interestingly, the contact zone is consistently fixed through a cilium-driven stereotypical rotation of the neurula-stage embryo, called the "neurula rotation" [63]. These data, once more linking Nodal and ciliary function, suggest that cilia could act in more than one way for L/R determination. Finally, in the sea urchin pluteus larva, the adult rudiment (the progenitor tissue for the future sea urchin) forms on one side of the mesodermal tissues [64,65]. Here, Nodal and H^+/K^+ ATPase activities are also involved in L/R patterning [65,66]. But there is a twist to it, as in sea urchin, Nodal is not a left side marker or inducer but is instead found to be expressed on the larval right side, where it prevents left-sided development of the adult rudiment [65,66].

Left–right asymmetry determination in invertebrates

Although they do not all possess asymmetrically positioned organs, most bilaterian animals show some kind of internal L/R asymmetry. Bilateria is a big clade containing the Deuterostomes and Protostomes phyla. All the aforementioned species belong to the Deuterostomes, yet the Protostomes (usually referred to as "invertebrates") are key to understand the basis of L/R patterning both at the morphological and at the functional level [14,67]. Among those, studying three different genera, snails of the *Lymnaea* genus, the *Caenorhabditis elegans* nematode, and the *Drosophila melanogaster* fruit fly, led to some major advances in our understanding of L/R asymmetry, which are discussed below.

Lymnaea *snails*

In snails, L/R asymmetry can be seen in the asymmetric positioning of organs such as the gonad or renal organ but is most evident in the coiling of their shell, whose direction is firmly controlled. There

are snail species with dextral coiling, others with sinistral coiling of their shell. Yet, snails with inverted shell coiling can naturally occur within a strain and prove invaluable to the study of L/R axis determination and patterning. In snails, both *nodal* and *Pitx* homologues are asymmetrically expressed during embryogenesis. Their expression is localized to the right side of dextral snails and to the left in sinistral snails and is important for the normal asymmetric production of the shell. Indeed, treatment with a general chemical inhibitor of the TGF-β superfamily (to which Nodal belongs) led to some individuals with non-coiled shells, which could suggest a loss of asymmetry [68]. A possible downstream effector of *Nodal/Pitx* signaling guiding the asymmetric growth of the shell could be the morphogen Dpp, another TGF-β family member. Indeed, *Dpp* expression appears to predict shell coiling in several species [69].

What controls the asymmetric *Nodal/Pitx* expression in snails? The exact symmetry-breaking event is unknown, but it appears to happen at the earliest stages of embryo development. At the 8-cell stage, the blastomere arrangement appears chiral. The four micromeres on top have their "axis" slightly shifted to one side compared to the bottom macromeres (Fig 2A). This "spiral" positioning of the blastomeres occurs at the third cleavage and predicts the coiling direction of the shell. It is thus found to the left in sinistral species and to the right in dextral ones [68,70,71]. Yet, the situation is strikingly different between variants of a given species, at least for the first stages. Until the 8-cell stage, the *situs inversus* embryos have all their blastomeres aligned, thus lacking the top micromere tilt of the *situs solitus* embryos of the same species [70,71]. But from the 8-cell stage onwards, an inversed tilt happens and the *situs solitus* and *situs inversus* individuals appear to be mirror images. These observations raised the possibility that two distinct mechanisms could be at play to control the dextral and sinistral fates [70]. Furthermore, micromanipulations of the blastomere arrangement during the third cleavage (leading to the 8-cell stage) can impose lateralization on the embryos (Fig 2A). Indeed, inversing the normal tilt of the blastomeres in *situs solitus* embryos or restoring a spiral blastomeric arrangement in *situs inversus* ones triggers the coiling of the shell of the resulting adults in the direction imposed by the manipulation, as well as *Nodal* and *Pitx* asymmetric expression during development [70]. These results indicate the crucial importance of the early asymmetric mechanisms at play at the third cleavage stage for L/R axis establishment. Interestingly, treatment of 4-cell stage embryos with the microtubule depolymerizing agent nocodazole does not affect proper L/R development, whereas treatments with actin depolymerizing agents such as latrunculin A or B at the same four-cell stage do impair snail lateralization, indicating the importance of the actin cytoskeleton in this process [71].

In spite of these indications, the molecular mechanisms regulating snail chirality remain unknown. Genetic experiments have shown that shell chirality depends on a single gene [72,73]. Taking advantage of the naturally occurring sinistral individuals of *Lymnaea peregra*, geneticists performed crossing experiments and found that shell directionality depends on a single locus of the maternal genome [73]. Furthermore, injection of dextral egg cytoplasm into sinistral eggs was sufficient to induce normal dextral development, whereas the injection of sinistral egg cytoplasm into dextral eggs had no effect, indicating that the dextral allele is dominant over the sinistral one [73]. Interestingly, phylogeny modeling has shown that determination of shell coiling by a single gene is evolutionary conserved [74] and that it could reflect an adaptive prey/predator response to snake asymmetric mandibles [75]. However, the exact gene that controls dextral coiling has not yet been identified, despite several attempts [72]. And thus, the nature of this maternally inherited and dominant dextral cytoplasmic factor, which is present in the egg and likely acts on the actin cytoskeleton during the first developmental cleavages, remains unknown.

Caenorhabditis elegans

Caenorhabditis elegans is a popular model system, for which the stereotypical developmental fate of each of the one thousand or so cells has been precisely mapped. *Caenorhabditis elegans* possesses many LR asymmetric features as well as asymmetrically positioned organs, such as the gonad, spermatheca, or vulva (for review on L/R patterning in *C. elegans* see [76,77]). Although the exact symmetry-breaking event during *C. elegans* development is unknown, the genetic regulation controlling asymmetric morphogenesis has been carefully dissected.

The dextral positioning of blastomeres occurring at the 4- to 6-cell stage transition is the first apparent sign of L/R asymmetry. This process has been heavily used to study early L/R patterning [76,78,79]. During the transition from the 4- to 6-cell stage, the anterior and posterior dorsal blastomeres slightly turn to the right, thus orientating the mitotic spindle rightward (Fig 2B). Upon cytokinesis, this asymmetric division leads to the rightward daughter cells to be positioned posteriorly relative to the leftward ones, the whole embryo thus adopting a dextral orientation (Fig 2B). The bias in the direction of the mitotic spindle appears to originate from the earliest stage of embryonic development. The one-cell embryo stereotypically rotates by 120° always in the same direction prior to the first mitosis. This process relies on the organization of the actin cytoskeleton, as depletion of the WAVE-Arp2/3 complex or of the CYK-1 Formin homologue impairs embryo rotation and *C. elegans* laterality, thus revealing the existence of an actin-based intrinsic chirality [80]. This initial chirality seems to be transmitted to the astral microtubules of the spindle, through the cortical G-alpha protein encoded by the *gpa-16* gene. Loss of *gpa-16* G-alpha protein activity leads to random lateralization of the 6-cell stage blastomere [81]. Consistently, disruption of the spindle orientation process similarly results in the randomization of 6-cell blastomere positioning [81,82]. These data suggest that these mechanisms are used to orient the mitotic spindle in order to fix consistent L/R development. Among these mechanisms, the non-canonical Wnt signaling pathway has been suggested to act on the cytoskeleton and thereby control blastomere spindle orientation [83,84]. From stage 12 onwards, a series of Notch inductions controls L/R patterning [85]. Indeed, after the asymmetric blastomere division at the 6-cell stage, a first Notch induction instructs asymmetric L/R patterning [80]. Thus, the original L/R asymmetries in spindle orientation are at the basis of later L/R patterning in worms [80,86].

Finally, the *C. elegans* brain shows two kinds of neuronal L/R asymmetries. First is the stochastic expression of GFP in a reporter line in a set of two neurons that are thus termed "On/Off" [87,88]. Through calcium signals between these two neurons, only one of the pair expresses the odorant receptor gene *str-2* [88]. This process rather corresponds to anti-symmetry than to proper stereotyped L/R

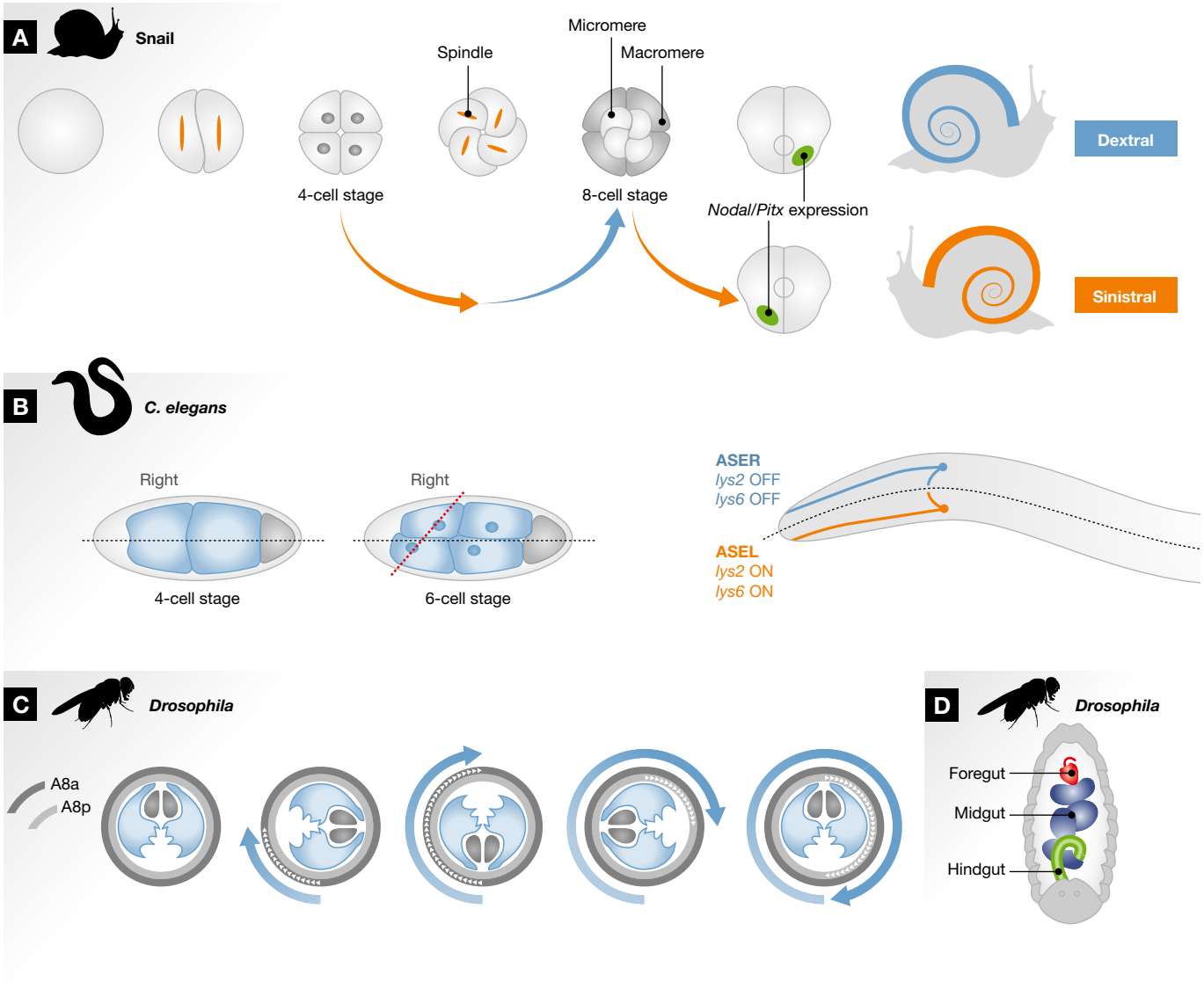

Figure 2. Left/right determination in Protostomes.
(A) In snails, L/R asymmetry is manifested in the coiling of the shell. The direction of this coiling depends on the orientation of the first two cell cleavages. The asymmetric spatial arrangement of the blastomeres leads to the spiral orientation of the spindles. Whereas forced inversion at the 2- to 4-cell stage causes only a temporal L/R perturbation, mended at the 4-cell stage, forced inversion at the 4- to 8-cell stage results in a permanent inversion of the L/R axis highlighted by asymmetric Nodal and Pitx expression (green spot). (B) The first clear asymmetric marker in *Caenorhabditis elegans* is the dextral placement of blastomeres during the 4–6 cell stage transition. The anterior cell and the posterior cell slightly spin so that the mitotic spindle orients rightward, with the result that the midline reorients slightly dextrally. This early asymmetry is propagated later on; one example is the appearance of the functionally asymmetric ASEL/ASER neurons, controlled by the specific expression of *lys2* and *lys6* genes. (C) Terminalia looping in *Drosophila* depends on the rotations of two independent rings, the A8a and the A8p, each contributing 180° (white arrowheads on A8a and A8p) to the 360° rotation (blue arrowheads). Although they are in close proximity, the direction of rotation of each of these rings, dextral or sinistral, is independent of each other and only depends on the presence and absence of the dextral determinant MyoID. (D) The gut of the *Drosophila* embryo is divided in three parts, foregut (red), midgut (blue), and hindgut (green), each displaying a complex L/R asymmetry pattern.

asymmetry. Second is the stereotyped L/R asymmetry of the neuron pair ASEL/ASER (Fig 2B). Although the ASEL/ASER fate also depends on the 6-cell stage blastomere asymmetry, their future differentiation is determined at the 24-cell stage through two rounds of Notch inductions that leave a L/R mark on the postmitotic neurons [89,90]. Recent work identified the nature of the L/R marks and found that a miRNA, encoded by the *lsy-6* locus, induced chromatin de-compaction in the neuron committed to the ASEL fate [91,92].

Drosophila melanogaster

In all the model systems reviewed so far, the animal L/R axis appears to be established sequentially from an initial symmetry-breaking event, yet in *Drosophila* the various L/R organs seem to be able to individually lateralize owing to the existence of L/R organizing centers [93,94 and González-Morales N *et al*, in preparation]. Furthermore, it is a striking feature of *Drosophila* that a reset of the lateralization can occur at metamorphosis (for review on L/R patterning in *Drosophila* see [95]). In *Drosophila*, most L/R research

has been performed on the lateralization of two organs at two different times of development: first, the dextral looping of the embryonic hindgut during embryogenesis, and second, the dextral 360° rotation of the male terminalia and the associated coiling of the spermiduct during metamorphosis (Fig 2C and D, [95,96]). The dextral orientation of these organs, as well as that of the other *Drosophila* L/R asymmetric organs, depends on the activity of a single gene: *myosin ID* (*myoID*). When *myoID* activity is missing, *Drosophila* L/R asymmetry is inverted, thus revealing the activity of an underlying sinistral pathway [94,97]. Interestingly, in some of these organs, L/R organizers could be identified in which MyoID activity was exclusively required for normal dextral development of the organ [94 and González-Morales N *et al*, in preparation]. Using temporally and spatially controlled genetic tools, it was shown that L/R establishment of the embryonic hindgut and terminalia is independent and happens at two distinct developmental times [94,97,98].

Further thorough analysis of *myoID* expression yielded unanticipated results. Indeed, in the L/R organizer controlling terminalia rotation, MyoID is expressed in two distinct cell rows [94]. Interestingly, these two MyoID expression domains each correspond to the two independent rings contributing to the 360° terminalia rotation. Selective depletion of *myoID* activity in one, the other, or both domains shows that each cell ring contributes 180° to the rotation and that they behave as two genetically independent mini-L/R organizers. Consequently, when *myoID* activity is present, the ring rotates dextrally by 180° and by 180° sinistrally when *myoID* activity is missing. These data open startling evolutionary perspectives which could explain the observed diversity in terminalia rotation in diptera, through the appearance and later duplication of a 180° L/R unit [99].

Recently, the Hox transcription factor Abd-B was identified as the upstream regulator of L/R determination in *Drosophila* (Fig 3A). *Abd-B* and other Hox genes are key to establish A/P identity [100], nevertheless this new function in L/R patterning appears to be separate. Upon depletion of *Abd-B* activity in the embryonic hindgut or the male terminalia L/R organizer, loss of *myoID* expression is observed [93]. Nevertheless, unlike *myoID* loss of function, *Abd-B* depletion does not result in an inverted asymmetric development of the L/R axis but in the loss of asymmetry leading to a symmetric development of the organs [93]. Remarkably, restoring MyoID expression is sufficient to rescue this phenotype indicating that Abd-B controls the expression of the symmetry-breaking factor, the dextral determinant MyoID. Furthermore, *Abd-B* depletion in a *myoID* null, and so sinistral, background similarly yields flies developing symmetrically, showing that a genuine sinistral pathway, also under the control of Abd-B, exists (Fig 3A) [93]. These data suggest that factors involved in L/R axis establishment might be able to "read" the A/P axis.

Molecularly, the dextral determinant MyoID is a type I unconventional myosin, a one-headed, monomeric actin-based motor, that is very well conserved in evolution [94,97,101]. Type I myosins comprise three domains: an N-terminal single-headed motor domain coupled to a C-terminal tail via an alpha-helical neck [102,103]. The motor domain binds actin and hydrolyses ATP. The neck contains a number of IQ domains and binds light chains acting as a lever-arm, thus transmitting the conformational changes that occur in the motor domain after ATP hydrolysis [104,105]. Finally, the tail

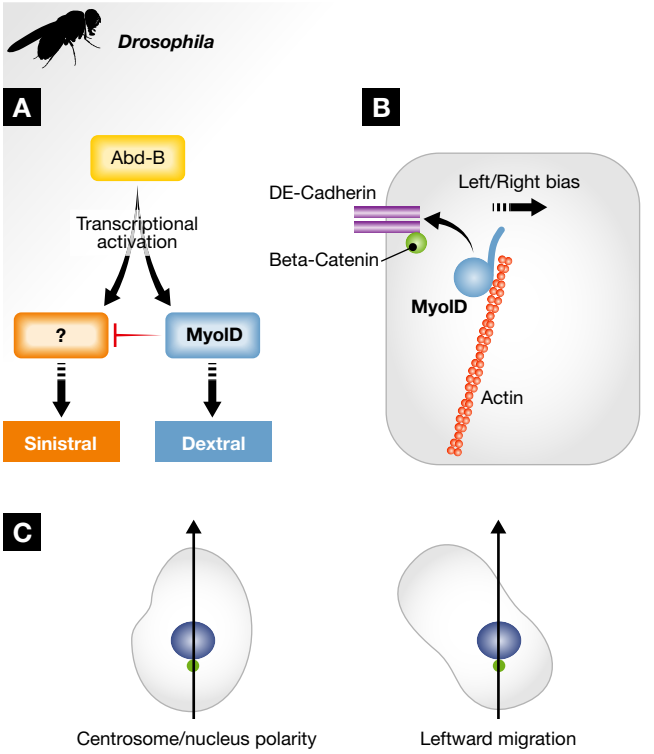

Figure 3. Genetic and cellular determination of *Drosophila* L/R asymmetry.
Schematic depiction of genetic and cellular aspects of *Drosophila* lateralization. (A) The wild-type, or "dextral", orientation depends on the activity of MyoID (Blue). Dextral determination is dominant over sinistral determination (Red), which only becomes apparent in *myoID* null flies. Interestingly, Abd-B (Yellow) controls the expression and/or activity of the two opposite pathways. In *Abd-B* depleted flies, the L/R organs develop symmetrically [93]. To date, the putative sinistral counterpart to MyoID is still unknown. (B) In the cells of the L/R organizer, MyoID (blue) binds to cortical actin (red) and needs to associate with the adherens junction components E-cadherin (yellow) and β-catenin (green) at the apical membrane for proper L/R determination [94,109]. (C) Several lines of cultured vertebrate cells orient themselves according to their nucleus–centrosome axis (arrow) and are thus able to migrate in a L/R asymmetric manner.

domain is thought to interact with cargos and binds membrane phospholipids through its Pleckstrin Homology domain, a positively charged lipid-binding region [106,107].

How does MyoID act during L/R determination? Interestingly, MyoID activity appears to be required only for a short time to induce a dextral bias [94]. To date, the exact mechanism of MyoID action remains unknown, but the actin-binding head domain appears to be central for L/R patterning [98]. Additionally, in the cells of the organizer, MyoID requires the adherens junction components β-catenin and E-cadherin as well as a properly organized cortical actin cytoskeleton (Fig 3B) to induce dextral L/R development [94,97,98,108,109]. In the epithelium of the embryonic hindgut, MyoID has been shown to cell-autonomously bias cell chirality and induce membrane bending [108]. Interestingly, computer simulations showed that mild membrane bending in each cell is sufficient to induce a complete dextral loop of the hindgut [108]. MyoID-dependent membrane bending appears to be mediated by E-cadherin, as membranes in *E-cadherin* null mutants do not

bend [108]. Taken together, these data suggest that L/R morphogenesis could originate from asymmetric membrane tension generated by a MyoID/E-cadherin complex. Interestingly, unlike in the absence of E-cadherin or β-catenin when no consistent orientation is seen, in the absence of MyoID cell membranes of the hindgut still bend, but this time in the opposite direction [108,109]. These observations suggest that the sinistral factor(s), whose activity is only apparent in the absence of MyoID, is also able to induce an orientated cell membrane bias.

Innate cellular chirality

As mentioned above, asymmetric traits are not specific to multicellular structures but can also appear at the single cell level. Indeed, numerous cell types exhibit chiral structures, orientated movements as well as chiral behaviors [110–113]. These observations argue that intracellular elements might underlie L/R asymmetry determination. This idea, termed the "intracellular model", has been around for some time and proposes that the origin of asymmetry in the body plan relies on intracellular structures and in particular the actin cytoskeleton [16]. Supporting this model is the fact that in cultured migrating cells, a clear 3D cell polarity can be seen. In addition to the first two axes, rear-front and top-bottom, a third one, drawn from the center of the nucleus to that of the centrosome, demonstrates clear cell chirality and corresponds loosely to the direction followed by these cells during their migration [113]. However, when cultured in contact with a repeated pattern, cells consistently migrate with a clear bias toward the left side of this third axis (Fig 3C), strongly suggesting the existence of an intracellular bias present in each individual cell [110,112,113].

The cell chirality depends on the cell cytoskeleton. Disrupting microtubule integrity leads to randomization, revealing the need for an intact microtubule cytoskeleton for this leftward bias [113]. Disruption of the actin cytoskeleton instead leads to the "inversion of the cell L/R axis" that is, a rightward bias in cell migration [110]. Consistently, the expression of constitutively active GSK3 similarly inverts the cell "L/R axis". The cells now polarize to the right of the nucleus-to-centrosome axis. These data suggest that GSK3 could act as a link between the unknown original chiral template and the cytoskeleton sensing the spatial cues and orienting cell polarity [113]. These data, obtained in vertebrate cells, are reminiscent of the link between the actin cytoskeleton and L/R patterning in *Drosophila*, *C. elegans* or the *Lymnaea* snails, suggesting a conserved mechanism. Furthermore, they also support the existence of a sinistral factor, as cell or organismal orientation can be consistently inverted and not simply randomized. However, a diversity of L/R orientations exists in cultured cells with some cell types having a dextral bias, others a sinistral one and some with no bias at all [111,112]. To conclude, cell culture experiments revealed the crucial role of actin dynamics for internal cell chirality and suggest that both dextral and sinistral L/R patterning might originate from intracellular polarity.

Indeed, several pieces of evidence obtained from studies of type I myosins and actin dynamics support the idea that L/R asymmetries can be created *de novo* from basic cell components [114]. Type I myosins, to which *Drosophila* MyoID belongs, are members of the myosin superfamily of actin-based motors and are found in most eukaryotic cells [115,116]. In vertebrates, eight type I myosins (myosin I a–h) are found, whereas only two members exist in *Drosophila* (myosin ID and IC) [117,118]. Recent work, using *in vitro* binding of murine MyoIc to actin, revealed that

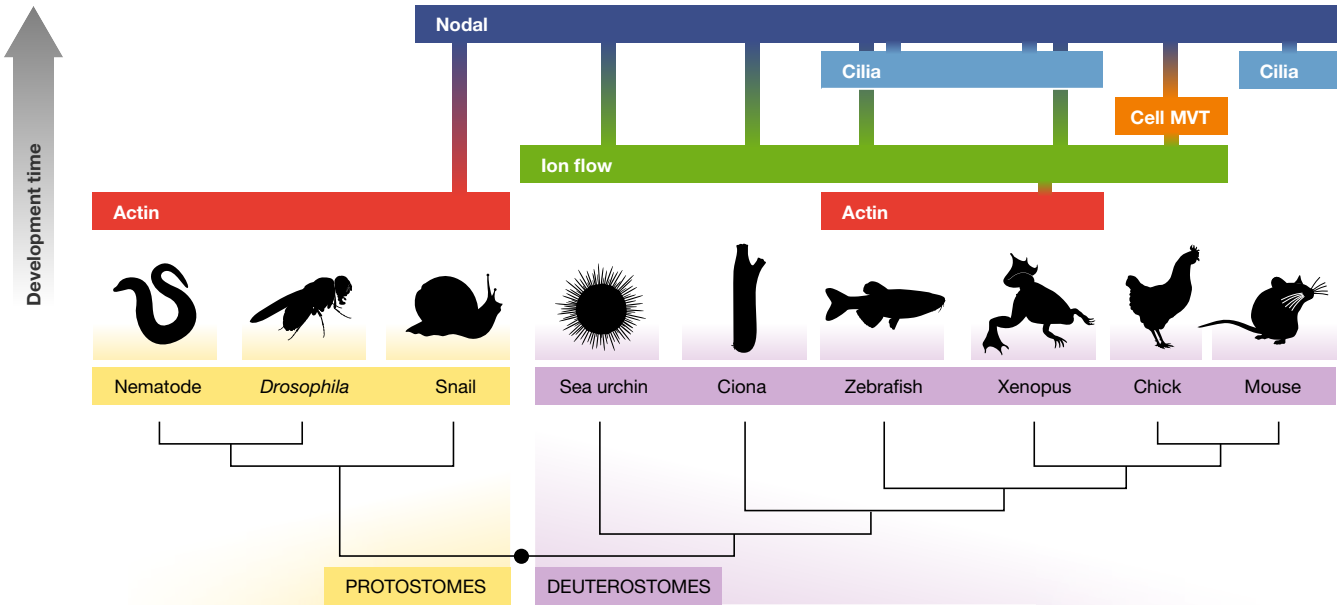

Figure 4. L/R asymmetry in metazoa: diversity and convergence.
Common and divergent principles of L/R asymmetry establishment in the model systems discussed in this review (see text for details). Species are aligned along a phylogenetic tree discerning Protostomes (yellow) and Deuterostomes (purple). The mechanisms breaking symmetry (actin-based: red; ion flow: green; cell movement (Cell MVT): orange; cilia-based Nodal flow (Cilia): light blue) are vertically aligned along the developmental time (DVPT TIME) at which they act (early, down; later, up). The direct link between a mechanism and a subsequent one or ultimately to the *Nodal*-signaling pathway (Nodal, dark blue) is indicated by the color gradient.

Sidebar A: In need of answers

(i) How is symmetry broken at the cellular level?
(ii) What are the mechanisms and molecular elements at the basis of *situs inversus* phenotypes?
(iii) What is, or what are, the origin(s) of L/R asymmetry?
(iv) How did L/R asymmetry establishment evolve in metazoa?

MyoIc can asymmetrically guide motility, leading to actin filaments that curl counterclockwise [114]. Importantly, this generation of asymmetric motility appears to be a property of MyoIc and not a universal characteristic of myosin I motors, since neither murine MyoIa nor Ib are able to generate a similar asymmetric actin movement [114]. Although it is not directly stated, the head domain seems to be responsible for this feature, which is consistent with the fact that, *in vivo*, the L/R activity of *Drosophila* MyoID also appears to depend on its head domain [98]. The finding that specific myosins can make actin fibers chiral are the earliest described signs of asymmetry somehow related to L/R patterning.

Taken together, it appears that from all the model systems discussed, Nodal flow is rather an exception in L/R axis establishment (Fig 4). Evolutionarily, it could correspond to a refinement that was added to earlier mechanisms happening at the cellular level. The conserved involvement of fundamental cellular elements such as ion channels or cytoskeletal components may point to common ancestral L/R asymmetry mechanisms. Additionally, they allow for the generation of a theoretical model for how, from core molecules at the cellular level, such as the actin cytoskeleton, L/R patterning may be created in metazoans.

Acknowledgements

Work in SN laboratory is supported by CNRS, Inserm, ANR, LABEX SIGNALIFE (Program reference # ANR-11-LABX-0028-01), ARC, FRM and University of Nice. We are grateful to Gaëlle Le Breton for critical reading of this manuscript. We apologize to the colleagues, whose work could not be cited due to space limitation.

Conflict of interest

The authors declare that they have no conflict of interest.

References

1. Boycott AE, Diver C (1923) On the inheritance of sinistrality in *Limnaea peregra*. *Proc R Soc Lond B, Contain Papers Biol Charact* 95: 207 – 213
2. Gurdon JB (2005) Sinistral snails and gentlemen scientists. *Cell* 123: 751 – 753
3. Danos MC, Yost HJ (1995) Linkage of cardiac left-right asymmetry and dorsal-anterior development in Xenopus. *Development* 121: 1467 – 1474
4. Fujinaga M, Baden JM (1991) A new method for explanting early postimplantation rat embryos for culture. *Teratology* 43: 95 – 100
5. Hoyle C, Brown NA, Wolpert L (1992) Development of left/right handedness in the chick heart. *Development* 115: 1071 – 1078
6. Hummel KP, Chapman DB (1959) Visceral inversion and associated anomalies in the mouse. *J Hered* 50: 9 – 13
7. Layton WM, Layton MW, Binder M, Kurnit DM, Hanzlik AJ, Van Keuren M, Biddle FG (1993) Expression of the IV (reversed and/or heterotaxic) phenotype in SWV mice. *Teratology* 47: 595 – 602
8. Schreiner CM, Scott WJ Jr, Supp DM, Potter SS (1993) Correlation of forelimb malformation asymmetries with visceral organ situs in the transgenic mouse insertional mutation, legless. *Dev Biol* 158: 560 – 562
9. Stalsberg H (1969) The origin of heart asymmetry: right and left contributions to the early chick embryo heart. *Dev Biol* 19: 109 – 127
10. Yokoyama T, Copeland NG, Jenkins NA, Montgomery CA, Elder FF, Overbeek PA (1993) Reversal of left-right asymmetry: a situs inversus mutation. *Science* 260: 679 – 682
11. Yost HJ (1991) Development of the left-right axis in amphibians. *Ciba Found Symp* 162: 165 – 176; discussion 176–181
12. Levin M, Johnson RL, Stern CD, Kuehn M, Tabin C (1995) A molecular pathway determining left-right asymmetry in chick embryogenesis. *Cell* 82: 803 – 814
13. Brown NA, Wolpert L (1990) The development of handedness in left/right asymmetry. *Development* 109: 1 – 9
14. Speder P, Petzoldt A, Suzanne M, Noselli S (2007) Strategies to establish left/right asymmetry in vertebrates and invertebrates. *Curr Opin Genet Dev* 17: 351 – 358
15. Hirokawa N, Tanaka Y, Okada Y, Takeda S (2006) Nodal flow and the generation of left-right asymmetry. *Cell* 125: 33 – 45
16. Vandenberg LN, Levin M (2013) A unified model for left-right asymmetry? Comparison and synthesis of molecular models of embryonic laterality. *Dev Biol* 379: 1 – 15
17. Lee JD, Anderson KV (2008) Morphogenesis of the node and notochord: the cellular basis for the establishment and maintenance of left-right asymmetry in the mouse. *Dev Dyn* 237: 3464 – 3476
18. Nonaka S, Tanaka Y, Okada Y, Takeda S, Harada A, Kanai Y, Kido M, Hirokawa N (1998) Randomization of left-right asymmetry due to loss of nodal cilia generating leftward flow of extraembryonic fluid in mice lacking KIF3B motor protein. *Cell* 95: 829 – 837
19. Takeda S, Yonekawa Y, Tanaka Y, Okada Y, Nonaka S, Hirokawa N (1999) Left-right asymmetry and kinesin superfamily protein KIF3A: new insights in determination of laterality and mesoderm induction by kif3A$^{-/-}$ mice analysis. *J Cell Biol* 145: 825 – 836
20. Supp DM, Witte DP, Potter SS, Brueckner M (1997) Mutation of an axonemal dynein affects left-right asymmetry in inversus viscerum mice. *Nature* 389: 963 – 966
21. McGrath J, Somlo S, Makova S, Tian X, Brueckner M (2003) Two populations of node monocilia initiate left-right asymmetry in the mouse. *Cell* 114: 61 – 73
22. Supp DM, Brueckner M, Kuehn MR, Witte DP, Lowe LA, McGrath J, Corrales J, Potter SS (1999) Targeted deletion of the ATP binding domain of left-right dynein confirms its role in specifying development of left-right asymmetries. *Development* 126: 5495 – 5504
23. Okada Y, Nonaka S, Tanaka Y, Saijoh Y, Hamada H, Hirokawa N (1999) Abnormal nodal flow precedes situs inversus in iv and inv mice. *Mol Cell* 4: 459 – 468
24. Kartagener H (1935) Bronchiektasien bei situs viscerum inversus. *Schweiz Med Wocshenschr* 65: 782 – 784
25. Nonaka S, Shiratori H, Saijoh Y, Hamada H (2002) Determination of left-right patterning of the mouse embryo by artificial nodal flow. *Nature* 418: 96 – 99
26. Shinohara K, Kawasumi A, Takamatsu A, Yoshiba S, Botilde Y, Motoyama N, Reith W, Durand B, Shiratori H, Hamada H (2012) Two rotating

cilia in the node cavity are sufficient to break left-right symmetry in the mouse embryo. *Nat Commun* 3: 622

27. Nakamura T, Mine N, Nakaguchi E, Mochizuki A, Yamamoto M, Yashiro K, Meno C, Hamada H (2006) Generation of robust left-right asymmetry in the mouse embryo requires a self-enhancement and lateral-inhibition system. *Dev Cell* 11: 495 – 504
28. Sampaio P, Ferreira RR, Guerrero A, Pintado P, Tavares B, Amaro J, Smith AA, Montenegro-Johnson T, Smith DJ, Lopes SS (2014) Left-right organizer flow dynamics: how much cilia activity reliably yields laterality? *Dev Cell* 29: 716 – 728
29. Brennan J, Norris DP, Robertson EJ (2002) Nodal activity in the node governs left-right asymmetry. *Genes Dev* 16: 2339 – 2344
30. Meno C, Shimono A, Saijoh Y, Yashiro K, Mochida K, Ohishi S, Noji S, Kondoh H, Hamada H (1998) Lefty-1 is required for left-right determination as a regulator of lefty-2 and nodal. *Cell* 94: 287 – 297
31. Yamamoto M, Mine N, Mochida K, Sakai Y, Saijoh Y, Meno C, Hamada H (2003) Nodal signaling induces the midline barrier by activating nodal expression in the lateral plate. *Development* 130: 1795 – 1804
32. Logan M, Pagan-Westphal SM, Smith DM, Paganessi L, Tabin CJ (1998) The transcription factor Pitx2 mediates situs-specific morphogenesis in response to left-right asymmetric signals. *Cell* 94: 307 – 317
33. Piedra ME, Icardo JM, Albajar M, Rodriguez-Rey JC, Ros MA (1998) Pitx2 participates in the late phase of the pathway controlling left-right asymmetry. *Cell* 94: 319 – 324
34. Ryan AK, Blumberg B, Rodriguez-Esteban C, Yonei-Tamura S, Tamura K, Tsukui T, de la Peña J, Sabbagh W, Greenwald J, Choe S *et al* (1998) Pitx2 determines left-right asymmetry of internal organs in vertebrates. *Nature* 394: 545 – 551
35. Yoshioka H, Meno C, Koshiba K, Sugihara M, Itoh H, Ishimaru Y, Inoue T, Ohuchi H, Semina EV, Murray JC *et al* (1998) Pitx2, a bicoid-type homeobox gene, is involved in a lefty-signaling pathway in determination of left-right asymmetry. *Cell* 94: 299 – 305
36. Okada Y, Takeda S, Tanaka Y, Izpisua Belmonte JC, Hirokawa N (2005) Mechanism of nodal flow: a conserved symmetry breaking event in left-right axis determination. *Cell* 121: 633 – 644
37. Nonaka S, Yoshiba S, Watanabe D, Ikeuchi S, Goto T, Marshall WF, Hamada H (2005) *De novo* formation of left-right asymmetry by posterior tilt of nodal cilia. *PLoS Biol* 3: e268
38. Cartwright JH, Piro O, Tuval I (2004) Fluid-dynamical basis of the embryonic development of left-right asymmetry in vertebrates. *Proc Natl Acad Sci USA* 101: 7234 – 7239
39. Goodrich LV, Strutt D (2011) Principles of planar polarity in animal development. *Development* 138: 1877 – 1892
40. Antic D, Stubbs JL, Suyama K, Kintner C, Scott MP, Axelrod JD (2010) Planar cell polarity enables posterior localization of nodal cilia and left-right axis determination during mouse and Xenopus embryogenesis. *PLoS ONE* 5: e8999
41. Borovina A, Superina S, Voskas D, Ciruna B (2010) Vangl2 directs the posterior tilting and asymmetric localization of motile primary cilia. *Nat Cell Biol* 12: 407 – 412
42. Hashimoto M, Shinohara K, Wang J, Ikeuchi S, Yoshiba S, Meno C, Nonaka S, Takada S, Hatta K, Wynshaw-Boris A *et al* (2010) Planar polarization of node cells determines the rotational axis of node cilia. *Nat Cell Biol* 12: 170 – 176
43. Song H, Hu J, Chen W, Elliott G, Andre P, Gao B, Yang Y (2010) Planar cell polarity breaks bilateral symmetry by controlling ciliary positioning. *Nature* 466: 378 – 382
44. Mahaffey JP, Grego-Bessa J, Liem KF Jr, Anderson KV (2013) Cofilin and Vangl2 cooperate in the initiation of planar cell polarity in the mouse embryo. *Development* 140: 1262 – 1271
45. Norris DP (2012) Cilia, calcium and the basis of left-right asymmetry. *BMC Biol* 10: 102
46. Tanaka Y, Okada Y, Hirokawa N (2005) FGF-induced vesicular release of Sonic hedgehog and retinoic acid in leftward nodal flow is critical for left-right determination. *Nature* 435: 172 – 177
47. Field S, Riley KL, Grimes DT, Hilton H, Simon M, Powles-Glover N, Siggers P, Bogani D, Greenfield A, Norris DP (2011) Pkd1l1 establishes left-right asymmetry and physically interacts with Pkd2. *Development* 138: 1131 – 1142
48. Pennekamp P, Karcher C, Fischer A, Schweickert A, Skryabin B, Horst J, Blum M, Dworniczak B (2002) The ion channel polycystin-2 is required for left-right axis determination in mice. *Curr Biol* 12: 938 – 943
49. Yoshiba S, Shiratori H, Kuo IY, Kawasumi A, Shinohara K, Nonaka S, Asai Y, Sasaki G, Belo JA, Sasaki H *et al* (2012) Cilia at the node of mouse embryos sense fluid flow for left-right determination via Pkd2. *Science* 338: 226 – 231
50. Kamura K, Kobayashi D, Uehara Y, Koshida S, Iijima N, Kudo A, Yokoyama T, Takeda H (2011) Pkd1l1 complexes with Pkd2 on motile cilia and functions to establish the left-right axis. *Development* 138: 1121 – 1129
51. Gardner RL (2010) Normal bias in the direction of fetal rotation depends on blastomere composition during early cleavage in the mouse. *PLoS ONE* 5: e9610
52. Armakolas A, Klar AJ (2007) Left-right dynein motor implicated in selective chromatid segregation in mouse cells. *Science* 315: 100 – 101
53. Sauer S, Klar AJ (2012) Left-right symmetry breaking in mice by left--right dynein may occur via a biased chromatid segregation mechanism, without directly involving the Nodal gene. *Front Oncol* 2: 166
54. Noel ES, Verhoeven M, Lagendijk AK, Tessadori F, Smith K, Choorapoikayil S, den Hertog J, Bakkers J (2013) A Nodal-independent and tissue-intrinsic mechanism controls heart-looping chirality. *Nat Commun* 4: 2754
55. Feistel K, Blum M (2006) Three types of cilia including a novel 9+4 axoneme on the notochordal plate of the rabbit embryo. *Dev Dyn* 235: 3348 – 3358
56. Stephen LA, Johnson EJ, Davis GM, McTeir L, Pinkham J, Jaberi N, Davey MG (2014) The chicken left right organizer has nonmotile cilia which are lost in a stage-dependent manner in the talpid ciliopathy. *Genesis* 52: 600 – 613
57. Cui C, Little CD, Rongish BJ (2009) Rotation of organizer tissue contributes to left-right asymmetry. *Anat Rec* 292: 557 – 561
58. Gros J, Feistel K, Viebahn C, Blum M, Tabin CJ (2009) Cell movements at Hensen's node establish left/right asymmetric gene expression in the chick. *Science* 324: 941 – 944
59. Levin M, Thorlin T, Robinson KR, Nogi T, Mercola M (2002) Asymmetries in H^+/K^+-ATPase and cell membrane potentials comprise a very early step in left-right patterning. *Cell* 111: 77 – 89
60. Adams DS, Robinson KR, Fukumoto T, Yuan S, Albertson RC, Yelick P, Kuo L, McSweeney M, Levin M (2006) Early, H^+-V-ATPase-dependent proton flux is necessary for consistent left-right patterning of non-mammalian vertebrates. *Development* 133: 1657 – 1671

61. Aw S, Adams DS, Qiu D, Levin M (2008) H,K-ATPase protein localization and Kir4.1 function reveal concordance of three axes during early determination of left-right asymmetry. *Mech Dev* 125: 353 – 372
62. Shimeld SM, Levin M (2006) Evidence for the regulation of left-right asymmetry in Ciona intestinalis by ion flux. *Dev Dyn* 235: 1543 – 1553
63. Nishide K, Mugitani M, Kumano G, Nishida H (2012) Neurula rotation determines left-right asymmetry in ascidian tadpole larvae. *Development* 139: 1467 – 1475
64. Raff RA, Snoke Smith M (2009) Chapter 7. Axis formation and the rapid evolutionary transformation of larval form. *Curr Top Dev Biol* 86: 163 – 190
65. Molina MD, de Croze N, Haillot E, Lepage T (2013) Nodal: master and commander of the dorsal-ventral and left-right axes in the sea urchin embryo. *Curr Opin Genet Dev* 23: 445 – 453
66. Duboc V, Rottinger E, Lapraz F, Besnardeau L, Lepage T (2005) Left--right asymmetry in the sea urchin embryo is regulated by nodal signaling on the right side. *Dev Cell* 9: 147 – 158
67. Frasnelli E, Vallortigara G, Rogers LJ (2012) Left-right asymmetries of behaviour and nervous system in invertebrates. *Neurosci Biobehav Rev* 36: 1273 – 1291
68. Grande C, Patel NH (2009) Nodal signalling is involved in left-right asymmetry in snails. *Nature* 457: 1007 – 1011
69. Shimizu K, Iijima M, Setiamarga DH, Sarashina I, Kudoh T, Asami T, Gittenberger E, Endo K (2013) Left-right asymmetric expression of dpp in the mantle of gastropods correlates with asymmetric shell coiling. *Evodevo* 4: 15
70. Kuroda R, Endo B, Abe M, Shimizu M (2009) Chiral blastomere arrangement dictates zygotic left-right asymmetry pathway in snails. *Nature* 462: 790 – 794
71. Shibazaki Y, Shimizu M, Kuroda R (2004) Body handedness is directed by genetically determined cytoskeletal dynamics in the early embryo. *Curr Biol* 14: 1462 – 1467
72. Liu MM, Davey JW, Banerjee R, Han J, Yang F, Aboobaker A, Blaxter ML, Davison A (2013) Fine mapping of the pond snail left-right asymmetry (chirality) locus using RAD-Seq and fibre-FISH. *PLoS ONE* 8: e71067
73. Freeman G, Lundelius JW (1982) The developmental genetics of dextrality and sinistrality in the gastropod *Lymnaea peregra*. *Wilhelm Roux's Arc Dev Biol* 191: 69 – 83
74. Ueshima R, Asami T (2003) Evolution: single-gene speciation by left-right reversal. *Nature* 425: 679
75. Hoso M, Kameda Y, Wu SP, Asami T, Kato M, Hori M (2010) A speciation gene for left-right reversal in snails results in anti-predator adaptation. *Nat Commun* 1: 133
76. Pohl C (2011) Left-right patterning in the *C. elegans* embryo: unique mechanisms and common principles. *Commun Integr Biol* 4: 34 – 40
77. Wood WB (1998) Handed asymmetry in nematodes. *Semin Cell Dev Biol* 9: 53 – 60
78. Hutter H, Schnabel R (1995) Establishment of left-right asymmetry in the *Caenorhabditis elegans* embryo: a multistep process involving a series of inductive events. *Development* 121: 3417 – 3424
79. Hutter H, Schnabel R (1995) Specification of anterior-posterior differences within the AB lineage in the *C. elegans* embryo: a polarising induction. *Development* 121: 1559 – 1568
80. Pohl C, Bao Z (2010) Chiral forces organize left-right patterning in *C. elegans* by uncoupling midline and anteroposterior axis. *Dev Cell* 19: 402 – 412
81. Bergmann DC, Lee M, Robertson B, Tsou MF, Rose LS, Wood WB (2003) Embryonic handedness choice in *C. elegans* involves the Galpha protein GPA-16. *Development* 130: 5731 – 5740
82. Johnston CA, Afshar K, Snyder JT, Tall GG, Gonczy P, Siderovski DP, Willard FS (2008) Structural determinants underlying the temperature-sensitive nature of a Galpha mutant in asymmetric cell division of *Caenorhabditis elegans*. *J Biol Chem* 283: 21550 – 21558
83. Cabello J, Neukomm LJ, Gunesdogan U, Burkart K, Charette SJ, Lochnit G, Hengartner MO, Schnabel R (2010) The Wnt pathway controls cell death engulfment, spindle orientation, and migration through CED-10/Rac. *PLoS Biol* 8: e1000297
84. Bischoff M, Schnabel R (2006) A posterior centre establishes and maintains polarity of the *Caenorhabditis elegans* embryo by a Wnt-dependent relay mechanism. *PLoS Biol* 4: e396
85. Hermann GJ, Leung B, Priess JR (2000) Left-right asymmetry in *C. elegans* intestine organogenesis involves a LIN-12/Notch signaling pathway. *Development* 127: 3429 – 3440
86. Wood WB (1991) Evidence from reversal of handedness in *C. elegans* embryos for early cell interactions determining cell fates. *Nature* 349: 536 – 538
87. Hobert O, Johnston RJ Jr, Chang S (2002) Left-right asymmetry in the nervous system: the *Caenorhabditis elegans* model. *Nat Rev Neurosci* 3: 629 – 640
88. Troemel ER, Sagasti A, Bargmann CI (1999) Lateral signaling mediated by axon contact and calcium entry regulates asymmetric odorant receptor expression in *C. elegans*. *Cell* 99: 387 – 398
89. Poole RJ, Hobert O (2006) Early embryonic programming of neuronal left/right asymmetry in *C. elegans*. *Curr Biol* 16: 2279 – 2292
90. Bertrand V, Bisso P, Poole RJ, Hobert O (2011) Notch-dependent induction of left/right asymmetry in *C. elegans* interneurons and motoneurons. *Curr Biol* 21: 1225 – 1231
91. Cochella L, Hobert O (2012) Embryonic priming of a miRNA locus predetermines postmitotic neuronal left/right asymmetry in *C. elegans*. *Cell* 151: 1229 – 1242
92. Zhang F, O'Meara MM, Hobert O (2011) A left/right asymmetric neuronal differentiation program is controlled by the *Caenorhabditis elegans* lsy-27 zinc-finger transcription factor. *Genetics* 188: 753 – 759
93. Coutelis JB, Geminard C, Speder P, Suzanne M, Petzoldt AG, Noselli S (2013) Drosophila left/right asymmetry establishment is controlled by the Hox gene abdominal-B. *Dev Cell* 24: 89 – 97
94. Speder P, Adam G, Noselli S (2006) Type ID unconventional myosin controls left-right asymmetry in *Drosophila*. *Nature* 440: 803 – 807
95. Geminard C, Gonzalez-Morales N, Coutelis JB, Noselli S (2014) The myosin ID pathway and left-right asymmetry in Drosophila. *Genesis* 52: 471 – 480
96. Coutelis JB, Petzoldt AG, Speder P, Suzanne M, Noselli S (2008) Left-right asymmetry in *Drosophila*. *Semin Cell Dev Biol* 19: 252 – 262
97. Hozumi S, Maeda R, Taniguchi K, Kanai M, Shirakabe S, Sasamura T, Spéder P, Noselli S, Aigaki T, Murakami R *et al* (2006) An unconventional myosin in *Drosophila* reverses the default handedness in visceral organs. *Nature* 440: 798 – 802
98. Hozumi S, Maeda R, Taniguchi-Kanai M, Okumura T, Taniguchi K, Kawakatsu Y, Nakazawa N, Hatori R, Matsuno K (2008) Head region of unconventional myosin I family members is responsible for the organ-specificity of their roles in left-right polarity in *Drosophila*. *Dev Dyn* 237: 3528 – 3537
99. Suzanne M, Petzoldt AG, Speder P, Coutelis JB, Steller H, Noselli S (2010) Coupling of apoptosis and L/R patterning controls stepwise organ looping. *Curr Biol* 20: 1773 – 1778
100. Maeda RK, Karch F (2009) The bithorax complex of *Drosophila* an exceptional Hox cluster. *Curr Top Dev Biol* 88: 1 – 33

101. Speder P, Noselli S (2007) Left-right asymmetry: class I myosins show the direction. *Curr Opin Cell Biol* 19: 82 – 87
102. Krendel M, Mooseker MS (2005) Myosins: tails (and heads) of functional diversity. *Physiology (Bethesda)* 20: 239 – 251
103. Nambiar R, McConnell RE, Tyska MJ (2010) Myosin motor function: the ins and outs of actin-based membrane protrusions. *Cell Mol Life Sci* 67: 1239 – 1254
104. Barylko B, Binns DD, Albanesi JP (2000) Regulation of the enzymatic and motor activities of myosin I. *Biochim Biophys Acta* 1496: 23 – 35
105. Greenberg MJ, Ostap EM (2013) Regulation and control of myosin-I by the motor and light chain-binding domains. *Trends Cell Biol* 23: 81 – 89
106. Hokanson DE, Laakso JM, Lin T, Sept D, Ostap EM (2006) Myo1c binds phosphoinositides through a putative pleckstrin homology domain. *Mol Biol Cell* 17: 4856 – 4865
107. Hokanson DE, Ostap EM (2006) Myo1c binds tightly and specifically to phosphatidylinositol 4,5-bisphosphate and inositol 1,4,5-trisphosphate. *Proc Natl Acad Sci USA* 103: 3118 – 3123
108. Taniguchi K, Maeda R, Ando T, Okumura T, Nakazawa N, Hatori R, Nakamura M, Hozumi S, Fujiwara H, Matsuno K (2011) Chirality in planar cell shape contributes to left-right asymmetric epithelial morphogenesis. *Science* 333: 339 – 341
109. Petzoldt AG, Coutelis JB, Geminard C, Speder P, Suzanne M, Cerezo D, Noselli S (2012) DE-Cadherin regulates unconventional Myosin ID and Myosin IC in Drosophila left-right asymmetry establishment. *Development* 139: 1874 – 1884
110. Chen TH, Hsu JJ, Zhao X, Guo C, Wong MN, Huang Y, Li Z, Garfinkel A, Ho CM, Tintut Y *et al* (2012) Left-right symmetry breaking in tissue morphogenesis via cytoskeletal mechanics. *Circ Res* 110: 551 – 559
111. Wan LQ, Ronaldson K, Park M, Taylor G, Zhang Y, Gimble JM, Vunjak-Novakovic G (2011) Micropatterned mammalian cells exhibit phenotype-specific left-right asymmetry. *Proc Natl Acad Sci USA* 108: 12295 – 12300
112. Wan LQ, Vunjak-Novakovic G (2011) Micropatterning chiral morphogenesis. *Commun Integr Biol* 4: 745 – 748
113. Xu J, Van Keymeulen A, Wakida NM, Carlton P, Berns MW, Bourne HR (2007) Polarity reveals intrinsic cell chirality. *Proc Natl Acad Sci USA* 104: 9296 – 9300
114. Pyrpassopoulos S, Feeser EA, Mazerik JN, Tyska MJ, Ostap EM (2012) Membrane-bound myo1c powers asymmetric motility of actin filaments. *Curr Biol* 22: 1688 – 1692
115. Kim SV, Flavell RA (2008) Myosin I: from yeast to human. *Cell Mol Life Sci* 65: 2128 – 2137
116. Richards TA, Cavalier-Smith T (2005) Myosin domain evolution and the primary divergence of eukaryotes. *Nature* 436: 1113 – 1118
117. Berg JS, Powell BC, Cheney RE (2001) A millennial myosin census. *Mol Biol Cell* 12: 780 – 794
118. Tzolovsky G, Millo H, Pathirana S, Wood T, Bownes M (2002) Identification and phylogenetic analysis of *Drosophila melanogaster* myosins. *Mol Biol Evol* 19: 1041 – 1052

L/R asymmetry in Drosophila

1 Drosophila as a genetic model

Drosophila melanogaster has been extensively studied for over a century as a model organism for genetic investigations. It has many characteristics which make it an ideal organism for the study of animal development and behavior, neurobiology, and human genetic diseases. The fruit fly has many practical features: a short life cycle, an ease of culture and maintenance, and a small genome size. As the fruit fly has been heavily studied for over a century, which has lead to the creation of a vast amount of publicly available tools going from: stock collections carrying mutations and/or specific tools for modifying the expression of nearly every gene, and other *Drosophila* species for comparison analysis; DNA collections; and Internet based platforms devoted to aid the Drosophila research.

In Drosophila L/R asymmetric organs have been observed and documented since the beginning of the use of this animal as a genetic model. As a general and non exhaustive list the main L/R organs in Drosophila are the embryonic gut (both midgut and hindgut), the terminalia dextral looping, the testis dextral coiling and the adult gut (see figure 1 in next section review article). The dextral looping of the embryonic hindgut for example (For a more detailed explained in more detail in next chapter section: MARKERS OF LEFT–RIGHT ASYMMETRY IN DROSOPHILA) is clearly explained and documented in the seminal works of both Hartenstein (Hartenstein, 1995) and Bate,

Martinez-Arias (Bate, 1994). Other L/R markers, like the terminalia and testis looping have also been heavily described (Reviewed in Géminard et al., 2014; Ligoxygakis et al., 2001; Hayashi et al., 2005 and Figure 1 of next chapter). In fact, the terminalia looping has been used extensively for taxonomic classification in the Diptera order (reviewed as Supplementary content in: Suzanne et al., 2010).

Though, the underlying causes of these asymmetries were initially not investigated and to some extent are still unknown. A major breakthrough in the study of *Drosophila* L/R asymmetry was the discovery of an inverted L/R mutant (Speder et al., 2006; Hozumi et al., 2006). This mutant completely inactivates the function of *myosin ID (myoID)* a gene coding for an unconventional type 1 myosin (Speder et al., 2006). Before this huge discovery, there were a few attempts of elucidating the underlying cause of L/R asymmetry; the most famous example of these is the set of experiments done by the Averof's group. The main question was whether the anterior-posterior axis directly controls L/R looping; through a very elegant approach in which the duplication of the posterior segments was induced in the embryonic head, resulting in an embryo with two tails and no head (Ligoxygakis et al., 2001), they showed that, with some exceptions, most tails maintained their dextral condition; somehow showing that the looping is independent of the anterior-posterior axis. However the experiment was clever, it failed to give a clear answer as there were indeed some L/R defects in these embryos (Hayashi et al., 2005).

After *myoID* mutant was revealed in the two seminal papers published (Speder et

al., 2006; Hozumi et al., 2006). The idea of how L/R asymmetry is controlled in Drosophila radically changed: first the mutated gene encodes a myosin protein which directly links L/R patterning with actin cytoskeleton and not directly with gene regulation; second, though not clearly stated, based on *myoID* expression patterns and phenotypic rescue experiments, in both embryo and larva, the existence of at least two separate organizers appeared, in contrast to the unique organizer model, deduced from most animal models used, ranging from vertebrates to nematodes and snails where there is clearly only one symmetry breaking event (Reviewed in Coutelis et al., 2014). Finally the discovery of *myoID* opened a whole new set of questions in the L/R asymmetry field in a simple genetic model. This thesis, as the work done by others regarding the function of MyoID in Drosophila L/R establishment was devoted to answer some of these questions.

Broadly, the questions are: is there a specific L/R organizer for each L/R organ in Drosophila? If so, how are the asymmetries generated at a half-developed larval stage? And how are these asymmetries generated, maintained and propagated? Does MyoID function unveils an underlying actin cytoskeleton asymmetry? Is there a sinistral factor that takes over when MyoID is absent and thus explaining the inverted phenotype?

The work of two groups (Stéphane Noselli and Kenji Matsuno) has been extensively focused on answering these questions, and the simplified current overview of the system can be summarized as follows. *MyoID* transcription is controlled by the HOX-bearing protein Abdominal-B (Abd-B) that binds mainly the 1st and second intron and is necessary and sufficient for *myoID* expression (Coutelis et al., 2013). Once MyoID

is present in the cell it localizes at the adherent junctions where it binds DE-Cadherin and B-Catenin (Speder et al., 2006; Petzoldt et al., 2012). This binding is necessary for correct L/R pattering and is specifically blocked by the action of another type one myosin, MyoIC (Speder et al., 2006; Petzoldt et al., 2012). MyoIC is normally present in the same cells as MyoID, however in wild type situation it does not affect MyoID function while if the MyoID/MyoIC ratio is changed towards a more of the latest the process will fail (Petzoldt et al., 2012). These two myosins are quite similar structurally and in fact most of their domains can be completely interchanged without affecting their function (Hozumi et al., 2008). There is though one domain that cannot be exchanged and that is the head or motor domain (Hozumi et al., 2008). The motor domain is responsible for actin binding and so this reinforces the view that MyoID-actin interaction is crucial to L/R asymmetry (see figure 2 in next section review article).

Furthermore, the link between MyoID and DE-Cadherin has been used to point out several important details in MyoID function. As stated above this link is absolutely necessary for L/R pattering; but more interestingly is the fact that MyoID has been shown to kink or bend the cellular membranes at the sites of binding to DE-cadherin (the adherens junctions) in a cell autonomous L/R asymmetric fashion (Taniguchi et al., 2011). Consistently, a mathematical model of this bending explains the overall looping of the embryonic hindgut (Taniguchi et al., 2011). In a different study, MyoID action has been shown to be cell-autonomous (Taniguchi et al., 2011). Thus *myoID* is the key player in L/R patterning in Drosophila and acts in a cell autonomous manner, yet is has restricted spatial expression in all L/R asymmetric organs (Reviewed in Géminard et al.,

2014). How could, then, L/R patterning be propagated and maintained throughout development?

Another important detail about MyoID function is its transient function; for terminalia looping MyoID is necessary for a very narrow time-window of three hours; while DE-Cadherin is necessary for a slightly broader time-window (Speder et al., 2006; Petzoldt et al., 2012). These observations point out the logical existence of a propagation and/or maintenance system that transform MyoID functional asymmetric cues into proper L/R morphogenesis.

We have very recently published a review on L/R asymmetry in Drosophila with more details about particular experiments, detailed references and supporting data; this review is presented here in the next chapter as a support for what has been stated here.

2 The Myosin ID Pathway and Left–Right Asymmetry in Drosophila (Review article)

REVIEW

The Myosin ID Pathway and Left–Right Asymmetry in *Drosophila*

Charles Géminard,[1,2,3†] Nicanor Gonzalez-Morales,[1,2,3†] Jean-Baptiste Coutelis,[1,2,3†] and Stéphane Noselli[1,2,3*]

[1]Université de Nice Sophia Antipolis, institut de Biologie Valrose, iBV, Parc Valrose, Nice cedex 2, France

[2]CNRS, institut de Biologie Valrose, iBV, UMR 7277, Parc Valrose, Nice cedex 2, France

[3]INSERM, institut de Biologie Valrose, iBV, U1091, Parc Valrose, Nice cedex 2, France

Received 11 January 2014; Revised 20 February 2014; Accepted 21 February 2014

Summary: *Drosophila* is a classical model to study body patterning, however left-right (L/R) asymmetry had remained unexplored, until recently. The discovery of the conserved *myosin ID* gene as a major determinant of L/R asymmetry has revealed a novel L/R pathway involving the actin cytoskeleton and the adherens junction. In this process, the HOX gene *Abdominal-B* plays a major role through the control of *myosin ID* expression and therefore symmetry breaking. In this review, we present organs and markers showing L/R asymmetry in *Drosophila* and discuss our current understanding of the underlying molecular genetic mechanisms. *Drosophila* represents a valuable model system revealing novel strategies to establish L/R asymmetry in invertebrates and providing an evolutionary perspective to the problem of laterality in bilateria. genesis 52:471–480, 2014. © 2014 Wiley Periodicals, Inc.

Key words: genetic; morphogenesis; developmental biology; invertebrates; diptera; left–right asymmetry; asymmetric morphogenesis in invertebrates; symmetry breaking; unconventional type I myosin; HOX gene Abdominal-B

INTRODUCTION

Differentiating the left and right hand sides is essential for the development, positioning and looping of visceral organs like the heart and gut, and for the acquisition of new cognitive and behavioral functions. Improper establishment of left-right (L/R) asymmetry underlies a number of defects and syndromes, representing, for instance, the main cause of congenital heart disease and spontaneous abortion in humans (Aylsworth, 2001; Manner, 2009). Work done in the past 20 years has revealed unique molecular mechanisms and strategies to break symmetry and translate it into asymmetric tissue morphogenesis (Speder *et al.*, 2007). In vertebrates, such strategies include the generation of a directional fluid flow or asymmetric cell migration at the embryonic node (Levin *et al.*, 1995; Mercola and Levin, 2001; Tabin, 2005). However, in *Xenopus*, asymmetries have also been described before gastrulation (i.e. prior to node formation), with the formation of asymmetric pH gradients and gene expression as early as the four-cell stage (Levin *et al.*, 2002; Adams *et al.*, 2006; Danilchik *et al.*, 2006). There are therefore several mechanisms underlying L/R asymmetry in vertebrates and there is still debate on whether or not these can be common among bilateria (Speder *et al.*, 2007; Coutelis *et al.*, 2008; Raya and Izpisua Belmonte, 2008; Vandenberg and Levin, 2013).

L/R asymmetry in invertebrates has been less well studied making it unclear whether some mechanisms and/or principles are conserved with vertebrates (Speder *et al.*, 2007; Okumura *et al.*, 2008).

*Correspondence to: Stéphane Noselli, Université de Nice Sophia Antipolis, institut de Biologie Valrose, iBV, Parc Valrose, 06108 Nice cedex 2, France. E-mail: noselli@unice.fr

†C.G., N.G.-M., and J.-B.C. contributed equally to this work, order randomly assigned.

Contract grant sponsors: CONACYT (NGM); ANR (JBC); CNRS, Inserm, University of Nice, ARC, FRM, ANR; Contract grant sponsor: "Programmes Investissements d'Avenir" Labex SIGNALIFE, Contract grant number: ANR-11-LABX-0028-01

Published online 2 March 2014 in
Wiley Online Library (wileyonlinelibrary.com).
DOI: 10.1002/dvg.22763

Understanding how key L/R factors act at the cellular level to control cell chirality may help unify the current data.

In this review, we present our current knowledge of how L/R asymmetry is established in the fruit fly *Drosophila melanogaster*. First, we introduce the markers of asymmetry in this organism, which are found at all stages from embryo to adult and which are mostly related to tubular organs. Second, we discuss the role of the Myosin ID (MyoID) pathway, which plays a major role in the control of L/R asymmetry in flies.

MARKERS OF LEFT–RIGHT ASYMMETRY IN *DROSOPHILA*

The Brain

Brain activity and morphology show L/R asymmetry in many vertebrates (reviewed in Concha and Wilson, 2001; Roussigne *et al.*, 2012; Bishop, 2013; Morton, 2013). In *Drosophila*, data related to brain asymmetry is limited. One structure, called the asymmetric body, has a biased localization on the right hand side of the midline, next to the mushroom bodies (Fig. 1A). The asymmetric body appears asymmetric in 92% of wild type flies. Other flies showing a symmetric structure present long-term memory defects (Pascual *et al.*, 2004). Recently, efforts to characterize the expression pattern of randomly selected enhancers in the adult *Drosophila* brain identified a specific enhancer-trap line that is expressed in the asymmetric body (Fig. 1A). The enhancer is located in the *pog* gene encoding for a glutamate G-protein coupled receptor (Brody and Cravchik, 2000; Jenett *et al.*, 2012). The *pog* enhancer-trap does not drive asymmetric expression in the larval brain suggesting that asymmetry is established later, during metamorphosis. Note that asymmetry in the brain is not controlled by the same genes controlling MyoID-dependent visceral asymmetry (see below), suggesting the existence of an alternative L/R asymmetry mechanism controlling brain functions in flies, as is observed in vertebrates (Roussigne *et al.*, 2012; Aizawa, 2013).

Malpighian Tubules

The Malphighian tubules are an excretory organ mainly devoted to the clearing of toxic compounds. They consist of two bifurcated tubes attached to the midgut-hindgut junction. Malphighian tubules develop during embryogenesis and continue to grow during larval stages. Interestingly, they are among the few structures that remain functional and do not degenerate during pupal development (for review see Beyenbach *et al.*, 2010); thus, tissue asymmetry is maintained throughout metamorphosis. A recent microarray study revealed that Malphighian tubules are both morphologically and transcriptionally LR asymmetric (Chintapalli *et al.*, 2012).

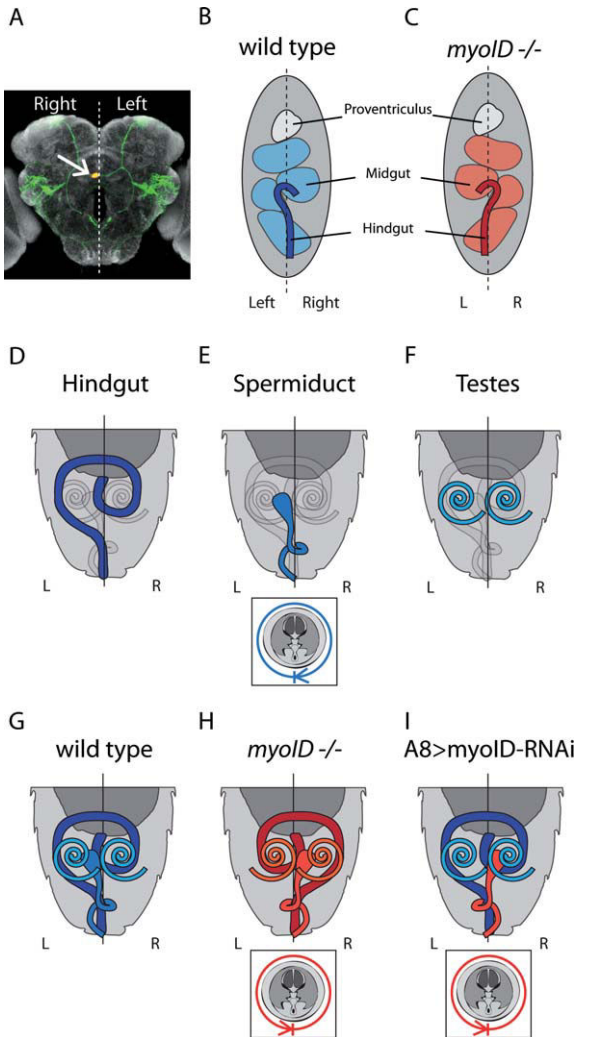

FIG. 1. (**a**) Frontal view of the *Drosophila* brain adapted from (Jenett *et al.*, 2012). The asymmetric body (yellow spot; white arrow) is a unique structure found on one side of the midline in most adult flies (see text for details). (**b** and **c**) Dorsal view of a schematized drosophila embryo: left (L), right (R). In wild-type (b), the three parts of the embryonic gut, the anterior proventriculus, the central midgut and the posterior hindgut, are oriented toward the right (Dextral, light gray and blue). In *myoID* null mutant embryos (c), both the midgut and hindgut are inverted, thus adopting a leftward orientation (Sinistral, red) whereas the proventriculus maintains its rightward orientation (Dextral, light gray). (**d–i**) Dorsal view of transverse sections of *Drosophila* adult male abdomen, highlighting the L/R asymmetric organs: hindgut (d), spermiduct and associated rotation of the terminalia (e), Testes (f) and their orientations (*Situs solitus* or Dextral, blue; *Situs inversus* or Sinistral, red) in various genetic contexts: wild-type male flies (g), *myoID* null flies (h) or flies in which myoID activity is selectively depleted in the L/R terminalia organizer (A8, I). See text for details.

The right pair of Malpighian tubules is directed anteriorly and wraps around the midgut, while the left pair is directed posteriorly and associates with the hindgut (Chintapalli *et al.*, 2012). It will be interesting to test this whether asymmetric gene expression indeed lead to malpighian tubules functional lateralization.

Testis

The two drosophila testes are elongated, spiral, blunt-ended tubes coiling around the seminal vesicle and located symmetrically on each side of the fly abdomen; they are inherently L/R asymmetric (chiral) and both testes are coiled toward the same direction (Fig. 1F).

Gonads in *Drosophila* develop from a group of embryonic primordial germ cells or pole cells, which, at the blastoderm stage, move with the rest of the germ band as it elongates, until they reach the fifth abdominal segment, forming two lateral symmetrical spheres. During larval stages, the stem cell niche is established at the apical pole of these gonads (Santos and Lehmann, 2004; Le Bras and Van Doren, 2006). Gonads keep a spherical shape until around 36 h after puparium formation (APF) at which stage they become attached to the *vas deferens*; then, they undergo dramatic morphological changes, elongating and coiling, to become two Dextral spirals (Fig. 1F).

Several signaling pathways have been shown to be involved in testis development, including TGF-β signaling for the maintenance of germline stem cells and the restriction of spermatogonial proliferation (Loveland and Hime, 2005), as well as Jak/Stat signaling which contributes to stem cell self-renewal (Hombria and Brown, 2002; de Cuevas and Matunis, 2011). On the other hand, the mechanisms underlying asymmetric coiling have not yet been addressed.

The Larval Gut

The gut is arguably the most obvious and conserved L/R asymmetric organ in the animal kingdom. In *Drosophila*, the gut is composed of the foregut, the midgut and the hindgut; all of these structures have clear L/R asymmetric features (Fig. 1B,D). The larval gut develops during embryogenesis (stages 13–17) through the invagination of precursor cells that initially form a continuous symmetrical tube, which later on adopts a global stereotyped L/R asymmetry. The asymmetric looping is sequential, appearing first in the hindgut with a 90° Dextral twist, then in the foregut with the right tilt of the proventriculus, and finally in the midgut with a more complex pattern (Fig. 1B) (Hayashi and Murakami, 2001; Lengyel and Iwaki, 2002; Myat, 2005). The cellular mechanism underlying gut lateralization is discussed further down.

The Adult Gut

Unlike the Malpighian tubules and the testes that are preserved throughout pupal development, the adult gut is almost completely renewed from imaginal tissues during metamorphosis (for review see Hartenstein, 1993). In the adult, L/R asymmetry is evident when looking at the morphology of the coiled midgut and hindgut. The adult midgut derives from the adult midgut precursors present in the larval midgut. The adult midgut precursors are located in between the larval enterocytes and can adopt two different fates, either becoming adult enterocytes or adult midgut-intestinal stem cells. During metamorphosis the larval midgut delaminates from the visceral mesoderm and basement membrane. Then, the adult midgut precursors divide and fuse to form the adult midgut epithelium, enterocytes and intestinal stem cells. Although both larval and adult guts are asymmetric organs, it is likely that they do not share common organizers since the L/R asymmetry of the larval midgut is lost before adult midgut coiling and some mutations affecting adult hindgut coiling do not affect embryonic hindgut coiling (Takashima *et al*., 2011).

Note that L/R asymmetry is preserved during intestinal epithelium constant turn over and adult midgut regeneration (Micchelli and Perrimon, 2006; Ohlstein and Spradling, 2006; Micchelli, 2012). Yet, the mechanisms maintaining L/R asymmetry during regeneration remain unknown. Thus, *Drosophila* midgut appears an excellent model to study the interaction between L/R asymmetry and regeneration (for review see, Jiang and Edgar, 2011, 2012; Micchelli, 2012).

Terminalia

Rotation of the male terminalia is a prominent L/R marker which has been extensively studied (Adam *et al*., 2003; Speder *et al*., 2006; Coutelis *et al*., 2008, 2013; Suzanne *et al*., 2010). The adult male terminalia, which includes all somatic tissues composing the genitalia and analia, originate from the male genital disc. The genital disc is unique in several respects: first, it is located at the ventral midline, whereas other imaginal discs are found paired on both sides of the larval body; second, it exhibits a strong sexual dimorphism; and, finally, it is a compound disc made of cells from three different embryonic segments, namely the A8, A9 and A10 (Fig. 3A). During metamorphosis, the genital disc evaginates to form the adult terminalia. During this process, the A8 segment forms a ring of cells around segments A9 and A10 (Keisman and Baker, 2001; Rousset *et al*., 2010) (Fig. 3B). Then, asymmetry is established through a stereotyped 360° clockwise (or Dextral) rotation, which leads to the coiling of the spermiduct around the gut (Adam *et al*., 2003; Speder *et al*., 2006) (Fig. 1E). This stereotyped rotation process last for about 15 h, taking place during the second day of pupal development, from 25 to 36 h APF (Suzanne *et al*., 2010). Importantly, circumrotation does not originate from a single rotation event but rather from the addition of two independent half-a-turn (180°) rotations (Suzanne *et al*., 2010) (Fig. 3C). Indeed, live imaging of terminalia rotation in pupae identified two distinct moving domains made of the A8a (for anterior) and A8p (for

posterior). The A8p moves first and is followed by A8a 2.5 h later. Thus, the observed 360° rotation is the result of a composite process involving two additive 180° movements reminiscent of the asynchronous appearance of the two rotations during evolution (Suzanne *et al*., 2010). Importantly, the same mechanism is responsible for both rotations (Suzanne *et al*., 2010; Coutelis *et al*., 2013) (see MyoID section below).

In *Drosophila pachea*, another *Drosophila* species, males show an additional kind of asymmetry of their terminalia, with the left external lobe being 1.5 times longer and thinner than the right one (Lang and Orgogozo, 2012). Surprisingly, 20% of males from one laboratory stocks possess fully symmetric external lobes, reminiscent of the incomplete asymmetry of the asymmetric body found in the brain. Symmetry of *Drosophila pachea* terminalia dramatically reduces mating efficiency compared to asymmetric flies (Lang and Orgogozo, 2012). The asymmetric lobes are proposed to be an adaptation optimizing terminalia coupling during mating and therefore increasing their efficiency. The mechanism controlling lobe asymmetry in *Drosophila pachea* is currently unknown.

GENES AND SIGNALING PATHWAYS CONTROLLING L/R ASYMMETRIC MORPHOGENESIS

The Myosin ID Pathway

Situs inversus genes, i.e. genes whose mutation leads to a complete and coordinated inversion of the L/R axis, are rare and valuable tools. To date only two have been molecularly characterized: i) *inversin* in mouse (Morgan *et al*., 1998) and ii) *myosin ID* (*myoID*) in *Drosophila* (Hozumi *et al*., 2006; Speder *et al*., 2006). MyoID is responsible for the wild-type Dextral orientation of all *Drosophila* L/R viscera (looping of the gut, coiling of the spermiduct, rotation of the male terminalia; see previous section) (Hozumi *et al*., 2006; Speder *et al*., 2006). In *myoID* mutants, the L/R axis is inverted and the flies develop sinistraly (Fig. 1 compare G and H), making MyoID a Dextral determinant. The genes specifically affecting the L/R development of a single organ are discussed elsewhere (Maeda *et al*., 2007; Coutelis *et al*., 2008; Okumura *et al*., 2010; Kuroda *et al*., 2012; Nakamura *et al*., 2013).

Class I myosins are members of the myosin family of actin-based motor proteins (for review see Kim and Flavell, 2008). They are found in eukaryotes from yeast to human and are thought to be one of the earliest myosin proteins (Richards and Cavalier-Smith, 2005). Mouse and human have eight class I myosin genes (MyoIa, b, c, d, e, f, g, and h) where *Drosophila* only has two (MyoIC and MyoID) (Berg *et al*., 2001). In vertebrates, these myosins play diverse roles in various processes such as actin cytoskeleton organization, cell motility, and endocytosis; for instance, Myo1a connects the structural actin cytoskeleton shafts of microvilli to the plasma membrane, MyoIC is involved in the vesicular transports to and from the plasma membrane in various cell types (for review see Kim and Flavell, 2008).

In *Drosophila*, *myoID* expression in the primordia of the various L/R tissues correlates with the fact that L/R patterning appears to be set-up independently (Hozumi *et al*., 2006; Speder *et al*., 2006). Indeed specific depletion of *myoID* in a given tissue leads to the reversal of its lateralization without affecting the other L/R organs (Hozumi *et al*., 2006; Speder *et al*., 2006; Speder and Noselli, 2007; Taniguchi *et al*., 2007). This notion appears particularly interesting as it differs from the vertebrate situation where L/R patterning seems to be set-up once and for all for the whole body plan. This independence of L/R patterning of *Drosophila* organs has made possible the identification of L/R organizers in which MyoID activity is required. This notion is best exemplified in the genital disc. At the end of the larval period, *myoID* is solely expressed in two rows of cells of the A8 segment – A8a and A8p - of the male genital disc (Fig. 3A). Exclusive depletion of MyoID activity in the A8 segment is sufficient to lead to the inversion (Sinistral) of the spermiduct coiling and of the associated male terminalia rotation whereas the other L/R organs (testes, hindgut, etc.) are unaffected (Fig. 1D). Conversely, restoring MyoID expression in the A8 segment alone of *myoID* null flies is sufficient to restore the normal Dextral development of both the spermiduct and terminalia rotation (Speder *et al*., 2006). These results show that the A8 segment is the terminalia L/R organizer.

To promote Dextral determination, the MyoID protein was shown to require a properly organized actin cytoskeleton and to bind to Armadillo, the *Drosophila* beta-catenin homolog (Hozumi *et al*., 2006; Speder *et al*., 2006; Petzoldt *et al*., 2012). This is of particular interest as the gene product of the mouse *inversin* locus, an ankyrin-repeat protein, also directly binds to beta-catenin (Nurnberger *et al*., 2002). This conserved property of both the *situs inversus* gene products led to the closer investigation of the role of the adherens junctions in the establishment of L/R asymmetry. Specific silencing of the adherens junction components DE-Cadherin, alpha-Catenin or beta-Catenin in the A8 segment leads to penetrant terminalia rotation defects, suggesting that adherens junctions as a whole are required for the establishment of L/R asymmetry (Petzoldt *et al*., 2012). Their participation was refined by looking at DE-cadherin temporal requirement for terminalia asymmetric rotation. Interestingly, two peaks are seen, the first synchronous with that of MyoID and the second occuring during the actual rotation process. Thus, DE-Cadherin is required both during L/R

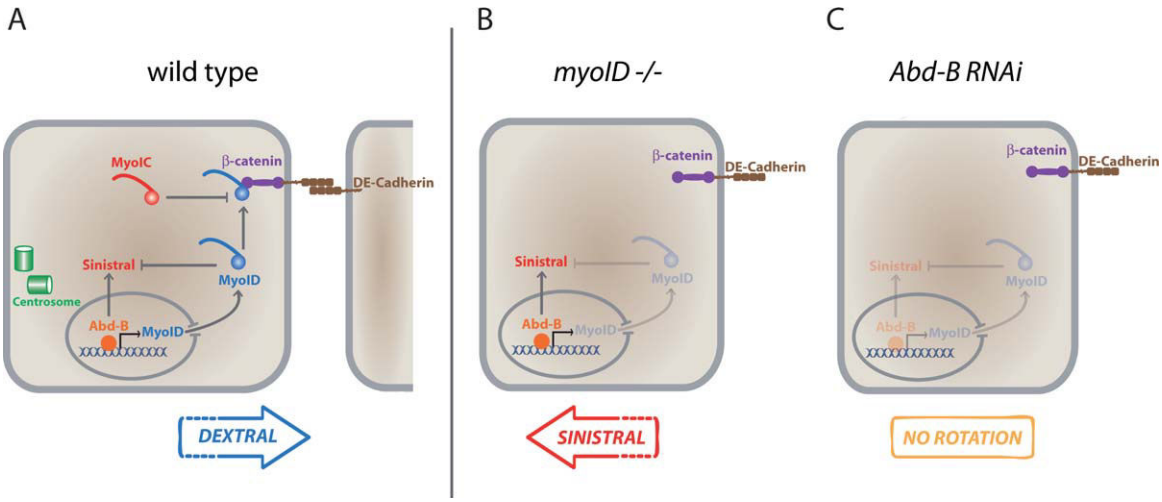

FIG. 2. Summary of the genetic and molecular interactions taking place in the L/R organizer cells. (**a**) The Hox family transcription factor Abd-B (orange) activates the expression of *myoID* in cells of the L/R organizer. MyoID (blue) localizes to the adherens junction via its interaction with beta-Catenin (purple) and DE-Cadherin (brown). This localization is essential for MyoID-dependent Dextral determination. Overexpression of the closely related MyoIC (red) displaces MyoID from the adherens junction thus antagonizing MyoID function, resulting in a *MyoID* null-like Sinistral phenotype (see text for details). Cells adopt oriented asymmetric shape and positioning of their centrosomes (green). (**b**) In *myoID* null mutant flies, recessive Sinistral activity leads to the full inversion of the L/R axis. (**c**) In *Abd-B* loss of function conditions, neither Dextral nor Sinistral are active, resulting in a no rotation phenotype.

determination and asymmetric morphogenesis (Petzoldt *et al*., 2012). Furthermore, in the A8 segment, DE-Cadherin, beta-Catenin and MyoID belong to a complex reinforcing the idea that the adherens junctions represent an essential signaling platform during L/R asymmetry determination required for MyoID activity (Fig. 2A).

The involvement of DE-Cadherin in L/R asymmetry was further investigated in the directional rotation of the embryonic hindgut. In the hindgut epithelial cells, DE-Cadherin is distributed in a polarized fashion to the cell boundaries, which predicts the direction of rotation. Indeed, in *myoID* mutant embryos, the L/R asymmetric distribution of DE-Cadherin is inverted and so is the coiling of the embryonic hindgut (Taniguchi *et al*., 2011). Interestingly, the embryonic hindgut cells show a MyoID-dependent L/R bias of DE-Cadherin and centrosome distributions as well as asymmetric cell shape within their plane leading to planar cell-shape chirality (Taniguchi *et al*., 2011). *In silico* modeling suggests that this intrinsic chirality could set up L/R asymmetric tissue morphogenesis (Taniguchi *et al*., 2011).

Abdominal-B

In a genetic screen for *myoID* interactors involved in L/R determination, the Hox gene *Abdominal-B* (*Abd-B*) was identified as a major upstream regulator of L/R determination in *Drosophila* (Coutelis *et al*., 2013). Abd-B is a homeobox transcription factor of the Bithorax complex known to specify segment identity along the Antero-Posterior axis (for review see Maeda and Karch, 2006). To circumvent the homeotic transformation phenotypes associated with classic *Abd-B* mutations, the authors used spatially and temporally controlled RNAi-mediated depletions of *Abd-B* activity. This led to specific L/R phenotypes without disturbance of Antero-Posterior identity and patterning or morphological defects indicating that this novel role for *Abd-B* is distinct from its function in Antero-Posterior patterning (Coutelis *et al*., 2013). Abd-B was shown to bind to *myoID* regulatory sequences and to be required for MyoID expression in the L/R organizer (Fig. 2A). Nevertheless, the L/R defects observed in both the hindgut and male terminalia upon *Abd-B* L/R activity depletion are neither an inversion nor a randomization of the asymmetry but rather resemble a lack of asymmetry. This strikingly differs from the situation of *myoID* null flies, in which the orientation of the L/R axis is fully inverted, thus revealing the activity of an underlying Sinistral activity only apparent in a *myoID* mutant context (Fig. 2B). It was therefore hypothesized that *Abd-B* could also be required for the Sinistral pathway. Indeed, in *myoID* null flies – in which the Sinistral determination is active – the depletion of *Abd-B* L/R activity leads to similar loss of asymmetry phenotypes indicating that *Abd-B* also controls the Sinistral activity (Coutelis *et al*., 2013). *Abd-B* therefore directs the earliest events of *Drosophila* L/R asymmetry establishment through control of both opposite Dextral and Sinistral determinants, allowing morphogenesis to reach a L/R asymmetric state from an initial symmetric situation. Thus, when *Abd-B* L/R activity is missing, no symmetry breaking occurs and flies develop symmetrically (Fig. 2C). This notion is particularly important as it indicates that in *Drosophila* the default state is symmetry. These data indicate that a

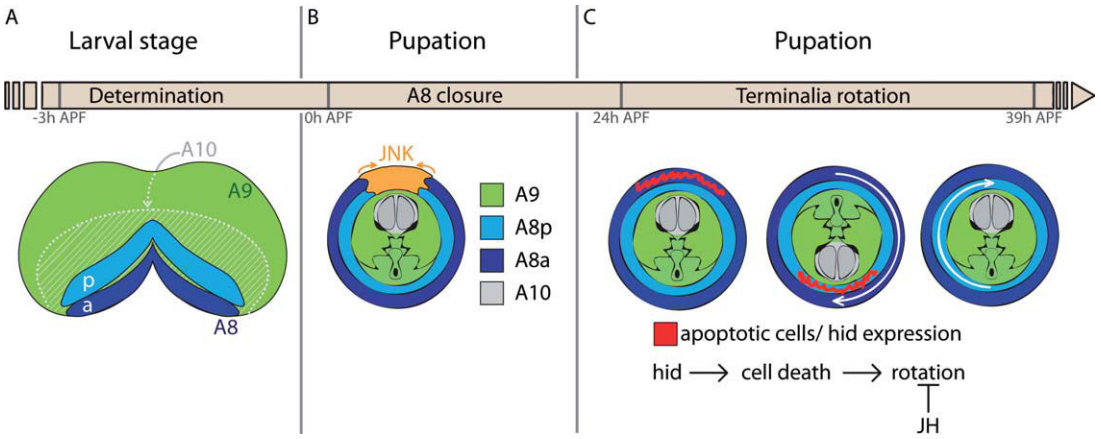

FIG. 3. (**a–c**) Schematic depiction of the developmental events leading to the directed rotation of the male terminalia. The developmental stages (upper part) are given relative to puparium formation (APF, after puparium formation). The larval genital disc (a) is composed of three segments (A8 (blue), A9 (green), and A10 (light gray and dashed)). In the A8 segment, which acts as the L/R organizer (see text for details), MyoID is expressed in two rows of Posterior (A8p, light blue) and Anterior (A8a, dark blue) cells. Following disc eversion upon puparium formation (b), A8 segment cells (anterior and posterior) fuse dorsally via a JNK-dependent process (light orange) to enclose the A9 (green) and A10 (light gray) cells that will give rise to the genital and anal parts, respectively. Between 24 and 39 h APF (c), each of the A8 compartments (posterior and anterior, dark and light blue) contribute half a turn each to the whole rotation (white arrows). Local cell death (red), triggered by the expression of the proapoptotic gene *hid*, works as a break release freeing the rotation of both A8 compartments. Increase in Juvenile Hormone (JH) levels or treatment with its analogs leads to an impaired terminalia rotation (see text for details).

Sinistral pathway exists, whose determinant(s) and molecular nature remain to be characterized.

Myosin IC

Interestingly, MyoIC, the other *Drosophila* class I myosin, has for a while represented a very good candidate for a Sinistral determinant. Indeed, MyoIC overexpression leads to the inversion of the L/R organs (gut looping, terminalia rotation, etc.) perfectly resembling a *myoID* loss of function situation (Hozumi *et al*., 2006, 2008; Petzoldt *et al*., 2012). Moreover, this effect of MyoIC overlaps with the temporal window of MyoID L/R determination (Petzoldt *et al*., 2012). Nevertheless, MyoIC does not appear to be the Sinistral determinant for several reasons: i) *myoID* and *myoIC* double mutant flies show the same *situs inversus* phenotype as *myoID* single mutants do (Petzoldt *et al*., 2012), ii) MyoIC overexpression does not seem to be able to rescue *Abd-B* L/R activity depletion as does the restoration of MyoID expression (Coutelis *et al*., 2013, unpublished results). In fact, thorough investigation of MyoIC function showed that MyoIC rather works as an antagonist of MyoID as MyoIC overexpression displaces MyoID from the adherens junction (Petzoldt *et al*., 2012). MyoIC antagonizes MyoID binding to the adherens junction components beta-Catenin and DE-Cadherin, both *in vitro* and *in vivo* (Petzoldt *et al*., 2012). Thus, MyoIC overexpression affects L/R asymmetry establishment by dislodging MyoID from the adherens junction (Fig. 2A).

Unlike the better-known Myosin-II class, unconventional type-I myosins are non-filamentous single peptide with three distinct domains, head, neck and tail. The N-terminal head bears the actin binding and motor domains; the central neck possesses several IQ motifs that are thought to bind regulatory light chains such as calmodulin; and the C-terminal tail is the site of putative cargo loading and of interaction with membranous phospholipids (for review see Coluccio, 1997; Barylko *et al*., 2000). In *Drosophila*, MyoID and MyoIC sequences are close, however short stretches of amino acids specific to one or the other can be found. This led to the investigation of the L/R activities of chimeric MyoID and MyoIC proteins in which their head, neck and tail domains were swapped. Very interestingly, MyoID and MyoIC specific L/R activities are not due to cargo-binding tail regions of the proteins but rather to their Actin- and ATP-binding head regions (Hozumi *et al*., 2008; Spéder *et al*., unpublished results). These results are of particular interest as they correlate with the striking observation that *in vitro* the motor domain of MyoIC has the singular property of generating asymmetric motility (Pyrpassopoulos *et al*., 2012). This ability to generate counterclockwise turns in the actin filaments could represent a way for class I myosins to establish asymmetry *in vivo*.

In *Drosophila*, the processes linking early L/R patterning with late morphogenesis are still poorly understood. For instance, in the terminalia, Dextral determination through MyoID occurs 24 h before the actual rotation process. In the following sections, we discuss the role of JNK signaling, cell death and hormones which are important for tissue morphogenesis, after the L/R patterning has taken place.

JNK Signaling

The Jun N-terminal Kinase (JNK) signaling pathway is known to be involved in a wide variety of processes including programmed cell death, cell competition, immunity, stress response, cell reprogramming, as well as tissue remodeling and cell elongation during morphogenesis and regeneration (Glise *et al*., 1995; Glise and Noselli, 1997; Holland *et al*., 1997; Adachi-Yamada, *et al*., 1999; Agnes and Noselli, 1999; Agnes *et al*., 1999; Noselli and Agnes, 1999; Zeitlinger and Bohmann, 1999; Manjon *et al*., 2007; Thomas *et al*., 2009; Gettings *et al*., 2010). Recently though, JNK signaling has also been shown to play a role in L/R asymmetry in *Drosophila*. Indeed, terminalia rotation defects are observed in males carrying loss or gain of JNK function. Mutant alleles for the JNK Kinase *hemipterous* (*hep*) or the over-expression of the JNK phosphatase Puckered (Puc) lead to an absence or a partial rotation of terminalia (Glise *et al*., 1995; Holland *et al*., 1997; Macias *et al*., 2004). Interestingly, JNK signaling controls two separate aspects of terminalia development which are crucial for rotation. First, the loss of JNK activity leads to improper fusion of the A8 segment in its dorsal part, which normally takes place prior to rotation. In the absence of fusion, rotation is strongly affected (Fig. 3B). Negative feedback of JNK activity through the serine protease Scarface, a novel JNK target gene, is required for the perfect fusion of the A8 segment and the genital arch, eliciting the rotation of the terminalia (Rousset *et al*., 2010). Once the rotation is completed, JNK signaling is required in the A8 segment for proper fusion of the terminalia with the abdomen (Rousset *et al*., 2010).

In addition to controlling terminalia rotation, JNK signaling is also involved in the asymmetric development of the embryonic anterior midgut (Taniguchi *et al*., 2007). Both down-regulation or hyper-activation of JNK signaling affects the asymmetric cell rearrangements in the circular visceral muscle surrounding the embryonic gut epithelium, leading to the subsequent randomization of L/R asymmetric development of the anterior midgut (Taniguchi *et al*., 2007).

Cell Death

Affecting apoptosis was long known to perturb terminalia rotation (Abbott and Lengyel, 1991; Grether *et al*., 1995; Macias *et al*., 2004). However, only recently has the role of cell death during terminalia looping been unraveled (Suzanne *et al*., 2010). Indeed, localized apoptosis at the boundary of the A8a and A8p rings is essential for uncoupling rings at the onset of their rotation. This break releaser activity takes place as two waves of cell death in the A8 segment, coinciding spatially and temporally with the rotation of the A8a and A8p rings, where MyoID is expressed (Fig. 3C) (Suzanne *et al*., 2010). This localized cell death is proposed to free tissues for proper morphogenetic looping and to control their speed to ensure developmental coordination (Suzanne *et al*., 2010; Kuranaga *et al*., 2011).

Hormones

As mentioned above, terminalia rotation occurs in the pupae during metamorphosis, a process under tight endocrine regulation. Previously, it has been shown that juvenile hormone levels can impact on terminalia rotation (Adam *et al*., 2003). Indeed, ectopic juvenile hormone activity during the pupal stage through injection of JH analogs or in a specific Fasciclin2 mutant condition, induces terminalia rotation defects (Adam *et al*., 2003). Importantly, the juvenile hormone is a terpenoid hormone related to retinoic acid (RA) which also plays a crucial role in vertebrate LR asymmetric development (Harmon *et al*., 1995; Hall and Thummel, 1998). However, in *Drosophila*, the homologue of the RA co-receptor (RxR) is not the JH receptor Met but Ultraspiracle which dimerizes with the receptor of the steroid hormone Ecdysone, the key hormone controlling puparium formation (Hall and Thummel, 1998). Nonetheless, we have observed that Ecdysone and JH interplay to control terminalia rotation (Géminard *et al*., unpublished data), consistent with JH receptor ability to bind to USP and EcR (Jones and Sharp, 1997). Thus, the encouraging parallel between the hormonal control of *Drosophila* and vertebrates L/R asymmetry should be worth digging into.

CONCLUSIONS

Drosophila represents a new valuable model to study L/R asymmetry. The identification of the Myosin ID pathway has revealed the clear role of actin and associated molecular motors in patterning the L/R body axis. A striking feature of *Drosophila*, not found in vertebrates, is the finding that organs can have their own independent organizers. However, despite the use of multiple organizers, organ asymmetry depends on the same MyoID core pathway.

How MyoID activity then connects to cell and organ chirality and whether events downstream of MyoID are conserved in different organs remain to be determined. In the organizer cells, the interaction of MyoID with beta-catenin and DE-cadherin suggests an important role of the adherens junction in connecting up L/R asymmetry with cell and organ polarity. Following initial establishment of asymmetry, several processes and pathways need to be coordinated downstream of MyoID for proper L/R morphogenesis. Recent work has identified JNK signaling and cell death for control of discrete steps during the process of genitalia rotation. Furthermore, L/R development is under hormonal control

for correct coordination with other morphogenetic events.

L/R asymmetry relies on a two-determinant system, Dextral/MyoID and Sinistral. Identifying the genes responsible for Sinistral development represents a critical step toward understanding the molecular basis of L/R asymmetry. The identification of Abd-B as a major factor of asymmetry important for both Dextral and Sinistral development should help identify the still elusive Sinistral pathway.

Whether vertebrates and invertebrates share common mechanisms and principles to set up L/R asymmetry still remains unclear. Data suggest that a number of mechanisms have emerged that can act at different developmental stages or in different organisms. Interestingly, our recent results suggest a conservation of MyoID function in some vertebrates (Coutelis *et al.*, unpublished data), which may provide some new perspectives on the evolution of L/R asymmetry.

LITERATURE CITED

Abbott MK, Lengyel JA. 1991. Embryonic head involution and rotation of male terminalia require the Drosophila locus head involution defective. Genetics 129:783–789.

Adachi-Yamada T, Fujimura-Kamada K, et al. 1999. Distortion of proximodistal information causes JNK-dependent apoptosis in Drosophila wing. Nature 400:166–169.

Adam G, Perrimon N, et al. 2003. The retinoic-like juvenile hormone controls the looping of left-right asymmetric organs in Drosophila. Development 130:2397–2406.

Adams DS, Robinson KR, et al. 2006. Early, H+-V-ATPase-dependent proton flux is necessary for consistent left-right patterning of non-mammalian vertebrates. Development 133:1657–1671.

Agnes F, Noselli S. 1999. [Dorsal closure in Drosophila. A genetic model for wound healing?]. C R Acad Sci III 322:5–13.

Agnes F, Suzanne M, et al. 1999. The Drosophila JNK pathway controls the morphogenesis of imaginal discs during metamorphosis. Development 126:5453–5462.

Aizawa, H. 2013. Habenula and the asymmetric development of the vertebrate brain. Anat Sci Int 88:1–9.

Aylsworth AS, 2001. Clinical aspects of defects in the determination of laterality. Am J Med Genet 101: 345–355.

Barylko B, Binns DD, et al. 2000. Regulation of the enzymatic and motor activities of myosin I. Biochim Biophys Acta 1496:23–35.

Berg JS, Powell BC, et al. 2001. A millennial myosin census. Mol Biol Cell 12:780–794.

Beyenbach KW, Skaer H, et al. 2010. The developmental, molecular, and transport biology of Malpighian tubules. Annu Rev Entomol 55: 351–374.

Bishop DV. 2013. Cerebral asymmetry and language development: Cause, correlate, or consequence? Science 340:1230531.

Brody T, Cravchik A. 2000. Drosophila melanogaster G protein-coupled receptors. J Cell Biol 150: F83–88.

Chintapalli VR, Terhzaz S, et al. 2012. Functional correlates of positional and gender-specific renal asymmetry in Drosophila. PLoS One 7: e32577.

Coluccio LM. 1997. Myosin I. Am J Physiol 273: C347–359.

Concha ML, Wilson SW. 2001. Asymmetry in the epithalamus of vertebrates. J Anat 199(Pt 1-2):63–84.

Coutelis JB, Geminard C, et al. 2013. Drosophila left/right asymmetry establishment is controlled by the Hox gene abdominal-B. Dev Cell 24:89–97.

Coutelis JB, Petzoldt AG, et al. 2008. Left-right asymmetry in Drosophila. Semin Cell Dev Biol 19:252–262.

Danilchik MV, Brown EE, et al. 2006. Intrinsic chiral properties of the Xenopus egg cortex: An early indicator of left-right asymmetry? Development 133: 4517–4526.

de Cuevas M, Matunis EL. 2011. The stem cell niche: Lessons from the Drosophila testis. Development 138:2861–2869.

Gettings M, Serman F, et al. 2010. JNK signalling controls remodelling of the segment boundary through cell reprogramming during Drosophila morphogenesis. PLoS Biol 8: e1000390.

Glise B, Bourbon H, et al. 1995. hemipterous encodes a novel Drosophila MAP kinase kinase, required for epithelial cell sheet movement. Cell 83:451–461.

Glise B, Noselli S. 1997. Coupling of Jun amino-terminal kinase and Decapentaplegic signaling pathways in Drosophila morphogenesis. Genes Dev 11:1738–1747.

Grether ME, Abrams JM, et al. 1995. The head involution defective gene of Drosophila melanogaster functions in programmed cell death. Genes Dev 9: 1694–1708.

Hall BL, Thummel CS. 1998. The RXR homolog ultraspiracle is an essential component of the Drosophila ecdysone receptor. Development 125:4709–4717.

Harmon MA, Boehm MF, et al. 1995. Activation of mammalian retinoid X receptors by the insect growth regulator methoprene. Proc Natl Acad Sci U S A 92: 6157–6160.

Hartenstein, V. 1993. Atlas of Drosophila Development, Cold Spring Harbor Laboratory Press.

Hayashi T, Murakami R. 2001. Left-right asymmetry in Drosophila melanogaster gut development. Dev Growth Differ 43:239–246.

Holland PM, Suzanne M, et al. 1997. MKK7 is a stress-activated mitogen-activated protein kinase kinase

functionally related to hemipterous. J Biol Chem 272:24994–24998.

Hombria JC, Brown S. 2002. The fertile field of Drosophila Jak/STAT signalling. Curr Biol 12: R569–575.

Hozumi S, Maeda R, et al. 2006. An unconventional myosin in Drosophila reverses the default handedness in visceral organs. Nature 440:798–802.

Hozumi S, Maeda R, et al. 2008. Head region of unconventional myosin I family members is responsible for the organ-specificity of their roles in left-right polarity in Drosophila. Dev Dyn 237:3528–3537.

Jenett A, Rubin GM, et al. 2012. A GAL4-driver line resource for Drosophila neurobiology. Cell Rep 2: 991–1001.

Jiang H, Edgar BA. 2011. Intestinal stem cells in the adult Drosophila midgut. Exp Cell Res 317:2780–2788.

Jiang H, Edgar BA. 2012. Intestinal stem cell function in Drosophila and mice. Curr Opin Genet Dev 22:354–360.

Jones G, Sharp PA. 1997. Ultraspiracle: An invertebrate nuclear receptor for juvenile hormones. Proc Natl Acad Sci USA 94:13499–13503.

Keisman EL, Baker BS. 2001. The Drosophila sex determination hierarchy modulates wingless and decapentaplegic signaling to deploy dachshund sex-specifically in the genital imaginal disc. Development 128:1643–1656.

Kim SV, Flavell RA. 2008. Myosin I: From yeast to human. Cell Mol Life Sci 65:2128–2137.

Kuranaga E, Matsunuma T, et al. 2011. Apoptosis controls the speed of looping morphogenesis in Drosophila male terminalia. Development 138:1493–1499.

Kuroda J, Nakamura M, et al. 2012. Canonical Wnt signaling in the visceral muscle is required for left-right asymmetric development of the Drosophila midgut. Mech Dev 128:625–639.

Lang M, Orgogozo V. 2012. Distinct copulation positions in Drosophila pachea males with symmetric or asymmetric external genitalia. Contributions to Zoology 81:87–94.

Le Bras S, Van Doren M. 2006. Development of the male germline stem cell niche in Drosophila. Dev Biol 294:92–103.

Lengyel JA, Iwaki DD. 2002. It takes guts: The Drosophila hindgut as a model system for organogenesis. Dev Biol 243:1–19.

Levin, M., Johnson RL, et al. 1995. A molecular pathway determining left-right asymmetry in chick embryogenesis. Cell 82:803–814.

Levin M, Thorlin T, et al. 2002. Asymmetries in H+/K+-ATPase and cell membrane potentials comprise a very early step in left-right patterning. Cell 111: 77–89.

Loveland KL, Hime G. 2005. TGFbeta superfamily members in spermatogenesis: Setting the stage for fertility in mouse and Drosophila. Cell Tissue Res 322:141–146.

Macias A, Romero NM, et al. 2004. PVF1/PVR signaling and apoptosis promotes the rotation and dorsal closure of the Drosophila male terminalia. Int J Dev Biol 48:1087–1094.

Maeda R, Hozumi S, et al. 2007. Roles of single-minded in the left-right asymmetric development of the Drosophila embryonic gut. Mech Dev 124:204–217.

Maeda RK, Karch F. 2006. The ABC of the BX-C: The bithorax complex explained. Development 133: 1413–1422.

Manjon C, Sanchez-Herrero E, et al. 2007. Sharp boundaries of Dpp signalling trigger local cell death required for Drosophila leg morphogenesis. Nat Cell Biol 9:57–63.

Manner, J. 2009. The anatomy of cardiac looping: A step towards the understanding of the morphogenesis of several forms of congenital cardiac malformations. Clin Anat 22:21–35.

Mercola M, Levin M. 2001. Left-right asymmetry determination in vertebrates. Annu Rev Cell Dev Biol 17: 779–805.

Micchelli CA. 2012. The origin of intestinal stem cells in Drosophila. Dev Dyn 241:85–91.

Micchelli CA, Perrimon N. 2006. Evidence that stem cells reside in the adult Drosophila midgut epithelium. Nature 439:475–479.

Morgan D, Turnpenny L, et al. 1998. Inversin, a novel gene in the vertebrate left-right axis pathway, is partially deleted in the inv mouse. Nat Genet 20:149–156.

Morton BE. 2013. Behavioral laterality of the brain: Support for the binary construct of hemisity. Front Psychol 4: 683.

Myat MM. 2005. Making tubes in the Drosophila embryo. Dev Dyn 232:617–632.

Nakamura M, Matsumoto K, et al. 2013. Reduced cell number in the hindgut epithelium disrupts hindgut left-right asymmetry in a mutant of pebble, encoding a RhoGEF, in Drosophila embryos. Mech Dev 130:169–180.

Noselli S, Agnes F. 1999. Roles of the JNK signaling pathway in Drosophila morphogenesis. Curr Opin Genet Dev 9:466–472.

Nurnberger J, Bacallao RL, et al. 2002. Inversin forms a complex with catenins and N-cadherin in polarized epithelial cells. Mol Biol Cell 13:3096–3106.

Ohlstein B, Spradling A. 2006. The adult Drosophila posterior midgut is maintained by pluripotent stem cells. Nature 439:470–474.

Okumura T, Fujiwara H, et al. 2010. Left-right asymmetric morphogenesis of the anterior midgut depends on the activation of a non-muscle myosin II in Drosophila. Dev Biol 344:693–706.

Okumura T, Utsuno H, et al. 2008. The development and evolution of left-right asymmetry in invertebrates: Lessons from Drosophila and snails. Dev Dyn 237:3497–3515.

Pascual A, Huang KL, et al. 2004. Neuroanatomy: Brain asymmetry and long-term memory. Nature 427: 605–606.

Petzoldt AG, Coutelis JB, et al. 2012. DE-Cadherin regulates unconventional Myosin ID and Myosin IC in Drosophila left-right asymmetry establishment. Development 139:1874–1884.

Pyrpassopoulos S, Feeser EA, et al. 2012. Membrane-bound myo1c powers asymmetric motility of actin filaments. Curr Biol 22:1688–1692.

Raya A, Izpisua Belmonte JC. 2008. Insights into the establishment of left-right asymmetries in vertebrates. Birth Defects Res C Embryo Today 84:81–94.

Richards TA, Cavalier-Smith T. 2005. Myosin domain evolution and the primary divergence of eukaryotes. Nature 436:1113–1118.

Rousset R, Bono-Lauriol S, et al. 2010. The Drosophila serine protease homologue Scarface regulates JNK signalling in a negative-feedback loop during epithelial morphogenesis. Development 137:2177–2186.

Roussigne M, Blader P, et al. 2012. Breaking symmetry: The zebrafish as a model for understanding left-right asymmetry in the developing brain. Dev Neurobiol 72:269–281.

Santos AC, Lehmann R. 2004. Germ cell specification and migration in Drosophila and beyond. Curr Biol 14: R578–589.

Speder P, Adam G, et al. 2006. Type ID unconventional myosin controls left-right asymmetry in Drosophila. Nature 440:803–807.

Speder P, Noselli S. 2007. Left-right asymmetry: Class I myosins show the direction. Curr Opin Cell Biol 19: 82–87.

Speder P, Petzoldt A, et al. 2007. Strategies to establish left/right asymmetry in vertebrates and invertebrates. Curr Opin Genet Dev 17:351–358.

Suzanne M, Petzoldt AG, et al. 2010. Coupling of apoptosis and L/R patterning controls stepwise organ looping. Curr Biol 20:1773–1778.

Tabin, C. 2005. Do we know anything about how left-right asymmetry is first established in the vertebrate embryo? J Mol Histol 36:317–323.

Takashima S, Younossi-Hartenstein A, et al. 2011. A novel tissue in an established model system: The Drosophila pupal midgut. Dev Genes Evol 221:69–81.

Taniguchi K, Hozumi S, et al. 2007. D-JNK signaling in visceral muscle cells controls the laterality of the Drosophila gut. Dev Biol 311:251–263.

Taniguchi K, Maeda R, et al. 2011. Chirality in planar cell shape contributes to left-right asymmetric epithelial morphogenesis. Science 333:339–341.

Thomas C, Rousset R, et al. 2009. JNK signalling influences intracellular trafficking during Drosophila morphogenesis through regulation of the novel target gene Rab30. Dev Biol 331:250–260.

Vandenberg LN, Levin M. 2013. A unified model for left-right asymmetry? Comparison and synthesis of molecular models of embryonic laterality. Dev Biol 379:1–15.

Zeitlinger J, Bohmann D. 1999. Thorax closure in Drosophila: Involvement of Fos and the JNK pathway. Development 126:3947–3956.

Planar cell polarity (PCP)

1 Definition

Cell polarity is a fundamental feature of many types of cells. From a three dimensional point of view, the cell have 3 axes (X, Y and Z). The Z axis is represented by the Apico/Basal (A/P) polarity system. As an example of a polarized cell type, the intestine epithelial cells feature an apical domain, facing the intestine lumen, and a basal plasma membrane domain, facing the internal side of the organism (Figure 2).

The orthogonal plane to the Z axis is then the X, Y axis; in cell biology this axis is called the planar cell polarity axis. The term planar polarity was first used by Nübler-Jung (Nübler-Jung, 1987) to describe the spatial organization of polarized structures such as bristles on the insect cuticle (Figure 3). Planar polarity is a common property of animal tissues that is most obvious when cells are organized in epithelial sheets. (For definitions of planar polarity, see: Adler, 2002; Lewis and Davies, 2002; Lawrence et al., 2007; Segalen and Bellaïche, 2009; Wang and Nathans, 2007).

In Drosophila, planar cell polarity is evident in a variety of tissues, including the larval epidermis (Donoughe and DiNardo, 2011), the ommatidia (Das et al., 2002), the wing and abdomen hairs (Lawrence et al., 2002; Adler, 2012), and the stretching of cells during different developmental processes (Rauzi et al., 2010; Bosveld et al., 2012). The positioning of wing hairs serves as a good example to explain PCP because it is a well characterized model and, given the strong evidence that the principles seen in the wing

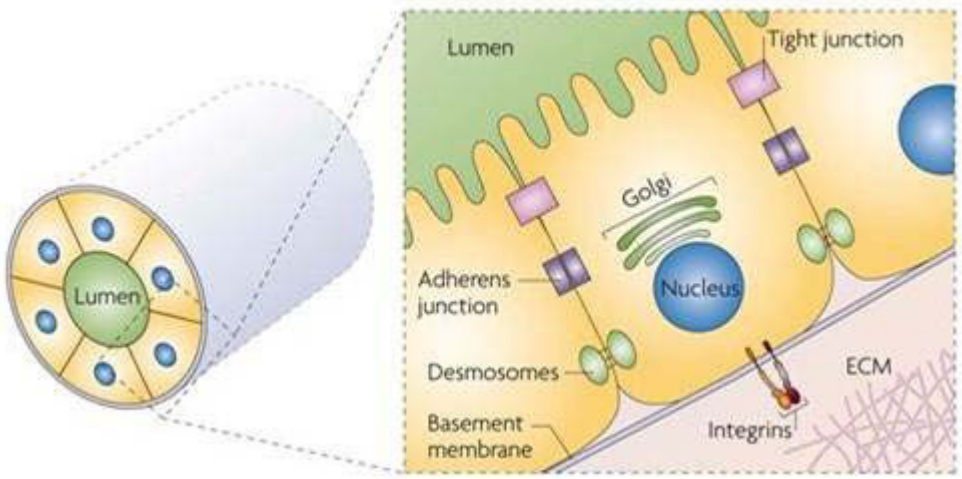

Figure 2. The apicobasal polarity in epithelial cells

In epithelial cells, the individual cells are split into two regions, the apical and basolateral regions, which are chemically and structurally different from each other. The apical region is defined as the area lying above the tight junctions and contains the apical membrane which faces the lumen or the outer surface. The basolateral region is the side that is below the tight junctions and contains the basolateral membrane which is in contact with the basal lamina. Image from (Bryant and Mostov, 2008)

are at least partially conserved across tissues and species (Carroll and Yu, 2012), it serves to provide a framework for understanding planar polarity establishment. Though, there are some controversies in the field

In the Drosophila wing PCP is evident by the positioning of single distally pointing trichomes (insect small hair). Two main cellular systems govern the cell-cell interactions that underlie the local alignment of cell polarity in the wing and in most PCP tissues studied so far: the so-called core planar polarity pathway and the global Fat/Dachsous (Ft/Ds) pathway (Figure 4). Both systems act through an underlying common logic; they generate asymmetric contacts between cells through heterophilic interactions between proteins located in the cell membrane, which in turn exhibit asymmetric sub-cellular activities and/or distributions. Finally, the activity of these PCP components restrict the formation of the trichomes to the distal site of the cell, leading to a distally located and pointing trochome.

The logic behind PCP establishment can be viewed as a three step process: First the activity of a signal coming from the tissue axes (dorso-ventral and proximo-distal) orients the tissue PCP axis, then the intracellular activity of PCP components which read and interpret the incoming signal and translate this signal to the rest of the component in a cell-autonomous manner. Finally the newly oriented cell is able to transmit its PCP information to neighboring cells thus propagating PCP information throughout a specific tissue (for reviews see Lawrence and Casal, 2013; Peng and Axelrod, 2012; Adler, 2012; Matis and Axelrod, 2013; Goodrich and Strutt, 2011; Segalen and Bellaïche, 2009; Singh

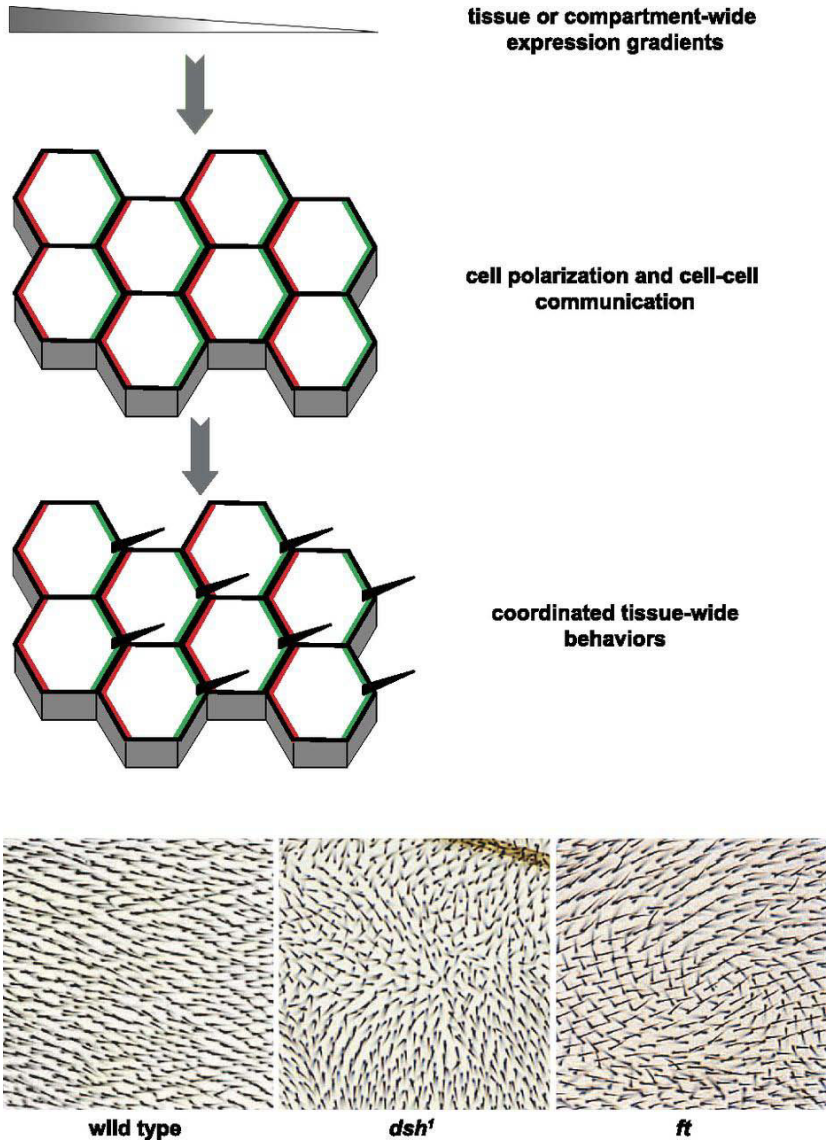

Figure 3. Planar Cell Polarity in the Drosophila wing epithelium.

A three step process to adquire proper PCP in the wing epithelium trichomes: First the tissue axis directional cues, in the form of expression gradients or selective diffusion of secreted factors, provide directional information about the tissue. Then the core PCP module adjust the inta-cellular PCP to match while coordinating and amplifying the polarity by intercellular communication and feedback mechanisms. Then while the components of the core PCP pathway localize distinct protein complexes to opposite sides of the cell they maintain PCP. Finally cells respond with appropriate tissue-specific behaviors, shown here is the production of a trichome (or hair) from the distal side of the cell that points distally. Mutations in components that affect PCP result a very characteristic patterns of trichome orientation defects: aligned and ponting distally in normal flies, random pointing in *dsh* mutants and non-random but non-aligned in mutants. Adapted from (Matis and Axelrod, 2013)

and Mlodzik, 2012; Eaton and Jülicher, 2011).

As stated PCP is a complex system receiving both intracellular and extracellular feedback signals. Though, it is an oversimplification of the actual process to present each pathway separately, to try to streamline the main components of the PCP pathways in *Drosophila,* I will present first the core-PCP pathway, then the global-PCP pathway and finally the relationship between the two pathways.

2 The core planar cell polarity pathway

The core pathway in flies is composed by six proteins; they had all been described based on their similar activities, their mutant phenotypes and by their localization at the adherens junctions. During wing development, before the appearance of the distal hair, in the wing disc during larval stages, the core PCP proteins exhibit a transient asymmetric localization in the epithelial plane (Strutt and Strutt, 2009; Goodrich and Strutt, 2011) (Figure 4). On the distal side of the cell junctions resides Frizzled (Fz), a seven-pass transmembrane protein, along with the ankyrin containing protein Diego (Dgo) and the PDZ bearing protein Dishevelled (Dsh), located both in the cytoplasm. On the other side of the cell (proximal) lays Strabismus (Stbm), a four-pass transmembrane protein and Prikled (Pk) a cytosolic protein. Finally, Flamingo (a.k.a. Starry Night Fmi/Stan) a seven-pass transmembrane cadherin, is present on both sides of the cell (Strutt and Strutt, 2009; Goodrich and Strutt, 2011 and Figure 5). Complete or partial loss of activity of any of the core proteins leads to mislocalization of other

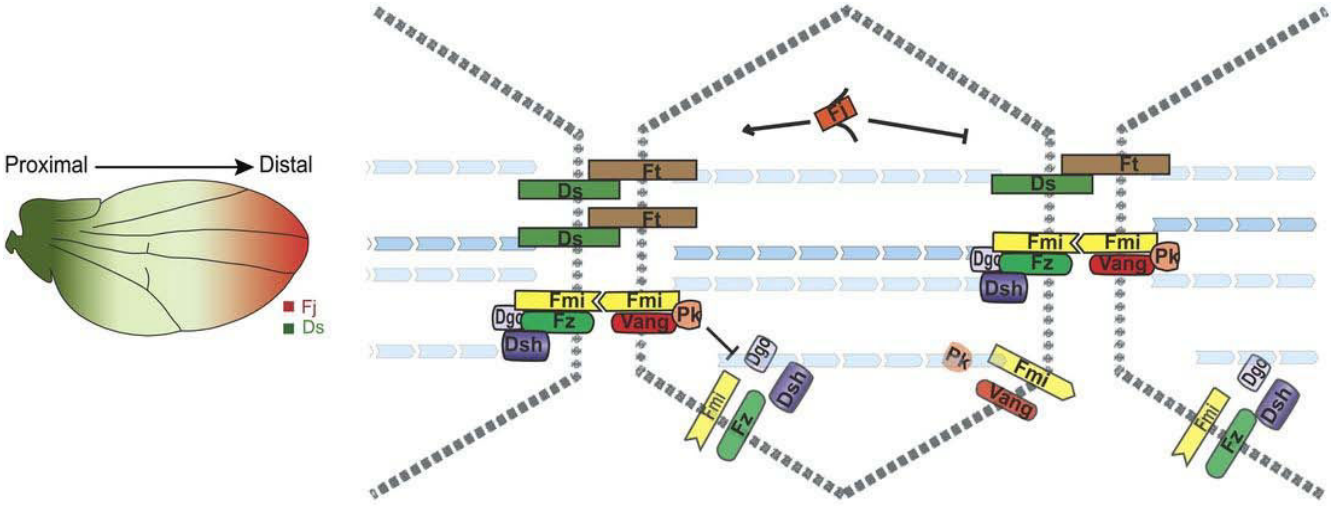

Figure 4. Subcellular localization of PCP components and polarization

The Ft/Ds pathway, through the oppositely oriented gradients of Ds and Fj, may provide directional information. The core proteins (Fmi, Fz, Dsh, Dgo, Vang, and Pk) segregate to opposite sides of the cell. Adapted from (Matis and Axelrod, 2013).

In contrast to Ft homogeneous distribution Fj and Ds exhibit opposite expression gradients in the wing. This opposite gradients are thought to establish an aligning cue for the proper PCP in the wing. The endokinase Fj, present in the Golgi (orange) is able to phosphorylate both Ds (green) and Ft (brown) , this prosphorylation changes the binding affinity of the ECD of these atypical cadherins. From the outter membrane space DsECD is able to stably bind FtECD however no such stable binding is made from homodimers. This mechanism is thought to be responsible for the opposite segregation of Ds and Ft to different sides of the membrane. In turn the microtubule network orients following the polarity dictated by Ft/Ds localizations and this microtubule orientation is finally read through Pk or Sple (pink). Pk in turn restricts Dgo ((ight blue) to the plus end of the microtubules and which is able to bind Fz and Fmi (Yellow and green) and stabilize Vang and Fmi the minus ends.

core-PCP components with an associated loss of planar cell polarity as evidenced by the trichome positioning/pointing (Wong and Adler, 1993).

Core-PCP is originally established at a cellular level; consistently, all of the core-PCP components mentioned above localize within the plane of the epithelium in a specific side of the cell and the disruption of one component affects the other in a cell autonomous manner (Jenny et al., 2003; Das et al., 2004; Bastock et al., 2003 Axelrod, 2001). However, the general asymmetric coordination seems to also require cell-cell contacts and the formation of asymmetric intercellular contacts, the removal of one component also affects the neighbor cell's components (Chen et al., 2008; Strutt and Strutt, 2008; Tree et al., 2002; Wu and Mlodzik, 2008). Thus the core PCP pathway is a complex process that receives intracellular and extracellular inputs within an epithelium.

Since mutations in any component of the core PCP pathways affect the localization of the other components it seems that the planar-polarized localization of each protein is reinforced by both positive (when a component is anchored to the membrane by other component) or negative (when one component is excluded from one side of the membrane) interactions (Peng and Axelrod, 2012; Carroll and Yu, 2012).

Finally, the core PCP pathway has the peculiar function to transmit or propagate its intracellular PCP directionality, thus it has a non-cell autonomous function. The most clear evidence for the non cell-autonomous function of the core PCP in coordinating polarity over the wing is that when groups of cells that lack Fz are induced, neighboring cells (with normal Fz) point their hairs towards the mutant cells; similarly, loss of Stbm

causes neighboring cells to point their hairs away (Wu and Mlodzik, 2008; Strutt and Strutt, 2002). This suggests that polarity is generated inside the cell and further propagated to neighboring cells (Figure 4 and Goodrich and Strutt, 2011).

3 The global planar cell polarity pathway

The global pathway is composed of the Fat (Ft), Dachsous (Ds) and Four-jointed (Fj) proteins (Figure 6). The *ft* and *ds* genes both encode atypical cadherins that preferentially bind heterophilically to each other at the cell surface (Ma et al., 2003; Matakatsu and Blair, 2004), and this interaction is modulated by phosphorylation of both extracellular domains by the Golgi-localized ectokinase protein Fj (Strutt et al., 2004; Brittle et al., 2010; Simon et al., 2010).

The Drosophila Fat and Ds proteins are members of the cadherin super family, a group of type I integral membrane proteins characterized by the presence in the extracellular domain of cadherin-type repeats composed of two β sheets mediating Ca2+-dependent binding. ft is predicted to encode a 5147-amino-acid protein with a calculated mass of 560 kDa, it contains three basic domains, an intracellular domain (ICD), a transmembrane domain and a large extracellular domain (ECD), the latter region containing five epidermal growth factor like repeats, 34 tandem cadherin-type domains,

and two laminin domains (Matis and Axelrod, 2013). In contrast, *ds* is predicted to encode a 3503-amino-acid protein with a calculated mass of 380 kDa with 27 cadherin repeats in its extracellular domain, a transmembrane domain and an intracellular domain (Figure 7) (Goodrich and Strutt, 2011; Matis and Axelrod, 2013).

Although Ft and Ds exhibit weak asymmetric subcellular localizations (Strutt and Strutt, 2002; Ma et al., 2003) their activity leads to the strong polarized subcellular distribution of Dachs, a downstream-acting atypical myosin (Ambegaonkar et al. 2012; Brittle et al. 2012; Bosveld et al. 2012; Mao et al., 2006; Rogulja et al., 2008). Dachs localizes to one side of the apical membrane in a planar-cell polarity fashion in response to a Ds gradient. Dachs is thought to control the proximo-distal elongation in the wing disc cells by controlling cell geometry, and thus indirectly influencing the mitotic spindle (Mao et al., 2011). Since Dachs is planar-polarized it has been suggested to act as a selective cell-cell junction constrictive force (Mao et al., 2011). Consistently mutant clones for *dachs* are small and rounded as opposed to the stereotyped elongated form of wild-type clones (Mao et al., 2011). Therefore, Ds asymmetric localization promotes the strong asymmetric accumulation of Dachs at one side of the cell through direct binding to the intracellular domain of Dachsous (DsICD) (Ambegaonkar et al. 2012; Brittle et al. 2012; Bosveld et al. 2012). Since Dachs is more strongly asymmetrically accumulated than Ds, an amplification mechanism has been suggested, and very recently has been identified: the ubiquitin ligase FbxI7 that binds to the intracellular domain of Ft (FtICD) but not the intracellular domain of Ds (DsICD) is able to promote the proteolytic degradation of Dachs specifically where Ft is highly localized; thus

explaining the stronger asymmetric accumulation of Dachs in relationship with Dachsous (Bosch et al., 2014; Rodrigues-Campos and Thompson, 2014).

The other component of the pathway, the kinase Fj is largely localized to the Golgi (Strutt et al. 2004) where it phosphorylates the cadherin domains of Ft and Ds in four and three cadherin domains respectively (Ishikawa et al. 2008). However this phorsphorylation leads to opposite effects: phosphorylated Ft increases the binding affinity to Ds (Simon et al. 2010) while phosphorylation of Ds decreases its affinity for Ft. Finally this phosphorilation is important for the polarity function of Ds (Brittle et al. 2010; Simon et al. 2010). Unlike Ft, Ds and Fj are expressed in gradients that may contribute to their ability to provide directional information and growth regulatory activity (Zeidler et al. 1999; Casal et al. 2002; Yang et al. 2002; Ma et al. 2003; Lawrence et al. 2004). *Fj* is expressed in opposite gradients to Ds along the proximo-distal axis in imaginal discs (Zeidler et al. 1999; Casal et al. 2002; Yang et al. 2002; Ma et al. 2003; Lawrence et al. 2004). This opposite effect, coupled with the gradient imposed by Fj, is thought to be the basis of planar cell polarity of this system. Finally, as a refinement of the system, Ft is further processed at two cleavage sites located in the extracellular domain in a Ds-dependent fashion revealed by biochemical analyses, with consequences in the regulation of the final wing size, revealing an even more complex signaling pathway (Feng and Irvine 2009).

However there is also some type of regulation between Ft and Ds happening in the intracellular space which function has not been completely resolved but it existence

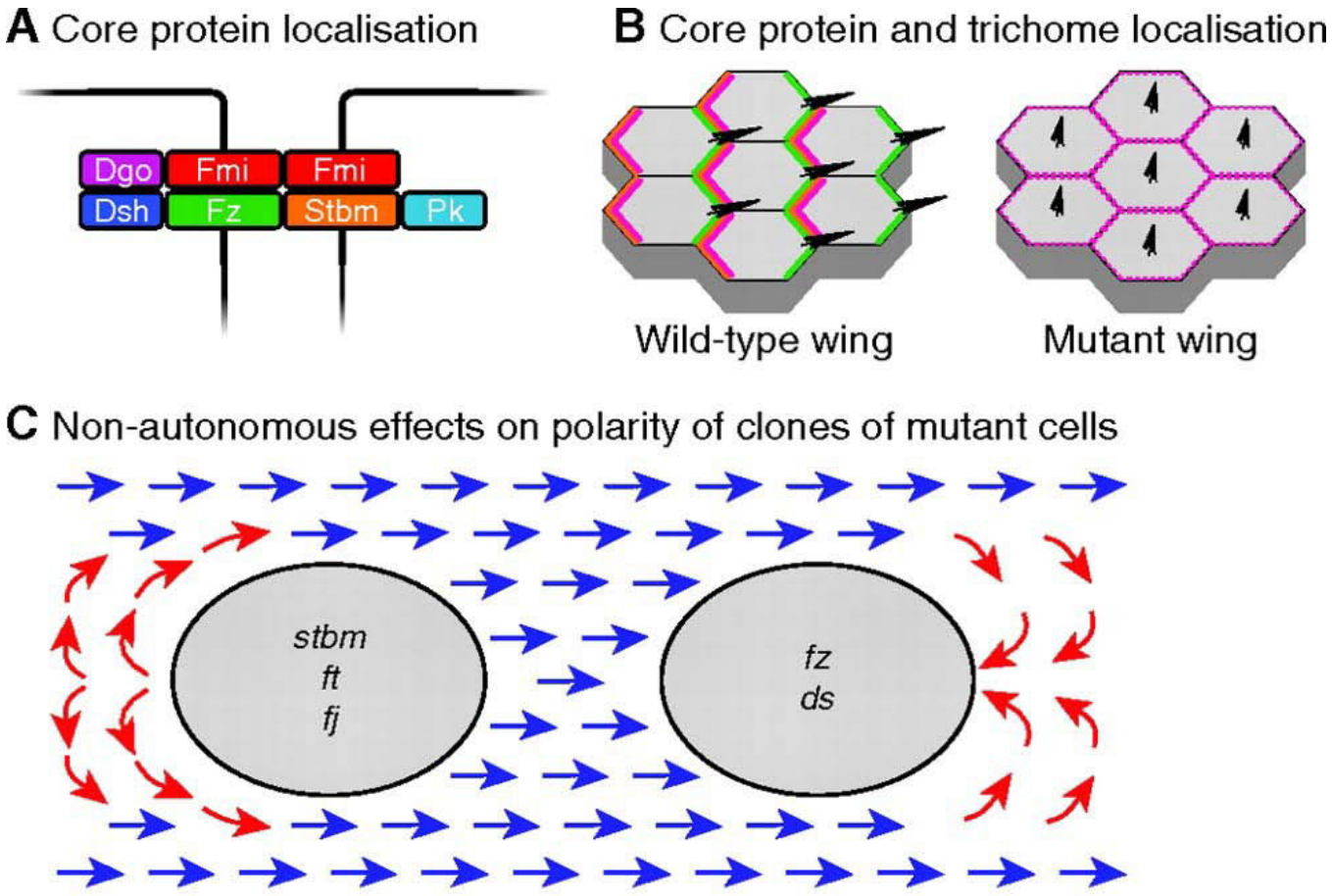

Figure 5. Properties of the core planar polarity proteins in Drosophila wing development.

(A) The core protein arrangement and localization at the adherens junction in the Drosophila wing. An intercellular asymmetric junction complex forms, with the transmembrane proteins Fz (green) and Fmi (red), and the cytosolic proteins Dsh (dark blue) and Dgo (purple) in one cell, associating with the transmembrane proteins Stbm (orange) and Fmi, and the cytosolic protein Pk (pale blue) in the adjacent cell. (B) The core-PCP components and some trichome formation effectors show a clear subcellular distribution in the pupal wing. Here the core-PCP components are shown using the same color code as in panel A and the effectors are drown as a black arrow (representing a growing trichome). In mutant cells for the PCP-components or in which the activity of these components in uniformly localized the trichome production happens randomly or in the cell center. (C) Normal trichome polarity shown in blue arrows can be affected in a non-autonomous manner by making clones of cells lacking planar polarity gene function (big gray circles). However the non-automomous effect is somehow different depending on the missing protein: clones of cells lacking stbm, ft or fj activity (left) cause cells proximal to the clone to invert their polarity (red arrows), in turn groups of cells lacking fz or ds function (right) cause trichomes distal to the clone to invert their polarity. Adapted from (Goodrich and Strutt, 2011)

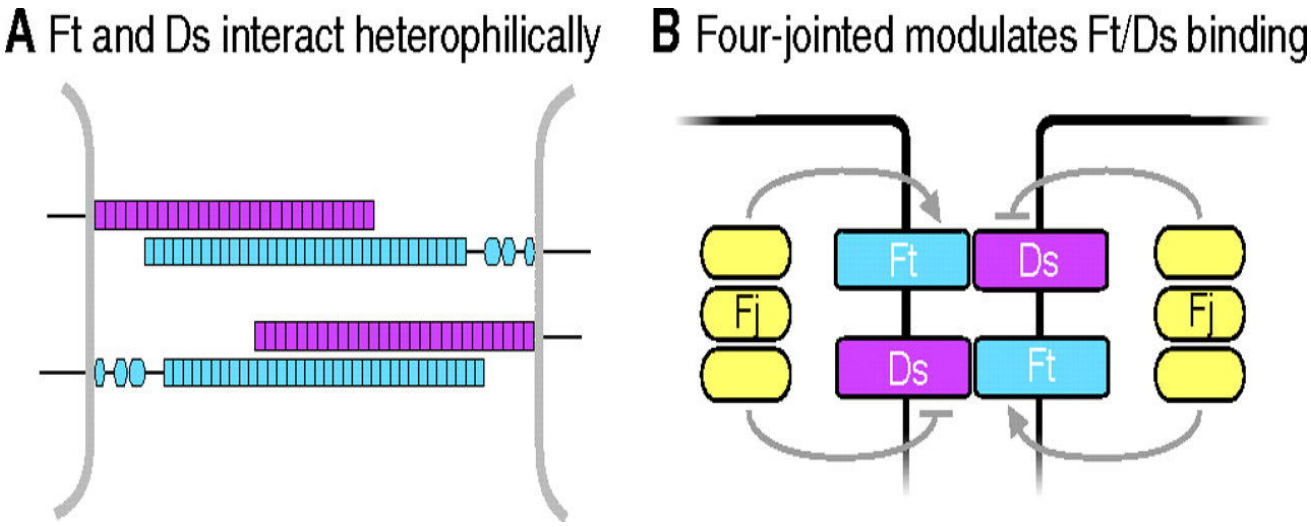

Figure 6. Fat Four-jointed and Dachsous interactions in the Drosophila wing.

Model of the interactions between the components of the Global pathway (Fat and Dachsous) at the adherens junctions of epithelial cells in the Drosophila imaginal discs. (A) Ft (blue) and Ds (magenta) are large atypical cadherin molecules that prefferable interact heterophilically thus creating an asymmetric junction. (B) The heterophilic interactions between Fat and Dachsous are modulated by the kinase activity in the Golgi Four-jointed (yellow), FJ phosphorylates the extracellular cadherin repeats in both Ft and Ds as they traffic through the Golgi apparatus to the cell surface; this Fj-mediated phosphorylation in Ft increases its binding affinity for Ds, while phosphorylation of Ds decreases its affinity for Ft. Adapted from (Goodrich and Strutt, 2011)

has been demonstrated to be of PCP consequences (Matis and Axelrod, 2013). The most noteworthy series of experiments that overall suggest a functional intracellular Ft/Ds interactions are: If a clone of cells in which the Ds protein is present in higher concentrations, the cells the border of the clone show a clear polarity reversal phenotype, pointing towards the highest peak of Ds expression; this same phenotype can be achieved using a form of Ds lacking the extracellular domain (DsΔECD). Though the repolarization phenotype observed using the DsΔECD form is weaker than the one induced using the full-length form of Ds, this experiment questions the necessity of the ECD to transmit non-cell autonomous PCP information (Sharma and McNeill, 2013). Surprisingly, the non-autonomy phenotype observed by the overexpression of either Ds or DsΔECD depends on the presence of Ft within the clone, as evidenced by the rescue of the ectopic polarity reversals when the clones are depleted of Ft protein. Therefore, since the interaction is restricted to the intracellular space and the ICD of Ds, there is a functional PCP signal transmitted by the ICD of Ds that depends on Ft (Sharma and McNeill 2013). While the experiment of also removing the ECD in this already complex system was not done, since the ICD of Ds cannot bind the, ECD of Ft it is plausible to postulate that there is an ECD-free PCP signal coming from the interaction between Ds/Ft. A mechanism to explain how is this ECD-free signal able to propagate throughout the epithelial tissue is, to my knowledge, not been reported.

In summary, though there are plenty of interaction between the members of the

global pathway happening in which has become a very complex system, it is clear that the Ft/Ds system converts transcription gradients of Fj and Ds into sub cellular asymmetries of Ds/Ft heterodimers that reside at adherent junctions (Yang et al. 2002; Ma et al. 2003). The essential feature of this mechanism is that it captures information about the direction of the tissue axes and provides sub cellular asymmetric molecular cues that are available to orient PCP relative to the tissue axes.

Another particularity of the system is that though the original PCP asymmetric localization of Ds, Ft and therefore Dachs are generated inside of the cell. This asymmetric localization propagates to the neighboring cells throughout several cell diameters. The basis for this mechanism is that the accumulation of Ft in one cell would recruit Ds within neighboring cells or *vice versa* on the opposite side of the neighboring cell (Matis and Axelrod, 2013). A propagation mechanism for the Ft/Ds/Fj module was first predicted computationally (Ma et al. 2008), and then seen in wing discs. In order to test the propagation of the global PCP pathway signal an elaborated experimental set-up was used: in wing discs with clones overexpressing Ds, the polarity of the neighboring cells is inverted, and this inversion was seen not only by the positioning of the trichomes but also by tagging the endogenous Ds and Dachs outside of the clone (Ambegaonkar et al. 2012; Brittle et al. 2012). The observed non-autonomous effect of the Ft/Ds/Fj module is reminiscent of that produced by the core PCP module (Figure 4; Matis and Axelrod, 2013).

However, there is some controversy in the field based on a particular experiment

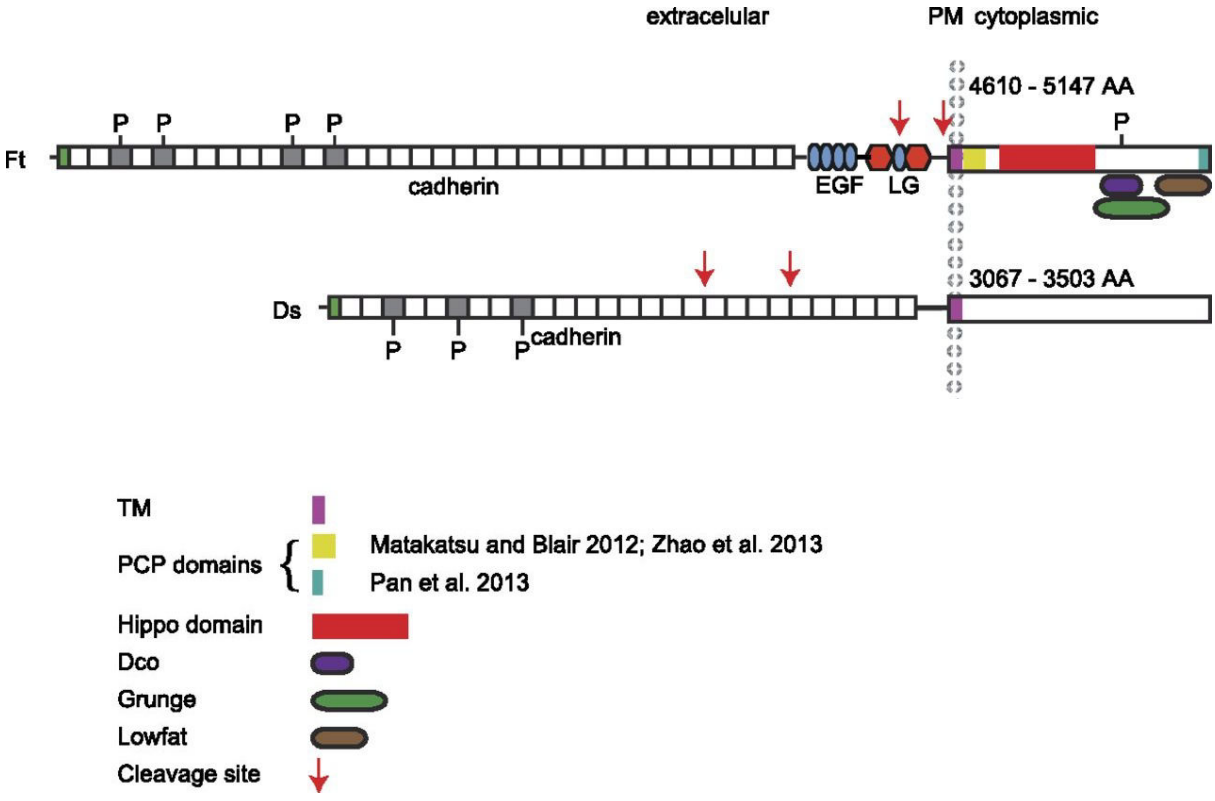

Figure 7. Illustrative views of Fat and Dachsous atypical cadherins.

Conserved extracellular domains are indicated. Sites of phosphorylation by Fj are marked with "P," and cleavage sites are marked with arrows. Known intracellular binding sites are shown, as are putative functional domains identified by various structure/function studies. Adapted from (Matis and Axelrod, 2013).

that comes from the analysis of Fat truncated forms in their ability to rescue both growth and PCP defects. Fat protein forms lacking the cadherin domains (FtΔECD) provide substantial polarity-rescuing activity in *ft*-null mutant wing and abdominal tissue (Matakatsu and Blair 2006, 2012; Zhao et al. 2013) Even more surprising, a smaller form FtΔECDΔ1-C construct lacking the complete extracellular domain and all binding regions identified in the ICD is also able to rescue *ft* mutant overgrowth and PCP defects (Matakatsu and Blair 2012). Interestingly, the remaining domains in the FtΔECDΔ1-C are not strongly conserved (Matis and Axelrod, 2013). This particular experiment seems to question the validity of the heterophilic binding of Ft to Ds for proper planar cell polarity propagation and also question the role of the domains present in the ICD of Ft. However since the evidence for the interaction between Ds and Ft are enormous some side explanations can be pointed to solve the apparent paradox of the rescuing activity of FtICD: first it could be that the mutant used was not completely abolishing Ft, for example if it generates a truncated protein that is normally useless but that can form dimmers with the overexpressed truncated form; second it could be that the rescuing activity is mediated by forming protein complexes with another Fat-like atypical cadherin (possibly encoded by the *fat2* gene) and third it could be that the truncated forms used to rescue *ft* mutants are able to self polarize the tissue independent of the global pathway: in such a way that can only be observed when the tissue is mispolarized. Of course this explanations are somehow not the standard view f rescuing experiments in *Drosophila* however since the implication of FtICD rescuing activity are so huge some side explanations have to be drawn.

Never the less and apart the strange and unresolved paradox the global pathway is a very studied system that translates information about the tissue axis into cellular asymmetries which are then propagated throughout the tissue.

4 Interaction between Global and Core PCP pathways

How is the core PCP pathway aligned with the dorsoventral and anteroposterior axes of the wing? The answer to this question is at present not clear. Since PCP is broadly aligned to the tissue axes, it was originally speculated that the pathways involved in the generation of these axes might somehow cue PCP. The dorso-ventral and the antero-posterior axes of the wing are broadly specified by gradients of the morphogens Wingless (Wg, a member of the Wnt family) and Decapentaplegic (Dpp), respectively (For a recent review on the integration of morphogen signaling into the wing growth see: Baena-Lopez et al., 2012). In vertebrates, a link between the Wnt non-canonical pathway and planar cell polarity has been suggested through the activation of β-catenin (Gao, 2012). However, the absence of planar polarity phenotypes upon loss of *Wg* suggests that Wg does not signal to the core PCP pathway (Lawrence et al., 2002; Goodrich and Strutt, 2011).

On the other hand, mutations affecting the Global-Fat/Ds (Ft/Ds) pathway (explained in more detail after) lead to the separation of the core-PCP pathway from the proximo-distal axis, together with the fact that the Global-Fat/Dachsous pathway forms a proximo-distal gradient in the wing, has lead to the proposal that the Ft/Ds pathway

might be responsible for the global coordination of the core PCP pathway to the tissue axes, hence its name as a global coordinator of PCP (Ma et al., 2003). The current view is that the Global-Ft/Ds pathway provides indirect cues that serve to align the core-PCP pathway to the body axis. This alignment is done either indirectly by controlling the cell geometry through accumulation of a downstream myosin Dachs (Goodrich and Strutt, 2011; Matis and Axelrod, 2013; Mao et al., 2011; Bosveld et al., 2012) or by guiding the planar polarity of the microtubule network which is finally read through one of the two isoforms in the *prickle* locus: pricke (*pk) or spiny-legs (sple)* (Ayukawa et al., 2014; Merkel et al., 2014; Olofsson et al., 2014; Matis et al., 2014).

When originally proposed the Ft/Ds pathway provided an elegant solution to the problem of how the core PCP components orient the global tissue axes. However, the accumulating data followed this proposal has proved it not to be completely accurate.

The main experiments that lead to the idea that the Ft/Ds pathway provides a cue to the core PCP pathway are: 1) mutant clones of *ft, ds,* or *fj* generated in the wing or in the eye, dissociates the core module orientation from the tissue axes, indicating a loss of global directional input; and 2) *Ft* overexpression influences ommatidial PCP polarity only if Fz is active, suggesting an epistatic behavior (Yang et al. 2002). These two experiments strongly suggest that the Ft/Ds system guides the orientation of the core PCP pathway.

However, recent experiments suggest that the relationship between these two pathways is not completely direct. For example, artificially flattening of the Ds and Fj

gradients does not affect PCP in the wing, suggesting that the proximo-distal information present in these gradients is not necessary for PCP. Similarly, like in all tissues studied in the abdomen the Ds system has an intrinsic capacity to non-cell autonomously re polarize cells (Ambegaonkar et al. 2012; Brittle et al. 2012), however in this particular tissue, this repolarization happens even when the cells are *stan* mutant. Therefore the Global pathway is able to induce PCP polarization without the core-PCP pathway (Simon 2004; Casal et al. 2006; Mao et al. 2006; Repiso et al. 2010; Donoughe and DiNardo 2011).

Though the exact mechanism has not been resolved yet and the genetic interaction between the Ft/Ds and the core PCP pathways suggest the existence of several links, alternative possibilities have been suggested to explain how the Ft/Ds pathway indirectly cues the alignment of the core PCP pathway. One way is through the alignment of the microtubule cytoskeleton. In the wing, the microtubules are aligned along the P/D axis, with a modest excess of plus ends on the distal side of the cell, this alignment contributes to the transport of Fz (Shimada et al. 2006). The apical microtubule cytoskeleton shows strong correlation with the core protein PCP pathway during wing development (Eaton et al., 1996; Shimada et al., 2006; Harumoto et al., 2010). Consistently, a mutation of *ds* has been found to alter microtubules orientation in a specific region of the wing, pointing towards a model in which polarization of Ft and Ds patterns the microtubules cytoskeleton, which in turn contributes to alignment of core module polarization (Harumoto et al. 2010). However, not always the core-PCP components respond equally to the Ds/Ft imposed polarity. The orientation of the

microtubule network is proposed to be assimilated in different directions by the two isoforms of the *prickle* locus: *prickle* (*pk*) and *spiny-legs* (*sple*) thus explaining the diversity of polarities observed by the core-PCP pathway in relationship with Ds and Fj gradients (Ayukawa et al., 2014; Merkel et al., 2014; Olofsson et al., 2014; Matis et al., 2014). However, this does not explain the repolarization induced by Ds in the absence of Stan protein or the lack of defect phenotype observed by the artificial flattening of the Ds gradient.

Another possible mechanism that has been proposed to explain the direction imposed by the Global pathway to the core PCP pathway comes from the observation of the Ds-dependent contraction of the hinge region of the wing during pupal development . This contraction has been surprisingly found to induce tissue remodeling in large regions of the proper wing (Aigouy et al. 2010). This contraction mechanism is based on a more mechanical signal than a mere gradient could impose: the hindge contraction was proposed to impose anisotropic tension on the wing blade, thereby inducing cell flow through cellular rearrangements, cell elongation, and consequently oriented cell divisions; all of which finally exert a mechanical tissue remodeling force that would reorient PCP domains (Sagner et al. 2012). Although it is not known what causes the contraction of the hinge region, it is partially dependent on Ds function, and one might imagine a mechanism similar to the Dachs-mediated anisotropic polarization which remodels the notum (Bosveld et al. 2012). While this model is appealing, it does not explain the induced repolarization of the core PCP components in clones over-expressing Ds (Adler et al. 1998; Strutt and Strutt 2002; Ma et al. 2003, 2008).

Finally, it is important to note that though the direct relationship between the Ft/Ds pathway and the core PCP pathway seems complex and several apparent paradoxes have been raised (several feedback relationships going on; the existence of some tissues where one pathway is needed but not the other; the biphasic response of the core PCP pathway which can be aligned or in the reversed to the global pathway signal, depending on the relative levels of Pk/Sple isoforms; and that some details in the intrinsic regulatory feedbacks happening in each system which are not completely resolved) these two systems constitute the molecular basis for planar cell polarity in most tissues already analyzed.

5 L/R asymmetry and PCP

L/R asymmetry and Planar Cell Polarity establishments operate on similar bases: 1) they both generate an asymmetric cue based on existing coordinated axes (namely Dorso/Ventral, Antero/Posterior axis and/or the Apico/Basal, Proximo/Distal); 2) they both are generated intracellularly and 3) they are both propagated throughout a tissue in a non-cell autonomous fashion. These similar and common features have lead to the tempting hypothesis that L/R asymmetry is a form of planar cell polarity (Aw and Levin, 2009).

But far from being an hypothetical idea, a link between these two pathways has been demonstrated; for example, the *inversin* mutant mouse strain which causes a near complete inversion of the L/R axis in mouse is mutated in a gene coding for a distant

homolog of the core-PCP related protein Diego (Morgan et al., 1998). Consistently, hair PCP defects are observed in the *inversin* mutant and the Inversin protein has been shown to localize and bind the core-PCP proteins Vang and Pk (Simons et al., 2005). All of these experiments show that information related to L/R asymmerty and PCP establishments are both present in one single protein. Two other components of the core-PCP pathway, Vang and Dishevelled, are also necessary for the correct cilia positioning in the node (the L/R organizer) thus reinforcing the role of PCP in L/R establishment. If Vang or Dsh proteins are absent the L/R axis becomes randomized (Antic et al., 2010; Borovina et al., 2010; Hashimoto et al., 2010). Another good example of the relationship between these pathways came from the analysis of the mouse mutant for the *bbs4* gene which induces classical PCP phenotypes (Ross et al., 2005). Noticeably the *bbs4* gene is one of the most common mutated genes in human patients that exhibit Bardet-Biedl syndrome, a condition that leads to clear L/R randomization defects (Ansley et al., 2003).

Finally, though a clear link between the core-PCP pathway and L/R asymmetry establishment has been showed in higher vertebrates; no such link has ever been made in *Drosophila*, nor it has been made between the Global-Ft/Ds pathway and L/R asymmetry establishment in any animal model studied so far.

The adult hindgut

The typical gut of an insect consists of the foregut, the midgut, and the hindgut (Lemaitre and Miguel-Aliaga, 2013). While the foregut and the midgut are the main sites for nutrient assimilation, the hindgut is where most of water and ions are reabsorbed if needed (Lemaitre and Miguel-Aliaga, 2013). In the last decades, there has been a substantial advance towards the understanding of the development and the function of the intestine in Drosophila. However, most studies in the *Drosophila* fly have been focused on the midgut and in contrast not so much is known about the last portion of the gut, the hindgut (Figure 8).

Originally, an enormous set of genetic evidence, made in the *Drosophila* embryo, described the basic principles of hindgut development in embryogenesis (Lengyel and Iwaki, 2002; Myat, 2005). Yet the adult counterpart has remained obscure. Only recently, followed by the identification of putative stem cell population in the adult hindgut (Takashima et al., 2008) some advances have been done in the study of the development of the adult hindgut (Takashima et al., 2013; Fox and Spradling, 2009).

The adult and the larval hindguts are morphologically similar (Figure 9); they are broadly divided into the pyloric region, the ileum and the rectum (Gupta and Berridge, 1966; Takashima et al., 2008; Fox and Spradling, 2009). The larval pyloric region is

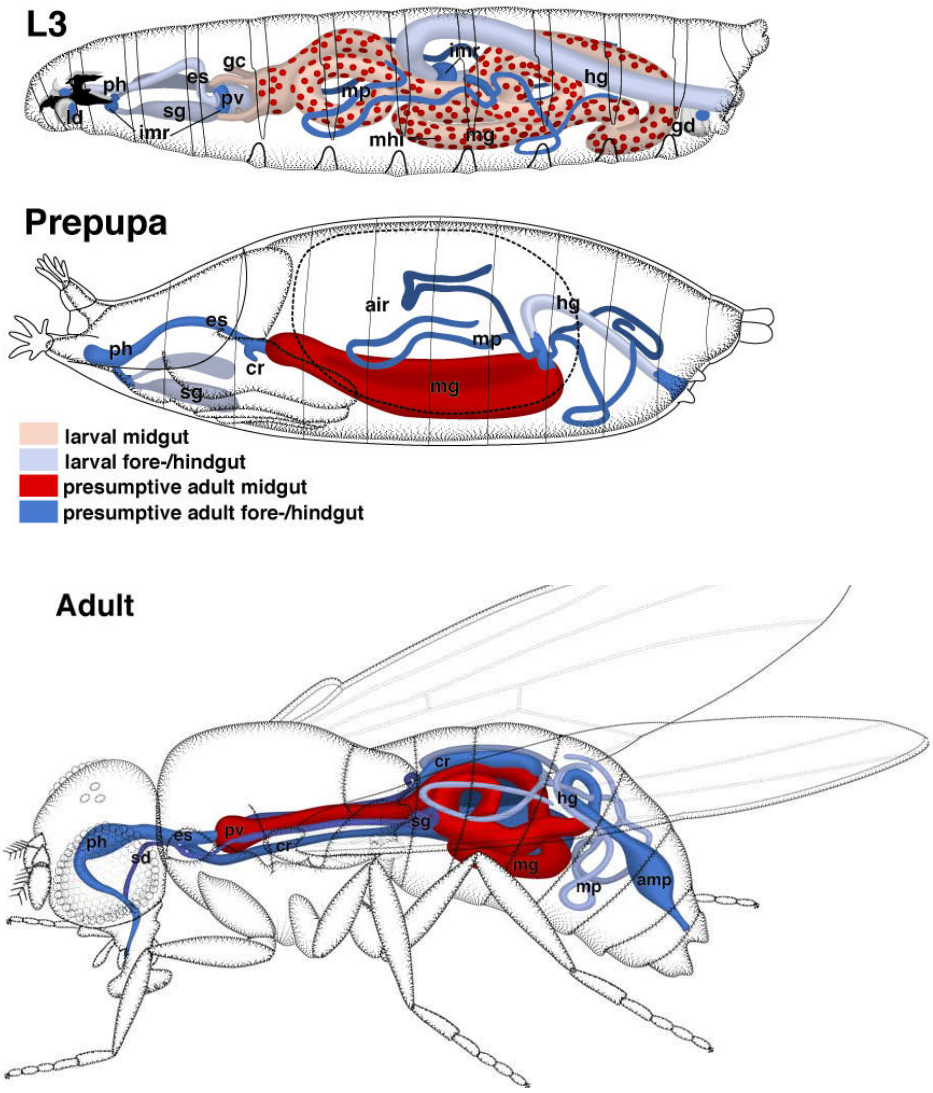

Figure 8. Structure and development of the alimentary tract of the fly

The typical gut of an insect consists of the foregut (blue), the midgut (red), and the hindgut (blue).
During pupa development the epithelium of the larval gut degenerates completely and is by imaginal cells. Precursors of the imaginal gut, present at larval stages, (dark blue or red) are integrated into the larval gut epithelium (light blue or red). The midgut is replaced by midgut histoblasts (*mhi*) scattered throughout the larval midgut epithelium (*mg*). Precursors of the adult hindgut (*hg*) lie in an imaginal ring (imr)located at the junction between larval hindgut and midgut; the posterior hindgut is replaced by cells originating in the genital disc (*gd).* At the end of the prepupal stage (12 hr apf), most of the larval gut has been replaced by imaginal cells. The primordium of the adult midgut forms a cylindrical chamber that encloses the remnants of the larval midgut (yellow body). The hindgut has been partly replaced. Components present in the adult fly that had not been present in the larva are the crop (*cr*), an unpaired outgrowth of the esophagus, and the rectal ampulla (*amp*), a specialization of the posterior hindgut. Conversely, the gastric caeca (*gc*), outgrowths of the anterior larval midgut, are not replaced in the adult gut. (*air*) Air bubble; (*ph*) pharynx (also called cibarium in the adult); (*pv*) proventriculus (also called cardia in the adult). proventriculus (*pv*) Malpighian tubules (*mp*) adult salivary duct (*sd*) glands (*sg*). Adapted from (Hartenstein, 1995)

subdivided by the imaginal ring and the actual pyloric valve. It controls the passage of fluid from the midgut and the malpighian tubules into the hindgut, and thus it is surrounded by strong visceral musculature (Coast, 2007; Cohen, 2013; Lemaitre and Miguel-Aliaga, 2013). The imaginal ring contains around 600 diploid cells that are recognized to be the adult hindgut (AHG) precursors (Murakami and Shiotsuki, 2001; Murakami et al., 1994; Fox and Spradling, 2009). The adult pylorus is formed by the pyloric valve and adjacent to the AHG, the stem cells of the pylorus. The exact nature of these stem cells is not completely resolved. They have been shown to be normally quiescent but to divide upon stress and their progeny in the AHG has been followed until the pylorus, but never in the ileum or rectum (Fox and Spradling, 2009).

The larval ileum consists of big polyploid cells and covers most of the hindgut length. During metamorphosis it degrades together with the larval pyloric valve and so the adult ileum is formed *de novo* from the imaginal ring (Murakami and Shiotsuki, 2001). The adult ileum is very similar to its larval counterpart; it is formed by only one type of big polyploidal cells and is also the biggest part of the AHG (Takashima et al., 2008).

The larval rectum consists of the rectum and the anal pads; they are formed by big polyploidal cells (Murakami and Shiotsuki, 2001). Interestingly, these cells are not degraded during metamorphosis but they mitotically divide to form the adult rectum, they are a very unusual case of polyploidal mitosis (Fox and Spradling, 2009). The adult rectum, though it comes directly from polyploidal mitotic divisions of the larval rectum,

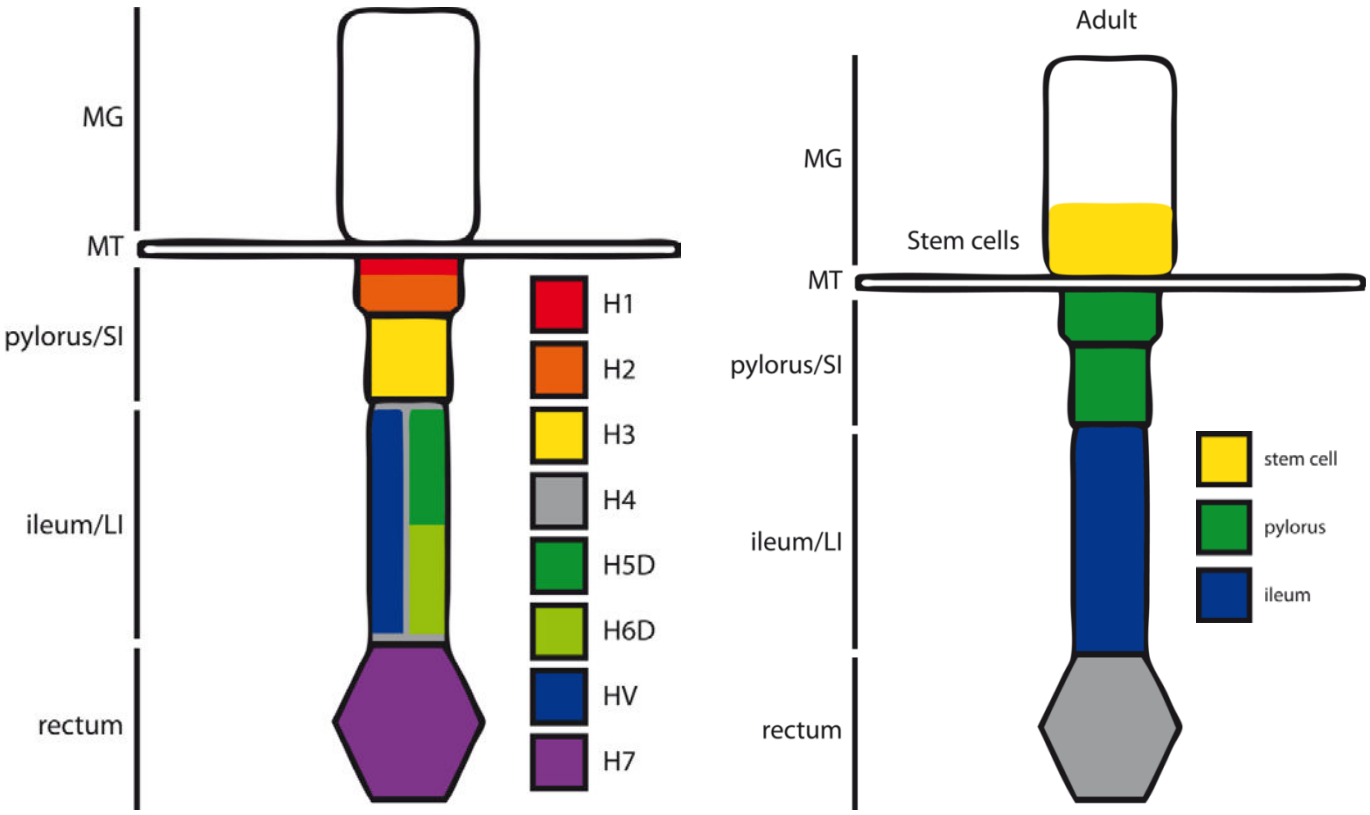

Figure 9. Comparison between larval and adult hindguts.

The adult and the larval hindguts are morphologically similar; they are broadly divided into the pyloric region, the ileum and the rectum. In color are shown the different proposed regions fro the larval hindgut , redrawn from (Murakami et al., 1994). Colors in the adult hindgut represent the homologous regions.

it is morphologically very different. It is a rounded structure that host 4 conic structures called rectal papillae that serve as the last water reapportion organ (Fox et al., 2010). From the outside the rectum is covered by strong musculature and the rectal sheath epithelium and from lumen side it hosts a dense layer of cuticle (Fox et al., 2010; Peacock and Anstee, 1977).

In terms of function, the seminal work on non-Drosophila insects have gave a good impression about the physiology of the hindgut (Hopkins, 1967; Cohen, 2013; Lemaitre and Miguel-Aliaga, 2013) yet until very recently these ideas have begun to be tested in the Drosophila genetic model (Cognigni et al., 2011; Seisenbacher et al., 2011). Though, functional studies have confirmed a role in the hindgut in osmoregulation (Seisenbacher et al., 2011), there are likely more functions to be uncovered; evidence to this is that most genes highly expressed in the adult hindgut are currently uncharacterized (Chintapalli et al., 2013).

General Experimental procedures

II General Experimental procedures

1 Fly strains

Flies were grown on standard cornmeal molasses agar medium with crosses performed at 25°C unless indicated otherwise. Strains are described in FlyBase (http://flybase.org) or otherwise specified. *w1118* flies or sibling controls were used as wild type. During the course of this work a large amount of different Drosophila strains have been produced an exhaustive list of stocks used is provided as Supplementary Table 1.

2 UAS/GAl4 system

The bipartite UAS/Gal4 transcription system derived from the budding yeast Saccharomyces cerevisiae is used in Drosphila melanogaster to express a given construct, e.g. RNAi or coding gene sequences, in a tissue of choice (Brand and Perrimon, 1993). The transcriptional activator Gal4 has been inserted in the fly genome and lays downstream of a promoter sequence of interest (enhancer trap). The regulatory sequence targets Gal4 expression into the tissue of interest (Figure 10). This construct is denominated "driver". Flies carrying the driver construct are crossed to transgenic flies encoding the UAS- gene/construct of interest. UAS stands for Upstream Activation

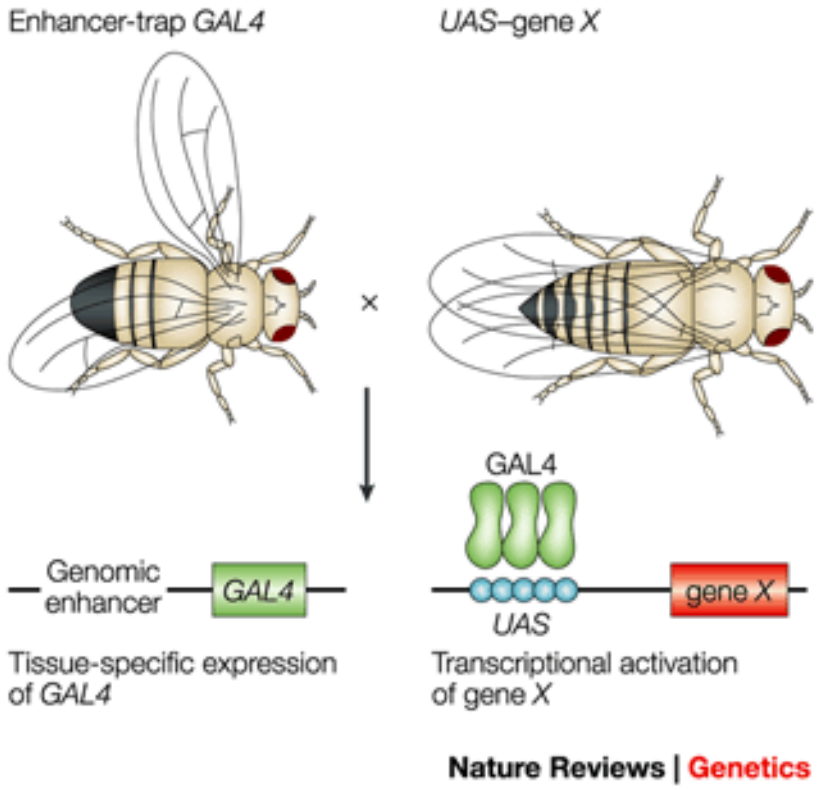

Figure 10. Overview of the UAS/GAL4 system in *Drosophila.*

The yeast transcriptional activator Gal4 can be used to regulate gene expression in Drosophila by inserting the upstream activating sequence (UAS) to which it binds next to a gene of interest (gene X). The GAL4 gene has been inserted at random positions in the Drosophila genome to generate 'enhancer-trap' lines that express GAL4 under the control of nearby genomic enhancers, and there is now a large collection of lines that express GAL4 in a huge variety of cell-type and tissue-specific patterns. Therefore, the expression of gene X can be driven in any of these patterns by crossing the appropriate GAL4 enhancer-trap line to flies that carry the UAS–gene X transgene. This system has been adapted to carry out genetic screens for genes that give phenotypes when misexpressed in a particular tissue. Image adapted from St Johnston , 2002.

Sequence, a specific Gal4 binding site. The UAS sequence is cloned upstream of the construct or gene of interest. Consequently, in the F1 generation, the gene or construct of interest adopts the temporal and special expression pattern of the driver. The system is temperature sensitive and expression is strongest at 30°C as this is the optimal temperature for yeast growth and is less efficient at 25°C.

3 Gal80TS and temperature dependent expression

The *Gal80* gene is a repressor of the Gal4 activator and acts by binding to the activation domain of Gal4, thus preventing the interaction between Gal4 and the transcriptional machinery in yeast (Ma et al., 1987) and has been introduced in fly (Lee et al., 1999). Conditional gene expression can be achieved by use of a ubiquitously expressed Gal80, e.g. by fusion to a ubiquitous promoter as *tubulin* (Tub-Gal80), which is temperature sensitive (ts). The repressor is inactive at 30°C and the Gal4 activator is transcribed and activates gene expression, therefore 30°C is the permissive temperature. The Gal80 repressor is active at 25°, inhibiting the Gal4 driven expression of the gene, hence 25°C is the restrictive temperature. Shifts between both temperatures permit the expression of the gene or construct at any time- window in development (McGuire et al., 2004).

4 RNAi silencing

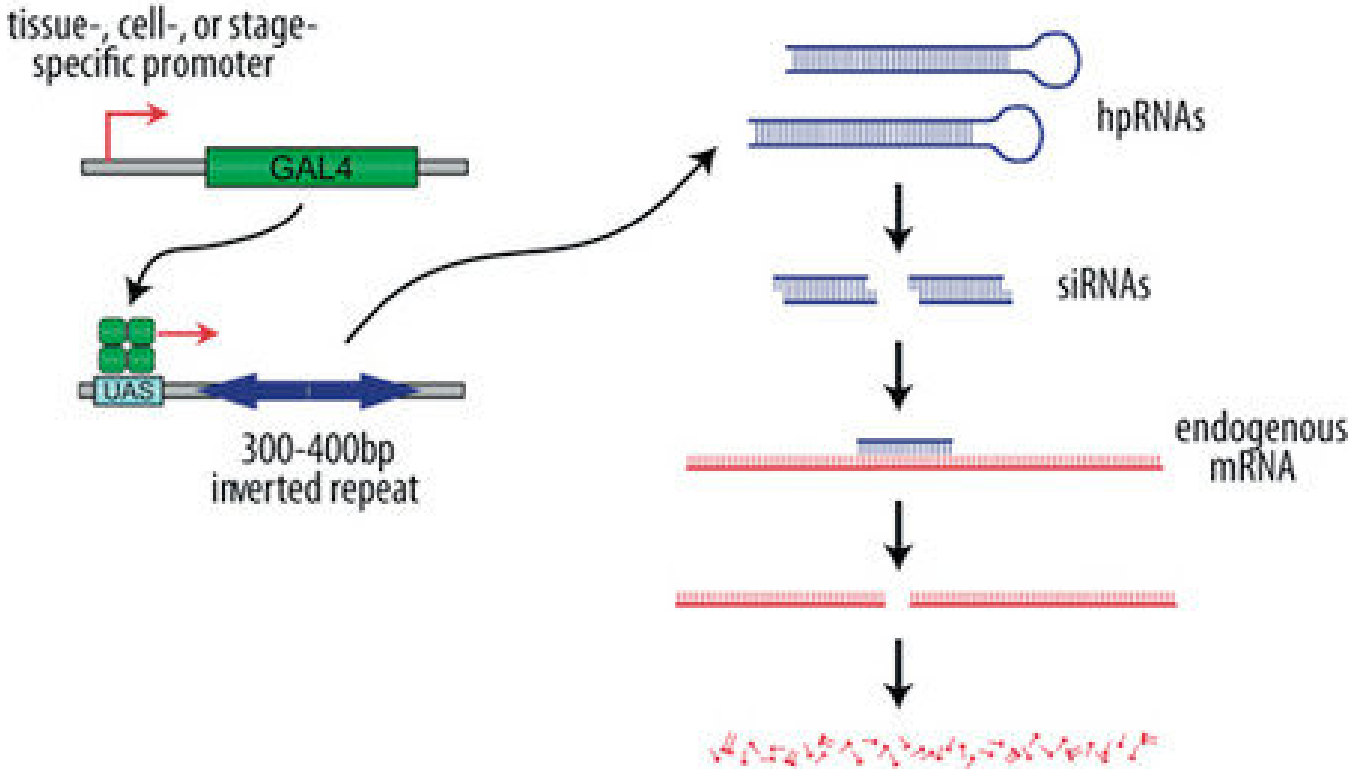

Figure 11. Overview of the transgenic RNAi mediated depletion system in *Drosophila*.

The generic GAL4/UAS system is used to drive the expression of a hairpin RNA (hpRNAs). These double-stranded RNAs are processed by Dicer into siRNAs which direct sequence-specific degradation of the target mRNA. Modified from VDRC website http://stockcenter.vdrc.at

RNAi silencing is used as a loss of function approach and acts through posttranscriptional depletion. The mRNA transcript of a gene of interest is destroyed by the RISC complex (RNA-induced silencing complex) of the cell, for review see (Sontheimer, 2005). Double stranded RNA is recognised by the ribonuclease-III enzyme dicer and cut into 21-23 nt short interfering siRNAs (Figure 11). Upon assembly of the RISC complex triggered by the siRNAs, the former recognizing the unwounded target mRNA by siRNAi-mRNA base pairing, the mRNA is cleaved and degraded. This mechanism is part of the cellular defense against viral infections and implied in endogenous control of gene transcription. By use of the UAS-Gal4 system the RNAi construct can be driven into the tissue of interest. RNAi is advantageous, if loss of function analysis is required in only a subset of cells or tissues and can be used for temporal analysis of protein requirement in connection with the $Gal80^{ts}$ allele. Drawbacks of this method are that the efficiency of silencing can vary largely between different constructs, and depends on protein half-live and turn-over. Gene silencing can be successful with only 19 nucleotides of sequence identity and off-targets that is involuntary silencing of proteins, can be responsible for observed phenotypes (Ma et al., 2006). Silencing efficiency can be increased by the simultaneous overexpression of dicer, a component of the RISC complex (Dietzl et al., 2007).

5 FLP/FRT mitotic clones

The FLP/FRT system permits to induce somatic clones in the tissue of interest by

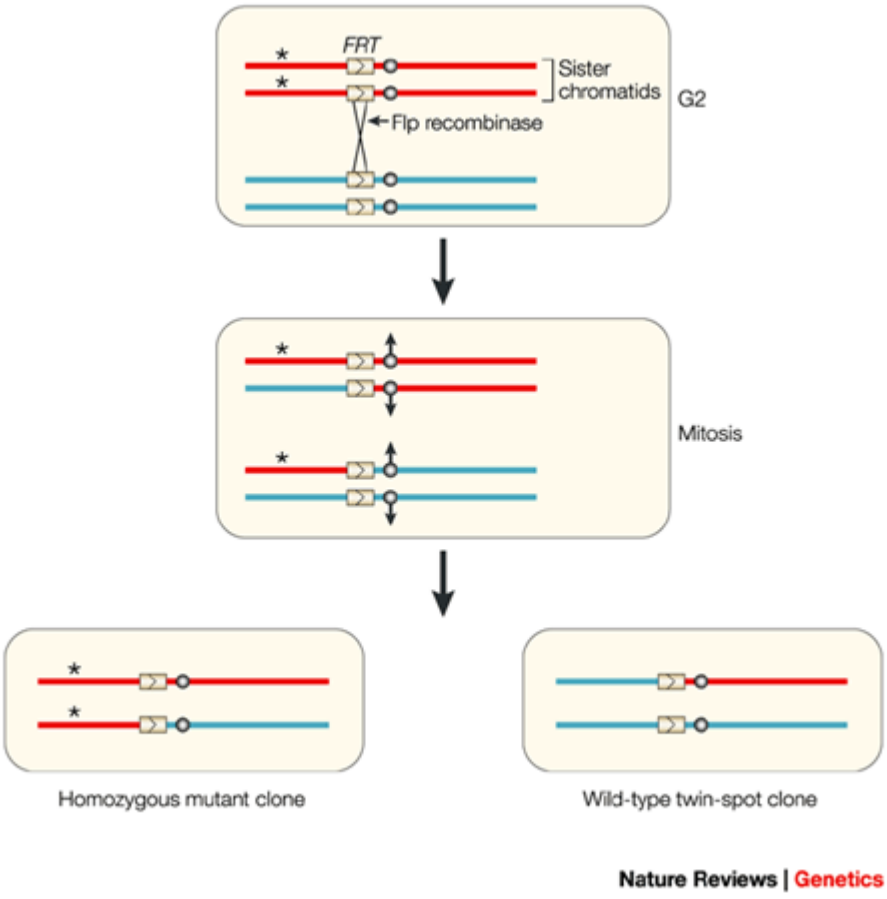

Figure 12. Overview of the FRT/FLP mediated clone induction system in *Drosophila*.

Flp recombinase mediates site-specific recombination between FRT (Flp recombinase target) sites during replication very efficiently when expressed in Drosophila. Flp-mediated recombination can be used to generate mitotic clones by creating flies with transgenic FRT sites at identical positions on homologous chromosomes. If the site-specific recombination between homologues occurs after DNA replication, and the daughter chromatids segregate appropriately, the region of the chromosome arm that lies distal to the FRT site will be made homozygous, with each daughter cell inheriting two copies of this region from one of the parental chromosomes. This site-specific recombination event can be used to make a mutagenized chromosome arm (red) homozygous in clones of cells, which can then be screened for a phenotype. Image adapted from St Johnston , 2002.

use of the site-specific recombinase FLP (flipase) to force mitotic crossing-over at the target FRT sites (Xu et al., 1993; Stowers, 1999) and (Figure 12). Mutant clones can be marked by cell autonomous markers, e.g. GFP. The *flipase* coding sequence is either under the control of a heat shock promoter or the UAS-Gal4 system regulating the temporal and/or spatial generation of mutant clones. The advantage of clonal analysis is the possibility to directly compare adjacent wildtype and mutant cells and to detect minor differences in protein localisation or expression. For the induction of mitotic clones in the A8 segment of the genital disc we first constructed a line containing *Ubi:GFP, frt40a/Cyo; AbdB^{LDL}-Gal4, UAS-flp/TM6b.* We then crossed this line to *chic^{p5202}, FRT40A.*

6 Visualization of terminallia rotation

We determined the terminallia rotation phenotype by dissection of the abdomen of the male adult flies. Parallel observation of the position of the male terminallia from the exterior and looping of the spermiduct around the hindgut in the dissected flies permitted the determination of the degree and direction of the plate rotation. The rotation degree phenotype was broadly measured and expressed as degrees (from-360° up to 360°).

7 Visualization of adult hindgut looping

In order to visualize the looping of the AHG and preserve the structure of the abdomen we followed two strategies.

Blue Erioglaucine staining

Flies were fed on a mixture of agar 3%, sucrose 5% and erioglaucine 2.5% (Sigma#861146) for at least 6 hours. Then the AHG position was examined in a LeicaMZ6 stereoscope.

Wholemount for confocal microscopy

Headless flies were fixed in formaldehyde 4% overnight; following washes in PBS with 0.1% Triton, the dorsal part of the abdominal cuticle was carefully removed using forceps. Abdomens were then stained with FITC- TRITC-phalloidin of overnight. Complete abdomens were mounted in 2% agarose in a concaved slide and image in an SPE Leica upright confocal

8 Standard procedures

For all standard molecular techniques (PCR, ligation, digestion and sequencing) we followed to common protocols of Sambrook and Russell (2001). Bacteria transformation was performed by electroporation. For purification of PCR products we

used the QIAquick PCR purification protocol (Invitrogen). For purification of PCR products from gel we used QIAquick Gel Extraction Kit (Invitrogen). For DNA purification from bacteria we used QIAquick Spin Miniprep or Midiprep Kit (Invitrogen).

DNA preparation from single fly

Smash one fly in 50 µl of squishing buffer (10mM Tris-HCl pH 8.2, 1 mM EDTA, 25 mM NaCl, 200µg/mlfresh proteinase K). Incubate for 30 min at 25-37°C. Inactivate proteinase K by heating to 95°C for 2 min.

Fosmid/BAC modification

The fosmid FlyFos transgenes rescue mutant phenotypes, recapitulate endogenous gene expression patterns and in some cases allow imaging of gene products in living animals. The D.pseudoobscura transgenes rescue RNAi phenotypes when introduced into the D.melanogaster genome, providing a convenient control for the specificity of the knockdown (Langer et al. 2010). For RNAi rescue experiments the ortholog region containing the desire gene from D.pseudoobscura were obtained from the Flybase Blast. Then the specific fosmid was selected from the FlyFos project website (https://transgeneome.mpi-cbg.de/transgeneomics/). The obtained Fosmids were prepared for injection and sent to Best gene. The fosmids are inserted into the pFlyFos backbone containing inducible oriV, the attB sequence for φC31-mediated gene

integration and eye promoter–driven dsRed selectable marker (Langer et al., 2010; Kondo et al., 2009)

Co-immunoprecipitation and Western Blott

Drosophila Schneider line-2 R+ cells (S2R+) were maintained in Schneider's Insect medium (PAA) containing heat inactivated Fetal Bovine Serum (10%, Lonza) and Penicillin-Streptomycin cocktail (100 Unit/ml, Gibco). S2R+ cells were transfected using Lipofectamine (Invitrogen) and protein expression was performed using MyoID-GFP and DsICD-FLAG Drosophila expression vectors under the control of a constitutive actin promoter and actin::Gal4 vector.

Transfected cells were lysed 3 days after transfection in lysis buffer (10 mM Tris-HCl pH 7.5, 150 mM NaCl, 0.5mM EDTA and 0.5% NP-40, protease inhibitors). Cell extracts (200ug of protein) were incubated overnight at 4°C with 20ul of GFP-Trap® beads (Chromotek), beads were then washed and treated according to the Chromotek protocol. Immuno-complexes were denatured for 5 minutes at 75°C and loaded onto NuPAGE Novex gel (12%, Bis-Tris Gel, Invitrogen). Proteins were detected by Western blotting using anti-Flag mouse antibody (1/2000, Sigma), anti-GFPN-term rabbit antibody (1/2000, Sigma). Antibody detection was performed using Odyssey® Infrared imaging system (Li-cor).

9 Antibodies and staining reagents

Antobody name	*origin*	*species*	*Dilution IF*	*Dilution WB*
B-galactosidase	Promega/ Invitrogen	Mouse,chicken	1/100, 1/500	
DE-Cadherin	DSHB	Rat	1/50	
Dlg	DSHB	Mouse	1/100	
Chicadee	DSHB	Mouse	1/10	1/50
Wg	DSHB	Mouse	1/50	
Cora	DSHB	Mouse	1/50	
GFP	Invitrogen/Sigma	Mouse, Rabbit	1/100	1/1000, 1/50 CoIP
HA	Covance	Mouse	1/100	1/500
Flag	?	Mouse		1/50 CoIP
Alexa-546 or Cy3	Invitrogen		1/200	
Cy5	Invitrogen		1/200	
DAPI /Höchst		NA	1/100	
Phalloidin-TRITC	Invitrogen	NA	1/500	

IF=Immunoflourescence, WB=WesternBlott, CoIP=Co-immunoprecipitation assay

10 Hobo mediated deficiency generation

P{wHy} is a compound element comprised of *P*-transposon carrier arms and a central deleter transposon, *hobo*, which is flanked by *white* and *yellow* genes. Flanking deletions are obtained by introducing a source of *hobo* transposase, followed by recombination between the original and second copy of *hobo*; the direction of the deletion is indicated by the particular *P{wHy}* marker lost. The genetic schemes and strains for the basic manipulation of *P{wHy}* transposition are described in (Huet et al., 2002; Myrick et al., 2009).

All initial *D. melanogaster* strains used for deletion generation had genetic backgrounds devoid of hobo elements. Hobo-mediated deletions were generated by using P{wHy}DG30510 insertion on chromosome 2 at 2L:66,953..66,953 [-]. G0 crosses were matings of Df (1)w67c23, y1 w67c23; P{wHy,w+y+} with Df (1)w67c23, y1 w67c23; In (2LR)Gla, wgGla-1/CyO P{hsH\T-2}. P{hsH\T-2} contains the hobo transposase gene placed under a heat-shock promoter. Crosses were brooded three times every other day. The progeny were heat-shocked three times during development for 30 min at 37°C at 2-day intervals to elevate the expression of the hobo transposase. Each G1 cross consisted of two males of the genotype y1 w67c23; P{wHy}/CyO, P{hsH\T-2} and virgin females of the genotype y1 w67c23; In (2LR)Gla, wgGla-1/SM6a. G2 matings consisted of one y1 w67c23; P{5′wHy,w+y−} or P{3′wHy,w−y+}/SM6a male crossed to virgin y1 w67c23; In (2LR)Gla, wgGla-1/SM6a females. From these latter crosses, stocks of the

P{5'wHy} or P{3'wHy} derivatives were established, balanced with SM6a.

11 CRISPR/CAS9 mutagenesis

CRISPRs (clustered regularly interspaced short palindromic repeats) and the CRISPR-associated Cas9 nuclease function as part of an adaptive immune system in bacteria and archaea (Barrangou et al., 2007). In type II CRISPR systems, a CRISPR RNA (crRNA), which contains sequence complementary to invading virus or plasmid DNA, and a trans-activating CRISPR RNA (tracrRNA) interact with Cas9 to direct sequence-specific cleavage of exogenous DNA. A minimal two-component system required for the site-specific cleavage of DNA are the Cas9 endonuclease and a chimeric RNA (chiRNA), comprising the crRNA and tracrRNA (Jinek et al., 2012). The introduccion of two chiRNA induces a deletion flanked by the two chiRNAs (Gratz et al., 2013).

We made two injections, each comprising two chiRNAs the first one aiming for a 3.3kb deletion of the first intron; the second one for a small 1.4kb deletion of the putative AHG enhancer. Both injections were done in flies bearing a M(vas-cas9)ZH transgene (Bloomington #51323). G0 crosses were matings of all the survival males mass crossed against w1118; If/Cyo. The progeny were individually crossed against either w1118; If/Cyo (enhancer mutant) or against w1118; myoID k2, shg p(w+k03401)/Cyo.

Finally, efficient deletions were selected by PCR and the exact breaking points detected by sequencing the amplicon. Eight enhancer mutants were kept but as they all had similar phenotipes only one w; myoID$^{AHG\#A2}$ was further analyzed; Three intron mutants were kept, one w; myoID$^{intron\#E2}$ was mostly used.

Aims

III Aims

This thesis aims to contribute to the understanding of L/R patterning in *Drosophila*. The main focus is to further investigate the mechanisms that convert MyoID function in the *Drosophila* alimentary canal into a stereotypical dextral looped tube. We focused on a particular region of the adult Drosophila gut called the hindgut. Through the use of genetic and molecular approaches we now present our current view on a possible mechanism that translates original asymmetries from MyoID into a whole asymmetric organ.

Two main objectives were set: i) set up, as a collaborative approach together with other members of the L/R asymmetry group, a genome-wide screen in an effort to identify new components of the MyoID L/R machinery involved in the dextral looping of the terminalia and ii) understand how MyoID controls the adult hindgut dextral looping and thus set up this organ as a new model for the study of L/R patterning.

Results

IV Results

The result section is divided in four parts. The first one is presenting the data concerning the interaction between the unconventional myosin, MyoID and the planar cell polarity pathway through the regulation of the atypical cadherin Dachsous and its binding partner Fat. This novel regulatory interaction seems to be controlling the establishment of the dextral coil in the Adult hindgut. The data suggesting this interaction are summarized in the manuscript "The Atypical Cadherin Dachsous and Planar Cell Polarity control Left-Right Asymmetry in Drosophila", which is currently in the revision process for publication.

The second part constitutes an evolutionary approach to understand the origin of AHG looping in *Drosophila*. The original experiment that led to this approach was kindly suggested by Francisco (Paco) Martin during a seminar session in the institute. Briefly, He asked whether the dextral coiled was conserved among flies, that led us to screen for some *Drosophila* species apart from *D.melanogaster,* the description of what we found out is described in Part 2 of the results section.

The third part includes a short story on clarifying the AHG precursor cells located in the larva. It came out as a logical consequence on focusing on the study of the development of the AHG, which has not been studied. The results of this part include the screen for gene expression patterns in the AHG and the lineage tracing experiments that allowed the identification of specific cell precursors. This story is summarized in the

chapter “Regional division and development of the Adult Hindgut in Drosophila”.

The four part is a collection of experiments that were originally thought to be included as part 1 or 2 but they were left aside for different reasons. Alone they do not constitute a complete story; however I thought to include them as a complete section as they provide insights into the general process of AHG looping.

The fifth part is the summary of the results obtained during a genome wide genetic screen for genes interacting with *myoID* and the further identification of Profilin homolog in flies, *chickadee.* This project was done in collaboration with a former Ph.D student Nicolas Porquet, a researcher Charles Géminard and a post-doc Jean-Baptiste Coutelis.

The Atypical Cadherin Dachsous and Planar Cell Polarity control Left-Right Asymmetry in Drosophila

The manuscript "The atypical cadherin Dachsous and planar cell polarity control left-right asymmetry in Drosophila" which is now under revision process, we show a new role for the components of the Global Fat/Dachsous and core planar cell polarity (PCP) pathways in controlling the asymmetric left/right looping of the adult Drosophila hindgut. Using tissue-specific *myoID* knockdown we show that MyoID regulates terminalia rotation and hindgut looping independently, this indicates that MyoID is required in two different L/R organizers for two different tissues. We further show that MyoID is expressed in the H1 region of the larval hindgut, and by the specific MyoID knockdown in different regions, we conclude that the H1 of the imaginal hindgut ring domain represents a critical, transiently present organizer domain that is responsible for asymmetric looping of the entire hindgut structure. Consistently, we found an early L/R asymmetric orientation of the hindgut primordium (H2 cells) which direction is under the control of MyoID activity in the adjacent H1 cells. Also we further demonstrate a biochemical interaction between MyoID and Dachsous using co-immunoprecipitation experiments and show that loss of Dachsous results in a misloop phenotype which we interpret as a loss of asymmetry phenotype.

Finally using biochemical experiments we characterize the interaction between MyoID and Dachsous and found it to require the Dachsous intracellular domain. This interaction is also likely required for proper L/R asymmetric patterning based on misexpression experiments. Finally, we demonstrate that not only Dachous but all the components of both planar cell polarity pathways are required to maintain the asymmetric orientation and thus the final adult hindgut L/R looping.

Overall our results identify a novel role for components of the core and global PCP pathways in a novel cellular system, adult hindgut looping, and identify key cellular structures within this system that are important for the initiation or transmission of L/R asymmetry signals. This is the first time components of the global Fat/Dachsous pathway have been shown to play a role in L/R asymmetry in animals and the first time for the core-PCP components in insects.

Developmental Cell

The Atypical Cadherin Dachsous and Planar Cell Polarity control Left-Right Asymmetry in Drosophila

--Manuscript Draft--

Manuscript Number:	
Full Title:	The Atypical Cadherin Dachsous and Planar Cell Polarity control Left-Right Asymmetry in Drosophila
Article Type:	Research Article
Keywords:	L/R Asymmetry; planar cell polarity; Myosin I; Dachsous; organizer; organ looping; body axis; Drosophila
Corresponding Author:	Stéphane Noselli University of Nice Nice, FRANCE
First Author:	Nicanor Gonzàlez-Morales
Order of Authors:	Nicanor Gonzàlez-Morales
	Charles Géminard
	Jean-Baptiste Coutelis
	Delphine Cerezo
	Stéphane Noselli
Abstract:	Left-Right (L/R) asymmetry is essential for organ development and function in metazoans. Yet, how initial L/R cue is relayed to tissues still remains unclear. Here, we uncover a mechanism by which the Drosophila L/R determinant Myosin ID (MyoID) transfers L/R information to neighboring cells through the planar cell polarity (PCP) atypical cadherin Dachsous (Ds). Molecular interaction between MyoID and Ds in a specific L/R organizer controls dextral cell polarity of adjoining hindgut progenitors and is required for organ looping in adults. Loss of Ds blocks hindgut tissue polarization and looping, indicating that Ds is a crucial factor for both L/R cue transmission and asymmetric morphogenesis downstream of MyoID. We further show that the Ds/Ft and Frizzled PCP pathways are required for the spreading of L/R asymmetry throughout the hindgut progenitor tissue. These results identify a direct functional coupling between the L/R determinant MyoID and PCP, essential for non-autonomous propagation of early L/R asymmetry.
Suggested Reviewers:	
Opposed Reviewers:	

The Atypical Cadherin Dachsous and Planar Cell Polarity control Left-Right Asymmetry in *Drosophila*

González-Morales N.[1,2,3], Géminard C.[1,2,3], Coutelis J.B.[1,2,3] , Cerezo D.[1,2,3] and Noselli S.[1,2,3,4]

[1] University of Nice Sophia Antipolis, institut de Biologie Valrose, iBV, 06108 Nice, France
[2] CNRS, institut de Biologie Valrose, iBV, UMR 7277, 06100 Nice, France
[3] INSERM, institut de Biologie Valrose, iBV, U1091, 06100 Nice, France

[4] Corresponding author. Email: noselli@unice.fr

ABSTRACT

Left-Right (L/R) asymmetry is essential for organ development and function in metazoans. Yet, how initial L/R cue is relayed to tissues still remains unclear. Here, we uncover a mechanism by which the *Drosophila* L/R determinant Myosin ID (MyoID) transfers L/R information to neighboring cells through the planar cell polarity (PCP) atypical cadherin Dachsous (Ds). Molecular interaction between MyoID and Ds in a specific L/R organizer controls dextral cell polarity of adjoining hindgut progenitors and is required for organ looping in adults. Loss of Ds blocks hindgut tissue polarization and looping, indicating that Ds is a crucial factor for both L/R cue transmission and asymmetric morphogenesis downstream of MyoID. We further show that the Ds/Ft and Frizzled PCP pathways are required for the spreading of L/R asymmetry throughout the hindgut progenitor tissue. These results identify a direct functional coupling between the L/R determinant MyoID and PCP, essential for non-autonomous propagation of early L/R asymmetry.

INTRODUCTION

Left/Right asymmetry is a prominent feature of bilateria (for recent review, see Blum et al., 2014; Coutelis et al., 2014; Nakamura and Hamada, 2012; Namigai et al., 2014; Vandenberg and Levin, 2013; Yoshiba and Hamada, 2014). Differentiating two body sides is essential for positioning organs, controlling their looping and ultimately their function. Abnormalities in L/R patterning can lead to a range of defects including loss of asymmetry (isomerism), loss of concordance between organs (heterotaxia, *situs ambiguous*) and inversion of the L/R axis (*situs inversus*); several congenital health threatening or lethal conditions are indeed linked to defects in L/R asymmetry (Peeters and Devriendt, 2006). Understanding how symmetry is initially broken and how *de novo* asymmetry is transferred to tissues during development represent major questions. Studies using a range of deuterostome/vertebrate model organisms have revealed some original patterning mechanisms, including the generation of ion flux in pre-gastrula embryos, the generation of a leftward flow at the embryonic node through rotating cilia, and asymmetrical cell movement (Adams et al., 2006; Blum et al., 2014; Coutelis et al., 2014; Cui et al., 2009; Gros et al., 2009; Lenhart et al., 2013; Levin et al., 2002; Namigai et al., 2014; Vandenberg and Levin, 2013; Yoshiba and Hamada, 2014). These early events contribute to symmetry breaking, ultimately leading to asymmetric activation of the conserved nodal/TGF-beta pathway which then controls organ asymmetrical morphogenesis (Raya and Izpisua Belmonte, 2006).

Studies of highly stereotypical L/R asymmetric organs in *Drosophila* suggest that distinct symmetry breaking mechanisms have emerged during evolution since *Drosophila* mostly lack primary cilia (except in some sensory neurons) and a Nodal signaling cascade (Coutelis et al., 2008; Géminard et al., 2014). In contrast to vertebrates, *Drosophila* L/R markers are relatively simple and homogeneous as they are restrained to tubular organs which undergo directional morphogenesis towards dextral; these include male terminalia rotation, looping of the larval and adult gut, and testis (Hozumi et al., 2006; Géminard et al., 2014; Speder et al., 2006 Coutelis et al., 2008;). Genes controlling L/R asymmetry in flies have only recently been identified. The conserved type ID myosin gene (Myosin ID, MyoID; aka Myo31DF) (Mooseker and Cheney, 1995; Morgan et al., 1995) is unique as *myoID* loss of function

leads to complete *situs inversus* with all asymmetric organs developing as sinistral (Hozumi et al., 2006; Géminard et al., 2014; Speder et al., 2006 Coutelis et al., 2008;). The expression of MyoID, and hence L/R symmetry breaking, is under the direct control of the HOX transcription factor Abdominal-B (Coutelis et al., 2013). Further, binding of MyoID to the adherens junction proteins beta-catenin and E-cadherin is important for its function in both the terminalia and embryonic hindgut (Petzoldt et al., 2012; Taniguchi et al., 2011). Interestingly, tissue-targeted invalidation of *myoID* in the genital disc has revealed the existence of a restricted domain controlling dextral terminalia rotation, termed the terminalia L/R organizer (Speder et al., 2006). Knockdown of *myoID* in this specific terminalia L/R organizer inverts the rotation of the terminalia; other organs, however, develop normally suggesting the existence of additional tissue-specific L/R organizers which remain to be characterized.

The *Drosophila* adult hindgut represents an attractive yet uncharacterized model to study MyoID-dependent control of *de novo* L/R asymmetry. Indeed, adult hindgut L/R asymmetry is established independently of larval hindgut asymmetry as it derives from dedicated precursor cells clustered in the larval imaginal ring. The imaginal ring comprises two subdomains (H1 and H2), which are thought to give rise to the adult sphincter-like pylorus, the absorptive ileum and the stem-cell region (Fox and Spradling, 2009, Takashima et al., 2008; Takashima et al., 2013). During pupal development, imaginal ring derivatives proliferate and differentiate, while larvae counterparts degenerate (Fox and Spradling, 2009; Robertson, 1936) (Fig. 2E). The transition from larval to adult hindgut thus provides an interesting model to characterize the mechanisms responsible for asymmetry cue transmission downstream of MyoID, which, we show here, is dependent on planar cell polarity (PCP) signaling (Gray et al., 2011; Wallingford, 2012; for recent reviews, see also Yang, 2012).

In *Drosophila*, PCP is involved in the polarity of hair-like structures in many organs including the wing, eye, abdomen and notum (Adler, 2012; Lawrence et al., 2007; Lawrence and Casal, 2013; Matis and Axelrod, 2013; Singh and Mlodzik, 2012). The well-studied *Drosophila* PCP genes are known to belong to two major pathways: the ‘core system’ and the ‘global system’ (Axelrod, 2009; Goodrich and Strutt, 2011 Lawrence and Casal, 2013; Matis and Axelrod, 2013). The core system comprises the distally located (relative to the

anterior-posterior (A/P) axis) proteins Frizzled (Fz), Dishevelled (Dsh) and Diego (Dgo), the proximally located proteins Van Gogh (Vang, aka Strabismus) and Prickle (Pk) and symmetrically localized Flamingo (Vinson and Adler, 1987; Krasnow et al., 1995; (Bastock et al., 2003; Das et al., 2002; Tree et al., 2002; Wolff and Rubin, 1998;). The global system includes the atypical cadherins Fat (Ft) and Dachsous (Ds) and the Golgi kinase Four-Jointed (fj) (Sharma and McNeill, 2013; Simon et al., 2010; Thomas and Strutt, 2012; Yang et al., 2002). Both systems rely on extracellular protein interactions and feedback signaling to ensure proper polarization of tissues (Axelrod, 2009; Goodrich and Strutt, 2011; Peng and Axelrod, 2012). Current studies suggest that the two pathways can interact in different ways depending on the cell context with Ds gradient direction and core module polarization oriented either parallel or anti-parallel (Zeidler et al., 2000; Casal et al., 2002; Ma et al., 2003; Matakatsu and Blair, 2004; Rogulja et al., 2008). Interestingly, it has been proposed that the global system provides a directionality cue which is then used by the core system to align the polarity of each cell with that of their neighbors (Ayukawa et al., 2014; Hogan et al., 2011; Ma et al., 2003; Olofsson et al., 2014).

The first hint of a role of PCP in L/R asymmetry initially came from the identification of the mouse *inversin* gene (a distant homolog of the *diego* PCP gene), mutations of which lead to a high percentage of *situs inversus* (Morgan et al., 1998). More recently, the mouse PCP core pathway has been shown to control cilia positioning in the embryonic node, important for nodal flow and correct L/R asymmetry (Antic et al., 2010; Song et al., 2010). However, no study so far has linked global PCP and L/R asymmetry.

In this study, we characterize a new role of both core and global PCP pathways in *de novo Drosophila* adult hindgut L/R asymmetry downstream of MyoID. We identified the hindgut imaginal ring subdomain H1 as the L/R organizer controlling the directional looping of the adult hindgut. In H1 cells, MyoID physically interacts with the intracellular domain of Ds to polarize H2 hindgut precursor cells towards dextral. Polarization is inverted (sinistral) in *myoID* loss-of-function while it is absent when Ds is specifically invalidated in the H1 domain. In addition, MyoID and Ds interact genetically to polarize the H2 cells. Therefore, Ds is essential to convey MyoID-dependent L/R information to neighboring H2 hindgut precursors. We further show that spreading of L/R polarity within H2 precursor cells depends on both global and core PCP

pathways. These results thus reveal a novel mechanism allowing cell non-autonomous transmission of symmetry breaking information from a L/R organizer to organ precursors essential for proper L/R morphogenesis.

RESULTS

Myosin ID controls directional looping of the adult hindgut through a specific L/R organizer

In wild type flies, the adult hindgut coils clockwise forming a single stereotyped loop localized on the right hand side of the abdomen when viewed from dorsal (Fig. 1A, D). Looping can be visualized by transmission microscopy using a non-invasive 'blue feeding' method which stains the gut lumen while keeping organs in their native configuration. The phenotype can be further analyzed by dissecting the whole fly abdomen followed by confocal microscopy. Using these methods, we show that in *myoID* null mutants, the adult hindgut displays an inverted sinistral phenotype in 80% of individuals (Fig. 1B ,E, G); the remaining 20% of the population show a twisted phenotype, whereby the adult hindgut does not form a loop but a roughly symmetrical 'S' shape (Fig. 1C, F, G) (Hozumi et al., 2006). This phenotype can be reproduced when expressing *myoID-RNAi* driven by either *MyoID-Gal4*, which mimics the *myoID* expression pattern (Coutelis et al., 2013; Petzoldt et al., 2012 ; Speder et al., 2006), or *byn-Gal4* (hereafter referred to as *hindgut-GAL4*), which is expressed in hindgut precursor cells (Fig. 1G). Altogether, these observations show that, like in other L/R organs, MyoID controls the directionality of adult hindgut looping towards dextral.

At the posterior end of the adult hindgut is the rectum which is part of the rotated terminalia but derives from both the genital disc and rectal larval cells (Fox et al., 2010). As *myoID* expression in the genital disc A8 segment controls dextral rotation of the terminalia we asked whether MyoID activity in the genital disc and/or rotation of the terminalia itself might be involved in adult hindgut looping. In order to test these possibilities, we knocked-down *myoID* by RNAi specifically in the A8 segment (using Abd-B^{LDL}-Gal4, hereafter referred to as A8-GAL4) or in the hindgut (using *hindgut*-Gal4) and looked at terminalia rotation and adult hindgut looping in both cases. *myoID* invalidation in the hindgut did not affect terminalia rotation but was sufficient to induce a sinistral and mislooped adult hindgut (Fig. 1G); reciprocally, when *myoID* was specifically silenced in the A8 segment the terminalia was misrotated but the hindgut properly looped (Fig. 1G). These results show that i) terminalia rotation and adult hindgut looping are two independent events and ii) hindgut looping is

controlled by a hindgut specific MyoID-dependent organizer. Thus, we reveal that MyoID controls hindgut looping and terminalia rotation through two distinct tissue-specific organizers.

We next asked when MyoID activity is required for adult hindgut looping. Therefore, we knocked down *myoID* at different time periods during development using the Tub-Gal80ts/Gal4 system (TARGET method; McGuire et al., 2003). Using this approach, we show that *myoID* activity is required during days 3-5 of larval development for proper adult hindgut looping. Note that this functional timeframe overlaps with the requirement of *myoID* activity during terminalia rotation (Fig. 1H)(Petzoldt et al., 2012; Speder et al., 2006), indicating that, although terminalia and hindgut MyoID-dependent organizers are spatially distinct, they are temporally synchronous.

The hindgut L/R organizer lies in the H1 domain of the larval imaginal ring

As mentioned earlier, the adult hindgut derives from the larval imaginal ring which comprises two domains, a small anterior domain called H1, and a larger posterior domain called H2 (see Fig. 2E) (Murakami and Shiotsuki, 2001). To precisely map *MyoID* expressing cells in the imaginal ring, we analyzed the expression of several MyoID reporter lines (*MyoID-Gal4*, *MyoID-lacZ* and *MyoID::GFP*) relative to that of known markers in the larval hindgut (Fig. 2A-D) (Fox and Spradling, 2009; Takashima et al., 2013). We found that MyoID expressing cells co-localize perfectly with Wg expression which marks all H1 cells (Fig. 2B). To check whether MyoID expression is exclusive of H1 cells, we used the posterior H1 and anterior H2 marker *ptc>GFP* (*ptc-Gal4, UAS-MCD8GFP)* which overlaps the H1-H2 boundary. Importantly, MyoID colocalized with *ptc>GFP in posterior H1 cells* but not in H2 cells (Fig. 2C). These results were confirmed by checking the absence of MyoID expression from the H2 domain using an exclusive H2 marker (*GBE-Su(H)-Gal4, UAS-MCD8GFP)* (Fig. 2C, D). From these data we conclude that MyoID is precisely expressed in the H1 domain.

To test if H1 cells may represent the adult hindgut L/R organizer, *myoID* function was knocked down by RNAi using Gal4 drivers expressed in different portions of the ring domain. The sinistral phenotype observed using *MyoID-*

Gal4 (H1 driver) was also obtained using *hindgut-Gal4*, which is expressed in both the H1 and H2 domain and *ptc-Gal4* which is expressed in a subset of posterior H1 cells as well as in anterior H2 cells (Fig. 2C, E). However, no phenotype was observed using the H2-specific driver (*GBE-Su(H)-Gal4*) indicating that H2 cells do not play a role in L/R determination. Altogether, these data show that MyoID activity in the H1 domain is necessary and sufficient for proper L/R asymmetry of the adult hindgut. Furthermore, these data show that the newly identified *Drosophila* MyoID-dependent L/R organizer is localized in the H1 domain of the imaginal ring.

The hindgut L/R organizer is a transient structure

Although lineage tracing experiments have identified the adult pylorus and ileum precursors, the exact contribution of the H1 domain to different parts of the tissue has not been revealed (Takashima et al., 2013). Therefore, we analyzed the contribution of H1/MyoID cells to the adult hindgut through a lineage tracing method using the *MyoID-Gal4* line (see Materials & Methods). We confirmed that the progeny of H1+H2 cells (*hindgut-Gal4* lineage) or H2 cells alone (*GBE-Su(H)-Gal4* lineage) covers the entire adult hindgut, including the recently identified posterior terminal midgut (Fig. 3A, B) (Takashima et al., 2013). However, the progeny of H1 cells (*myoID-Gal4* lineage) does not cover any cell population of the adult hindgut or midgut (Fig. 3C), suggesting that in fact, the adult hindgut derives solely from H2 cells.

To further determine the fate of H1 cells, we followed their behavior during pupal development. Consistent with our lineage tracing experiments, *MyoID-Gal4* is not expressed in the developing hindgut during late pupa stages, indicating that H1 cells have indeed a distinct fate from that of H2 cells (Fig. 3I). In fact, at 10hrs after pupal formation (APF), H1 cells (expressing both MyoID and hindgut-Gal4) are physically separated from the rest of the imaginal ring (Fig. 3D). Then, at 24hrs APF, H1 cells are found in the pupal midgut, a transient structure responsible for larval midgut degradation prior to its elimination in the meconium by young adults (Takashima et al., 2011). Consistently, H1 cells are also found in the meconium (Fig. 3J-M), indicating that the H1 cells are degraded in the pupal midgut along with other transient larval tissues. Note that H1 domain detachment is normal in *myoID* null mutants indicating that

myoID does not have a role in this process (Fig. 3E, H). Altogether, this analysis demonstrates that the H1 domain is a transient structure. Thus, we hypothesized that intervention of the H1 domain in hindgut asymmetry breaking occurs prior to H1 detachment.

To test this model, H1 cells were ablated at different time points by driving expression of the pro-apoptotic gene *reaper* in a temperature-dependent manner (using *myoID-Gal4;tub:Gal80^{ts}*). Strikingly, ablating the H1 domain between 0 and 10hrs APF resulted in a mislooped phenotype, whereas ablation of H1 after 10hrs APF (*i.e.* after normal H1 detachment) had no effect on adult hindgut looping. Importantly, the overall adult hindgut integrity and in particular the midgut-hindgut junction was not compromised by H1 ablation as shown by histochemical analysis and retention of blue food dye in adult guts (Supplementary Fig. 1). These results are consistent with the fact that H1 cells do not structurally constitute the adult hindgut and further demonstrate that the H1 domain is essential prior to detachment to control hindgut asymmetry.

Furthermore, our results redefine the adult hindgut fate map. Indeed, previous work has shown that the boundary between the hindgut and the midgut is not stable, with some anterior hindgut cells crossing the border to invade the midgut to form the posterior terminal midgut. However, we show that the most anterior MyoID/Wg/H1 cells are eliminated and thus do not contribute to the posterior terminal midgut. Thus, we propose that H2 cells are the adult hindgut proper primordial cells (with the most anterior H2 cells invading and constituting part of the midgut), whereas H1 cells are in fact transient, non-structural, regulatory cells that provide the L/R directional cue guiding adult hindgut looping (Fig. 3M).

H1 cells transmit directionality to the hindgut precursor cells

Since the H1 domain detaches from the adult hindgut primordium well before hindgut looping and morphogenesis (approximately 50hrs before), it raises the question of how H1-MyoID-generated L/R information is translated to H2 cells. Therefore we analyzed cell behavior in the H2 domain during early pupal development. Cell shape changes and orientation were characterized by measuring the orientation of cellular membranes relative to the A/P axis

(Viktorinova and Dahmann, 2013) (Fig. 4A, B). Before pupal formation (L3 larval stage), H2 cells are cuboidal in shape with no visible L/R asymmetry (Fig. 4C, F, I). Strikingly though, the first visible cell shape changes occur at 10hrs APF when H2 cells become oriented with a +50° bias relative to the A/P axis; we call this orientation dextral by convention (Fig. 4D, G, J). Importantly, H2 cells in *myoID* mutants are inverted compared to wild type, showing an orientation of -50° (sinistral) (Fig. 4E, H, K). These data indicate that MyoID activity in H1 cells orchestrates the early H2 cell shape changes underlying directional looping of the adult hindgut. Thus, *myoID* has an instructive and cell non-autonomous function in H1 to direct L/R asymmetry of the H2 hindgut precursor cells.

Planar cell polarity mediates L/R polarity of H2 cells

However, the question remains as to how L/R asymmetry is transmitted and maintained in H2 cells from H1 detachment to looping morphogenesis. It is noteworthy that cell shape changes in H2 cells occur in the plane of the epithelium. Therefore, we asked whether the PCP pathways which set and maintain planar cell polarity in other epithelia (Goodrich and Strutt, 2011; Peng and Axelrod, 2012), are also required for hindgut L/R polarity. To do so, we drove RNAi targeting components of the 'core' and 'global' PCP pathways in either H1 (*myoID-Gal4*) or H1+H2 cells (*hindgut-Gal4*). Knocking down any of the core system components in H1+H2 cells resulted in a penetrant mislooped adult hindgut phenotype (Fig. 5 B, C, D, E). In contrast, RNAi depletion solely in H1 cells did not lead to any looping defect (Fig. 5F), suggesting that the core PCP genes are required in H2 cells alone for maintaining proper polarity and looping of the adult hindgut.

Similar to the core system, RNAi depletion of the global *ft, ds or fj* genes in H1+H2 or H2 cells resulted in a highly penetrant mislooped phenotype (Fig. 5G, H, I, K and Supplementary Fig. 2). Surprisingly though, and unlike any other member of the PCP pathways, knockdown of *ds* specifically in H1 cells resulted in a highly penetrant mislooped phenotype, indicating that Ds is essential in the H1 domain for adult hindgut asymmetry (Fig. 5J, L and Supplementary Fig. 2). Thus, the *ds* H1-specific loss-of-function phenotype reveals that Ds plays a non-autonomous role in H1 cells to direct H2 directionality. Altogether, these results indicate that adult hindgut looping relies on proper PCP signaling in both H1

and H2 compartments. Although both Fz and Ft/Ds systems participate in maintaining L/R orientation in H2 cells, the atypical cadherin Ds achieves a specific function in the H1 domain.

Dachsous interacts with MyoID to control early L/R polarity of H2 cells

To further assess the role of Ds in H1 cells, we specifically removed *ds* function from H1 cells using *myoID-Gal4* and analyzed H2 cell orientation. Interestingly, the quantification of membrane orientation showed a complete loss of H2 cell orientation bias (Fig. 6A, B). Thus *ds* is essential in H1 cells for H2 cell L/R polarity (Fig. 5). Importantly, the absence of bias inversion in *ds* mutants as observed in *myoID* mutant conditions indicates that *ds* is essential in H1 to transmit both dextral and sinistral orientations. Therefore, in the absence of *ds*, directional guidance cannot be conveyed to H2 cells, thus the tissue remains naïve.

The unique involvement of Ds in the H1 domain suggests a possible interaction with MyoID to direct L/R asymmetry. To test this hypothesis, we evaluated potential genetic interactions between the two genes. Heterozygous mutant flies for *ds* or *myoID* show none or very low penetrance (~2%) mislooped phenotypes, respectively (Fig. 6C and D). However, in double heterozygous flies mutant for one *myoID* and one *ds* allele, the frequency of mislooped defects is significantly raised (Fig. 6E and F), indicating that *myoID* and *ds* interact for proper adult hindgut looping and suggesting they act in the same genetic pathway controlling L/R asymmetry.

Ds intracellular domain is responsible for MyoID-dependent L/R polarization

Previously, MyoID has been shown to bind beta-catenin and DE-cadherin for proper looping of the terminalia (Petzoldt et al., 2012; Taniguchi et al., 2011). Since Ds is an atypical Cadherin whose expression is needed in the same domain as *myoID* in the imaginal ring (see Fig. 5), we tested if MyoID and Ds also interact molecularly. For this purpose, we expressed both MyoID::GFP and Ds::HA tagged proteins in the H1 domain. In this experiment, genomic constructs were used to drive tagged proteins at physiological levels (Fig. 6H).

Co-immunoprecipitation with anti-HA antibodies from larval hindgut extracts led to the specific pull-down of MyoID::GFP (Fig. 6G). These data show that MyoID and Ds bind in a same complex and interact together in H1 cells for proper L/R morphogenesis of the hindgut.

MyoID is known to act inside cells, thus we checked whether MyoID specifically interacts with the Ds intracellular domain (ICD). Tagged forms of MyoID (MyoID-GFP) and the Ds intracellular domain (Ds amino-acids 3120-3556; Ds-ICD-Flag) were co-expressed in *Drosophila* S2R+ cells. Interestingly, we noticed that both proteins co-localize and accumulate at membrane sites in contact with neighboring cells (Fig. 7A). This co-localization was further supported biochemically in a co-immunoprecipitation assay showing that MyoID-GFP is able to co-immunoprecipitate the full-length intracellular domain of Ds (Fig. 7A).

In other planar polarized epithelia, *ds* overexpression induces long-range polarity rearrangements due to Ds protein mislocalization (Ambegaonkar et al., 2012; Brittle et al., 2012; Bosveld et al., 2012; Matakatsu and Blair, 2006). Interestingly, overexpression of *ds* in H1 cells induces a gain-of-function adult mislooped phenotype in about 40% of flies (Fig. 7D), suggesting that stoichiometry between MyoID and Ds should be maintained in H1 cells. Thus, overexpression of MyoID would be expected to at least partially rescue Ds-overexpression phenotype. In fact, the *ds* overexpression phenotype was fully rescued by co-overexpression of *myoID* in H1 cells (Fig. 7G, J), corroborating the importance of the Ds-MyoID interaction in H1 for proper looping.

We used this rescue assay to further probe which of the Ds domains is required for interaction with MyoID *in vivo* by overexpressing truncated forms of Ds, lacking either the intracellular (*dsΔICD*) or extracellular (*dsΔECD*) domain (Matakatsu and Blair, 2006). Expression of these truncated forms also led to a gain-of-function mislooped phenotype (Fig. 7E, F). However, the phenotype induced by overexpression of *dsΔICD* was not at all rescued upon co-expression of MyoID (Fig. 7H, K), confirming that the Ds intracellular domain is indeed important for the interaction with MyoID. The mislooped phenotype observed by overexpression of dsΔECD is likely due to the displacement of endogenous full-length Ds/MyoID complexes. Indeed, DsΔECD cannot bind to Ft and therefore cannot propagate planar polarity to other cells. Consistently, this

phenotype was rescued by MyoID co-overexpression which likely re-equilibrates the dose of active versus inactive complexes (Fig. 7I, L).

Altogether, these results suggest that Ds/MyoID stoichiometry is important *in vivo* and that MyoID in H1 cells propagates L/R asymmetry to H2 target cells through interaction with the intracellular domain of Ds in H1 cells.

DISCUSSION

In this work, we reveal the existence of a new, hindgut-specific L/R organizer having transient activity. We show that L/R information is transferred non-autonomously from this organizing center to the target tissue, through a unique MyoID-Ds interaction taking place at a PCP signaling boundary (the H1/H2 boundary). The initial MyoID-Ds-dependent L/R information is then relayed to the developing hindgut through Ds/Ft global PCP signaling and subsequently amplified through core PCP signaling. Importantly, these results reveal that MyoID can act as a directional cue to bias planar cell polarity.

So far, only a role for the core PCP pathway in cilia positioning and L/R asymmetry had been reported in mouse, chick and Xenopus (Antic et al., 2010; Song et al., 2010; Zhang & Levin, 2009). Here, we reveal a previously unknown role of the global PCP pathway in L/R asymmetry. We show that the atypical cadherin Ds is essential for early L/R planar polarization of hindgut precursors and later on for looping morphogenesis. Ds appears singular among other PCP genes, as it is unique in playing a specific role in the L/R organizing center (H1 domain) through interaction with the dextral factor MyoID. Further, Ds has a cell non-autonomous function, allowing transfer of L/R information from the H1 domain to H2 hindgut precursor cells. Ds therefore represents a critical relay factor acting at the boundary between – and linking – a L/R organizer and its target tissue.

In addition to a MyoID-dependent function in H1, the mislooped phenotype induced upon Ds silencing in the H2 domain (Fig. 5; Suppl. Fig. 2) suggests that Ds also has a MyoID-independent activity in H2 cells, likely through interaction with other PCP genes. Indeed, reducing the activity of PCP global or core gene functions reveals that the two pathways are important in the H2 region for adult hindgut looping. However, the results reveal important differences in the way these pathways control hindgut asymmetry. First, although the terminal adult phenotype is similar upon silencing of one or the other pathway, the early polarization of H2 cells in pupae (10hrs APF) is only affected when knocking down the activity of the global pathway (Fig. 5 and data not shown). These results show that the global pathway, but not the core pathway, is required for establishing early L/R polarity. Second, the phenotype is quantitatively different, since silencing of global PCP led to a consistent and

very strong phenotype while reducing core PCP signaling had a significantly less penetrant one. These data suggest a partly overlapping function of core and global signaling for late hindgut morphogenesis. Together, these genetic data show that the Ds/Ft pathway plays an early and predominant role for setting initial MyoID-dependent L/R polarity, whereas the core pathway likely intervenes at late morphogenesis to relay/amplify the global PCP polarizing information for proper L/R asymmetry of the adult hindgut (Fig. 5). Therefore, we propose the following sequential model (Fig. 7M): in H1 cells, MyoID interacts with Ds intracellular domain which becomes 'biased' towards dextral, through a currently unknown mechanism (discussed below). This initial L/R bias is then transmitted across the H1/H2 boundary through Ds/Ft heterophilic interaction. Then, boundary H2 cells relay the initial bias and spread it to the remaining H2 cells through classic Ds/Ft PCP. Interestingly, the local signaling boundary suggested by our model is consistent with recent studies showing that Ds can propagate polarity information in a range of up to 8 cells (Ambegaonkar 2012; Bosveld 2012; Brittle 2012; Sharma and McNeill, 2013), a distance that is consistent with the size of the H2 domain at 10 hrs APF (Fig. 4). Once initial polarity has been set up through the Ds/Ft pathway, this is in turn relayed to and amplified by the core pathway, acting as a secondary PCP program. Interestingly, a similar two-step mechanism has also been proposed for the wing (Hogan et al., 2011) and could apply to other tissues (Ayukawa et al., 2014; Olofsson et al., 2014).

The discovery of a coupling between the MyoID dextral factor and Ds is a nice example of crosstalk between signaling modules. In the simplest crosstalk model, the role of MyoID would just be to bias or tilt Ds function towards one side, possibly through Ds localization and/or activity polarization along the L/R axis. Using both *in vitro* and *in vivo* assays, we show that interaction between Ds and MyoID requires Ds intracellular domain, supporting a cytoplasmic interaction between the two proteins. These results along with recent findings suggest that Ds may represent a general platform for myosin function in different tissues. In particular, the intracellular domain of Ds was found to bind to the unconventional myosin Dachs, controlling Dachs polarized localization which is important for subsequent cell rearrangements underlying thorax morphogenesis (Bosveld 2012). However in contrast to thoracic Dachs, MyoID is expressed uniformly in H1 cells (Fig. 2, 6), suggesting that the interaction

between myosins and Ds may involve different mechanisms. Additionally, we could not detect any L/R polarized localization of MyoID or Ds in H1 cells, although we cannot exclude the existence of subtle asymmetries undetectable by available tools. Nevertheless, alternative means to generate the L/R bias in H1 include: i) L/R polarized expression of an unknown asymmetric factor, or ii) L/R asymmetric activity of Ds. These interesting possibilities are consistent with recent work showing that some type I myosins can generate directed spiral movement of actin filaments *in vitro* (Pyrpassopoulos et al., 2012). It is tempting to speculate that similarly, MyoID putative chiral activity could be translated into Ds asymmetrical function along the L/R axis. Future work will explore this possibility as well as others to unravel the molecular basis of MyoID L/R biasing activity in the H1 organizer.

The identification of the H1 domain as a specific adult tissue L/R organizer demonstrates the existence of multiple, independent tissue and stage-specific L/R organizers in flies. This situation echoes with what is known in other models including vertebrates, in which at least two phases of asymmetry establishment can be distinguished. A first pre-gastrula phase, as early as the 4-cell stage in Xenopus, involves the generation of asymmetric gradients of ions. Then a second phase takes place at gastrulation and involves Nodal flow and asymmetric cell migration, eventually leading to asymmetric expression of the *nodal* gene in the left lateral plate mesoderm (Adams et al., 2006; Levin et al., 2002; Raya and Izpisua Belmonte, 2006). In *Drosophila*, some interesting common and specific features can be drawn out by comparing the hindgut and terminalia organizers (Géminard et al., 2014; Speder et al., 2006). A first, major common feature is the fact that both organizers rely on MyoID function, showing the conserved role of this factor in *Drosophila* L/R asymmetry. Second, the two organizers show temporal disconnection, acting much earlier than L/R morphogenesis, which is expected of a structure providing directionality to tissues *per se* (24hrs for terminalia and approx. 72 hrs for hindgut looping). Such temporal disconnection of MyoID function with late morphogenesis is also observed in the terminalia where a peak of MyoID activity precedes terminalia rotation by 24hrs (Speder et al., 2006; Suzanne et al., 2010). Time lag in MyoID function requires L/R cue transmission and maintenance in developing tissues until directional morphogenesis. The finding of a role of Ds and PCP in hindgut L/R asymmetry provides a simple mechanism by which initial L/R information is

maintained and transmitted across a tissue through long-range PCP self-propagation.

Importantly, the two organizers also show distinct features. In terminalia, MyoID has a cell autonomous function in two adjacent domains (Suzanne et al., 2010). In addition, the terminalia organizer is permanent, developing as an integral component of the adult tissue. In contrast, MyoID in the imaginal ring has a cell non-autonomous function. And indeed a striking feature of the hindgut organizer is its transience as it detaches from the hindgut precursors 50hrs before full looping morphogenesis prior to its degradation and elimination, hence the need to transfer L/R information to the H2 hindgut primordium. An interesting question then is whether the MyoID-Ds/PCP interaction is conserved in terminalia? We have shown that terminalia rotation requires the activity of DE-cadherin, however invalidation of the atypical cadherins Ds or Ft or core PCP signaling in the terminalia organizer did not affect asymmetry (Petzoldt et al., 2012). The fact that PCP does not have a general role in *Drosophila* L/R asymmetry is not altogether surprising as MyoID cell autonomous function in terminalia and organizer persistence do not require that L/R information be transferred to and stored in other parts of the tissue, as is the case in the hindgut. Therefore, despite conservation of MyoID-dependent upstream dextral cue, significant differences in downstream morphogenetic pathways imply alternative cellular mechanisms controlling cue transmission and maintenance.

The L/R signaling module, comprising the dextral determinant MyoID and the still unknown sinistral determinant, can thus be coupled to distinct morphogenetic modules including PCP as shown in this study. We suggest that coupling between L/R asymmetry and PCP might be observed in processes requiring long distance patterning of tissues and organ precursors, both in invertebrate and vertebrate models. Understanding organ L/R morphogenesis clearly requires studying diverse and complementary models. In this context, the multiplicity of L/R organizers discovered in *Drosophila* represents a powerful model to study the diversity in coupling of L/R organizers with downstream programs responsible for late tissue morphogenesis. In particular, the *Drosophila* hindgut represents an invaluable model to study the genetic basis and molecular mechanisms coupling L/R asymmetry with PCP patterning.

Experimental Procedures

Fly stocks

Fly stocks were maintained on standard agar *Drosophila* medium. Crosses were done at 25°C and for the case of Gal4/UAS then transferred to 29°C. For detailed description of stocks and genetic analysis see Supplementary Experimental Procedures.

Histochemistry and Image analysis

Detailed description can be found in the Supplementary Experimental Procedures.

Acknowledgements

We thank J. Axelrod, Y. Bellaiche, S. Blair, S. Hou, K. Irvine, E. Sanchez-Herrero, and G. Struhl for sharing reagents and fly lines; JY. Tinevez for help with the directionality plug-in; the TRiP facility at Harvard Medical School [NIH/NIGMSR01-GM084947], BSDC and VDRC stock centers and DSHB for reagents; the iBV PRISM imaging facility for advice and support; and members of the laboratory for discussion and comments. NGM is supported by a CONACyT fellowship (288758 213221). Work in the S.N. laboratory is supported by CNRS, Inserm, University of Nice, ANR, LABEX SIGNALIFE [#ANR-11-LABX-0028-01], Fondation ARC and FRM.

References

Adams, D.S., Robinson, K.R., Fukumoto, T., Yuan, S., Albertson, R.C., Yelick, P., Kuo, L., McSweeney, M., and Levin, M. (2006). Early, H+-V-ATPase-dependent proton flux is necessary for consistent left-right patterning of non-mammalian vertebrates. Development 133, 1657–1671.

Adler, P.N. (2012). The frizzled/stan pathway and planar cell polarity in the Drosophila wing. Curr. Top. Dev. Biol. 101, 1–31.

Ambegaonkar, A.A., Pan, G., Mani, M., Feng, Y., and Irvine, K.D. (2012). Propagation of Dachsous-Fat planar cell polarity. Curr Biol 22, 1302–1308.

Antic, D., Stubbs, J.L., Suyama, K., Kintner, C., Scott, M.P., and Axelrod, J.D. (2010). Planar cell polarity enables posterior localization of nodal cilia and left-right axis determination during mouse and Xenopus embryogenesis. PLoS One 5, e8999.

Axelrod, J.D. (2009). Progress and challenges in understanding planar cell polarity signaling. Semin Cell Dev Biol 20, 964–971.

Ayukawa, T., Akiyama, M., Mummery-Widmer, J.L., Stoeger, T., Sasaki, J., Knoblich, J.A., Senoo, H., Sasaki, T., and Yamazaki, M. (2014). Dachsous-Dependent Asymmetric Localization of Spiny-Legs Determines Planar Cell Polarity Orientation in Drosophila. Cell Rep.

Bastock, R., Strutt, H., and Strutt, D. (2003). Strabismus is asymmetrically localised and binds to Prickle and Dishevelled during Drosophila planar polarity patterning. Development 130, 3007–3014.

Blum, M., Schweickert, A., Vick, P., Wright, C.V.E., and Danilchik, M.V. (2014). Symmetry breakage in the vertebrate embryo: When does it happen and how does it work? Dev. Biol.

Bosveld, F., Bonnet, I., Guirao, B., Tlili, S., Wang, Z., Petitalot, A., Marchand, R., Bardet, P.L., Marcq, P., Graner, F., et al. (2012). Mechanical control of morphogenesis by Fat/Dachsous/Four-jointed planar cell polarity pathway. Science 336, 724–727.

Brittle, A., Thomas, C., and Strutt, D. (2012). Planar polarity specification through asymmetric subcellular localization of Fat and Dachsous. Curr Biol 22, 907–914.

Coutelis, J.B., Petzoldt, A.G., Spéder, P., Suzanne, M., and Noselli, S. (2008). Left-right asymmetry in Drosophila. Semin. Cell Dev. Biol. 19, 252–262.

Coutelis, J.-B., Géminard, C., Spéder, P., Suzanne, M., Petzoldt, A.G., and Noselli, S. (2013). Drosophila left/right asymmetry establishment is controlled by the Hox gene abdominal-B. Dev. Cell 24, 89–97.

Cui, C., Little, C.D., and Rongish, B.J. (2009). Rotation of organizer tissue contributes to left-right asymmetry. Anat Rec (Hoboken) 292, 557–561.

Das, G., Reynolds-Kenneally, J., and Mlodzik, M. (2002). The atypical cadherin Flamingo links Frizzled and Notch signaling in planar polarity establishment in the Drosophila eye. Dev. Cell 2, 655–666.

Fox, D.T., and Spradling, A.C. (2009). The Drosophila hindgut lacks constitutively active adult stem cells but proliferates in response to tissue damage. Cell Stem Cell 5, 290–297.

Fox, D.T., Gall, J.G., and Spradling, A.C. (2010). Error-prone polyploid mitosis during normal Drosophila development. Genes Dev 24, 2294–2302.

Géminard, C., González-Morales, N., Coutelis, J.-B., and Noselli, S. (2014). The myosin ID pathway and left-right asymmetry in Drosophila. Genesis 52, 471–480.

Goodrich, L.V., and Strutt, D. (2011). Principles of planar polarity in animal development. Development 138, 1877–1892.

Gray, R.S., Roszko, I., and Solnica-Krezel, L. (2011). Planar cell polarity: coordinating morphogenetic cell behaviors with embryonic polarity. Dev. Cell 21, 120–133.

Gros, J., Feistel, K., Viebahn, C., Blum, M., and Tabin, C.J. (2009). Cell movements at Hensen's node establish left/right asymmetric gene expression in the chick. Science 324, 941–944.

Harumoto, T., Ito, M., Shimada, Y., Kobayashi, T.J., Ueda, H.R., Lu, B., and Uemura, T. (2010). Atypical cadherins Dachsous and Fat control dynamics of noncentrosomal microtubules in planar cell polarity. Dev. Cell 19, 389–401.

Hogan, J., Valentine, M., Cox, C., Doyle, K., and Collier, S. (2011). Two frizzled planar cell polarity signals in the Drosophila wing are differentially organized by the Fat/Dachsous pathway. PLoS Genet 7, e1001305.

Hozumi, S., Maeda, R., Taniguchi, K., Kanai, M., Shirakabe, S., Sasamura, T., Speder, P., Noselli, S., Aigaki, T., Murakami, R., et al. (2006). An unconventional myosin in Drosophila reverses the default handedness in visceral organs. Nature 440, 798–802.

Krasnow, R.E., Wong, L.L., and Adler, P.N. (1995). Dishevelled is a component of the frizzled signaling pathway in Drosophila. Development 121, 4095–4102.

Lawrence, P.A., and Casal, J. (2013). The mechanisms of planar cell polarity, growth and the Hippo pathway: some known unknowns. Dev. Biol. 377, 1–8.

Lawrence, P.A., Casal, J., and Struhl, G. (2002). Towards a model of the organisation of planar polarity and pattern in the Drosophila abdomen. Development 129, 2749–2760.

Lawrence, P.A., Struhl, G., and Casal, J. (2007). Planar cell polarity: one or two pathways? Nat. Rev. Genet. 8, 555–563.

Lenhart, K.F., Holtzman, N.G., Williams, J.R., and Burdine, R.D. (2013). Integration of nodal and BMP signals in the heart requires FoxH1 to create left-right differences in cell migration rates that direct cardiac asymmetry. PLoS Genet. 9, e1003109.

Levin, M., Thorlin, T., Robinson, K.R., Nogi, T., and Mercola, M. (2002). Asymmetries in H+/K+-ATPase and cell membrane potentials comprise a very early step in left-right patterning. Cell 111, 77–89.

Ma, D., Yang, C.H., McNeill, H., Simon, M.A., and Axelrod, J.D. (2003). Fidelity in planar cell polarity signalling. Nature 421, 543–547.

Matakatsu, H., and Blair, S.S. (2004). Interactions between Fat and Dachsous and the regulation of planar cell polarity in the Drosophila wing. Development 131, 3785–3794.

Matakatsu, H., and Blair, S.S. (2006). Separating the adhesive and signaling functions of the Fat and Dachsous protocadherins. Development 133, 2315–2324.

Matis, M., and Axelrod, J.D. (2013). Regulation of PCP by the Fat signaling pathway. Genes Dev. 27, 2207–2220.

McGuire, S.E., Le, P.T., Osborn, A.J., Matsumoto, K., and Davis, R.L. (2003). Spatiotemporal rescue of memory dysfunction in Drosophila. Science 302, 1765–1768.

Mooseker, M.S., and Cheney, R.E. (1995). Unconventional myosins. Annu Rev Cell Dev Biol 11, 633–675.

Morgan, D., Turnpenny, L., Goodship, J., Dai, W., Majumder, K., Matthews, L., Gardner, A., Schuster, G., Vien, L., Harrison, W., et al. (1998). Inversin, a novel gene in the vertebrate left-right axis pathway, is partially deleted in the inv mouse. Nat. Genet. 20, 149–156.

Morgan, N.S., Heintzelman, M.B., and Mooseker, M.S. (1995). Characterization of myosin-IA and myosin-IB, two unconventional myosins associated with the Drosophila brush border cytoskeleton. Dev Biol 172, 51–71.

Murakami, R., and Shiotsuki, Y. (2001). Ultrastructure of the hindgut of Drosophila larvae, with special reference to the domains identified by specific gene expression patterns. J Morphol 248, 144–150.

Nakamura, T., and Hamada, H. (2012). Left-right patterning: conserved and divergent mechanisms. Development 139, 3257–3262.

Nambiar, R., McConnell, R.E., and Tyska, M.J. (2009). Control of cell membrane tension by myosin-I. Proc Natl Acad Sci U S A 106, 11972–11977.

Namigai, E.K.O., Kenny, N.J., and Shimeld, S.M. (2014). Right across the tree of life: The evolution of left–right asymmetry in the Bilateria. Genesis 52, 458–470.

Olofsson, J., Sharp, K.A., Matis, M., Cho, B., and Axelrod, J.D. (2014). Prickle/spiny-legs isoforms control the polarity of the apical microtubule network in planar cell polarity. Development 141, 2866–2874.

Peeters, H., and Devriendt, K. (2006). Human laterality disorders. Eur J Med Genet 49, 349–362.

Peng, Y., and Axelrod, J.D. (2012). Asymmetric protein localization in planar cell polarity: mechanisms, puzzles, and challenges. Curr Top Dev Biol 101, 33–53.

Petzoldt, A.G., Coutelis, J.B., Geminard, C., Speder, P., Suzanne, M., Cerezo, D., and Noselli, S. (2012). DE-Cadherin regulates unconventional Myosin ID and Myosin IC in Drosophila left-right asymmetry establishment. Development 139, 1874–1884.

Pyrpassopoulos, S., Feeser, E.A., Mazerik, J.N., Tyska, M.J., and Ostap, E.M. (2012). Membrane-bound myo1c powers asymmetric motility of actin filaments. Curr Biol 22, 1688–1692.

Raya, A., and Izpisua Belmonte, J.C. (2006). Left-right asymmetry in the vertebrate embryo: from early information to higher-level integration. Nat Rev Genet 7, 283–293.

Robertson, C.W. (1936). The metamorphosis of Drosophila melanogaster, including an accurately timed account of the principal morphological changes. Journal of Morphology 59, 351–399.

Rogulja, D., Rauskolb, C., and Irvine, K.D. (2008). Morphogen control of wing growth through the Fat signaling pathway. Dev. Cell 15, 309–321.

Sharma, P., and McNeill, H. (2013). Regulation of long-range planar cell polarity by Fat-Dachsous signaling. Development 140, 3869–3881.

Simon, M.A., Xu, A., Ishikawa, H.O., and Irvine, K.D. (2010). Modulation of fat:dachsous binding by the cadherin domain kinase four-jointed. Curr. Biol. 20, 811–817.

Singh, J., and Mlodzik, M. (2012). Planar cell polarity signaling: coordination of cellular orientation across tissues. Wiley Interdiscip Rev Dev Biol 1, 479–499.

Song, H., Hu, J., Chen, W., Elliott, G., Andre, P., Gao, B., and Yang, Y. (2010). Planar cell polarity breaks bilateral symmetry by controlling ciliary positioning. Nature 466, 378–382.

Speder, P., Adam, G., and Noselli, S. (2006). Type ID unconventional myosin controls left-right asymmetry in Drosophila. Nature 440, 803–807.

Strutt, H., and Strutt, D. (2002). Nonautonomous planar polarity patterning in Drosophila: dishevelled-independent functions of frizzled. Dev Cell 3, 851–863.

Suzanne, M., Petzoldt, A.G., Speder, P., Coutelis, J.B., Steller, H., and Noselli, S. (2010). Coupling of apoptosis and L/R patterning controls stepwise organ looping. Curr Biol 20, 1773–1778.

Takashima, S., Mkrtchyan, M., Younossi-Hartenstein, A., Merriam, J.R., and Hartenstein, V. (2008). The behaviour of Drosophila adult hindgut stem cells is controlled by Wnt and Hh signalling. Nature 454, 651–655.

Takashima, S., Younossi-Hartenstein, A., Ortiz, P.A., and Hartenstein, V. (2011). A novel tissue in an established model system: the Drosophila pupal midgut. Dev. Genes Evol. 221, 69–81.

Takashima, S., Paul, M., Aghajanian, P., Younossi-Hartenstein, A., and Hartenstein, V. (2013). Migration of Drosophila intestinal stem cells across organ boundaries. Development 140, 1903–1911.

Taniguchi, K., Hozumi, S., Maeda, R., Okumura, T., and Matsuno, K. (2007). Roles of type I myosins in Drosophila handedness. Fly (Austin) 1, 287–290.

Taniguchi, K., Maeda, R., Ando, T., Okumura, T., Nakazawa, N., Hatori, R., Nakamura, M., Hozumi, S., Fujiwara, H., and Matsuno, K. (2011). Chirality in planar cell shape contributes to left-right asymmetric epithelial morphogenesis. Science 333, 339–341.

Thomas, C., and Strutt, D. (2012). The roles of the cadherins Fat and Dachsous in planar polarity specification in Drosophila. Dev. Dyn. 241, 27–39.

Tree, D.R.P., Shulman, J.M., Rousset, R., Scott, M.P., Gubb, D., and Axelrod, J.D. (2002). Prickle mediates feedback amplification to generate asymmetric planar cell polarity signaling. Cell 109, 371–381.

Vandenberg, L.N., and Levin, M. (2013). A unified model for left-right asymmetry? Comparison and synthesis of molecular models of embryonic laterality. Dev. Biol. 379, 1–15.

Viktorinova, I., and Dahmann, C. (2013). Microtubule polarity predicts direction of egg chamber rotation in Drosophila. Curr Biol 23, 1472–1477.

Vinson, C.R., and Adler, P.N. (1987). Directional non-cell autonomy and the transmission of polarity information by the frizzled gene of Drosophila. Nature 329, 549–551.

Wallingford, J.B. (2012). Planar cell polarity and the developmental control of cell behavior in vertebrate embryos. Annu. Rev. Cell Dev. Biol. 28, 627–653.

Wolff, T., and Rubin, G.M. (1998). Strabismus, a novel gene that regulates tissue polarity and cell fate decisions in Drosophila. Development 125, 1149–1159.

Yang, Y. (2012). Planar cell polarity during development. Preface. Curr. Top. Dev. Biol. 101, xi–xiii.

Yang, C., Axelrod, J.D., and Simon, M.A. (2002). Regulation of Frizzled by fat-like cadherins during planar polarity signaling in the Drosophila compound eye. Cell 108, 675–688.

Yoshiba, S., and Hamada, H. (2014). Roles of cilia, fluid flow, and Ca2+ signaling in breaking of left-right symmetry. Trends Genet. 30, 10–17.

Zeidler, M.P., Perrimon, N., and Strutt, D.I. (2000). Multiple roles for four-jointed in planar polarity and limb patterning. Dev. Biol. 228, 181–196.

FIGURE LEGENDS

FIGURE 1. *myosin ID* controls adult hindgut looping

(**A-C**) Dorsal views of adult fly abdomens after feeding with a blue dye to reveal hindgut shape. Wild type flies show hindgut dextral looping (**A**), whereas *myoID*$^{k2/k2}$ mutant flies show either looping inversion (sinistral, **B**) or mislooping (**C**).(**D-F**) Confocal microscopy images of the whole adult abdomen showing hindgut looping in wild type (**D**, dextral), inverted, and mislooped *myoID*$^{k2/k2}$ mutant flies (**E**, sinistral; **F**, mislooped). The hindgut is false-colored for clarity (blue=dextral; red=sinistral; orange=mislooped). This color-code is used hereafter. Scale bar: 100µm

(**G**) Histogram showing the adult hindgut and terminalia phenotypes following knockdown of *myoID* in either the terminalia L/R organizer (*myoID-Gal4*) or the whole hindgut precursor tissue (i.e. the imaginal ring; *hindgut-Gal4* - *HG-gal4*); same color-code as in D-E. N=100 for each genotype.

(**H**) Temporal requirement for MyoID activity during hindgut (green line) or terminalia (red line) L/R development. In both cases, MyoID function is required around day 5 of larval development, thus, 3 days before actual adult hindgut looping. N=50 flies for each time point.

FIGURE 2. MyoID is expressed and essential in the H1 domain for hindgut L/R asymmetry

(**A-E**) Confocal images of L3 imaginal rings stained with specific markers expressed in the larval imaginal ring. Expression patterns shown in A‘-E’ and A‘’-E‘’ panels are schematized on the right in gray. MyoID is expressed specifically in the H1 domain, overlapping with Wg-expressing cells. The yellow and orange line positions H1 cells and H2 cells, respectively. Scale bar: 50µm

(**F**) Schematic representation of the larval digestive tract. The H1 (yellow) and H2 (orange) domains of the imaginal ring are shown. Summary of the phenotypes induced by *myoID* RNAi expression in the larval imaginal ring. Expression of MyoID specifically in the H1 domain is essential for proper dextral looping of the adult hindgut.

FIGURE 3. The hindgut organizer is a transient structure

(**A-C**) Lineage tracing experiments showing the progeny (GFP, green) of H1+H2 (**A**), H2 (**B**) or H1 (**C**) cells. While the lineage from H1+H2 cells (**A**) or H2 cells alone (**B**) covers all the adult hindgut (AHG) and terminal posterior midgut (tPMG), the lineage from H1 cells alone does not produce any adult hindgut GFP positive cells. APF, after puparium formation. Scale bar in all panels: 50µm

(**D**) The H1 domain, marked by *hingut-Gal4* is separated from the H2 domain at 10HAPF. The yellow line shows the distance between H1 and H2 cells.

(**E**) Similar to (D). Detachment of H1 is not impaired in *myoID* mutants.

(**F**) At 24 hr APF, H1 cells (expressing GFP) are trapped inside the pupal midgut (PMG, encircled, white dashed line) together with the larval midgut (LMG); H2 cells on the other hand, are located in between the adult midgut (AMG) and the degrading larval hindgut (LHG, marked by white dashes). F' and F'' are magnification images from F.

(**G**) At 24 hr APF, H1 cells present in the pupal midgut still express *myoID::GFP* (red) and *hindgut-Gal4* (green).

(**H**) At 24 hr APF, *myoID* mutants H1 cells, marked with *hindgut-Gal4,* are also trapped in the pupal midgut.

(**I**) At 36 hr APF, *MyoID* expression is not detectable in H2 cells (orange line).

(**J**) The pupal midgut, together with the remnants of the larval midgut, is expelled during the first hours of adult life in the meconium.

(**K**) Confocal image of a meconium showing *hindgut-Gal4* positive cells.

(**L**) Schematic representation of H1 domain behavior at different time points showing the detachment of the H1 domain from the H2 domain.

(**M**) Schematic representation of the fate map of adult hindgut and posterior midgut.

FIGURE 4. MyoID controls early L/R polarization of H2 cells

(**A**) A representative L3 imaginal ring expressing *PH::GFP* to mark cell membranes (*hindgut-Gal4, UAS-PH::GFP*). The black box delineates the region used for quantitative measurements. It corresponds to the central region of the imaginal ring that is best aligned with the anterior-posterior (A/P) axis. R, right; L, Left

(**B**) Scheme showing the method used to measure cell orientation. The orientation of cells is measured by the angle (blue arrow) made between cell membranes and the A/P axis. By convention, angles between +67.5 and +22.5 were considered as dextral, while the ones between -67.5 and 22.5 were considered as sinistral.

(**C-E**) Representative images of H2 cells at different time points. At 0 hr APF, cells do not show any LR bias (**C**), whereas at 10 hr APF cells become elongated and orient towards the right hand side (**D**). In *myoID* mutants, cells show an inverted orientation towards the left hand side (**E**).

(**F-H**) Graphic plot showing the distribution of cellular angles found in H2 cells at 0H APF in wild type cells (control, **F**) and at 10H APF in wild type (**G**) and *myoID* mutant cells (**H**). Mean values are represented by a solid line and SEM is shown in gray. In (**F**) the peak at 90°/-90° represents symmetrical orientation along the A/P axis, whereas in (**G**) and (**H**) peaks indicate the preferential right or leftward orientations measured at 10H APF. N=10 for each genotype.

(**I-K**) Plot of the sum of rightward (R) against leftward oriented angles. At 0H APF, there is no significant L/R preference (**I**), while at 10H APF there is a clear 2.5 fold difference between R and L (**J**). In *myoID* mutants, this difference is inverted (**K**). Standard errors and p-values at statistical difference at 95% confidence values are shown.

FIGURE 5. Hindgut phenotypes of core and global PCP genes

(**A**-**D, G**-**J**) Hindgut phenotypes from control flies (**A**), flies expressing RNAi against core (green, **B**-**D**) or global (purple, **G**-**J**) PCP pathways genes and flies expressing Ds RNAi specifically in the H1 domain (**J**). Representative confocal

images are shown with false-colored hindguts for clarity (color code as in Fig. 1). Scale bar: 100µm

(**E**-**L**) Histogram showing the percentage of defects following RNAi depletion of the core and global system components in the entire imaginal ring (H1+H2 domains) using *hindgut-Gal4* (**E,K**) or specifically in H1 cells, using *myoID-Gal4* (**F,L**). N=100 for each genotype.

FIGURE 6. Genetic and biochemical interaction between MyoID and Ds in H1 cells

(**A**) Representative images of H2 cells at 10 hr APF, from control (top) or *ds-RNAi* flies (bottom). Cells are elongated and oriented towards the right hand side in control while in *ds-RNAi* flies, cells do not show any bias as in early O hr APF H2 cells (Fig. 4C).

(**B**) Knockdown of *ds* in the H1 domain results in a loss of LR polarity as revealed by the distribution of cellular angles found in H2 cells compared to the control (blue line). N=10 for each genotype.

(**C**) Plot of the sum of rightward (R) and leftward (L) oriented angles after depletion of Ds in H1 cells at 10H APF. Control cells show a bias towards the right hand side, while depletion of *ds* from H1 cells leads to a loss of the L/R bias. Standard errors and p-values at statistical difference at 95% confidence values are shown.

(**D-F**) Heterozygous *ds* (**D**) or *myoID* (**E**) flies show a wild type dextral phenotype. However, double *ds; myoID* heterozygotes show mislooped hindguts (**F**) indicating genetic interaction between the two genes. Representative confocal images are shown with false-colored hindguts for clarity (color code as in Fig. 1). N=100 for each genotype. Scale bar: 100µm.

(**G**) Histogram showing the percentage of defects in single and double heterozygous flies mutant for *ds* and/or *myoID*. Standard errors are shown and statistical difference at 95% confidence values are denoted by an asterisk. N=100 for each genotype.

(**H**). Co-immunoprecipitation experiment using *myoID-gal4, UAS-myoID::GFP; attpB-P(acman-ds::HA)* larval hindgut extracts. MyoID is specifically immunoprecipitated by Ds::HA.

(**I**) Confocal image of an imaginal ring from a larva overexpressing MyoID::GFP and Ds-HA at low levels (*myoID-Gal4, UAS-myoID::GFP; attpB-P(acman-ds::HA).* Ds expression is visible in both H1 (marked by *myoID-Gal4)* and H2 cells . White dashed line outlines the H1/H2 border.

FIGURE 7. MyoID interacts with Ds intracellular domain

(**A**) Co-expression of Ds-ICD and MyoID in *Drosophila* S2R+ cells showing membrane co-localization of both proteins at cell-cell contact sites (arrowheads). Heat map false colored confocal images showing protein concentration.

(**B**) Co-immunoprecipitation of Ds-ICD-Flag using MyoID::GFP as bait in *Drosophila* S2R+ cells.

(**C**) Cartoon of full length and truncated forms of Ds used in D-L panels, showing the intracellular domain (ICD, green), the transmembrane domain (orange) and the extracellular domain (ECD, blue).

(**D-I**) Hindgut phenotype from flies overexpressing different forms of Ds alone (**D-F**) or co-overexpressing different forms of Ds and MyoID (**G-I**). Scale bar: 100µm

(**J-L**) Histogram showing the percentage of defects shown in D-I. Standard errors are shown and statistical difference at 95% confidence values are denoted by an asterisk. n=100 for each genotype.

(**M**) Model of MyoID and Ds interaction in the H1 L/R organizer. Transient interaction between MyoID and Ds 'biases' Ds in H1 cells. This L/R bias is then transferred to H2 cells through Ds/Ft interaction at the H1/H2 boundary. At 10 hr APF, H2 cells become polarized along the L/R axis, initiating looping morphogenesis leading to a fully looped hindgut at 50 hr APF.

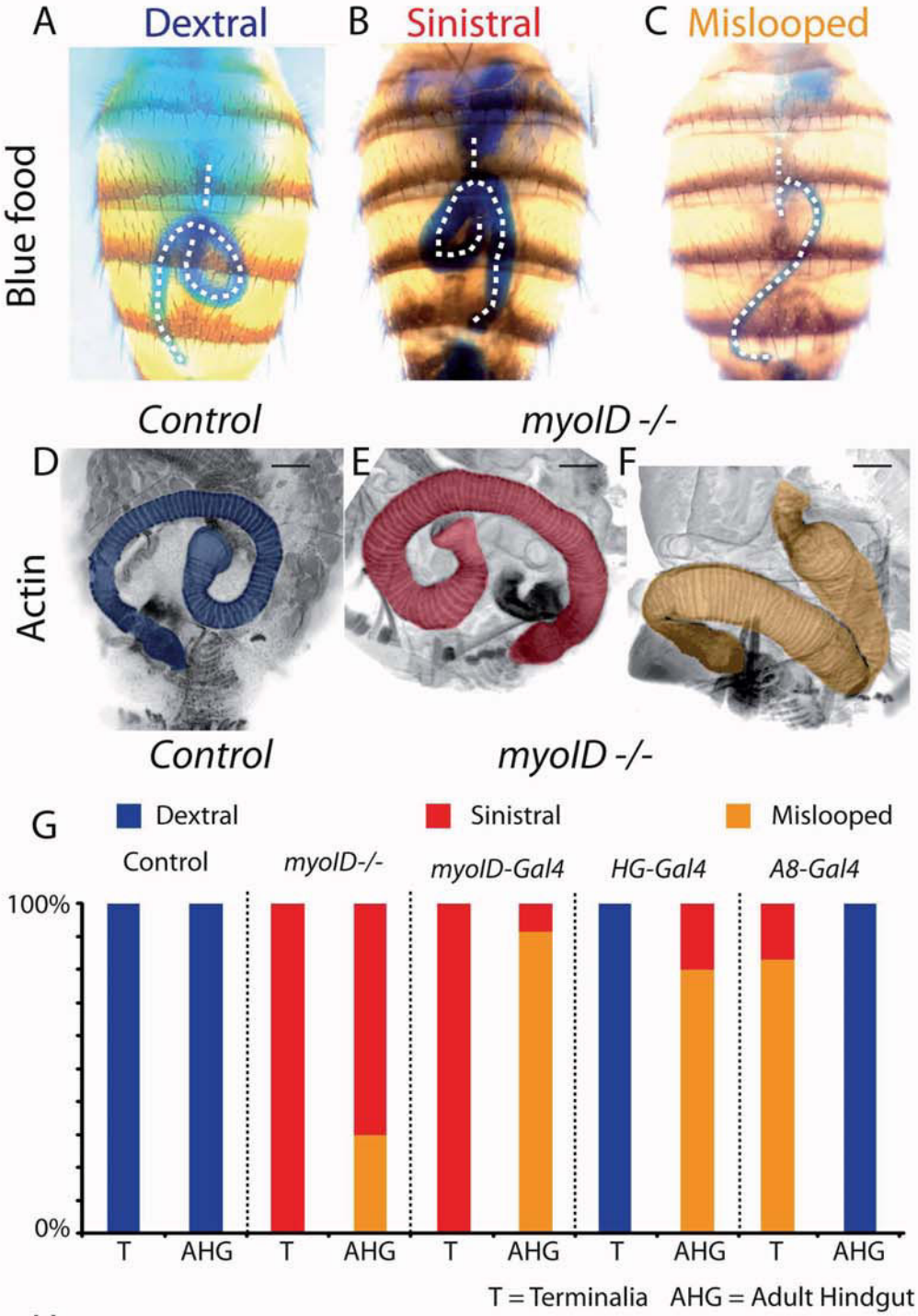

González-Morales et al. Figure 1

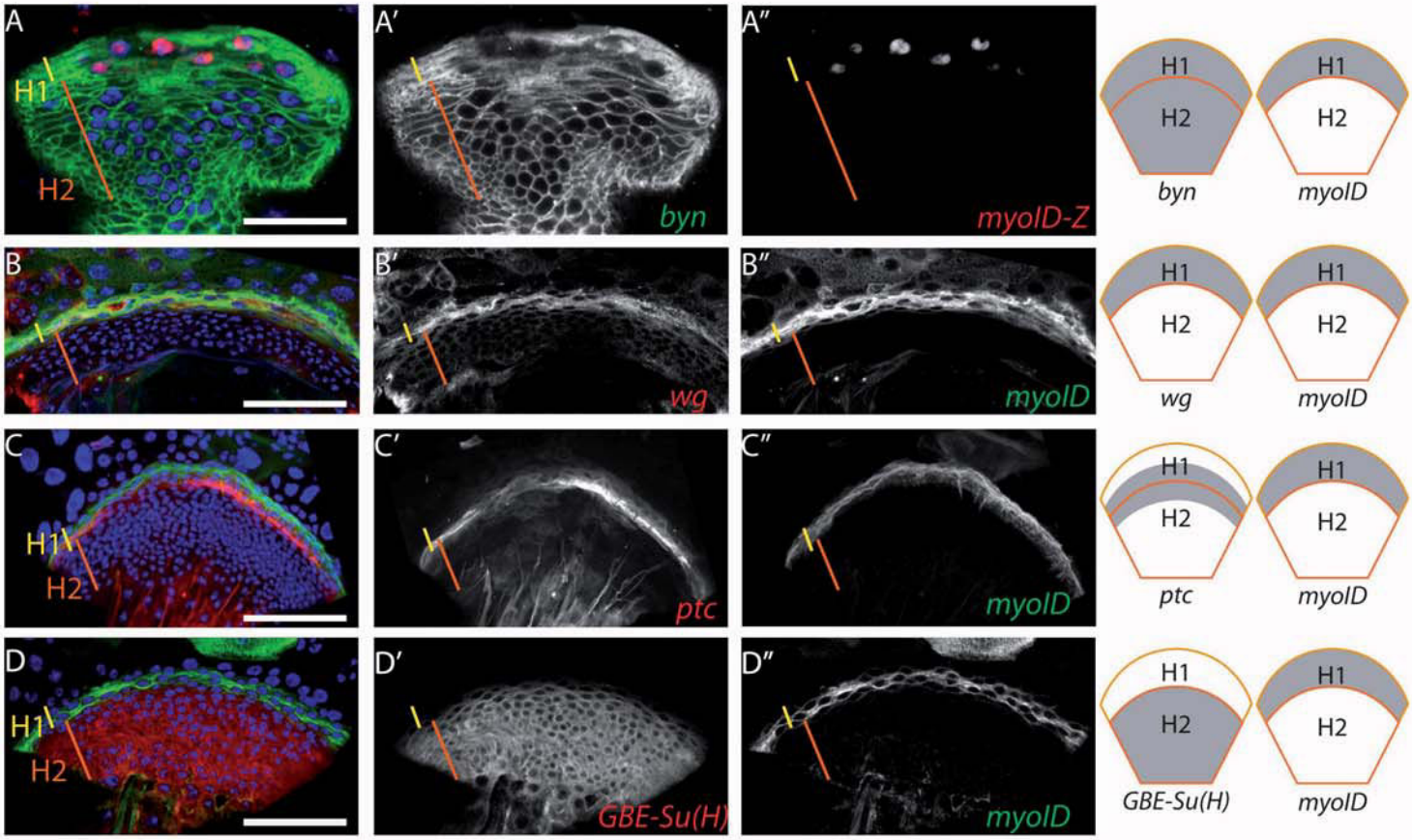

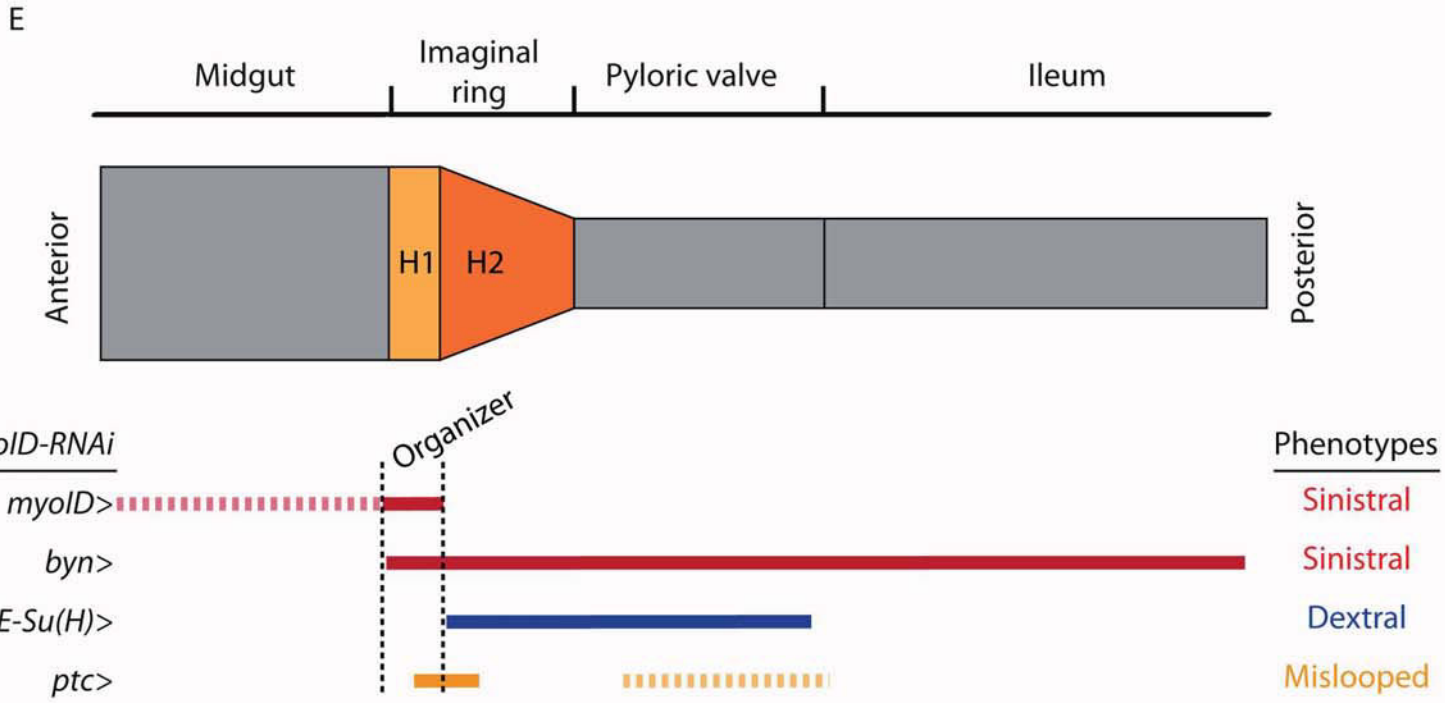

González-Morales et al. Figure 2

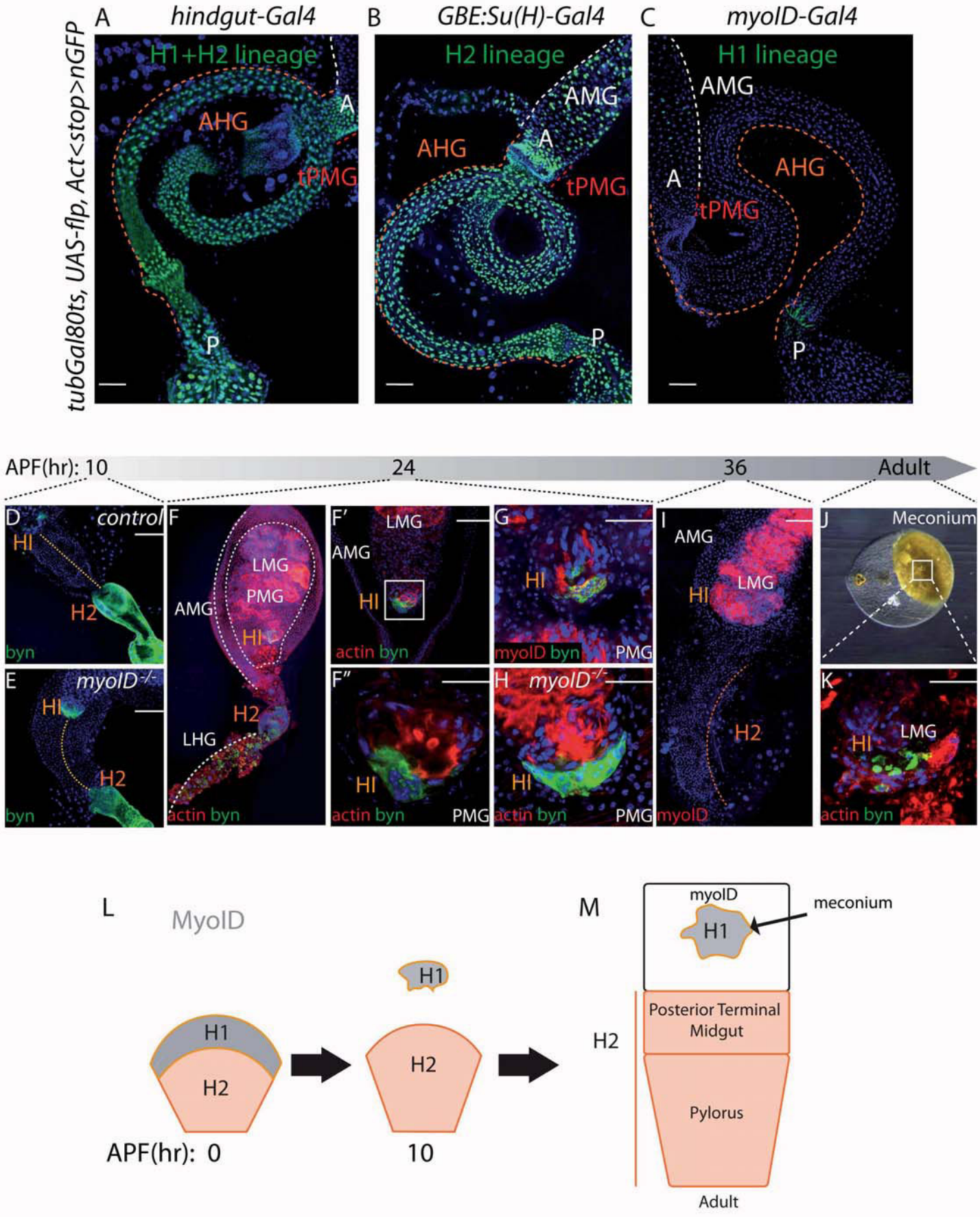

González-Morales et al. Figure 3

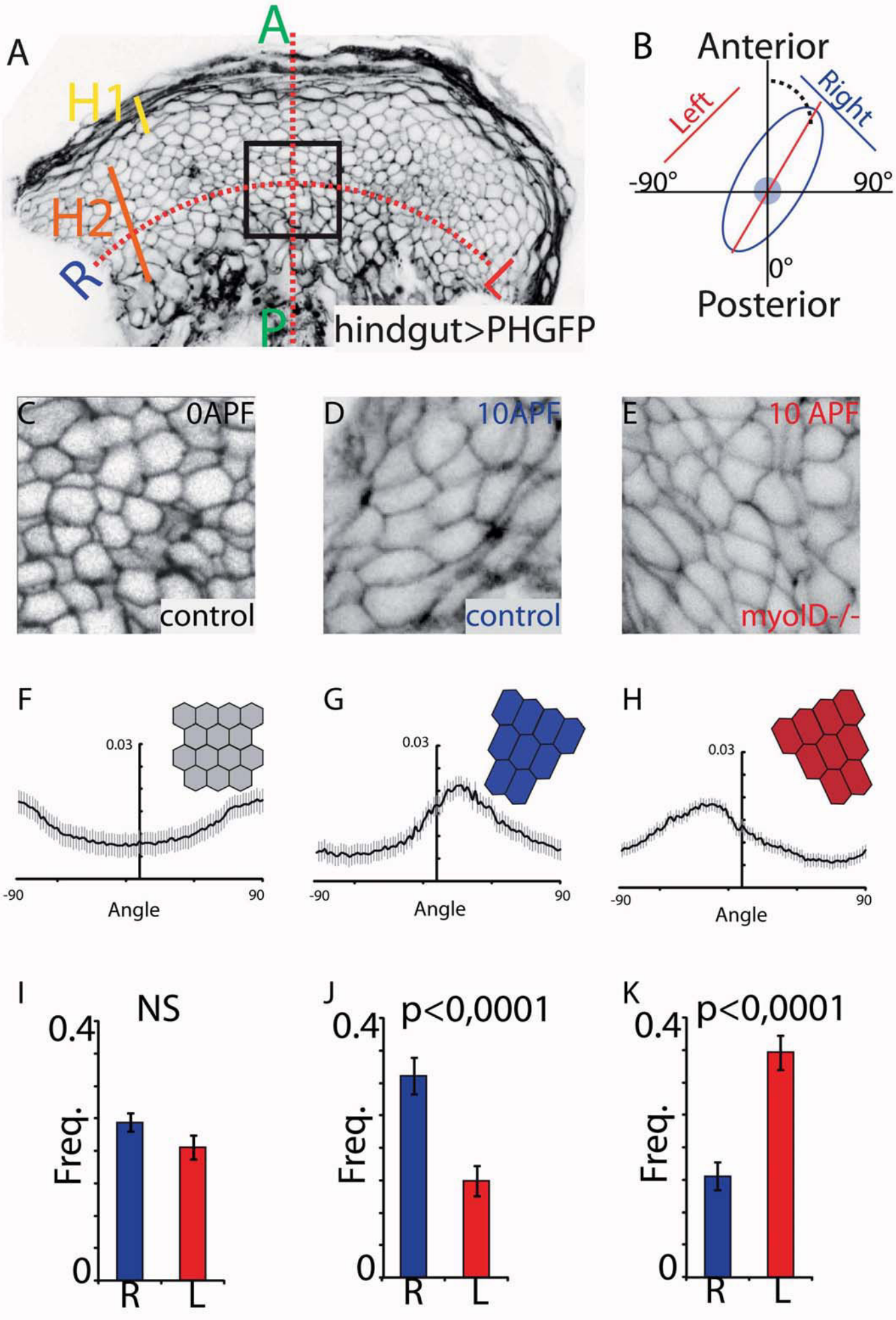

González-Morales et al. Figure 4

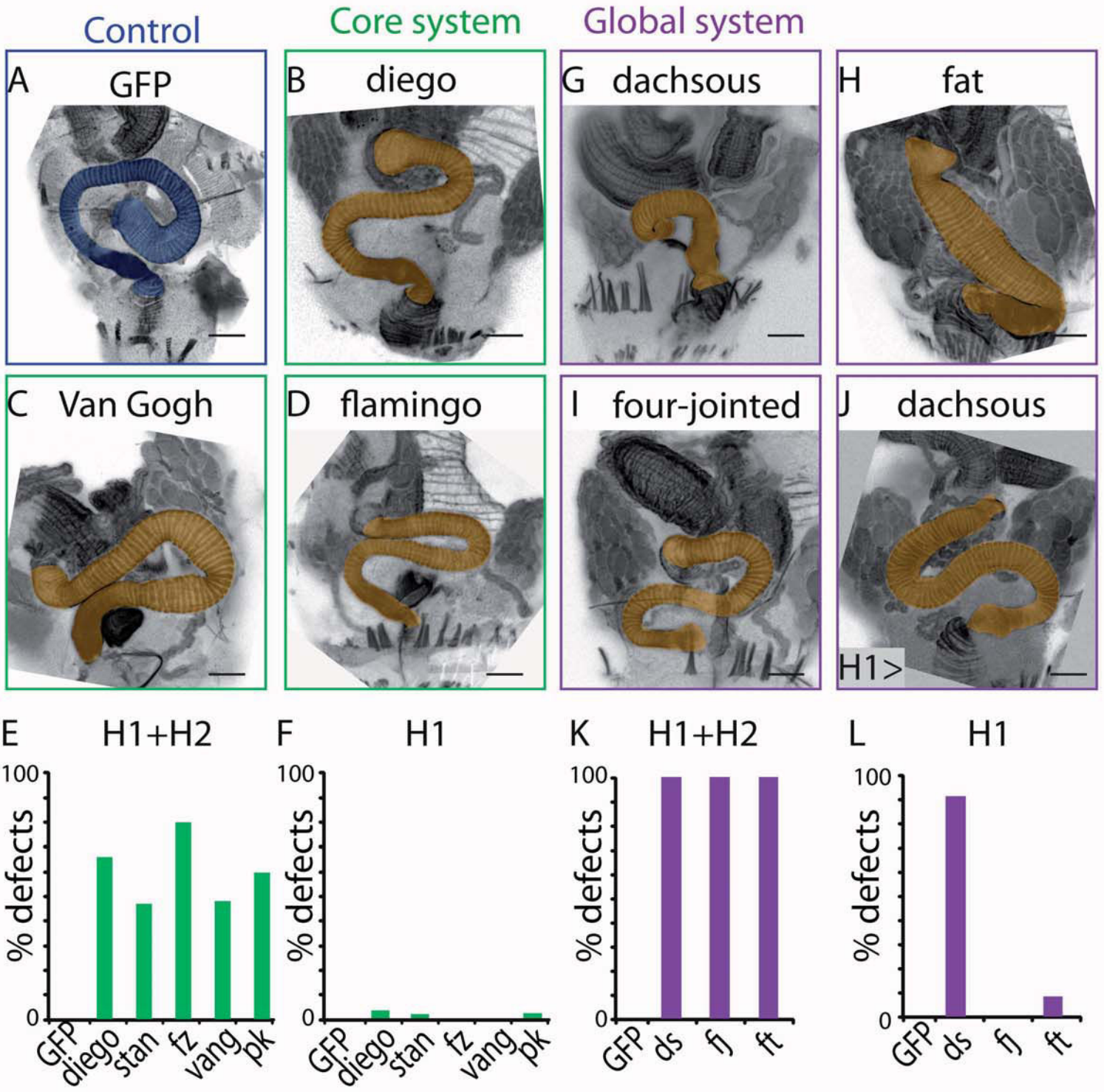

González-Morales et al. Figure 5

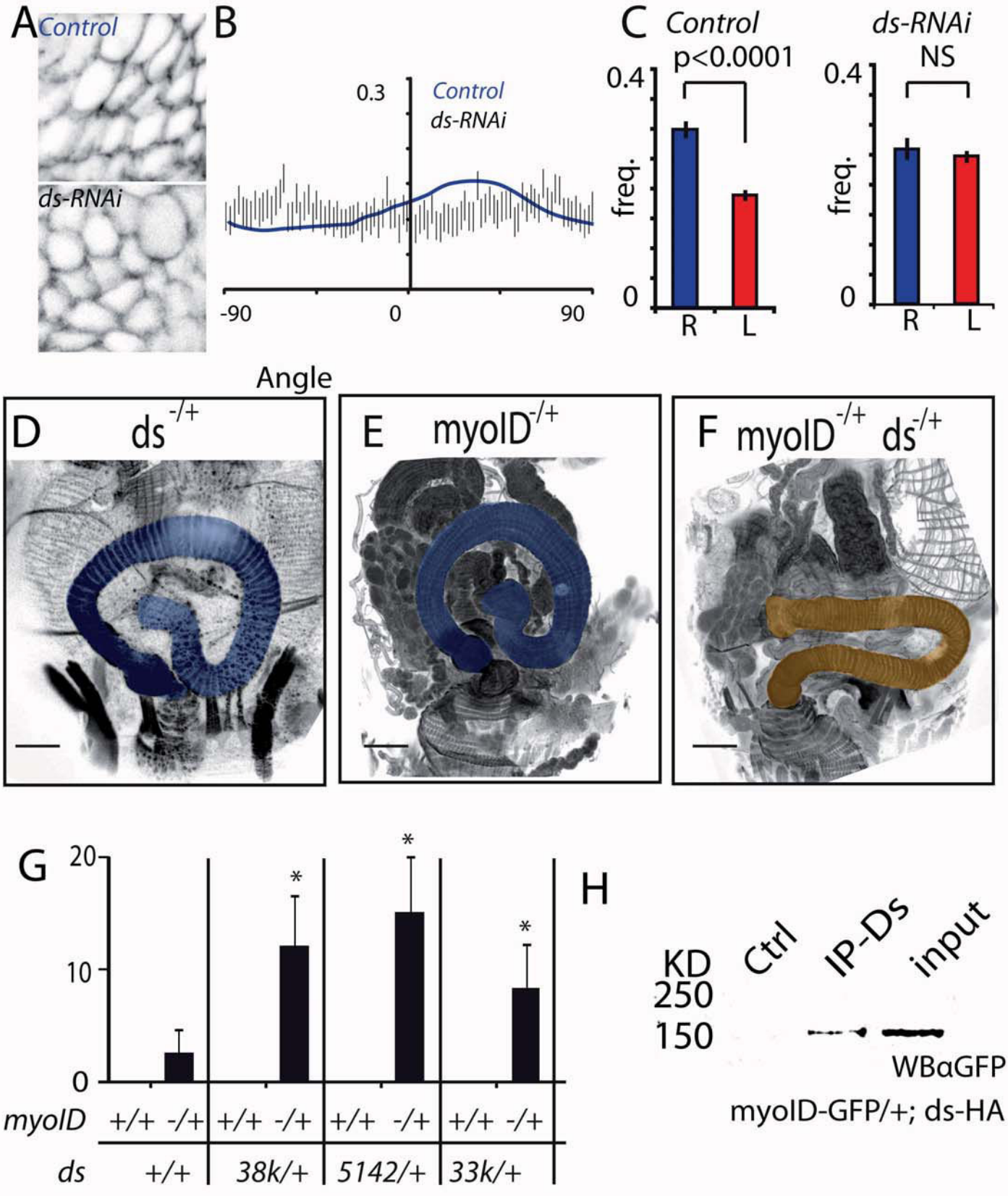

González-Morales et al. Figure 6

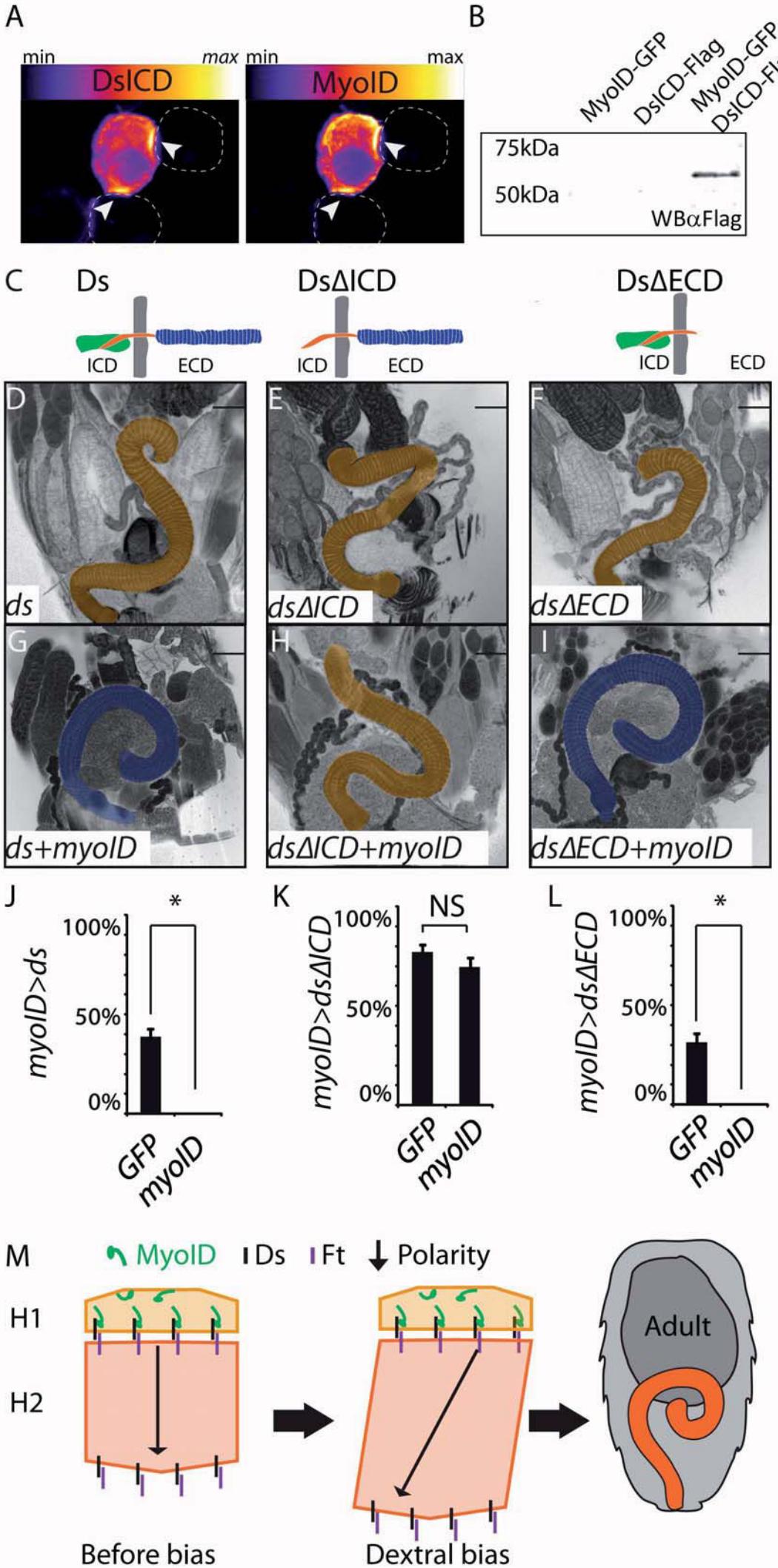

González-Morales et al. Figure 7

Supplemental Experimental Procedures

Fly stocks

The strain w^{1118} was used as control. *TubP:Gal80^{ts}, UAS-FLP, Ubi-p63E(FRT.STOP)Stinger, ds^{05142}, ds^{38k}, ds^{33k}, fj$^{9-11}$, UAS:PH(ɣ)-GFP, UAS:myrRFP, 10XStat92E-GFP, UAS:MCD8-GFP, UAS:dicer2*, were all obtained from Bloomington Drosophila Stock Center. The hindgut specific *byn^{Gal4}* was originally described by Judith Ann Lengyel (Iwaki and Lengyel, 2002), but was given to us by Kenji Matsuno. The A8 specific *AbdB$^{LDL\text{-}Gal4}$* was a gift from E. Sanchez Herrero (de Navas et al., 2006). *GBE-Su(H)^{Gal4}* drives expression in H2 cells and was a gift from Xiankun Zeng (Zeng et al., 2010). *ptc^{Gal4}, myoID$^{Gal4\text{-}(NP1458)}$, myoID^{LacZ}, myoID$^{k2/k2}$, UAS:myoID-RNAi-2X, UAS:myoID-GFP* have been previously described (Speder et al., 2006). *P(w+, genomic-myoID-GFP)* is a insertion in the 2nd chromosome that contains the genomic sequence of *myoID* in which a HA-GFP cassette has been placed before the stop codon, and which can rescue *myoID$^{k2/k2}$*. *attB-P(acman-ds-HA)* was a gift from Ken Irvine (Ambegaonkar et al., 2012). The following *RNAi* lines were used: *ds^{GD14350}, ds^{GD2646}, ds^{JM02842,} ds^{GD14350}, ft^{KK101190}, ft^{GD881}, ft^{JF03245}, fj^{GD430}, fj^{HMS01310,} fj^{JF02843}, dgo^{HMS01454}, dgo^{GD7575}, dgo^{KK}, fz^{GD4614}, fz^{kk108004}, pk^{GD1510}, stan^{HMS01464}, stan^{JF02047}, stan^{GD607}, stan^{GD607}, vang^{GD1889}, vang^{KK108814}* they were obtained from Bloomington Drosophila Stock Center and Vienna Drosophila RNAi Center.

Blue Erioglaucine staining

Flies were fed on a mixture of agar 3%, sucrose 5% and erioglaucine 2.5% (Sigma#861146) for at least 6 hours. Then the adult hindgut position was examined in a LeicaMZ6 stereoscope.

Wholemount for confocal microscopy

Headless flies were fixed in formaldehyde 4% overnight, following washes in PBS with 0.1% Triton, the dorsal part of the abdominal cuticle was carefully removed using forceps. Abdomens were then stained with FITC- TRITC-phalloidin of overnight. Complete abdomens were mounted in 2% agarose in a concaved slide and image in an SPE Leica upright confocal.

Antibodies and stainings

Larval and adult hindguts were dissected in PBS and fixed in 4% formaldehyde for 20 minutes. Subsequent washes and incubations were done in PBS with 0.1% Triton. Tissues were incubated overnight with primary antibody at 4°C, followed by two-hour incubation with secondary antibodies at room temperature. Antibodies used were mouse Wg (Developmental Studies Hybridoma Bank, 1:50), mouse B-Galactosidase (Promega 1:1000). Phalloidin-Cy3 –FITC (Molecular Probes 1:400). FITC-, Cy3-, and Cy5-conjugated secondary antibodies were obtained from Jackson Immunolabs and used at 1:200.

TARGET system

Synchronized fly populations of the genotype *myoD-Gal4, tub-Gal80TS/ UAS-myoID-RNAi* were raised at 25°C, where Gal4 system is off, then changed for 1 day to 29°. The same procedure was used in combination with UAS-reaper to genetically ablate H1 cells but in this case flies were kept at 29° one hour.

Lineage tracing strategy

Flies carrying *myoID-Gal4* (H1), *GBE-Su(H)-Gal4* (H2) or *byn-Gal4* (H1-2) in combination with all the constructs of the linage tracing were kept at 29° to allow the excision of the stop cassette; then, at white prepupa stage they were transferred to 18°C to prevent further GFP expression. Finally adults were dissected and analyzed for GFP presence.

Cell polarity measurements

A small square was selected in the middle of the H2 ring to minimize the effects of deformation caused by the architecture of a tube. Images were previously aligned along the A/P axis. L/R cell orientation was then analyzed with Fiji first manually by calculating the main axis of one cell and measuring its angle with the perpendicular A/P axis, and then using Fiji 'Directionality' plug-in created by Jean-Yves Tinevez (http://fiji.sc/Directionality). This plug-in gives the preferred orientation of structures present in the input image (cellular membrane) and plots them as a histogram of frequencies.

Supplementary References

De Navas, L., Foronda, D., Suzanne, M., and Sanchez-Herrero, E. (2006). A simple and efficient method to identify replacements of P-lacZ by P-Gal4 lines allows obtaining Gal4 insertions in the bithorax complex of Drosophila. Mech Dev 123, 860–867.

Iwaki, D.D., and Lengyel, J.A. (2002). A Delta-Notch signaling border regulated by Engrailed/Invected repression specifies boundary cells in the Drosophila hindgut. Mech Dev 114, 71–84.

Zeng, X., Chauhan, C., and Hou, S.X. (2010). Characterization of midgut stem cell- and enteroblast-specific Gal4 lines in drosophila. Genesis 48, 607–611.

SUPPLEMENTARY FIGURES

Supplementary FIGURE 1. (related to Figure 3)

Ablation of the H1 domain leads to mislooped adult hindguts

(**A**) Summary of 1hr-targeted expression of the pro-apoptotic gene reaper with *myoID-Gal4*. Expression in early stages (L1 to L3) results in lethality during larval stages. Expression between 0-10H APF induces mislooped hindguts, while expression after this stage does not affect hindgut development or looping.

(**B**-**C**) Confocal microscopy images of the whole abdomen showing hindgut looping phenotype from genetic ablation of H1 cells after 10 hrs APF (**B**), or between 0-10 hrs APF (**C**).

(**D**) Dorsal view of a mislooped hindgut phenotype in a H1 ablated adult fly fed with blue food. Note that the blue dye remains inside the adult hindgut confirming the integrity of the adult hindgut when the H1 domain is ablated after 10 hr APF.

(**E**) Confocal images of wild type (top) and mislooped (bottom) adult hindgut resulting from H1 ablation at 10H APF showing hindgut integrity.

(**F**) The general morphology of the adult pylorus is unaffected by H1 ablation.

Supplementary FIGURE 2. (related to Figure 5)

Core and global PCP pathway hindgut phenotypes

(**A**) Histogram showing the percentage of defects upon depletion of the Ft/Ds pathway components using different RNAi lines driven by *hindgut-Gal4*.

(**B**) Histogram showing the percentage of defects upon depletion of the Ft/Ds pathway components using different RNAi lines driven by *myoID-Gal4*.

(**C**) Histogram showing the percentage of defects upon depletion of the core PCP pathway components using different RNAi lines driven by *hindgut-Gal4*.

(**D**) Histogram showing the percentage of defects upon depletion of the Ft/Ds pathway components driven by the H2 specific *GBE-Su(H)-Gal4*.

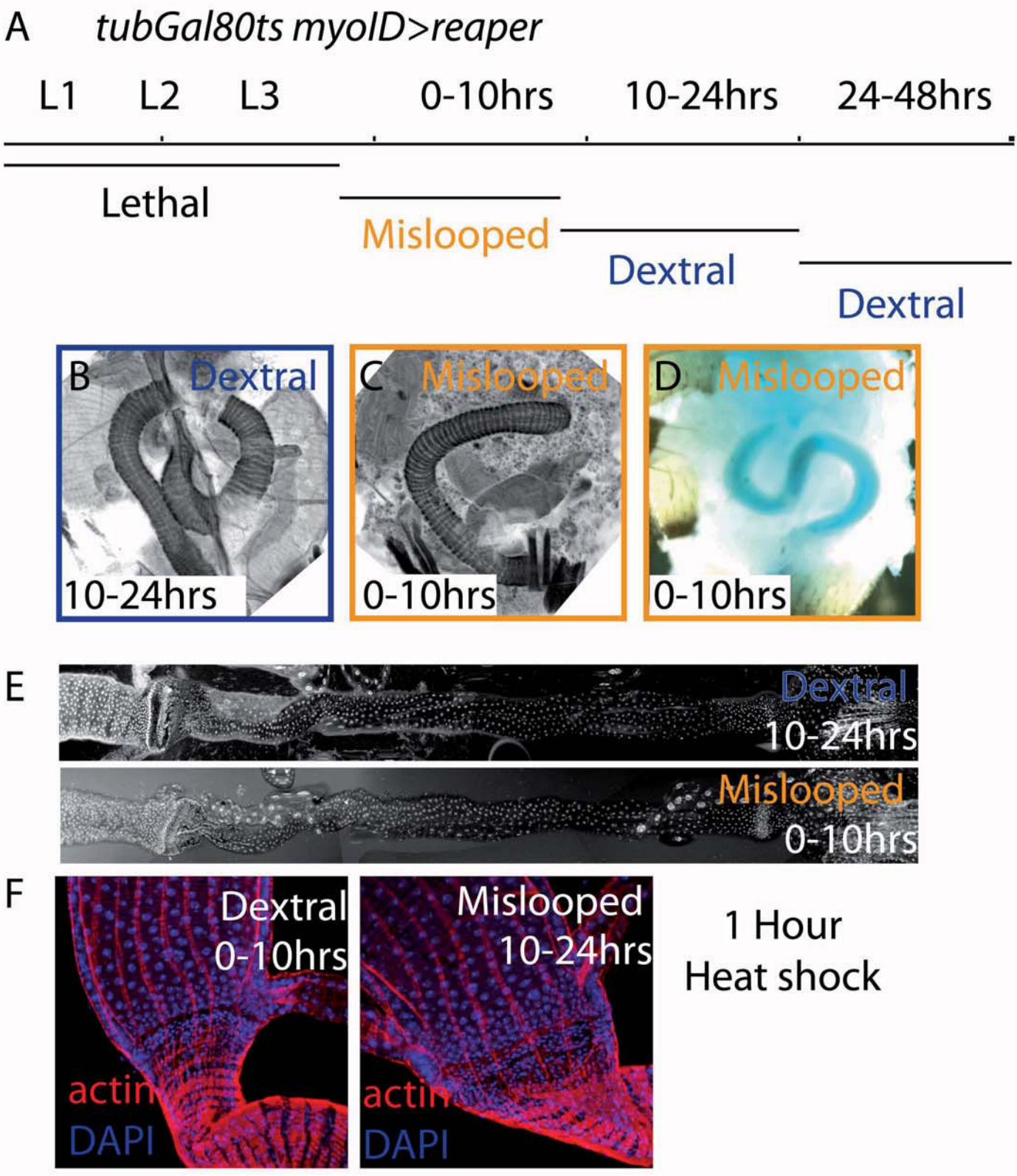

González-Morales et al. Supplementary Figure 1

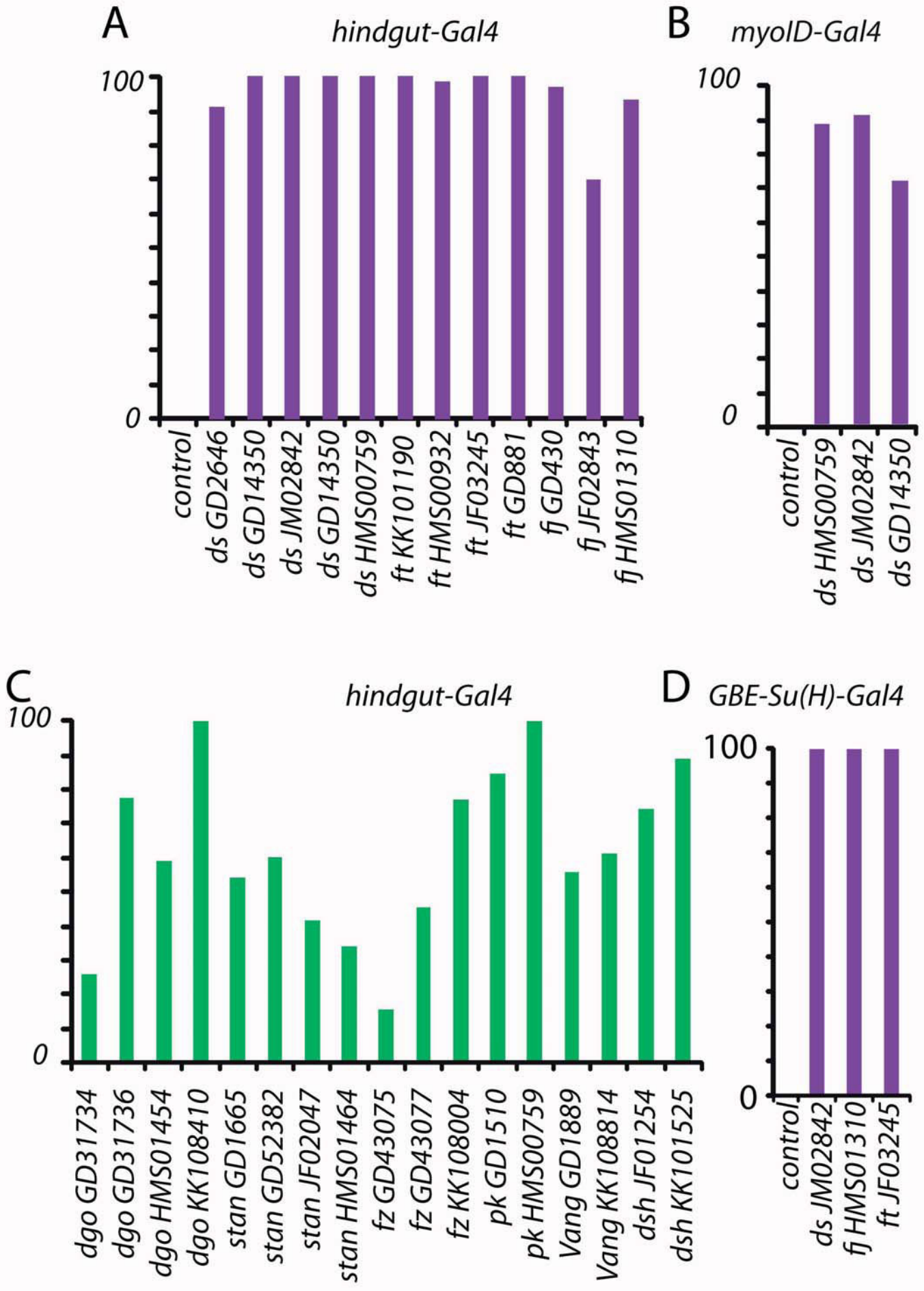

González-Morales et al. Supplementary Figure 2

Evolution of the Adult Hindgut loop

1 Summary

Left-Right organs have appeared multiple times during insect evolution. The most common form of asymmetry is the asymmetric gut looping, present in most insects. In Drosophila, the adult hindgut forms a dextal loop; the direction of this loop is under the control of the *myoID* gene. While *myoID* control all asymmetric organs in Drosophila, the appearance of these asymmetric events ocurred at different evolutionary times. Here we explore the recent appearance of the adult hindgut loop and use it to map a specific cis-regulatory element that likely caused its appearance during Drosophila evolution.

2 Adult hindgut looping is an evolutionary novelty of Sophophora flies

Proper gut packing is thought to be vital for correct gut functioning, and the general insect gut is quite similar among insect groups. However, the AHG shape seems less conserved among insects. In Diptera the AHG shape does not seem a conserved feature, *A. Gambiae* has a very short and straight AHG (Thompson, 2012), and the Glossina tsetse fly has semi looped AHG (Pollock, 1982). Unfortunately morphological descriptions of the AHG within *Drosophilidae* are not available, therefore, to test the conservation of the AHG looping in *Drosophilidae* we analyzed flies from different

Drosophila subgenus using a combination of blue dye feeding and confocal imaging in whole mount abdomens stained with TRITC-conjugated phalloidin.

The *Drosophilidae* family contains several subgenus the most important being *Sophophora* and *Drosophila,* strangely *D.melanogaster* belongs to *Sophophora* subgenus.

Interestingly, all flies that belong to the *Drosophilidae* subgenus *Sophophora*, including *D.melanogaster*, have a completely looped AHG, the exception is *D.takahashii* in which only half of the flies has a stereotyped dextral loop, however flies from the sister subgenus, *Drosophila*, have a randomized S shaped AHG which resembles H1 ablation experiments in *D.melanogaster,* with the exception of *D.hydei* and *D.albomicans* (Figure 13). This interesting phylogenetic pattern suggest that AHG looping appeared during evolution when *Sophophora* bifurcated from the rest of *Drosophila*, 25-40 millions of years ago (Drosophila 12 Genomes Consortium et al., 2007).

The evolutionary pattern suggests that AHG looping has appeared at least twice during Drosophila evolution, a last appearance happened at the Drosophila/Sophophora bifurcation. However to completely rule out the possibility that dextral looping was the ancient condition we screened two outer flies belonging to the same family but a different genus, *Zapronius indianus* and *Scaptodrosophila latifasciaeformis*, in both the

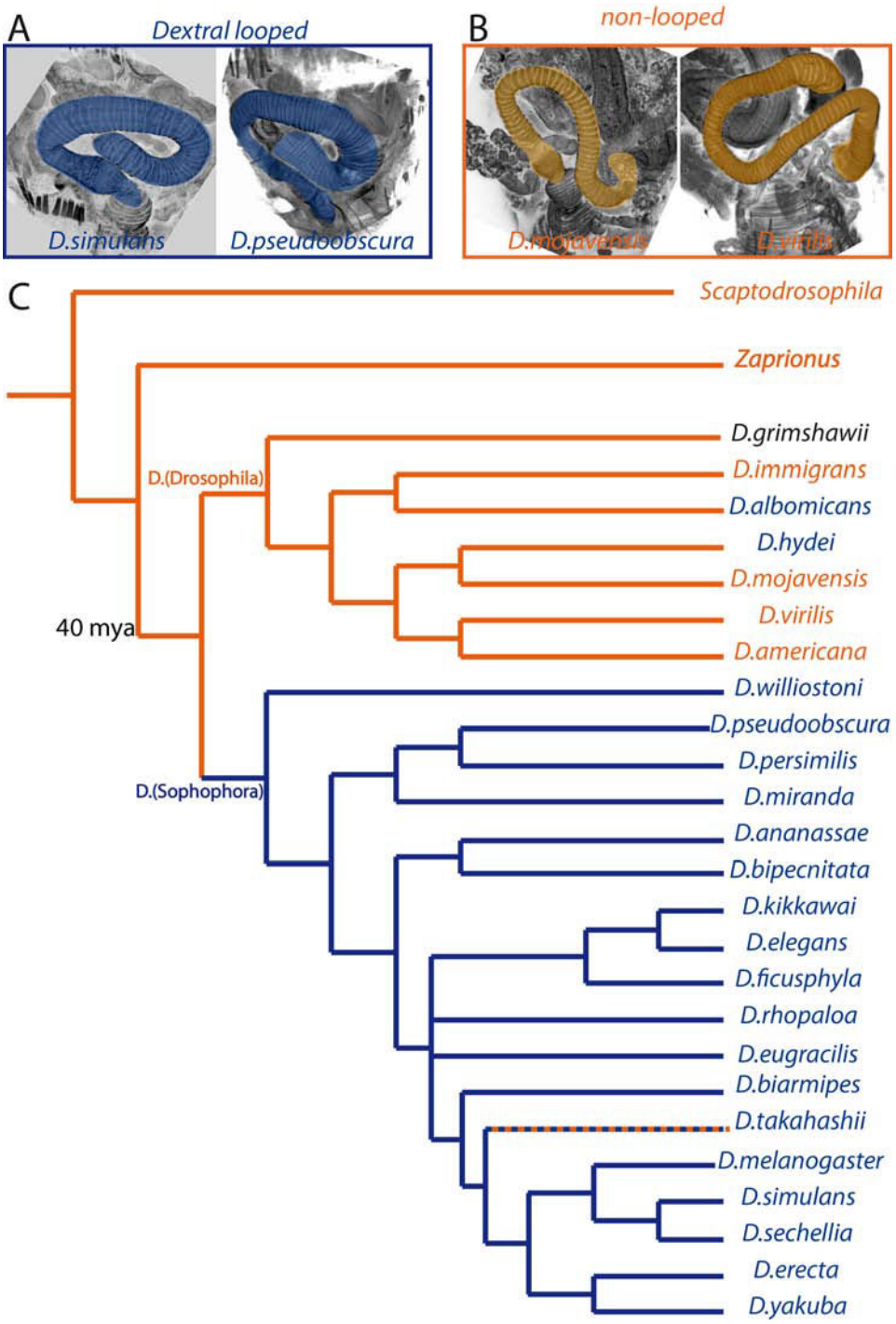

Figure 13. Evolution of the AHG looping direction in Drosophila.

A-B) Confocal images of the AHG of wholemount *Drosophila* species: *D.simulans* and *D.pseudoobscura* (A) , *D.virilis and D.mojavensis* (B). C) Phylogenetic tree of Drosophila family evolution adapted from (Drosophila 12 Genomes Consortium et al., 2007; Gao et al., 2011; van der Linde et al., 2010). Blue color denotes species with dextral loop, while orange denotes species without a clear dextral loop. Doted line for D.takahashii denotes that only half of the flies studied had a dextral loop.

AHG was not dextrally looped (Figure 13). Thus, suggesting that dextral loop was not lost in some Drosophila subgenus species and rather appeared as an evolutionary innovation in the *Sophophora* group, in *D.hydei* and in *D.albomicans* (Figure 13).

L/R asymmetry in Drosophila has been shown to be organ specific; that is the decision of whether a particular organ becomes dextral or not resides at a particular organizer that functions independently from the other L/R organs or organizers. Consistently, the inhibition of one particular organizer impacts only one tissue (i.e removing MyoID from the A8 segment only affects terminalia rotation) and has no effect on any other L/R organ (Taniguchi et al., 2011; Suzanne et al., 2010; Spéder et al., 2006; Petzoldt et al., 2012; Hozumi et al., 2006 Géminard et al., 2014; Coutelis et al., 2013).

In evolutionary terms, having separate organizers may provide the advantage of freely modifying one L/R organ without compromising the integrity on another. A particularly good example of this is the fact that all *Drosophilidae* flies tested have a completely dextrally rotated terminallia, in consistence with previous reports (Suzanne et al., 2010) despite whether or not they have a dextral looped AHG. This observation suggests that the AHG dextral looping appeared without modifying the existing L/R organs (such as the terminalia).

3 Putative AHG Cis-Regulatory Module revealed by conservation scores

MyoID function in L/R determination seem conserved among tissues, it is required in all asymmetric organs. Thus the question of how evolutionary forces act on the same gene (MyoID) to control the appearance of a new dextral organ, without affecting the other asymmetric organs seems to stand out. *myoID* complete gene span is 15kb and its expression is thought mostly to be controlled by specific Cis regulatory modules (CRM) located in the first intron, spanning 8kb (Coutelis et al., 2013;Nègre et al., 2011; Kharchenko et al., 2011).

We then wonder if the appearance of a specific regulatory sequence in *myoID* locus could be associated with the appearance of a dextral AHG loop. Cis regulatory modules or enhancers are normally classified according to their ability to bind specific transcription factors, their ability to promote expression of neighboring genes and its conservation among closely related species. *myoID* expression is controlled by the HOX-bearing protein Abd-B, which indeed binds to *myoID* 1st intron (Coutelis et al., 2013).

Apart from Abd-B binding sites we lacked information regarding functional TF binding to *myoID* locus, to overcome this problem we focused on analyzing functional conservation sites in non-coding regions in *myoId* locus. We reasoned that a particular regulatory element in *myoID* involved in AHG looping would likely be present in looped

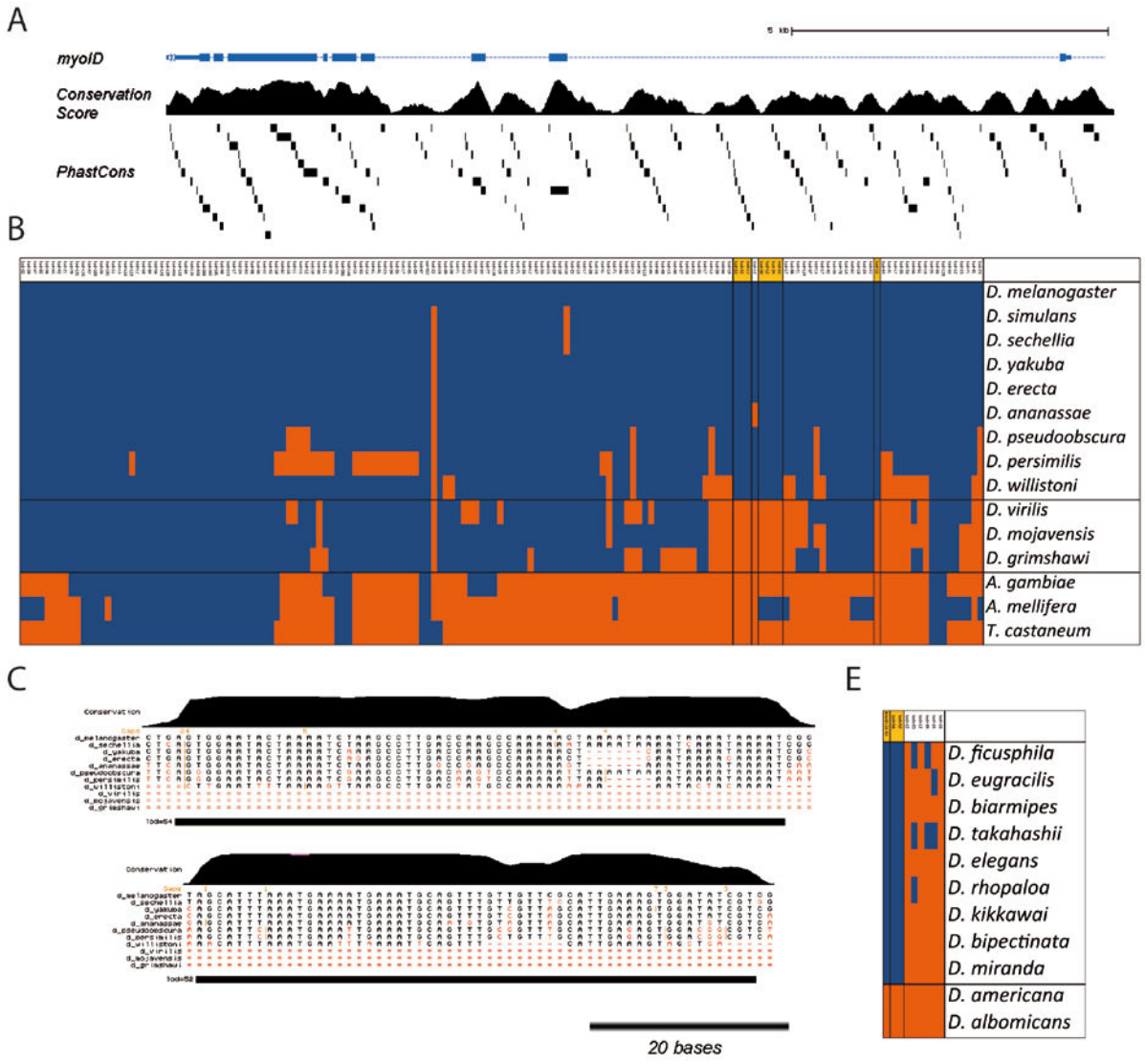

Figure 14. Putative AHG Cis-Regulatory Module revealed by conservation scores

A) MyoID gene span comprises 165 PhastCons sites based on the conservation score obtained from direct compassion to 12 Drosophila species and 3 insects. B) Graphic representation of blastn analysis for each PhastCon site, blue color notes that this sequence is conserved and orange means it was not found in each specied noted. C) Two neighbouring PhastCon sites located in the middle of the 1st intron are the only ones present in looped species and absent in non looped species.

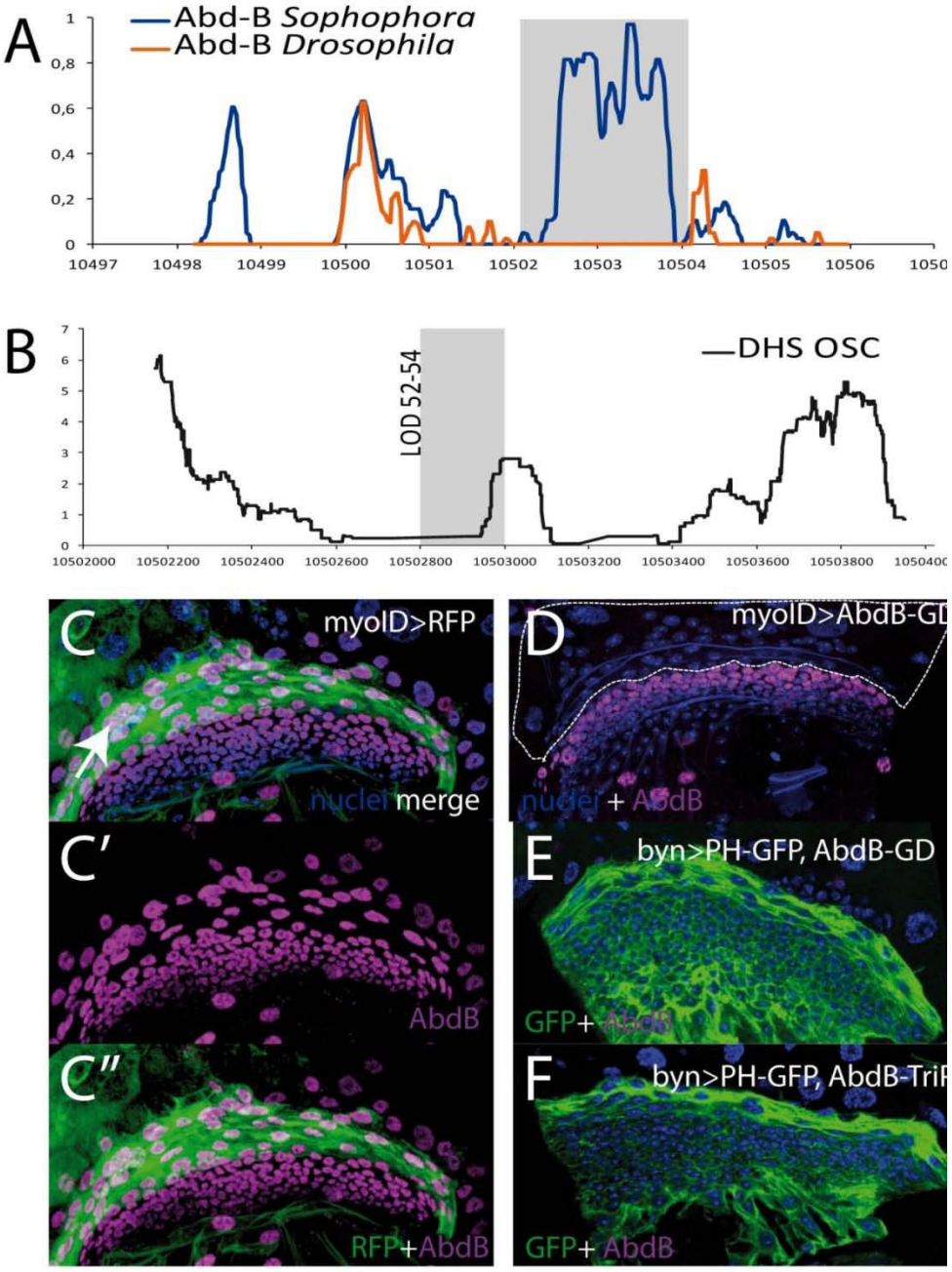

Figure 15. Abd-B in *myoID* regulation.

A) Graphic plot of scores for predicted Abd-B binding sites for all *Sophophora* flies (blue) and Drosophila flies (orange). The LOD52-54 region is highlighted in gray. B) DHS data plot showing the DNA availability in a different tissue, note that LOD52-54 region partially overlaps with one DNAse sensitive peak. C) Confocal image of the AHG precursor expressing RFP under the control of *myoID* regulatory elements (green) and stained for Abd-B. Abd-B is detected in a gratient starting at the anterior, *myoID* expressing cells with decreasing intensity at the posterior end. D) Specific down regulation of Abd-B following the expression of a specific RNAi in *myoID* expressing cells renders Abd-B protein undetectable in these cells (inside dotted line). E, F) Donwregulation of Abd-B in the complete AHG promordium using two different RNAi conditions.

flies and absent in non-looped flies. To test this, we first classified all regions in *myoID* locus with a high conservation score from a genome wide conservation score study from *D.simulans, D.sechellia, D.yakuba, D.erecta, D.ananassae, D.pseudoobscura, D.persimilis, D.willistoni, D.virilis, D.mojavensis, D.grimshawi, A.gambiae, A.mellifera and T.castaneum* (Siepel, 2005). We then isolated 160 highly conserved sites (PhastCon sites, LODs) spanning the entire *myoID* locus (Figure 14)

Conservation scores in these PhastCon sites was calculated by a mix of looped and non looped insects, thus to uncover the specific ones that are distinct from looped flies and non looped ones we performed a Blast-search for each PhastCon sequence from *D.melanogaster* against 12 *Drosophila* flies with genome sequence previously annotated. While most sites are conserved among all the 12 species (Figure 13B) we found 7 sites, clustered together in a 521 bp region which is present in all looped flies and missing in all non looped flies (Figure 13C).

During the course of this study, several other Drosophila flies genome became sequences, though not completely annotated. To confirm the specificity of the region to looped flies, we expanded our search to include 13 other Drosophila species whose genome complete sequence became recently available (*D. albomicans, D. americana, D. biarmipes, D. bipectinata, D. elegans, D. eugracilis, D. ficusphila, D. kikkawai, D. mauritiana, D. miranda, D. rhopaloa, D. santomea, D. suzukii and D. takahashii*). Using a similar strategy, we performed a BLAST search for *the PhastCons* we previously obtained.

Consistent with our hypothesis PhastCons sites (LOD52 and LOD54) inside the "Looped-specific-region" were found present in looped flies but absent in non-looped ones. Al together these data confirms that one region in *myoID* locus appeared at the same time as dextral looping (Figure 13E).

4 Abd-B expression/function in the AHG organizer

The identification of two PhastCon sites, LOD52 and LOD54, selectively present in looped species in a region annotated as enhancer containing at the middle of the 1st intron (Kharchenko et al., 2011) suggested the appearance of a cis regulatory module. As noted above, except for Abd-B we lacked information regarding transcription factor binding at the *myoID* locus, therefore we concentrated in analyzing AbdB binding sites. We then analyzed AbdB predicted binding sites in all Drosophila species along the 1st intron, using the FlySurvey Database of mapped predicted binding sites (Noyes et al., 2008; Christensen et al., 2012; (Brodsky and Wolfe, 2014).

Our analysis showed accumulation of Abd-B putative binding sites in one particular region overlapping with LOD52-54 when predicted in all looped species (Sophophora) but absent in that particular region all non-looped species (Drosophila) (Figure 15A).

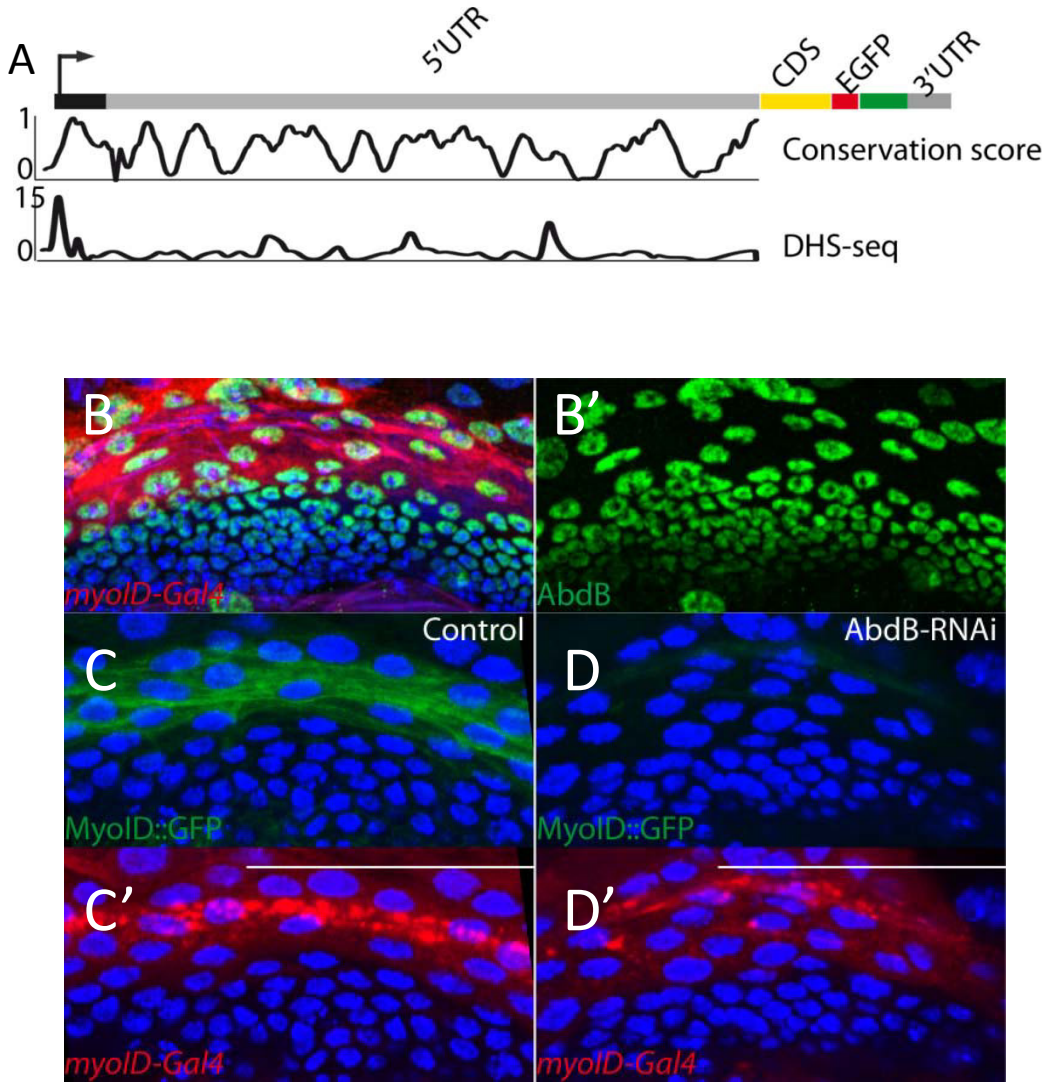

Figure 16. Abd-B downregulation affects *myoID* expression.

A) Schematic representation of genomic *myoID* reporter line containing the promoter (black) the 1st intron (gray), the coding sequence (yellow), HA and GFP (red and green); below is plotted the conservation score and the DNAse hypersensitive sites score. B) MyoID (red) and Abd-B (green) colocalize in H1 cells. C) The genomic *myoID* reporter line (green) is detected in the same pattern as *myoID-Gal4 UAS-RFP* (red), in H1 cells. D) Down regulation of Abd-B using a RNAi construct impacts *myoID* reporter expression.

Abd-B expression in *myoID* expressing cells has been documented in the genital disc, in the testis and in the embryonic gut (Coutelis et al., 2013; Papagiannouli et al., 2014). However, the expression of *Abd-B* in the AHG primordium remains elusive. We then stained for an antibody that specifically recognizes Abd-B in the AHG primordium; to mark *myoID* expressing cells (H1 cells) we used *myoID-Gal4* in combination with *UAS-RFP*. Abd-B can be detected as a gradient starting at *myoID* expressing cells with decreasing detection intensity towards the posterior end (Figure 15C). Consistently, expression of an RNAi hairpin directed against *Abd-B* in H1 cells renders Abd-B undetectable in H1 cells only (Figure 15D), and the expression of two different *Abd-B* RNAi constructs in the whole hindgut completely abolish Abd-B detection (Figure 15 E, F).

To demonstrate the role of Abd-B, previously described in other tissues, of controlling *myoID* expression (Coutelis et al., 2013; Papagiannouli et al., 2014), we first followed *myoID* expression in the imaginal ring using an reporter line carrying *myoID* promoter and 1st intron followed by *myoID* and *GFP* coding sequences, called *myoID::GFP* (Figure 16A). As previously reported *myoID::GFP* expression is detected in the first row of cells, H1 cells (Figure 16C) and this expression is no longer detected when Abd-B is depleted from *myoID* expressing cells using the H1 specific myoID-Gal4 (Figure 16D).

5 CRISPR/Cas9 mutants induce tissue specific phenotypes

Through the analysis of aligned sequences of all sequenced Drosopohila species we reached a region in the 1st intron of MyoID likely responsible for the appearance of the AHG looped throught the evolution of flies. In summary, this region i) is present only in looped species and absent in non-looped species; ii) it is classified as an enhancer from the modENCODE project and iii) it has conserved (in looped species) binding sites for the HOX bearing protein Abd-B, which has been shown to control *myoID* expression in other tissues.

In order to functionally test this region we took advantage of the recent method for inducing specific deletions anywhere in the genome through the induction of precise breaks via the CRISP/Cas9 system. Briefly there are two minimal components required for the induction of DNA breaks: the presence of the Cas9 nuclease and a chimeric RNA (chiRNA) comprising the crRNA and tracrRNA. Thus, in this modified CRISPR RNA/Cas9 system a common nuclease is directed to specific DNA sequences by a short, readily generated RNA (Ren et al., 2013; Port et al., 2014; Gratz et al., 2013). The injection of two chiRNA induces a specific deletion between the two chiRNA injected. We injected two chiRNA aiming for a deletion of the whole 1st intron or the looped-specific region (see materials and methods) Intron mutants were identified by the terminalia phenotype while the AHG enhancer mutants were identified by genomic PCR (Figure

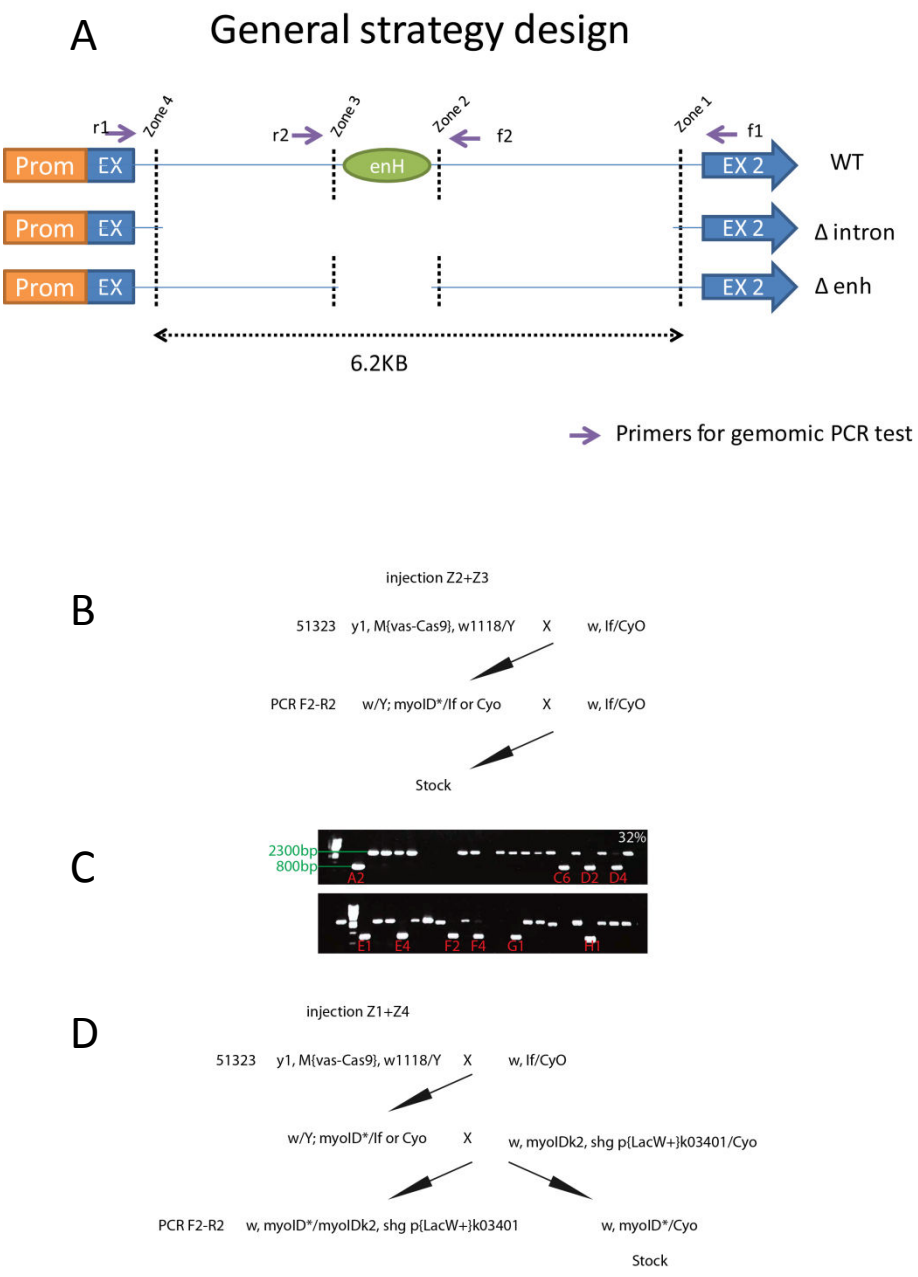

Figure 17. Generation of enhancer specific CRISP mutants in myoID locus.

A) General strategy scheme for generation *myoID* CRISP mutants. Prom: promoter, Ex: exon1, enH: hindgut enhancer, Ex2: exon 2, purple arrows denote primers and CRISP sgRNA target sites are noted by dotted lines (zone 1-4).

B) Crossing scheme for enhancer *myoID* mutant. Both Z2+Z3 sgRNA were injected in flies expressing *vas-Cas9,* the males were recovered and crossed to a balancer in mass, then individual males from the resulting progeny were crossed again against a balancer and were used as PCR template for primers F2-R2 right after copulation to maintain the progeny. Finally the progeny from males carrying a positive deletion were used to generate an stable stock.

C) Representative PCR product in 1% agarose gel. Wildtype PCR product f2+r2 results in a band of around 2.3Kb, while the expected deletion result in 0.8Kb. Positive lines are denoted by red text indicating the stock number. The overall efficiency was 32%

D)

Crossing scheme for 1st intron *myoID* mutant. Both Z2+Z3 sgRNA were injected in flies expressing *vas-Cas9,* the males were recovered and crossed to a balancer in mass, then individual males from the resulting progeny were crossed again against flies carrying a *myoID* null allele and a lethal p-element carrying a mini-white marker. The progeny was scored for defects and the stock if positive maintained.

E) Representative pictures from a non deleted *myoID* intron and a positive deleted intron with a mislooped terminalia.

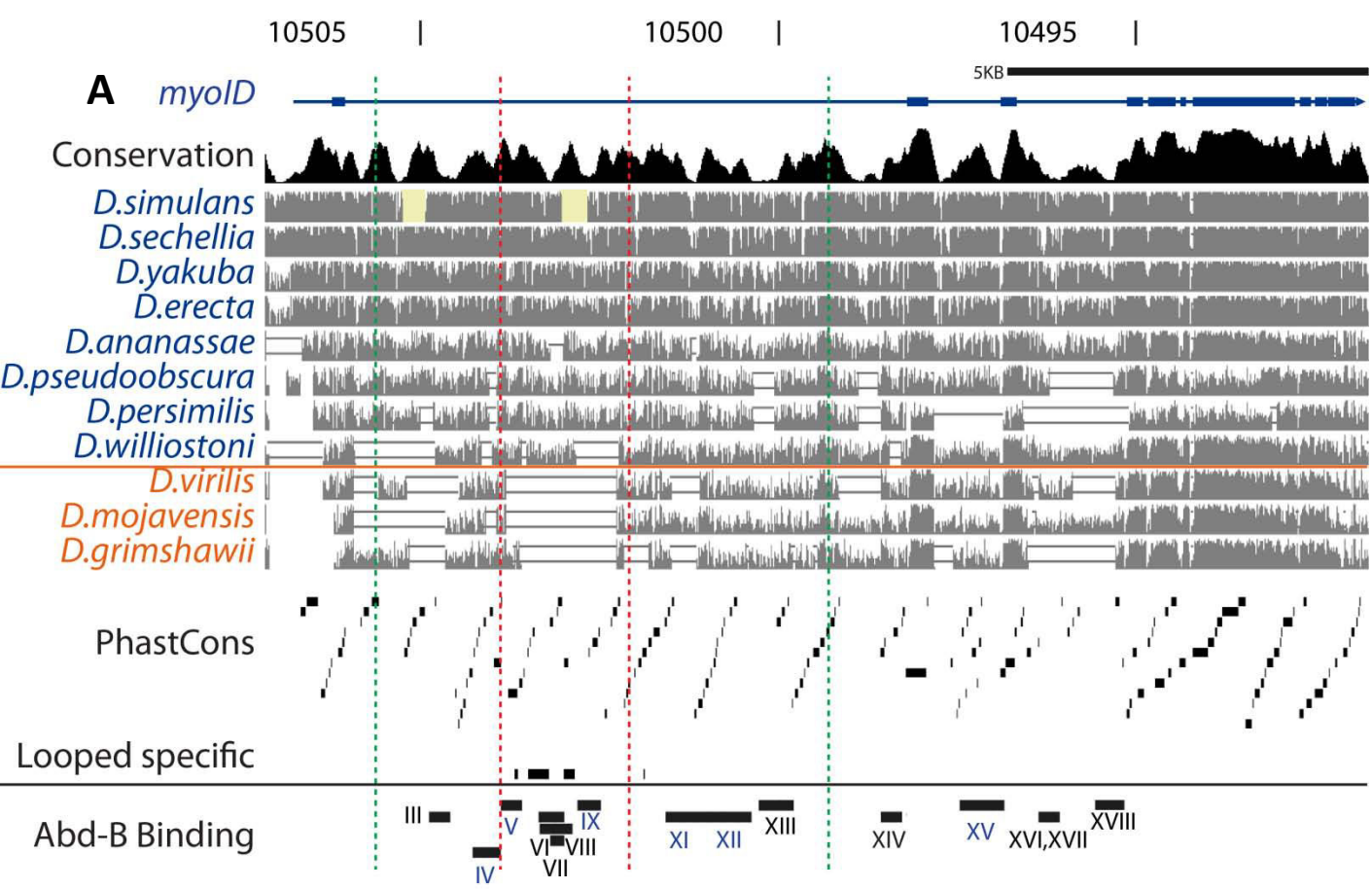

B

Genotype	Terminalia	Adult Hindgut	Testis
Wild Type (w-)	Dextral	Dextral	Dextral
myoID null	Inverted	Inverted	Inverted
myoID AHG enhancer	Dextral	Mislooped	Dextral
myoID 1st intron	Inverted	Inverted	Dextral

Figure 18. Genomic map of Crisp Mutants and regions specific for Sophophora (looped) flies.

(A) MyoID gene span comprises 15 Kb sites. Conservation score and local alignments for both looped (Sophophora in blue) and non-looped (Drosophila in orange) were calculated based on the alignment from 12 Drosophila species and obtained from the UCSC table Browser (Siepel et al., 2005). Abdb Binding regions (black) were obtained from (Coutelis et al., 2013). Looped specific regions were calculated from *myoID* alignements in Galaxy software. CRISPR induced specific mutants are shown as dotted green (AHG enhancer) and red (1st intron) lines . (B) Table of overall phenotypes induced by specific deletions in *myoID* locus.

17).

Consistent with our hypothesis, the deletion of the 1st intron of *myoID* phenocopies *myoID* null mutations in both the terminalia and the adult hindgut (Figure 18). Strangely, the testes appear normally looped, wild type appearance. A recently publish paper in which genome wide Abd-B binding sites were collected using a DAM-ID approach identified the promoter region in the myoID locus as the sole binding site for Abd-B in the testis (Papagiannouli et al., 2014). Consistent with this previous report our intronic mutant has a normal looped testis despite having an inverted terminalia and Adult hindgut (Figure 18). On the other hand, the *AHG enhancer* mutant, which completely deletes the looped-specific region in *myoID,* has a mislooped adult hindgut phenotype without affecting the terminalia or testes (Figure 18). This result alone, demonstrates that the region which appearance correlates with the appearance of dextrally looped adult hindgut during *Sophphora* bifurcation, around 40 million years ago is responsible for the looping of the AHG. As this region contains Abd-B binding sites is likely functioning as an enhancer of *myoID* expression in the AHG primordium (Figure 18). Therefore, in the enhancer mutant this expression is likely diminished but not completely absent since the overall phenotype is a mislooped AHG instead of a completely inverted one. Though at present we cannot rule out the possibility of a distinct role of this particular region involved in AHG looping independent of *myoID* expression we consider this possibility very unlikely.

Regional division and development of the Adult Hindgut in Drosophila

1 Introduction

The typical gut of an insect consists of the foregut, the midgut, and the hindgut (Lemaitre and Miguel-Aliaga, 2013). While the foregut and the midgut are the main sites for nutrient assimilation, the hindgut is where most of water and ions are reabsorbed if needed (Lemaitre and Miguel-Aliaga, 2013). In the last decades, there has been a substantial advance towards the understanding of the development and the function of the intestine in Drosophila. However, most studies have been focused in the Drosophila, midgut, and in contrast not so much is known about the last portion of the gut, the hindgut.

The adult hindgut is a specialized structure in insects that serves for water and ion re-absortion. It is broadly divided into the pyloric region, the ileum and the rectum (Gupta and Berridge, 1966; Takashima et al., 2008; Fox and Spradling, 2009). The adult pylorus is formed by the pyloric valve and adjacent to the HG, the stem cells of the pylorus. The exact nature of these stem cells is not completely resolved. They have been shown to be normally quiescent but to divide upon stress. Their progeny in the AHG has been followed until the pylorus, but never in the ileum or rectum (Fox and Spradling, 2009). The adult ileum is formed by only one type of big polyploidal cells and is the biggest part of the AHG (Takashima et al., 2008). Finally, the adult rectumIt is a rounded

structure that host 4 conic structures called rectal papillae that serve as the last water reapportion organ (Fox et al., 2010). From the outside the rectum is covered by strong musculature and the rectal sheath epithelium and from lumen side it hosts a dense layer of cuticle (Fox et al., 2010; Peacock and Anstee, 1977).

The adult hindgut stem-cell region, pylorus and ileum develop from the imaginal ring, a structure present in the larval gut that contains around 600 diploid cells. Based on lineage tracing experiments the imaginal ring is recognized to be the adult hindgut (AHG) precursor (Murakami and Shiotsuki, 2001; Murakami et al., 1994; Fox and Spradling, 2009). However the rectum has a completely different origin, it comes directly from polyploidal mitotic divisions of the larval rectum (Fox et al., 2010).

Most hindgut studies in *Drosophila* have been limited by the available genetic tools. In Drosophila, the Gal4-UAS system is widely used to manipulate gene expression in a tissue- or cell-specific manner (Brand and Perrimon, 1993), but in the Drosophila hindgut, there are no region-specific Gal4 lines available. Here we describe a set of Gal4 lines with restricted expression patterns in the adult hindgut and in their progenitors in the imaginal ring. Moreover, through the analysis of lineage tracing experiments we identify the progenitors of the AHG main regions.

In this study we use the recently constructed collections of enhancer trap lines containing putative enhancer fragments fused upstream of a Drosophila core synthetic promoter is followed by the yeast transcription activator protein GAL4 to assess the regional compartmentalization in the AHG (Pfeiffer et al., 2008). We report the

expression pattern of 21 Gal4 lines in the AHG and in the imaginal precursors. We further describe lineage tracing manipulations to show that the compartments are already present in larval precursor cell populations. Our work will facilitate the functional studies of the adult hindgut in Drosophila.

2 Selective screen for Gal4 lines differentially expressed in the AHG

In order to fast-screen for Gal4 lines driving expressing in the AHG we designated a biased approach based of known expression patterns.

More than 50 Gal4 lines from the Flylight project collection (Pfeiffer et al., 2008) were chosen among a collection of by their expression pattern in imaginal discs (Jory et al., 2012; Manning et al., 2012). Briefly, we selected exclusively lines which were expressed in all imaginal discs, thus raising the possibility of them to be expressed in the hindgut imaginal ring, and lines with a clear biased pattern in the anterior-posterior axis, thus selecting lines with higher chances of differential expression patterns along the adult hindgut and hindgut ring.

On the other hand, 20 Gal4 lines from the Vienna Tile collection were selected for their predicted associated gene that are known to be highly expressed in the AHG, according to the Fly Atlas project (Robinson et al., 2013).

Flies bearing the Gal4 constructs, from both collections, were then crossed to flies containing the UAS-MCD8cherry transgene and the F1 was analyzed at both adult

and Larval 3th stage for red fluorescence under an epifluorescence microscope.

We then selected 21 Gal4 lines (2 from the Vienna Tile collection and 19 from the Flylight project) with reproducible AHG expression pattern and 6 Gal4 lines with reproducible imaginal ring expression pattern (Supplementary Table 3).

3 AHG subdivision revealed by Gal4 expression patterns

In order to establish a proper comparison between Gal4 expression patterns we used an insertion carrying 10XStat92E-GFP (Stat-GFP) a GFP reporter, generated by placing Stat92E binding sites from a Stat92E target gene (Socs36E) upstream of enhanced GFP, that accurately reflect activity of the Drosophila JAK/Stat pathway (Bach et al., 2007).

In the Adult hindgut Stat-GFP is mainly detected in the stem-cell region anterior to the pylorus and in the rectal junction cells. In order to use Stat-GFP as a counter stain we first constructed flies carying the Gal4 and the UAS-MCD8cherry transgenes and crossed them to Stat-GFP bearing flies. The F1 adults were analyzed for both GFP and RFP fluorescence.

Non-overlapping regions were deduced from Gal4 expression patterns. From the 21 Gal4 lines with reproducible AHG expression pattern we divided the AHG in 9 genetically different sub regions (Figure 19A), several Gal4 lines were found to be

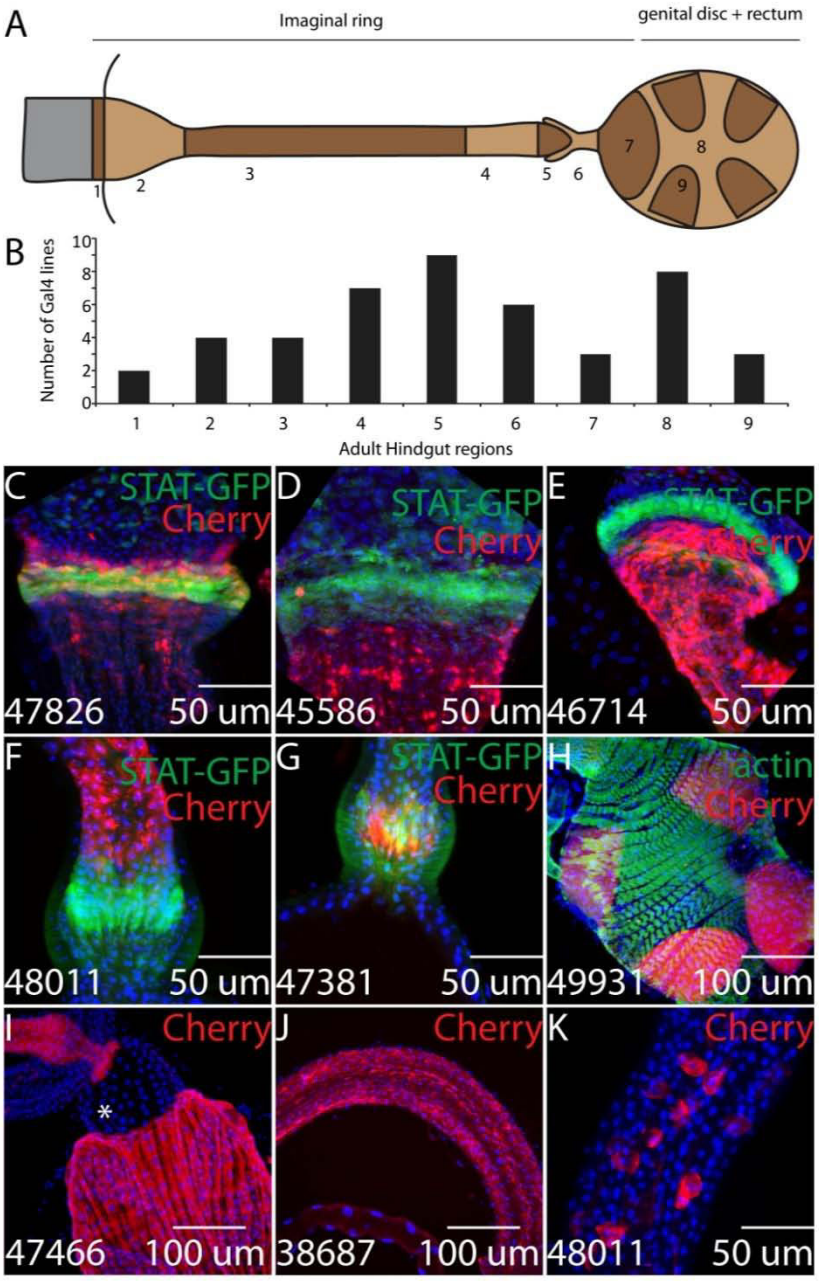

Figure 19. Subdivision of the AHG based on Gal4 expression patterns

A) Illustration describing the AHG regions identified in this study; regions are numbered starting from the most anterior; this include: 1 the stem cell region, 2 the pylorus , 3 the anterior ileum, 4 the posterior ileum, 5-7 the rectal junction, 8 the rectal sheath and 9 the rectal papillae.

B) Histogram of the number of Gal4 lines with expression in each AHG region.

C) *Stat-GFP* and *47826-Gal4, UAS:MCD8-cherry* are both expressed in the stem cell region

D) *45586-Gal4, UAS:MCD8-cherry* is expressed in the pylorus, abutting the *Stat-GFP* positive stem cell region.

E) *46714-Gal4* is also expressed in the pylorus and not in the stem cell region

F) *Stat-GFP* is detected in the rectal junction regions, while *48011-Gal4, UAS:MCD8-cherry* is detected immediately anterior to the rectal junction, in the posterior ileum.

G) *47381-Gal4, UAS:MCD8-cherry* is detected in the *Stat-GFP* positive cells in the rectal junction

H) *49931-Gal4* drives expression specifically in the rectal papillae, F-actin is shown in green as counter stain.

I) *47466-Gal4, UAS:MCD8-cherry* marks the rectal junction regions 5 and 6 but it is absent in region 7 (asterisk), it is also detected in the rectal sheath

J) *38687-Gal4, UAS:MCD8-cherry* is detected in the anterior ileum.

K) *48011-Gal4, UAS:MCD8-cherry* is also detected in the anterior ileum as random cell clusters.

All images are oriented anterior to the top, unless stated Stat-GFP is shown in green and Gal4 expression detected by Cherry fluorescence is shown in red. Scale bars are shown.

expressed at each region (Figure 19B). Lines expressed at the stem-cell region (region 1) were revealed by the overlapping expression of Stat-GFP (Figure 19C). Similarly lines with abutting expression posterior to Stat-GFP positive region were designated as the pylorus or region 2 (Figure 19D, E).

The ileum is considered a homogeneous organ, however we found two genetically distinct regions in the ileum; we designated these as Anterior and Posterior Ileum respectively (Figure 19F, K). Surprisingly, we found one particular line which drove expression in both the anterior and posterior ileum regions; it is noteworthy that its expression in the anterior ileum was observed in specific cell clusters (Figure 19K) and not homogeneously as other anterior Gal4 lines (Figure 19J). This specific pattern has never reported for this tissue before, however it might not represent a specific region on its own since this pattern was never found with any other Gal4 construct and we never found the opposite pattern. These result together show clearly that the ileum is not as homogeneous structure as previously thought and that is formed by distinct genetic regions.

The rectum containing the rectal sheath and the rectal papillae (Regions 8 and 9) develops from the genital disc and the larval rectal cells respectively. Thus in the most posterior part of the AHG that develops from the imaginal disc is the junction between the ileum and the rectum, the rectal junction. We found three genetically distinct regions in the rectal junction, regions 5 to 7. Region 5 being the region where most of Gal4 lines were expressed (Figure 19B). Region 5 and 6 together form a ball and socket

appearing structure, being region 5 the inner part and region 6 the outer part (Figure 19G). On the other hand, region 7 comprises a group of cells that invade the rectum, particularly *47466-Gal4* was particularly useful to detect this region as it is expressed in region 5, 6 and 8 but not in region 7 (Figure I9). Finally, the rectum is formed by the rectal sheath and the rectal papillae, regions 8 and 9, we found 8 lines expressed in the rectal papillae and 3 in the rectal sheath (Figure 19H, I).

4 Lineage tracing experiment confirms progenitors of all the AHG

We have previously shown that all the AHG except for the rectum comes from the H2 cells only; H1 cells instead do not proliferate and degrade during pupal development in a structure called the pupal midgut (See previous chapter and Takashima et al., 2011).

While looking for Gal4 lines expressed in the larval imaginal ring, we isolated two Gal4 lines, *49732-Gal4* and *bynVT-Gal4*, which are expressed in all H2 cells. *49732-Gal4* contains the promoter region of the *sixbanded* gene (*sba*) it's expression covers all the imaginal ring, H1+H2, from the most anterior Stat-GFP positive cells to the most posterior part in contact with the pylorus (Figure 20A and B). In contrast, *bynVT-Gal4* expression is restricted to H2 cells and is not present in H1 cells marked by *MyoID::GFP*, a constructed reporter for the expression of the H1 specific gene *myoID* (Figure 20D). Surprisingly, *bynVT-Gal4* is sometimes not expressed in all H2 cells and randomly

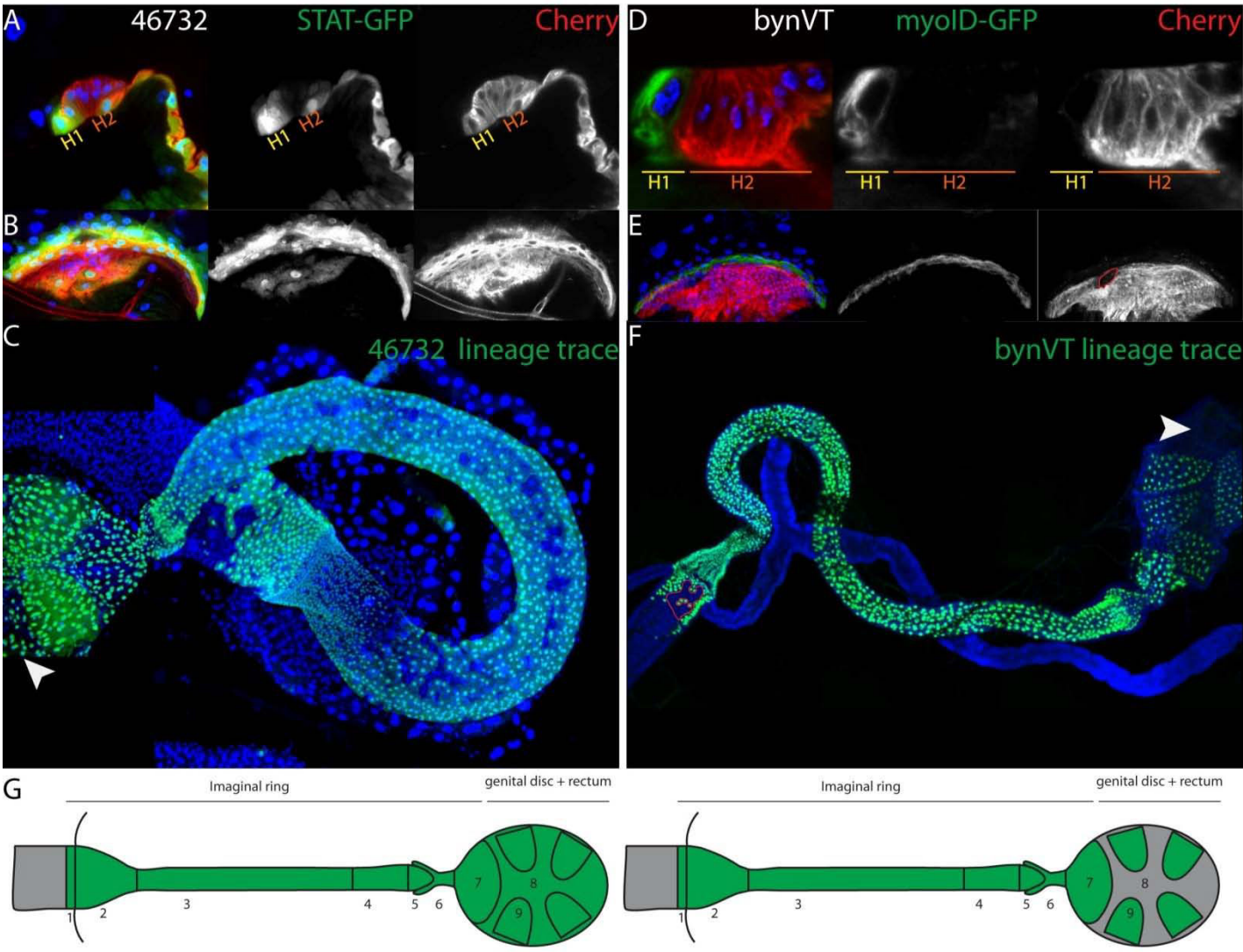

Figure 20 AHG precursors detection using linage tracing and selective Gal4 lines

A) Sagital view of an imaginal ring expressing *46732-Gal4, UAS:MCD8-cherry* (red) and *Stat-GFP* (green).
B) Top view of an imaginal ring expressing *46732-Gal4, UAS:MCD8-cherry* and *Stat-GFP*
C) Lineage descendent cells of *46732-Gal4*, *UAS:MCD8-cherry* larval expressing cells marked in the adult hindgut by nGFP, note all the AHG has nGFP including the rectal sheath (asterisk)
D) Section of an imaginal ring expressing *bynVT-Gal4*, *UAS:MCD8-cherry*(red) and *Stat-GFP* (green).
E) Top view of an imaginal ring expressing *bynVT-Gal4*, *UAS:MCD8-cherry* and *Stat-GFP*. Note the RFP negative spot encircled by a red line.
F) Lineage descendent cells of bynVT-Gal4 larval expressing cells marked in the adult hindgut by nGFP, note the lack of nGFP positive cells in the rectal sheath and the GFP negative region in the stem cell area marked by a red line.
G) Illustration describing in green the linage of *46732-Gal4* and *bynVT-Gal4* expressing cells respectively; regions are numbered as in Figure 1. All images are oriented anterior to the left.

distributed RFP-negative patches are often seen (Figure 20E).

Next we wondered whether we could follow lineage tracing experiments to evaluate the contribution of specific cell populations to the final AHG. To test this we crossed flies containing *49732-Gal4* and *bynVT-Gal4* to flies carrying *TubP:Gal80ts*, *UAS-FLP, Ubi-p63E(FRT.STOP.FRT)Stinger*. Following a temperature heat shock during larval period (see Materials and Methods section) the descendant cells are permanently marked in the adult tissues with nuclear GFP (Evans et al., 2009).

Consistently, with our previous report, the GFP positive cells, marking the lineage from the *49732-Gal4,* H1+H2 cells precisely, cover all the structures in the AHG (Figure 20C). Some GFP negative cells are often seen; their random positioning suggests that our lineage strategy is not perfectly efficient. It has already been shown that the Flipase dependant excision of the FRT.STOP.FRT "Flip-out" cassette is not 100% efficient and thus random GFP negative patches are often seen (Evans et al., 2009). Never the less, since a big proportion of cells for each region are GFP marked we conclude that this method is accurate enough to detect the specific cell lineages in the AHG.

The gene *byn* codes for a T-Box Transcription factor required for specification of the larval hindgut, with restricted expression to the hindgut (Singer et al., 1996). The *bynVT-Gal4* is a Gal4 containing line part of the Vienna Tile collection containing part of byn genetic regulatory elements. During Larval stages it drives expression in the entire hindgut except for H1 cells (Figure 20D and E).

The linage analysis from *bynVT-Gal4* revealed a GFP pattern all along the AHG

except for the rectal sheath, which originates from the genital disc (Figure 20F). As expected, some random GFP negative patches are also often seen, we assume these are the result of non saturated efficiency at the flip-out cassette lineage tracing method together with weak patchy Gal4 expression. Thus using this approach we confirmed that the whole adult hindgut comes from H2 cells only.

To our knowledge the specific progenitors that give rise to each region of the hindgut are not known. Therefore, in order to better clarify the specific origins of the hindgut regions we made lineage tracing experiments with Gal4 lines driving expression in specific patterns in the imaginal ring.

5 The progenitors of the rectal junction

The line *45926-Gal4* covers a small region in the 1st intron of the *invected* gene (*inv*), when crossed to flies bearing a *UAS-MCD8cherry* transgene it specifically marks all the pylorus and the last row of cells in the imaginal ring in the larval hindgut (Figure 21A and B). The pylorus is degraded during pupal development and therefore it is not likely to contribute to any adult structure, however *45926-Gal4* in the last row of cells of the imaginal ring, marked by Stat-GFP strongly suggests they are involved in the development of the adult hindgut.

Visualization of GFP fluorescence following by our lineage tracing method in

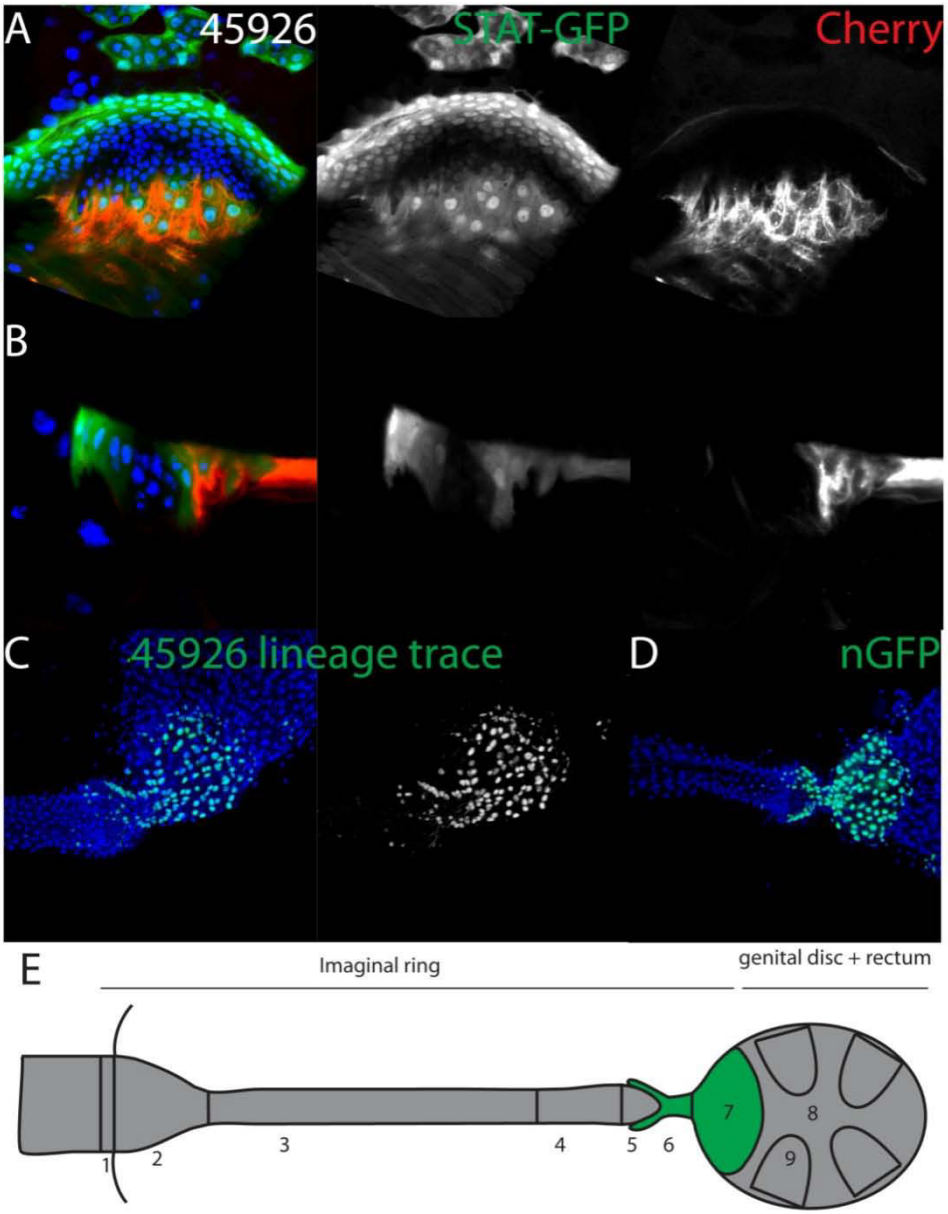

Figure 21 The rectal junction precursors

A) Top view of an imaginal ring expressing *45926-Gal4*, *UAS:MCD8-cherry* (red) in the pylorus and the rectal junction precursors in the imaginal ring, marked by *Stat-GFP*(green).

B) Sagital section of an imaginal ring expressing *45926-Gal4* and Stat-GFP.

C) Close-up image of the rectal junction expressing nGFP in the linage of *45926-Gal4* larval expressing cells, including regions 6 and 7.

D) Continuous lineage tracing results in similar linage expression pattern, containing regions 6 and 7.

E) Illustration describing in green the linage of 45926-Gal4 expressing cells; regions are numbered as in Figure 1. All images are oriented anterior to the left.

45926-Gal4 expressing cells revealed a portion of the adult hindgut in the rectal junction with GFP positive cells, regions 6 and 7 but not region 5 (Figure 21C). These regions are the most posterior ones deriving from the imaginal ring, the rectal rectal papilla and sheath have rectal and imaginal disc origins respectively.

To ensure that the lack of region 5 cells is due to the lack of gal4 expressing progenitors and not from a weak efficiency of the lineage flip-out cassette and since this particular Gal4 line does not drive expression in the AHG (Supplementary Table 3) we changed our Lineage strategy toward a continuous temperature shock thus increasing the flip-out efficiency but loosing the temporal resolution. Indeed, in an always active lineage analysis region 6 and 7 are GFP positive while cells in region 5 were not detected (Figure 21D) These results suggest that the most posterior cells of the imaginal ring give rise to the most posterior regions of the AHG, 6 and 7. Moreover, these results are in agreement with a model for AHG development in which cell migration does play an important role as has been already suggested based on the analysis of mitotic clones (Fox and Spradling, 2009).

6 The progenitors of the anterior ileum

The *38386-Gal4* line covers a specific enhancer for the predicted isoforms B and F of the *E2F transcription factor* (*e2f*). *38386-Gal4,* when crossed to flies bearing a *UAS-MCD8cherry* transgene, specifically marks a line of cells in the middle of the

Figure 22 . The anterior ileum precursors

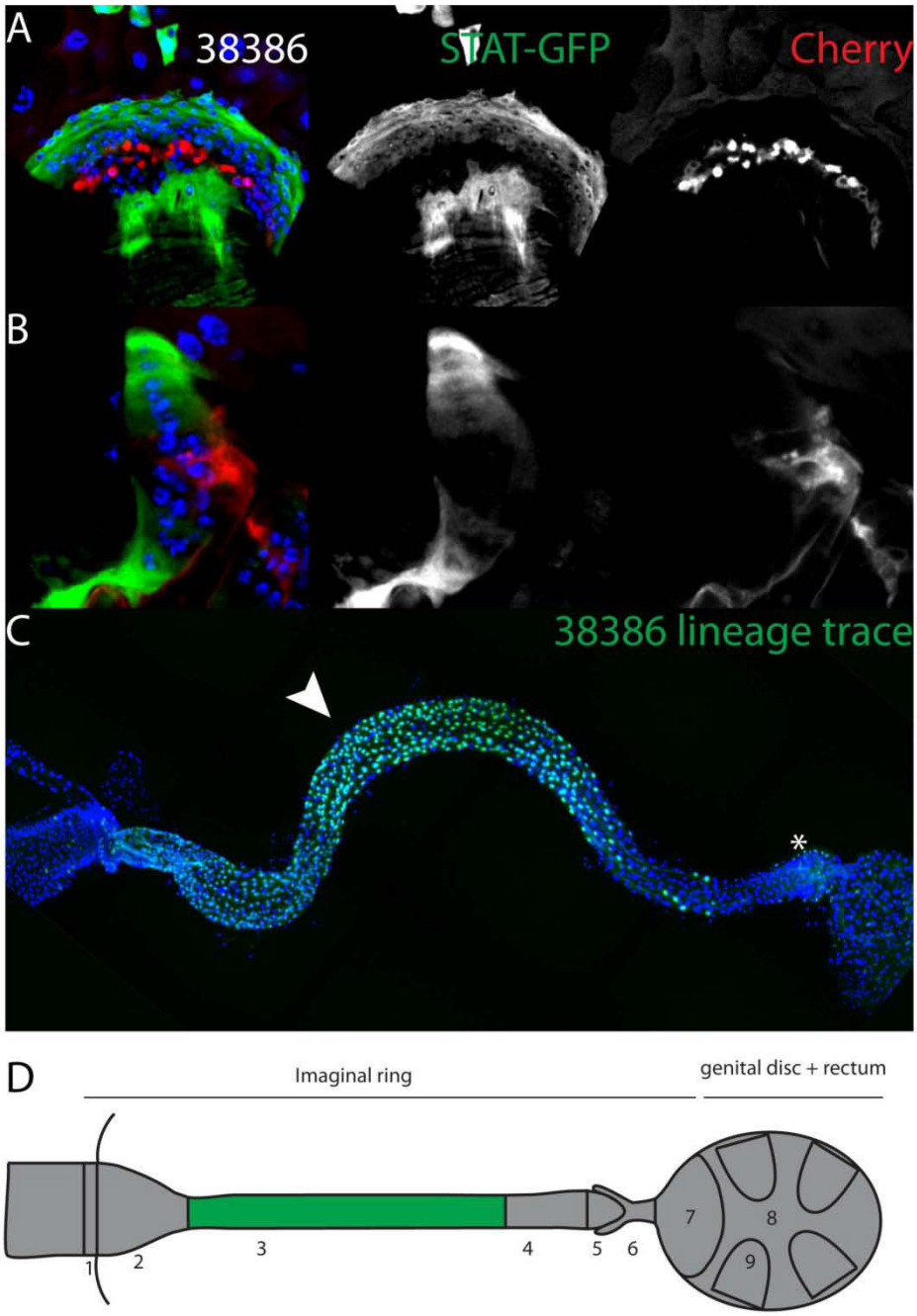

A) Top view of an imaginal ring expressing *38386-Gal4*, *UAS:MCD8-cherry* (red) in the ileum precursors, located in the *Stat-GFP* negative portion at the middle of the imaginal ring.
B) Sagital section of an imaginal ring expressing *38386-Gal4*, *UAS:MCD8-cherry* and *Stat-GFP*; note that Cherry positive cells are not *Stat-GFP* positive .
C) Complete AHG confocal image showing nGFP in the anterior ileum, the descendants of *38386-Gal4* larval expressing cells (arrowhead), nGPF is also seen at the muscles of the rectal junction (asterisk) which are not developing from the imaginal ring.
D) Illustration describing in green the linage of *38386-Gal4* expressing cells; regions are numbered as in Figure 1. All images are oriented anterior to the left.

Stat-GFP negative portion of the imaginal ring (Figure 22).

The anterior Stat-GFP positive cells are comprised by the H1 cells which degrade during pupal development and likely the progenitors of the AHG stem cells. Therefore, *38386-Gal4* positive cells, which do not overlap with Stat-GFP, are the precursors of the pylorus and the ileum. We then followed the lineage of these cells throughout development; following lineage tracing GFP positive cells appear mostly in the anterior ileum, but also as scattered cells in the posterior ileum and the pyloric region (Figure 22). Since the majority of cells are located in the anterior ileum (Region 3) we suggest that *38386-Gal4* marks the ileum progenitors, though there must be some weak leaky expression in other cells of the imaginal ring.

7 The progenitors of the Adult stem cells

The adult hindgut stem cells are controversial, they don't seem as prone to proliferate as their midgut counterpart and thought they divide when forced by strongly damaging the hindgut (Takashima et al., 2008), their progenitors do not seem to go farther that the adult pylorus (Fox and Spradling, 2009; Takashima et al., 2008; Xie, 2009). However, their active status as stem cells, the stem cell region is interesting because it is the most anterior part of the hindgut, and thought at very early adult stages it expresses *byn*, this expression is lost in one day old adult stages (Fox and Spradling, 2009). Like all the other hindgut regions, except the rectum, the adult

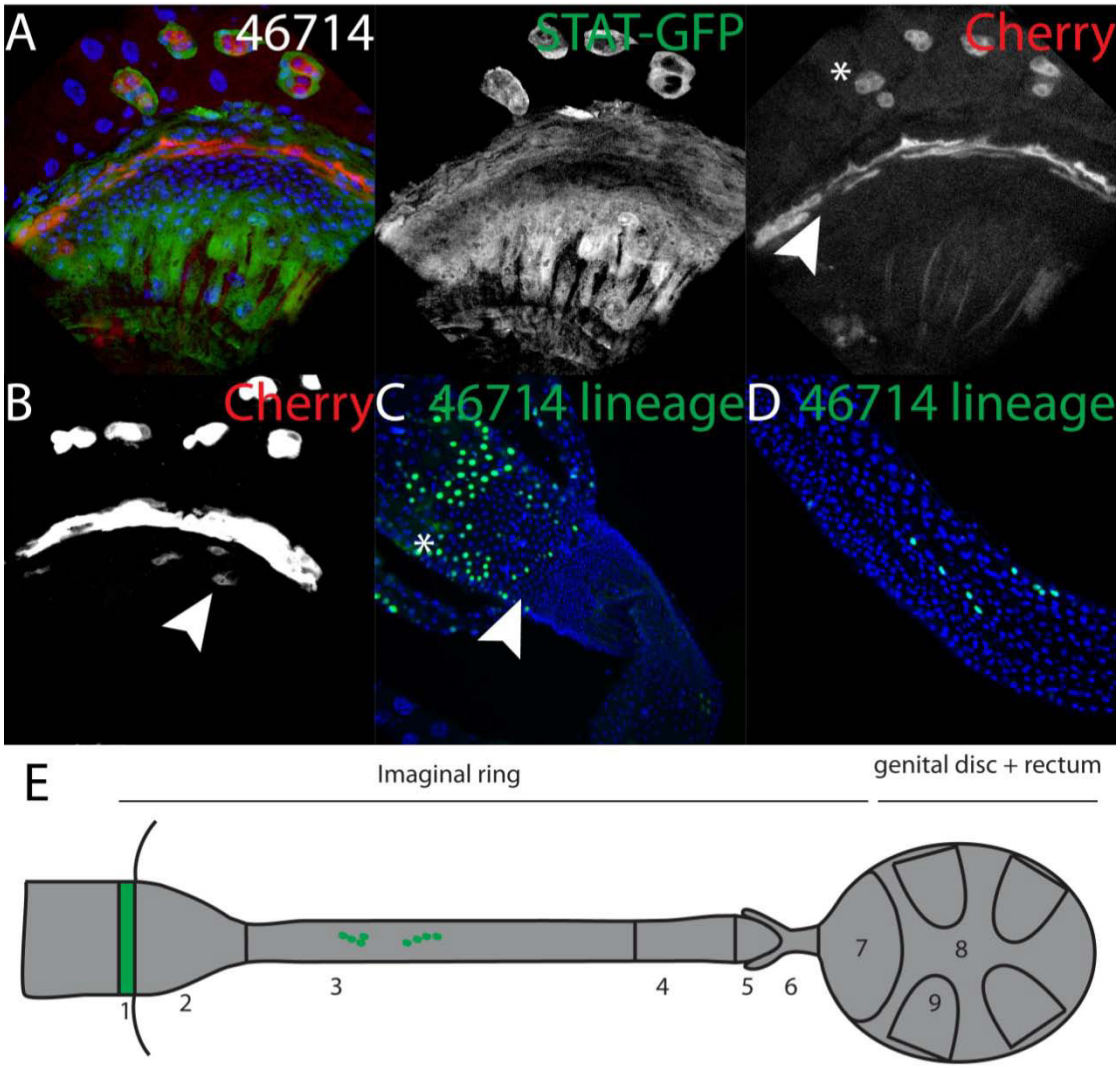

Figure 23. The stem-cell region precursors

A) Top view of an imaginal ring expressing *46714-Gal4*, *UAS:MCD8-cherry* (red) in the stem cells precursors, located in the *Stat-GFP* positive portion at the anterior of the imaginal ring (arrowhead). Note RFP expression is also in the adult midgut precursors (asterisk)
B) Higher contrasted image of a *46714-Gal4*, *UAS:MCD8-cherry* expressing imaginal ring reveals random cells located in the middle of the imaginal ring with weak RFP fluorescence (arrowhead)
C) Close-up image of the pyloric region expressing nGFP in the linage of *46714-Gal4* larval expressing cells in the posterior midgut (asterisk) and the AHG stem cell region (arrowhead). .
D) Close-up image of the anterior ileum region expressing nGFP in random 4-cell clones deriving from *46714-Gal4* expressing cells in the larval ileum precursors.
E) Illustration describing in green the linage of *46714-Gal4* expressing cells in the stem-cell region and in random 4-cell clones in the anterior ileum. Regions are numbered as in Figure 1. All images are oriented anterior to the left

stem-cell region derives from the imaginal ring (Figure20) (Takashima et al., 2013).

In the imaginal ring, the *46714-Gal4* line is mainly expressed in the 2 most posterior Stat-GFP positive cells in the imaginal ring (Figure 23A) and sometimes in individual randomly positioned cells in the middle of the imaginal ring; in the ileum precursor region (Figure 23B). Notable, the *46714-Gal4* line is also expressed in the AMG precursors located in small clusters in the larval midgut (Figure 23A). Consistently, lineage tracing experiments with this line results in nGFP marked cells mainly in the stem cell region and in the midgut (Figure 23C) and in rare 4-cell clones in the anterior ileum (Figure 5D).

8 Discussion

While the regionalization of the adult foregut and midgut, have been heavily studied using RNAseq from dissected regions, expression pattern analysis from selected Gal4 enhancer trap lines from the Flylight collection (Marianes and Spradling, 2013) and by microarrays (Buchon et al., 2013), the Drosophila adult hindgut has received very little attention and thus not so much is known about its development. Here we describe a similar strategy to the one used to analyze the regions in the Drosophila midgut but applied to the adult hindgut. Our results suggest a previously unrecognized complexity in the adult hindgut epithelia. We propose a regional classification of the AHG based of genetic expression data; it includes 9 regions, 7 of which are all comprised in the

imaginal ring.

Our lineage tracing experiments showed that as previously stated all the AHG except for the rectum comes from the hindgut imaginal ring (Fox and Spradling, 2009; Takashima et al., 2013) we have extended the understanding of the AHG development by showing that region 1-7 are also disc derived. Furthermore, we have shown the exact progenitors for regions 1, 3, 6 and 7. Interestingly, the progenitors of region 1 are the most anterior followed by the progenitors of region 3 and finally at the most posterior end the progenitors of regions 6-7. It has already been proposed, based on the analysis of GFP marked mitotic clones that the AHG develops without cell migration (Fox and Spradling, 2009) and thus the progenitors should be organized in the imaginal ring in sequential anteroposterior order as they will become the adult structure. Here we tested this hipotesis and our results are consistent with a model of sequential progenitor and no-migration development.

The insect AHG is recognized for its ability to reabsorb water and ions if under dry stress conditions. Metadata analysis from gene expression data at single tissue in Drosophila has shown that sodium regulation is conspicuous in the hindgut transcriptome, as are general substrate transporters of the Organic anion transporters family, consistent with its role in osmoregulation (Chintapalli et al., 2013). Consistently, at the functional level, salt unbalance impact a stress response in the hindgut led by the JNK and the p38/MK2 pathways (Seisenbacher et al., 2011). Yet, more strikingly the AHG is enriched in uncharacterized genes pointing out a yet uncharacterized function of this

organ (Chintapalli et al., 2013). Our newly described Gal4 lines will be useful for researchers interested in the physiology of the AHG as they will permit the specific manipulation of gene expression in specific parts of the AHG.

The AHG insights

1 The growth and looping

From an evolutionary perspective, the gut is looped as a consequence of its length, which is normally longer that the body itself; i.e. the human small intestine is around 7 meter long. This suggests that the looping process itself, but not the direction of the loop, might be the result of the intrinsic growth of the gut. However, this might not necessarily be true; the gut might loop by a combination of genetic factors and thus loop independently on its final length.

The *Drosophila* hindgut is around 4.5 times bigger than the length between the junction with the stomach (midgut) and the rectal junction (Figure 24A). We have shown, see previous sections, that the orientation of the AHG loop is genetically controlled by the L/R asymmetric controlling gene *myoID* and that the further amplification of the directionality signal is mediated by the Ft/Ds pathway and the core PCP components.

In order to explore whether the adult hindgut loop is forced by physical constrain, imposed by the differential length of the hindgut versus the abdominal cavity, or whether the loop is intrinsically looped, we tried to impair the hindgut loop simply by reducing the adult hindgut size in an otherwise normal fly. The insulin pathway is a mayor regulator of growth in metazoans, including *Drosophila, c*ell autonomous size reduction defects can be obtained by the specific removal or down-regulation of the

insulin Receptor (InR). Then, to test whether a smaller hindgut would fail to loop in a normal animal, we depleted the insulin receptor from the hindgut using a specific RNAi hairpin sin combination with the hindgut specific driver, *byn-Gal4*. The result flies were the same size as wild type flies, yet their adult hindgut was significantly smaller (Figure 24E). More interestingly was the fact that around half of them had an impaired hindgut loop. To properly correlate this looping defect with the relative AHG size, we first calculated the relative size (the AHG length divided by the abdominal cavity lenght). Interestingly, the mislooping defect was closely associated with the strength of the relative size reduction; flies with a relative size below 2.4 developed a mislooped phenotype, while flies with a relative size bigger than 2.4 did not (Figure 24B). This phenotype is interesting because i) it is a particularity of the gut, other organs do not behave in this way , i.e. depletion of InR in the wing results in a smaller yet properly patterned wing; and ii) it clearly shown that the final shape of the adult hindgut loop is influenced by size constrains.

In order to rule out any effect of insulin pathway other than growth control in the looping process we decided to analyze mutants for the insulin pathway that affect the whole fly. We focused on two insulin mutant conditions that develop into viable but unfertile and rather small flies. The first is a termosensible heteroallelic condition $InR^{GC25/E19}$ (Shingleton et al., 2005) and the second is the null mutant for the Insulin receptor substrate coding gene $chico^{1/1}$ (Oldham et al., 2002; Bohni et al., 1999). If the misloop phenotype observed before (*byn-Gal4, INR-RNAi*, Figure 24B) is the consequence of reducing the relative size of the hindgut, it should not be seen a whole

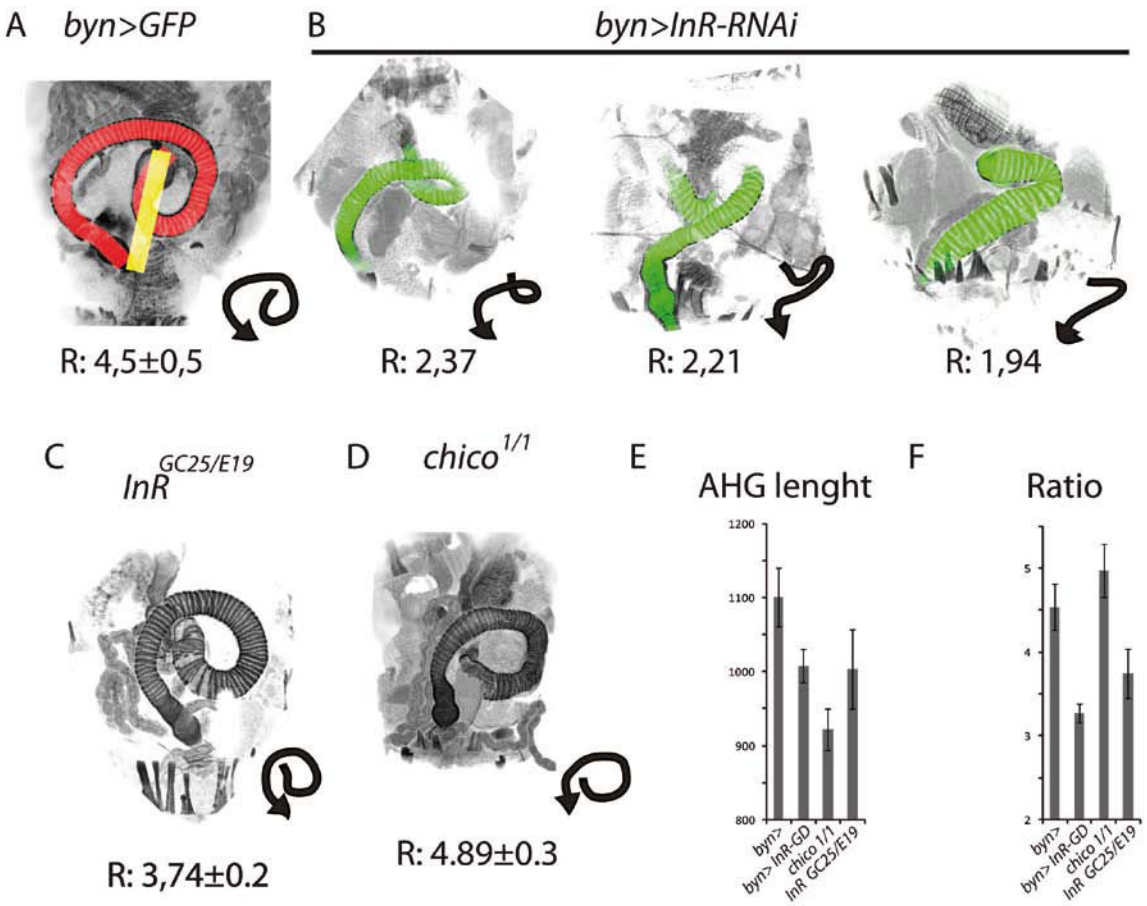

Figure 24. The relation between growth and looping in the AHG.

A) The AHG (red bar) is 4.5 folds longer than the abdominal length (yellow bar). B) Flies with smaller AHG in a normal abdomen develop dose dependent mislooped phenotypes . C-D) However, smaller flies with smaller AHG develop a properly looped AHG. E) Quantification of AHG length in different genetic conditions. F) Quantification of the AHG ratio, as in panel A in different genetic conditions.

body mutants as in these mutants the relative size remain unchanged, though the absolute size in reduced. Consistently with our hypothesis, neither *InR* mutants nor *chico* mutants have a mislooped phenotype despite having a strong reduction in adult hindgut size (Figure 24BC, D).

In summary, reducing the relative size of the adult hindgut directly affects the loop shape, however reducing the size of the whole fly size (the relative size remains unchanged) has no obvious effect on the adult hindgut shape. These results clearly indicate that the mislooped phenotype is indeed caused by the physical shortening of the AHG relative to the body size and not by a direct effect of insulin signaling because $InRE19^{/GC25}$ and $chico^{1/1}$ flies have a small yet fully looped AHG (Figure 24C, D).

Finally, to confirm our model in a wild type condition, we speculated that if the spatial limitation is the main force of the looping there should be an intermediate state of development in which the adult hindgut has started to grow but has not met its final size and therefore should be a straight tube. In order to find this state, *byn-Gal4, UAS-GFP* staged pupa were section using a standard vibratome in order to keep the general shape of the HG in the developing pupa. At 24h APF the AHG has not started to grow and the larval HG has started to degenerate. Later, at 50hAPF most of the larval HG has degenerated completely and its remnants are present as bright GFP dots in the abdominal cavity. The AHG has started to grow but has not reached its final length and at this moment is not looped. Finally at 60hAPF the loop is already achieved, though, the AHG has still not reached the final length (Figure 25). All of these data, together, suggest

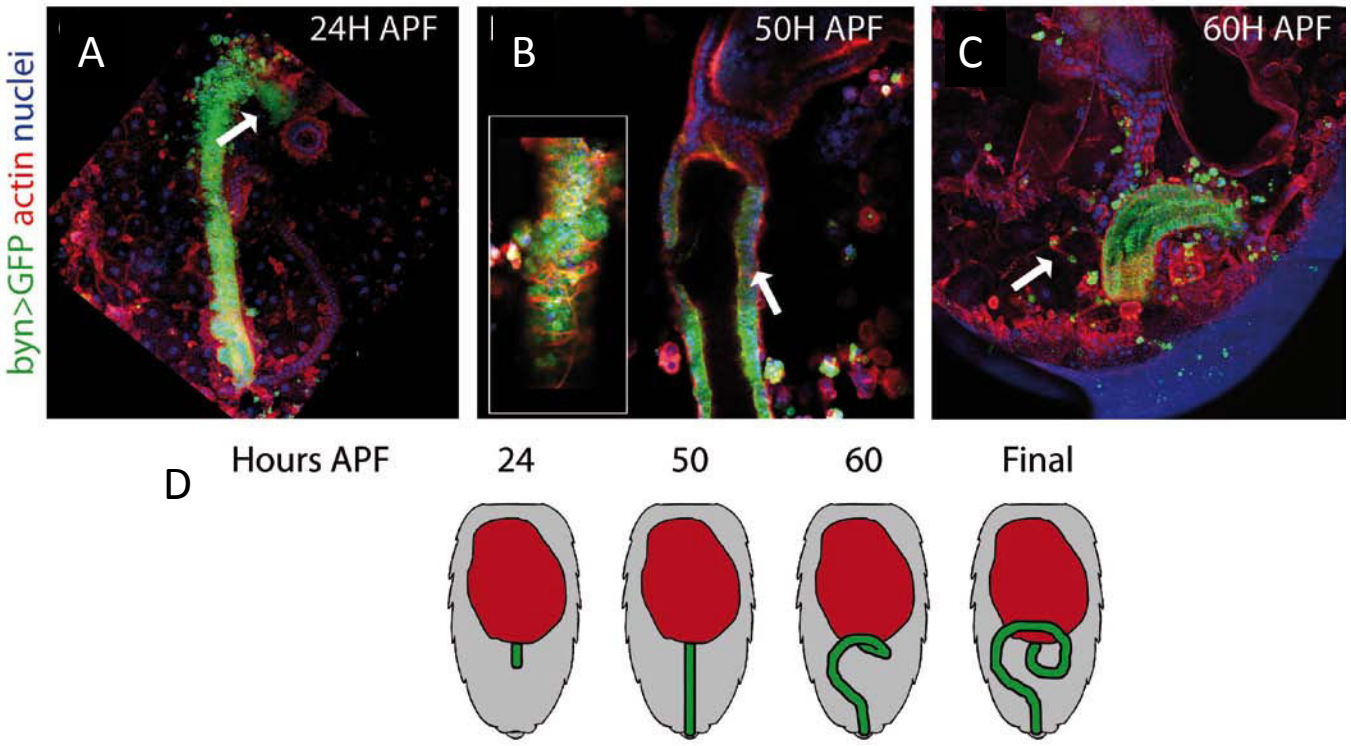

Figure 25. The looping moment revealed by time serial sections.

A-C) Confocal images of pupa at different hours of development expressing GFP under the control of *byn-Gal4,* to mark the hindgut. At 24h APF the AHG has not started to grow and the larval HG has started to degenerate (A). Later, at 50hAPF most of the larval HG has degenerated completely and its remnants are present as bright GFP dots in the abdominal cavity; the AHG has started to grow but has not reached its final length and at this moment is not looped (B). Finally at 60hAPF the loop is already achieved, though, the AHG has still not reached the final length (C). An illustration of the entire process is summarized as an illustration in panel D.

that the spatial limitation works as an amplification system that drives adult hindgut looping.

2 Abd-B in hindgut looping and hindgut morphogenesis

As noted in the previous section "Evolution of the Adult Hindgut loop" Abd-B plays an important role in controlling myoID expression in the genital disc (Coutelis et al., 2013) and likely in the AHG primordium. *Abd-B* is expressed in the hindgut imaginal ring as an anteroposterior gradient peaking in H1 cells (most anterior) and decreasing towards the posterior end. MyoID is solely detected in the H1 cells and is responsible only for directing the AHG looping direction. Using an RNAi hairpin directed against *Abd-B* either in H1 cells alone or in the entire imaginal ring (H1+H2), is able to render Abd-B protein undetectable using an antibody. Furthermore, in an imaginal ring depleted for Abd-B, MyoID::GFP reporter is no longer detected, suggesting that indeed Abd-B is responsible for *myoID* expression (see section Evolution of the Adult Hindgut loop).

However, Abd-B expression pattern extends towards the H2 cells suggesting another role for this HOX-bearing transcription factor in the development of the adult hindgut. In other to test the role of Abd-B in H2 cells, we depleted from the entire AHG primordium (H1+H2) using *byn-Ga4.* In this condition the adult hindgut is severely disrupted with: i) a huge reduction in size, ii) improperly formed rectal papillae (Figure 26)and in extreme cases the complete loss of terminallia structure (Figure 27).

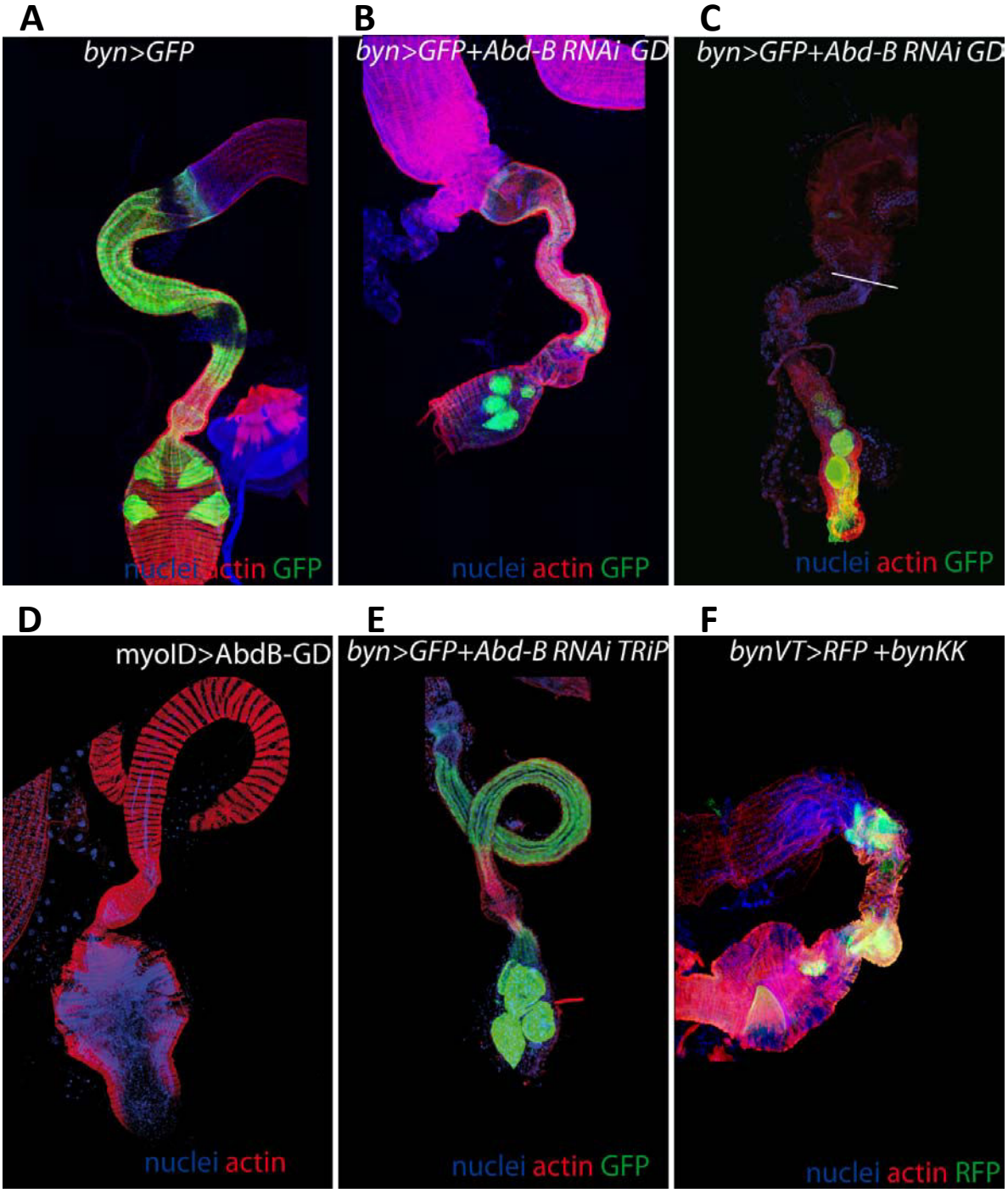

Figure 26. Depletion of Abd-B or Byn in the imaginal ring strongly impairs AHG formation.

A) Control fly bearing byn-Gal4, UAS-PH-GFP transgene. (B, C) Abd-B depletion in H1+H2 cells, using byn-Gal4 and AbdB-RNAi-GD, results in misformed smaller AHGs accompanied by loss of GFP. (D) Abd- depletion solely in H1 cells, using myoID-Gal4, does not affect AHG formation. Abd-B depletion in H1+H2 cells with a different RNAi transgene, Abd-B-TRiP, also results in smaller misformed AHGs. (F) Depletion of Byn in H1+H2 cells mimics Abd-B phenotype in B and C.

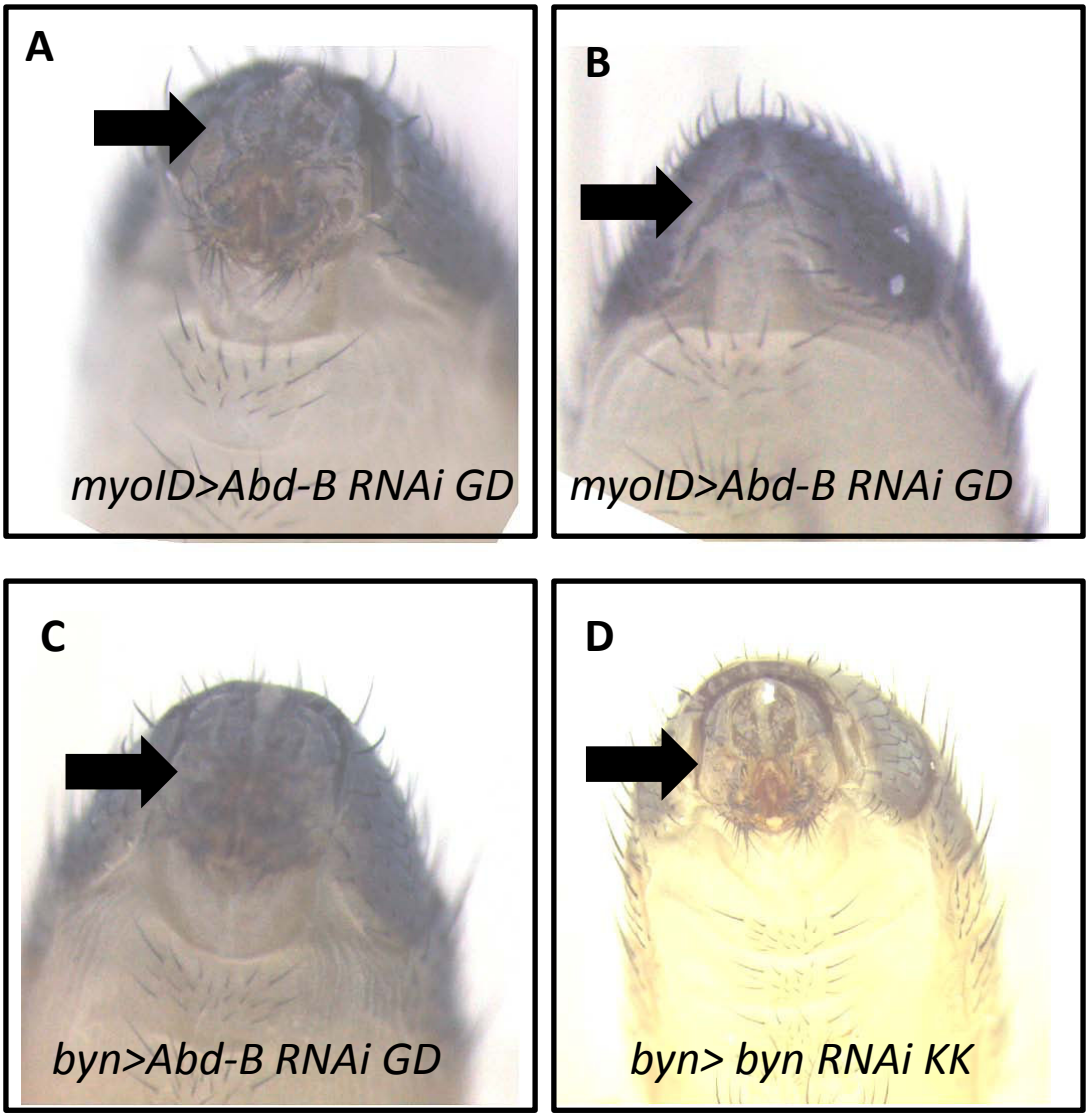

Figure 27. Depletion of Abd-B but not Byn in H2 cells results in absence of terminallia structures.

A) Depletion of Abd-B in H1 cells have no effect on terminalia structure. B) Depletion of Abd-B in H1+H2 in extreme cases results in the loss of extrenal terminalia stuctures (arrow). C) Depletion of Abd-B using a different , weaker, RNAi transgene does not affect the terminalia. D)Depletion of Byn in H2 cells do not affect the terminalia.

One surprising feature of *byn-Gal4, UAS-Abd-B*^{GDRNAi} flies is the expression of *byn-Gal4* which appears diminished, followed by a UAS-GFP construct (Figure 26). This phenotype was later confirmed by RT-Q-PCR for *byn* mRNA (Figure 28). We thus asked whether Byn depletion would affect similar the AHG morphology. There are two available RNAi lines for *byn (byn*^{GD} *and byn*^{KK}*)* both in combination with *byn-Gal4* result in early lethality, thus masking the adult phenotype. We then used a weaker Gal4 line with similar expression pattern as *byn-Gal4* but restricted to H2 cells: *bynVT-Gal4. T*his particular line comprises one regulatory element from the gene byn (for further description of this line see section "Regional division and development of the Adult Hindgut in Drosophila"). Consistently downregulation of *byn* using *bynVT-Gal4* line phenocopies the small AHG phenotype obtained from Abd-B depletion though it does not alter terminallia morphology (Figure 26 and 27).

Interestingly *byn* and *Abd-B* are of the most abundant transcription factors found in both larval and adult hindguts, consistent with a role in the specification/maintenance of the AHG identity (Figure 29).

Since depletion of Abd-B using *byn-Gal4* resulted in decreased *byn* expression assessed by RTqPCR and *byn-Gal4 reporter*>GFP levels we then thought to asses whether *Abd-B* affects also the expression of the reporter *byn-VTGal4* (which contains only a part of the complete cis-regulatory elements for *byn*). To test this we either overexpress Abd-B (isoform M) or deplete Abd-B using RNAi driven by *bynVT-Gal4*. Surprisingly we did not observed any difference at the GFP intensity levels between the overexpression

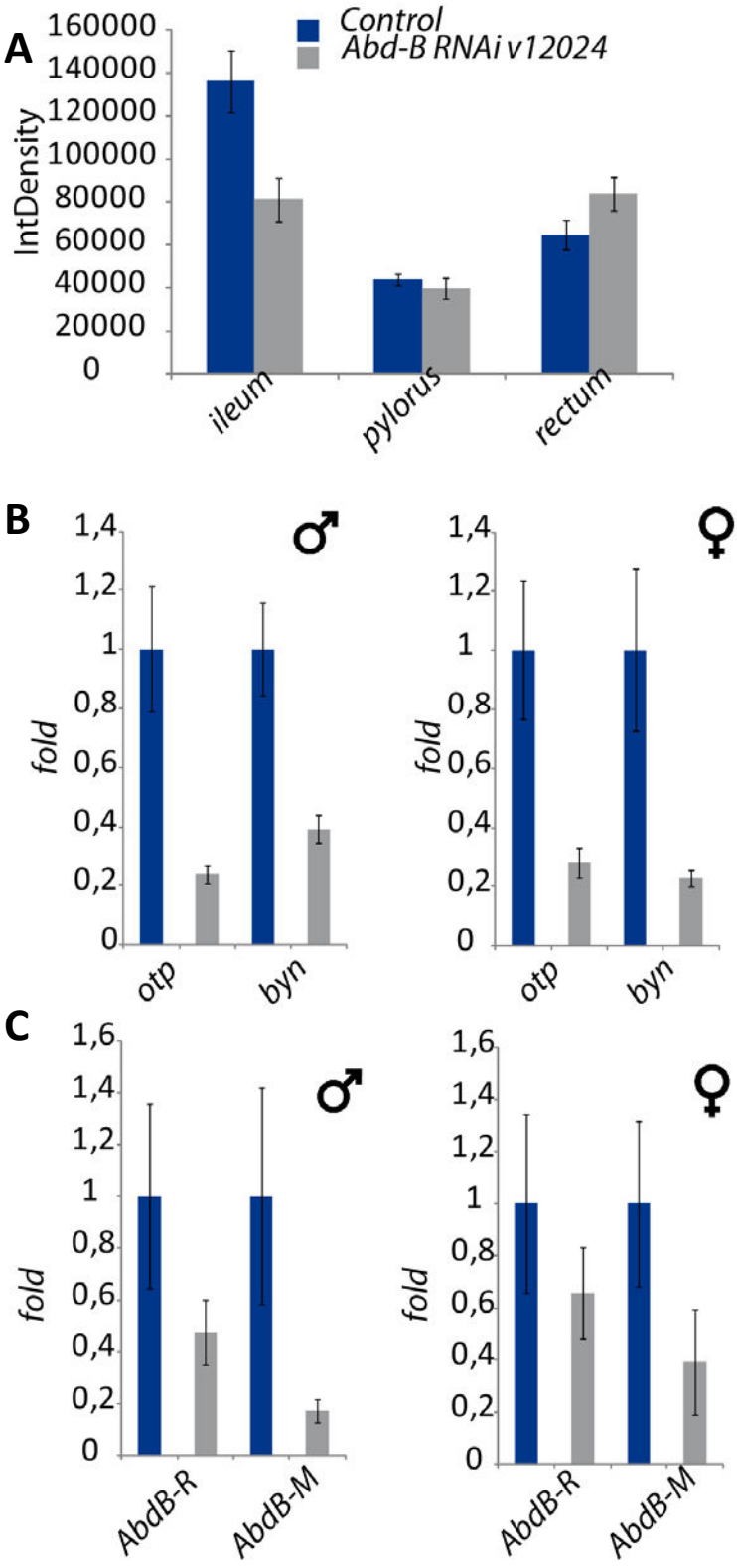

Figure 28. Abd-B depletion leads to *byn down regulation*

A) Byn>GFP fluorescence intensity plot from control a AbdB-GD flies, the GFP detections is clearly diminished in the ileum of Abd-B-GD flies. B) RT-Q-PCR in the same conditions from AHGs for *byn* and *otp,* another T-box transcription factor also present in the larval HG. C) RT-Q-PCR plot for both *Abd-B* forms showing efficient reduction of mRNA.

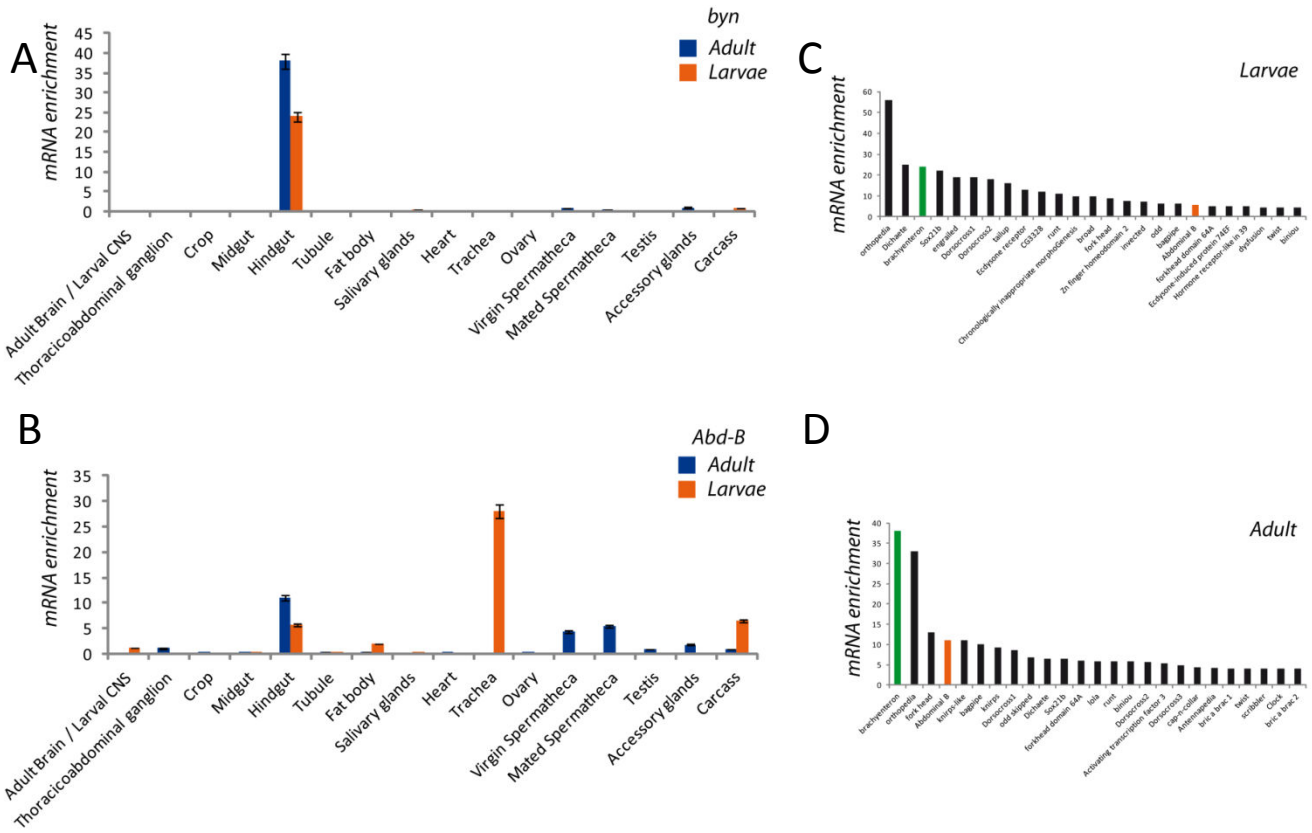

Figure 29. *Abd-B* and *byn* are highly enriched genes in the hindgut.

A) *Byn* mRNA expression plot along all tissues in both larva and adult stages. B) *Abd-B* mRNA expression plot along all tissues in both larva and adult stages . C) Most enriched genes plot in the larval hindgut, *byn* (green) and Abd-B (orange) and D) Most enriched genes in the larval hindgut, *byn* (green) and Abd-B (orange). *mRNA* data was obtained from the flyatlas proyect (Robinson et al., 2013)

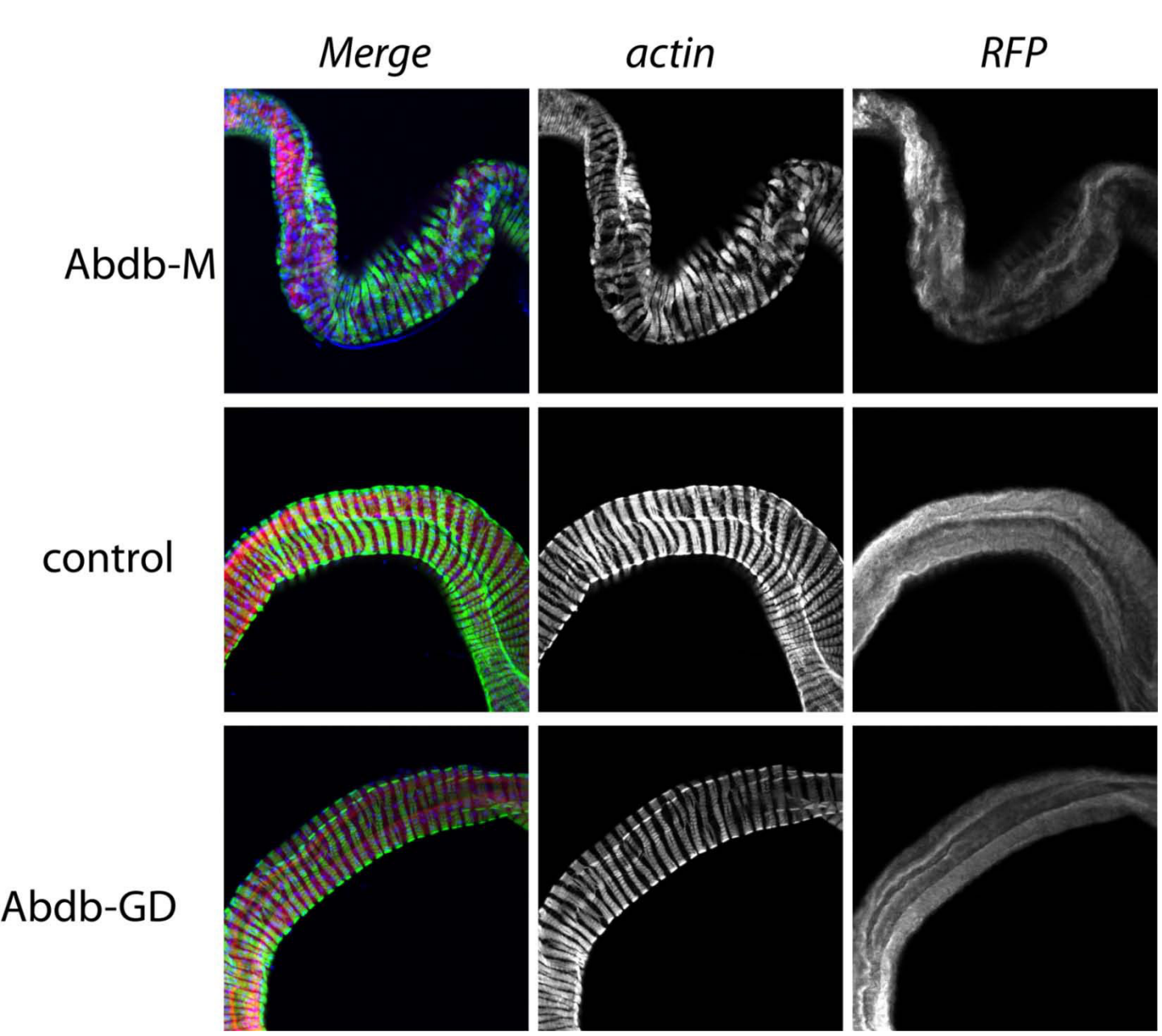

Figure 30. Effects on *bynVT-Gal4* expression upon increased and decreased Abd-B levels.

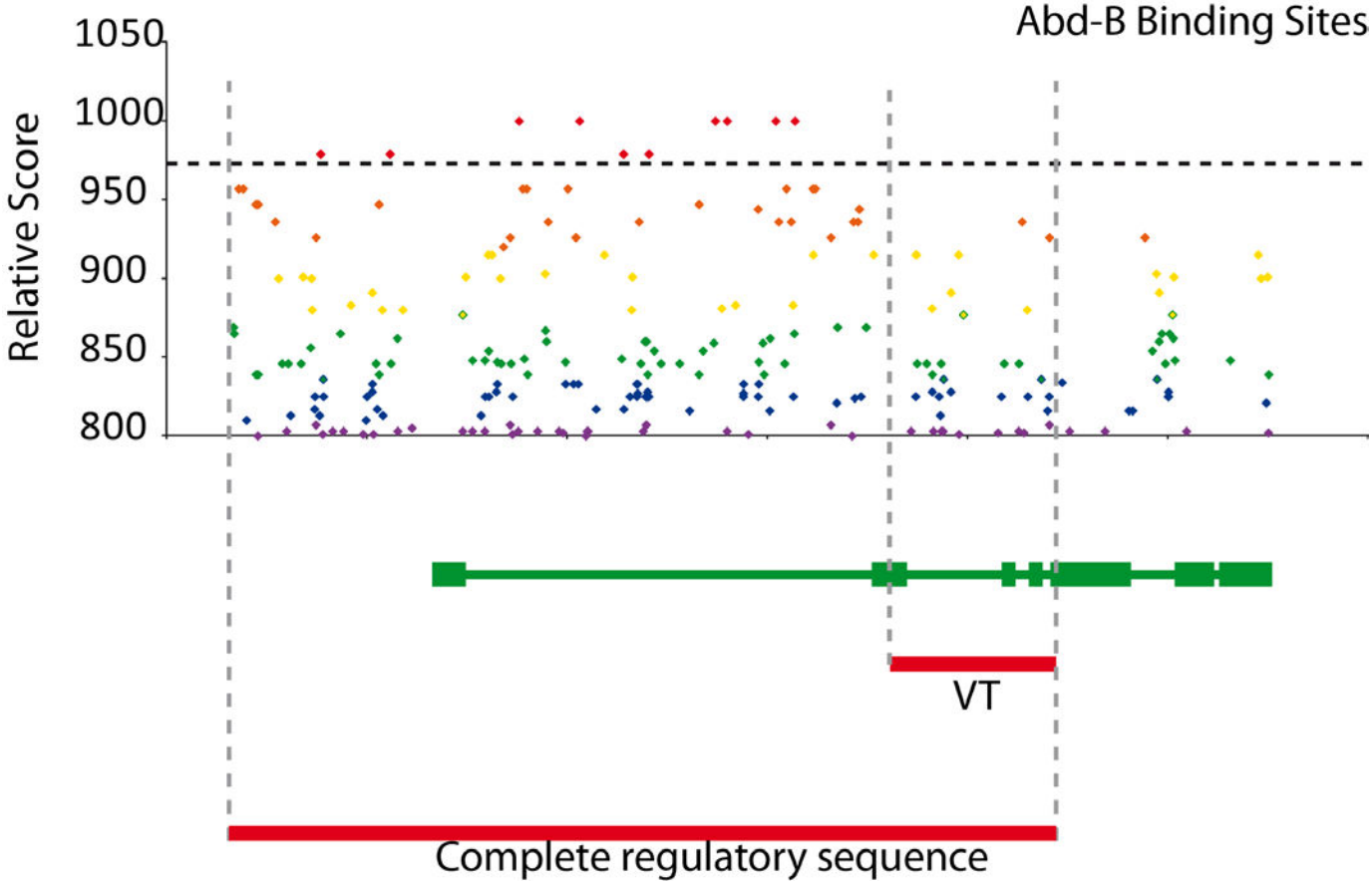

Figure 31. Localization of putative Abd-B BS at the *byn* locus.

Note the absence of High-scoring point within the VT region. *byn* gene is shown in green, with thick boxes representing the exons and a thin line for the introns, the promoter is the region before *byn* start, comprised by the complete regulatory sequence.

or the depletion of Abd-B in comparison to the control (Figure 30). Since *bynVT-Gal4* is an enhancer construct made with only one part of *byn* regulatory elements we then checked if any Abd-B binding sites were predicted to exist in this region. Consistently we found predicted Abd-B binding sites in the *byn* locus; however all of these were outside the regulatory element comprised in *bynVT-Gal4* (Figure 31). This explains why Abd-B affects the expression levels of *byn-Gal4* but not of *bynVT-Gal4.* Since both Gal4 lines are specifically expressed in the hindgut, the role of Abd-B is likely not to restrict *byn* expression to the hindgut but to control the expression levels of of *byn*. However, the presence of Abd-B binding sites, we have not been able to show a direct binding and thus we cannot rule out an indirect effect by which Abd-B might affect the expression of *byn.*

3 Imaginal ring culture

Arguably, the most interesting events of L/R asymmetry establishment and transmission happen in the imaginal ring in H1 cells during a small interval of time of 10H occurring at the onset of pupariation. The imaginal ring is located in the middle of the pupa covered by think opaque fat therefore dissection is necessary to observe this particular tissue under a microscope. Ruling out the possibility of observing the process in live, unless we manage to isolate the imaginal ring and culture it in a way that somehow resembles the endogenous place.

This section is devoted to explain the approach we used to film the imaginal ring

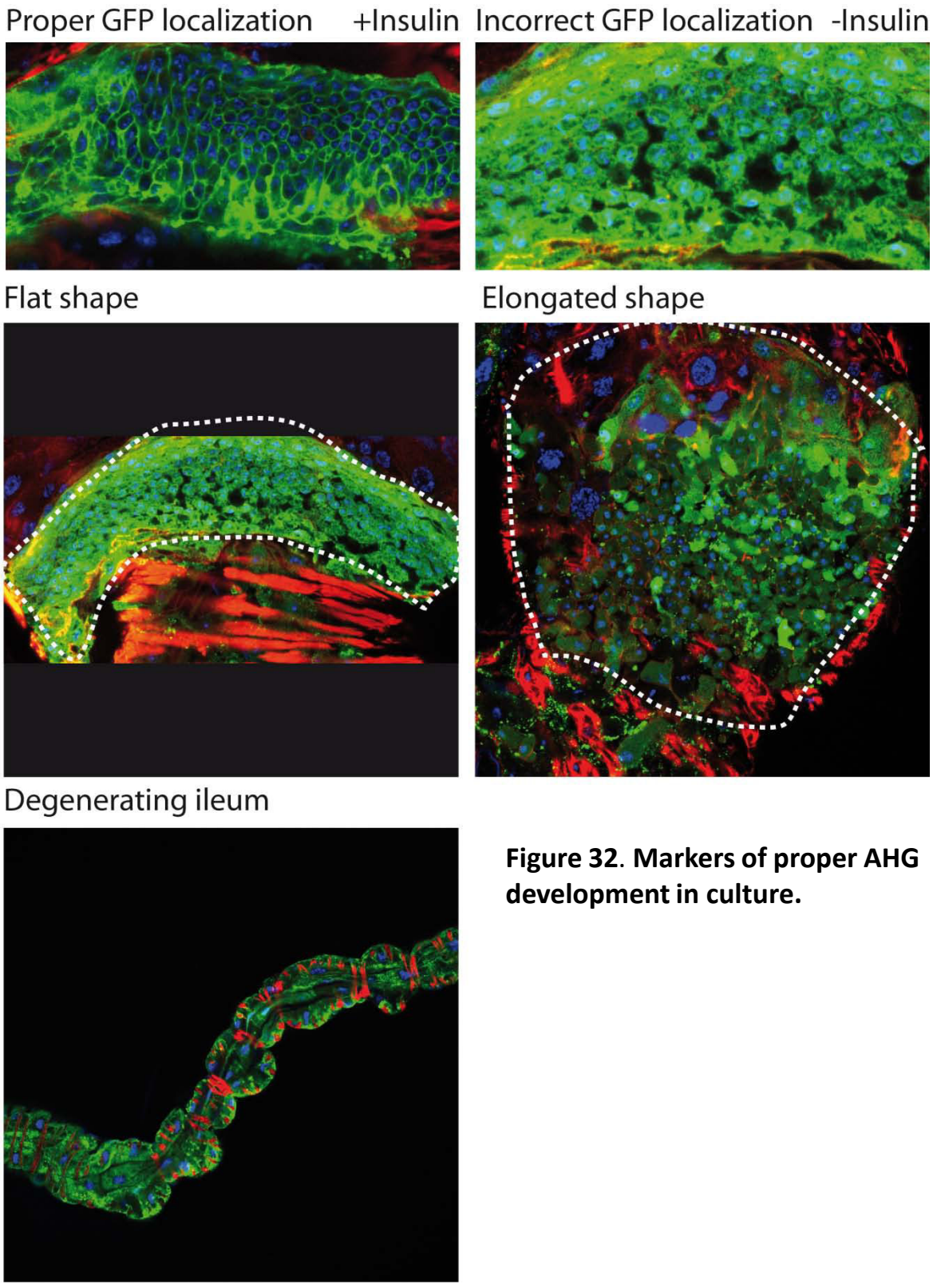

Figure 32. Markers of proper AHG development in culture.

under specific culture conditions, with specific reference to the problems we faced.

In order to image the imaginal ring under culture we had to first make sure that the imaginal ring would develop properly under this condition. We used S2 medium supplemented either with insulin or ecdyzone or both, without much difference in the final outcome in an incubator at constant 25°C. We dissected larval and white prepupa (0HAPF) hindguts for 12H, 24H and 48H. In order to assess the development of the AHG we asses 1) the detachment of H1 cells from H2 cells, 2) the degradation of the ileum 3) the change in shape of the H2 cell region from a flat trapezoid to an elongated rectangle and 4) the proper localization of Ph-GFP to the cytoplasmic membrane (Figure 32).

Table Summary of culture media effect on AHG development						
Stage	Hours in culture	Culture media	H1 detachment	Ileum degeneration	H2 change in shape	Proper GFP localization
L3	12	alone	no	no	no	yes
prepupa	12	alone	no	no	yes	yes
L3	24	alone	no	no	no	no
prepupa	24	alone	no	no	yes	no
L3	48	alone	no	yes	no	no
prepupa	48	alone	no	yes	yes	no
L3	12	ecdyzone	no	no	no	yes
prepupa	12	ecdyzone	no	no	yes	yes

L3	24	ecdyzone	no	no	no	no
prepupa	24	ecdyzone	no	no	yes	no
L3	48	ecdyzone	no	yes	no	no
prepupa	48	ecdyzone	no	yes	yes	no
L3	12	insulin	no	no	no	yes
prepupa	12	insulin	no	no	yes	yes
L3	24	insulin	no	no	no	yes
prepupa	24	insulin	no	no	yes	yes
L3	48	insulin	no	yes	no	yes
prepupa	48	insulin	no	yes	yes	yes
L3	12	both	no	no	no	yes
prepupa	12	both	no	no	yes	yes
L3	24	both	no	no	no	yes
prepupa	24	both	no	no	yes	yes
L3	48	both	no	yes	no	yes
prepupa	48	both	no	yes	yes	yes

Despite our efforts to set up the right conditions to culture the AHG development we failed to get a condition in which the H1 cells properly separate from the H2 cells. We managed to avoid membrane disruption, asses by GFP localization, by the addition of insulin. We also managed to induce H2 cell shape changes that end up with the elongation of the H2 region by simply dissecting prepupa instead of L3 late larvae. A peak of ecdyzone is responsible for the transition of L3 to prepupa (Andersen et al., 2013;

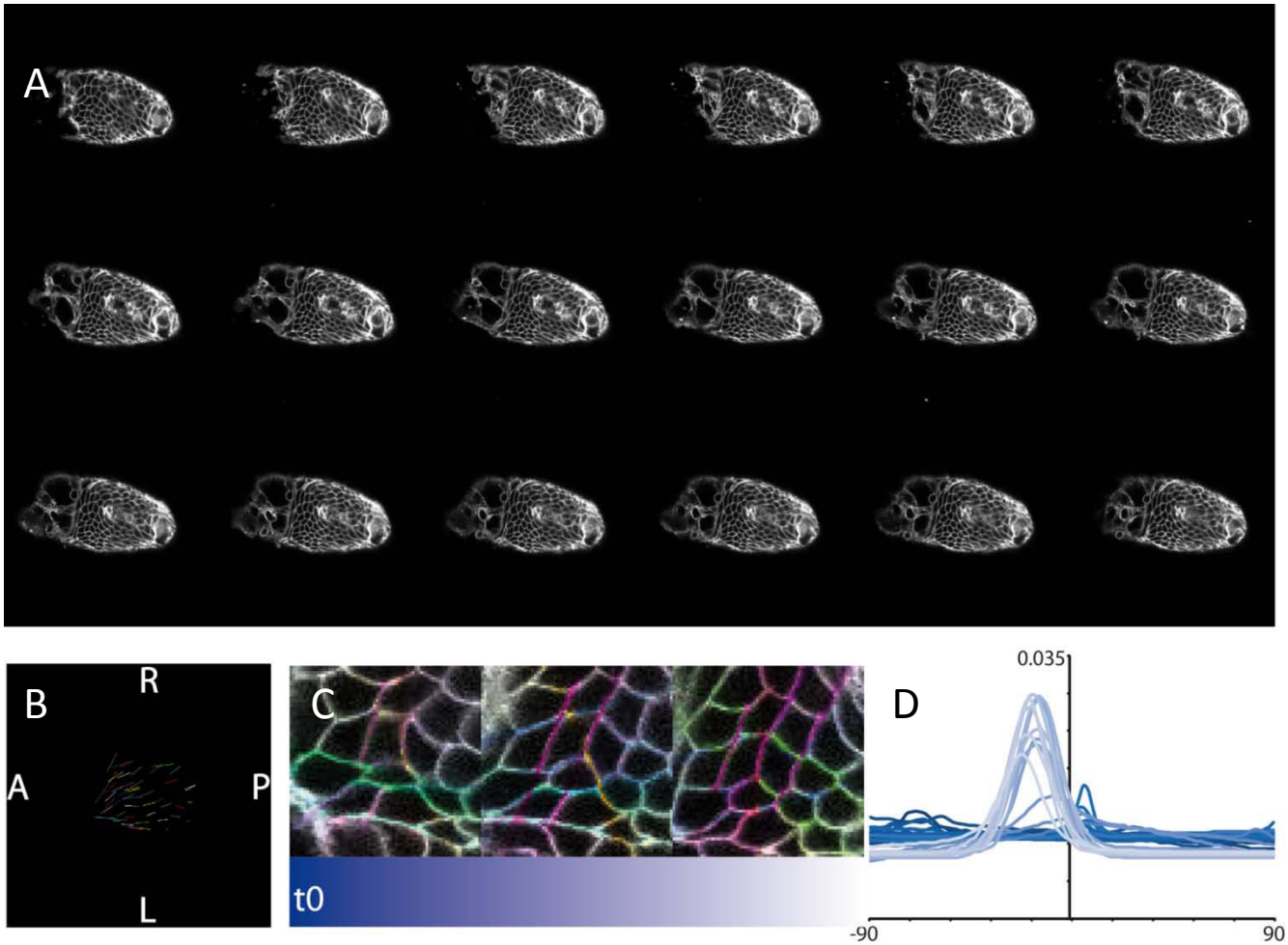

Figure 33. H2 dextral polarization revealed by time-lapse confocal microscopy.

A) Imaginal ring in culture at different time points, H1 cells extend towards the anterior . B) Tracked cell center trajectories show a slight displacement towards one side of the cell in a L/R asymmetric fashion. C) Color-coded H2 cell membranes reveal a time specific L/R asymmetric polarity pattern. D) Membrane polarity plots from all time points, color coded lines: darker blue at the starting time point and increasing in lighter blue towards the last time points.

Di Cara and King-Jones, 2013) and is likely also controlling the H2 rearrangements; however the addition of ecdyzone into the culture media had little effect on this. Finally ileum degradation is a strange marker as it does occur in normal development starting at 24H APF however in culture media we observed it later on suggesting that either the process is delayed under culture or that the degeneration we observe is not related to normal degeneration observed in flies.

Finally, as a last resort to try to set up this technique into the study of L/R morphogenesis in the AHG, we decided to film dissected cultured prepupa under a Lab-Tek cover slide chamber and an inverted confocal microscope. This approach is particularly hard as the malpigian tubules contract moving the HG constantly out of focus, however in some occasions this problem did not appear and then we were able to film the process. Our longest film is 8H long and shown from the stat the cell shape changes occurring in H2 cells, including the dextral polarization. However, H1 cells remained in place their behavior was completely different from H2 epithelial cells; long protrusions could be seen and a highly dynamic membrane was also apparent. This approach showed that H1 complete detachment is not necessary for H2 polarization, and proved to be a good model for measuring specific cell changes in vivo (Figure 33). Consistently *myoID* mutants showed the inverse polarization (data not shown)

4 L/R patterning and the Centrosomes

The centrosome is an organelle that serves as the main microtubule organizing center (MTOC) of the animal cell (Figure 34A). Centrosomes are composed of two orthogonally arranged centrioles surrounded by an amorphous mass of protein termed the pericentriolar material (PCM). The PCM contains proteins responsible for microtubule nucleation and anchoring including γ-tubulin, pericentrin and ninein. Interestingly, centrioles are not required for the progression of mitosis. When the centrioles are irradiated by a laser, mitosis proceeds normally with a morphologically normal spindle. Moreover, development of the fruit fly Drosophila is largely normal when centrioles are absent due to a mutation in a gene required for their duplication (Basto et al., 2006).

Nevertheless since the centrosomes are a unique organel at each cell they have been used as a way to infer the polarity of a single cell (Xu et al., 2007; Taniguchi et al., 2011; de Anda et al., 2005). The main principle is that if the center of mass of either the nucleus of a cell or the entire cell is linked by a line to the centrosome, then a polarity will be drawn, if this is done for several cells in a tissue the frequencies will tell is they are randomly oriented of if they follow a specific pattern. In cell culture they have been shown to be preferably localized to the left side of cells (Xu et al., 2007); neurons have been shown to localize their centrosomes and golgi apparatus to the side the axon will grow, before the axon is even detected (Figure 34B) (de Anda et al., 2005); and in the embryonic hindgut of *Drosophila* it was suggested that Centrosomin (Cnn-GFP) is able to mark the single pericentriolar material (Figure 34C), thus the centrosome, and this pattern was shown to be L/R asymmetric (Figure 34D) (Taniguchi et al., 2011).

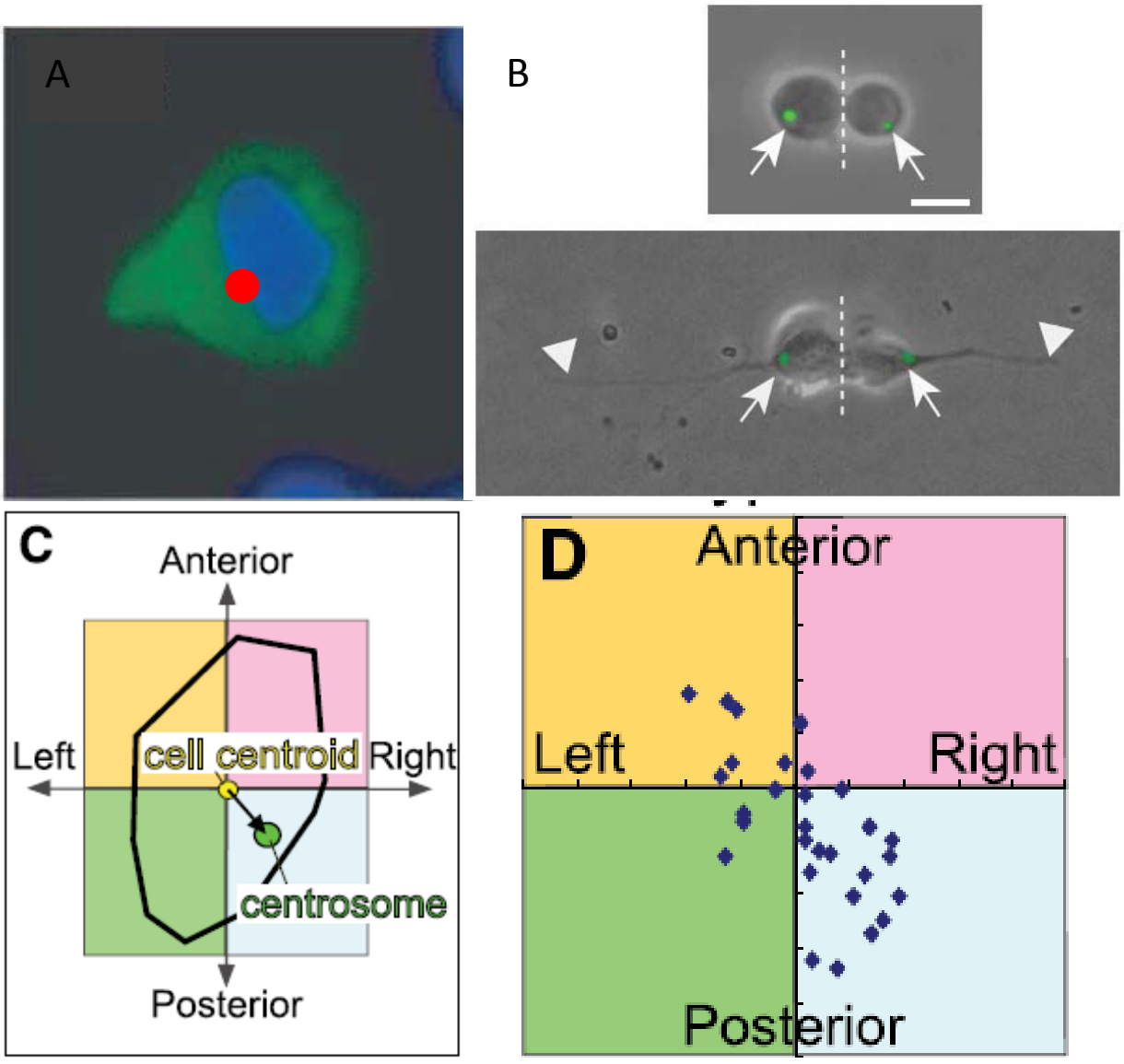

Figure 34. Examples of asymmetry revealed by tagged centrosomes.

A) the centrosome is an organelle that serves as the main microtubule organizing center of the animal cells, it is associated with the nuclear membrane and it serves as a polarity marker (shown in red). B) the polarized activities of the centrosome dictates the position of the neurite , thus precedes neuronal polarity; two neurons right after mitosis segregate their centrosome, top panel, to the place where the neurite will grow, bottom panel (de Anda et al., 2005). C) The centrosome position can be used to infer tissue polarity by comparing its position to that of the cell centroid. D) Using the centrosome as a PCP marker it has been shown that the embrionic gut is polarized to the right just before its asymmetric shape appears (Taniguchi et al., 2011).

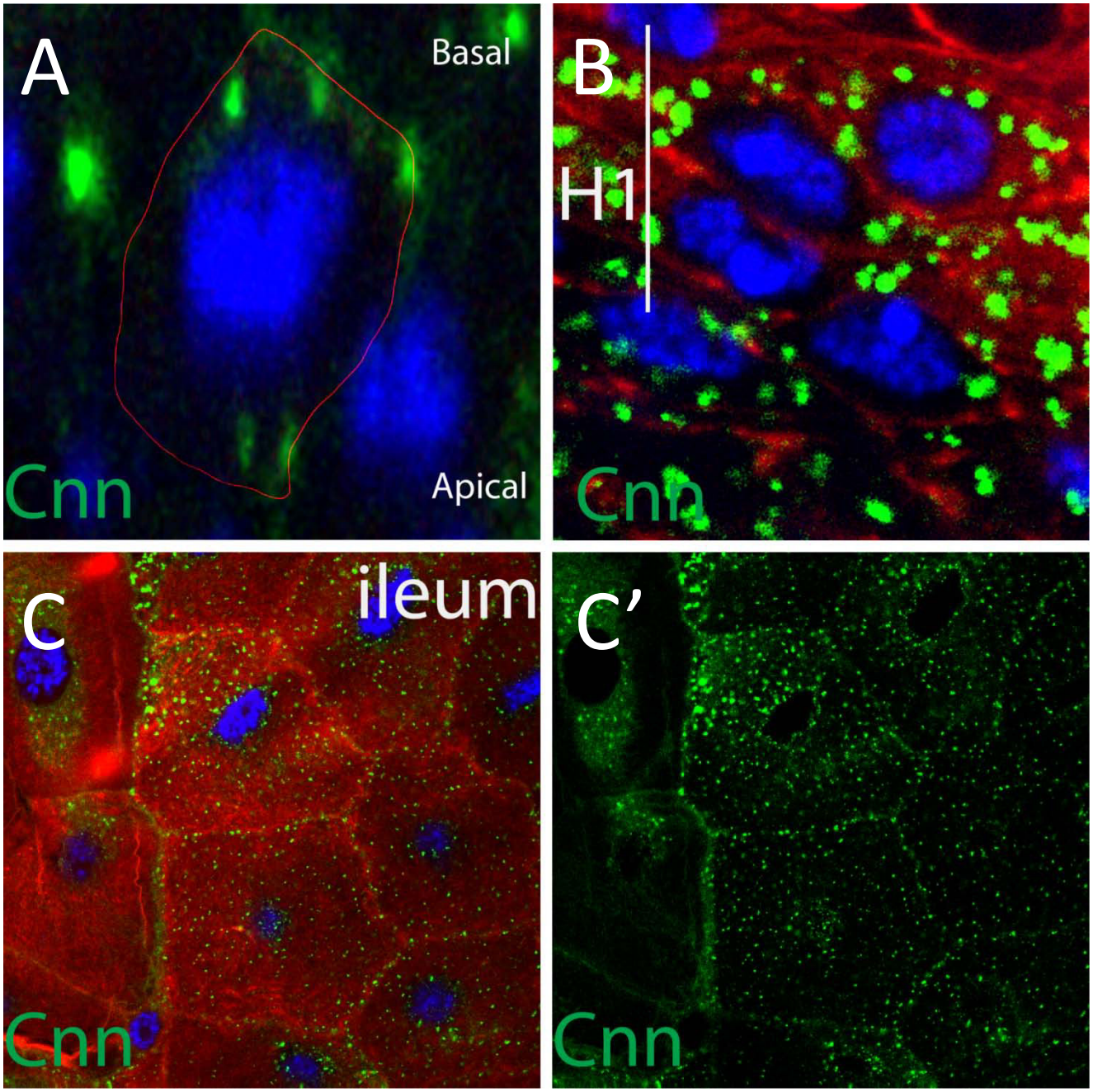

Figure 35. Multiple Cnn-positive structures uppon Cnn-GFP overexpression.

A) H2 cell close-up reveals ectopic centrosomes located at the apical and basal side of the cell, The red line denotes the cell membrane acquired with F-actin staining. B) The H1 cells also have ectopic centrosomes. C) The ectopic centrosomes are even more evident in a poliploid cell type, in this case ileum cells. The genotypes for all panels was *byn-Gal4, UAS-CNN-GFP* and cell membranes were visualized with phaloidin-TRITC

Thus, we tried to repeat this assay in the imaginal ring model. Briefly we expressed Cnn-GFP using byn-Gal4 and observed the centrosome pattern. We didn't go far on the polarity assessment since the most shocking observation was that over expression of *CNN-GFP* gave rise to ectopic supernumerary centrosome-like structures (Figure 35). The appearance of supernumerary centrosome-like structures might be caused by high doses of Cnn::GFP and therefore reducing the levels of expression of the *cnn::GFP* transgene might resolve solve this issue; however we were not able to find a condition in which the amount of Cnn::GFP was low enough to mark only one spot per cell.

Genome wide screen and the identification of Profilin homolog

1 Genome wide deficiency based interaction screen

Mutations that completely abolish *myoID* gene function result in a completely inverse terminallia looping, -360 degrees. However the knockdown of *myoID* transcript via RNAi results a wide range of intermediate positions between 0 and -360 degrees (Figure 36).

We constructed a line that gave a terminalia looping dominant phenotype (-185 degrees) when out crossed (Figure 36), we then used this line to screen for deficiencies that would modify this dominant phenoype. We screen for big deficienciess that covered all the 2nd and 3rd Chromosomes. We then narrowed the specific interacting location

using smaller deficiencies.

We identified 3 regions in chromosome 2: 50D 25D-E, 21A-B. We further identified the associated genes by RNAi depletion in combination with the tester line or by using null alleles for available genes. Here I will briefly describe the identification of two of these regions (50D and 21A-B), region 25D-E is described with more detail in next section.

Region 21A-B was originally identified as a region containing a *myoID* phenotype suppressor, deficiencies covering this region rescue *myoID* loss of function in the tester line, with different degrees. Most deficiencies in this region were originally generated by X-rays and the molecular lesion determined by genetic recombination rates and polytene bands analysis; thus the molecular lesion has not been precisely mapped; however one single deficiency, *Df2l)Ed50001*, originally generated by FRT/FLP method and then precisely mapped by PCR was available. This particular deficiency resulted in a weaker yet completely penetrant and significant suppression of the phenotype compared to the other deficiencies tested in this region. The *Df2l)Ed50001* uncovers 4 genes (*CG11023, lgl, Ir21a and Cda5*). From all of these only *lgl* null mutation is available; however in combination with the tester line did not phenocopy the suppression effect. Therefore we changed our strategy to RNAi mediated depletion of these genes; sadly, the depletion of any of these genes phenocopied the original deficiency. We then hypothesized that the suppression effect might be flanking the deficiency, in order to test this; we test deficiencies in the flanking regions. Df2l)Ed50001 is next to the start

of chromosome two and was made by directly fusioning chromosome two tip (21B) to chromosome 3, therefore removing region 21A. Thus *Df2l)Ed50001* has only one flank, being the other flank part of another chromosome. Deficiencies flanking *Df2l)Ed50001* in combination with the tester line did not significantly suppressed the phenotype. Therefore we can conclude that the suppressor effect lays in region 21A-B but we failed to map it precisely. Also shockingly is the fact that x-ray mutations around this area have a stronger suppression effect, this might be explained by the different genetic background, not shared between deficiencies and/or by additional mutations included in those deficiencies. However without a precise description of the molecular lesion in all deficiencies it is hard to speculate. Finally, as a last resort, we decided to generate small deficiencies around region 21A-B. We used a specific method based on HOBO transposon. This method allows the generation of nested deficiencies which direction can be positively selected based on eye-color change (see materials and methods). Briefly, we screened 1500 flies and recover 15 deficiencies; sadly none of these had the expected suppressor effect. Therefore, at present we cannot ascertain the locus involved in the genetic interaction with *myoID* in the terminalia looping process

The other region, 50D, was originally described as an enhancer of the tester line sinistral partial (-180°) phenotype. It was uncovered by 3 overlapping deficiencies. More detailed deficiency mapping showed that the enhancer activity was likely in a region uncovering 9 genes. Since there were no known mutants available we screened the RNAi loss of function phenotypes. From all RNAi tested only one, directed against *Tango7* gene, strongly modified the tester line phenotype. Strangely, the original effect of

removing one copy of *Tango7* gene in combination with the tester line resulted in an enhancement of the sinistral phenotype, from -180° to -270°, however the effect of the RNAi depletion resulted in a no-rotation phenotype (0° movement). We believe that Tango7 likely is required for normal rotation and thus complete RNAi depletion might mask the enhancement effect. Consistent with this hypothesis RNAi mediated depletion of Tango7 alone, resulted in impaired rotation. These data suggest that Tango7 is involved in terminalia rotation in both MyoID dependant and independent manner.

Tango7 is a Golgi resident protein identified in a genome wide screen for to identify genes required for constitutive protein secretion, therefore the name: Transport and Golgi Organization = Tango (Bard et al., 2006). This gene has been previously been implicated in apoptosis; in Tango7 depleted S2 *Drosophila* cells apoptotic induction by UV irradiation does not happen (Chew et al., 2009); later Tango7 role in apoptosis was confirmed in vivo (D'Brot et al., 2013). Briefly, Tango7 collaborates with the Drosophila apoptosome to drive a caspase-dependent remodeling process needed to resolve individual sperm from a syncytium. In these cells, Tango7 specifies the Drosophila apoptosome as an effector of cellular remodeling (D'Brot et al., 2013).

Given Tango7 involvement in apoptosome related tissue remodeling and the established role of apoptosis in remodeling the tissue before terminalia rotation actually takes place. Tango7 role in terminalia rotation might be related to apoptosis; we did not further test this hypothesis, however in noteworthy that though Tango7 depletion resulted in both terminally and AHG mislooping, the complete blockage of apoptosis by

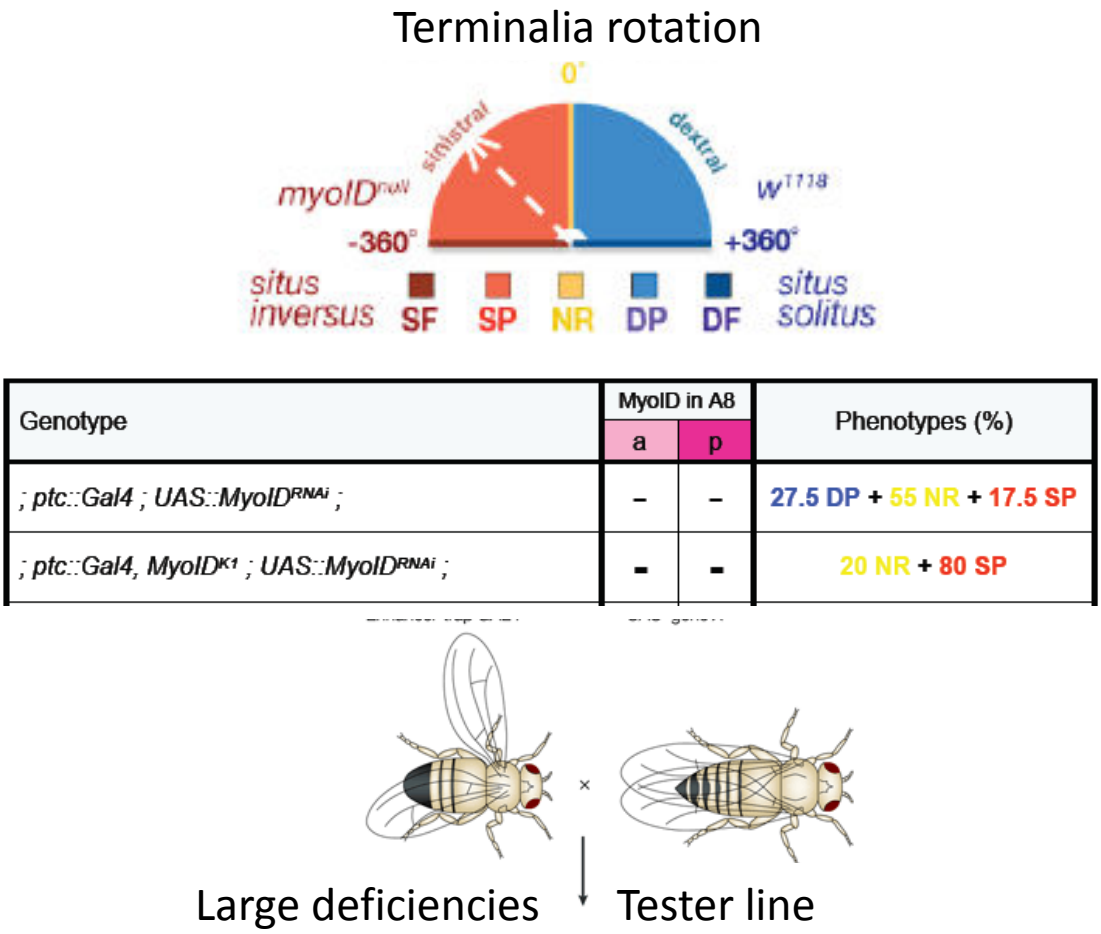

Figure 36. General strategy for deficiency-based genome wide screen.

The tester line composed (w; myoID-/+; ptc-Gal4, UAS-myoID-RNAi/+) has a terminalia rotation defect that ranges from -150° to -200° counterclockwise , while a wild type flies has a complete +360°. We collected female virgins from the tester line and crossed them agains males carrying large deficiencies.

the expression of the baculovirus protein p35 only blocks terminallia rotation and has no detectable effect on AHG looping; suggesting that Tango7 remodeling might not be completely dependent on apoptosis.

2 The role of chikadee in LR patterning

Deficiency based screen identified chic locus

Mutations that completely abolish *myoID* gene function result in a completely inverse terminallia looping, -360 degrees. However the knockdown of *myoID* transcript via RNAi results a wide range of intermediate positions between 0 and -360 degrees (Figure 36).

We constructed a line that gave a terminalia looping dominant phenotype (-185 degrees) when out crossed (Figure 36), we then used this line to screen for deficiencies that would modify this dominant phenoype. We screen for big deficienciess that covered all the 2nd and 3rd Chromosomes. We then narrowed the specific interacting location using smaller deficiencies.

Several interacting deficiencies were found, but we focused on the 2L25-27 region, where we found several deficiencies that strongly modified the tester line phenotype, from -185 to – 70 degree looping (Figure 37A-D). There was only one gene present in all interacting deficiencies tested in the 2L25-26 region, *chicadee (chic)*, which

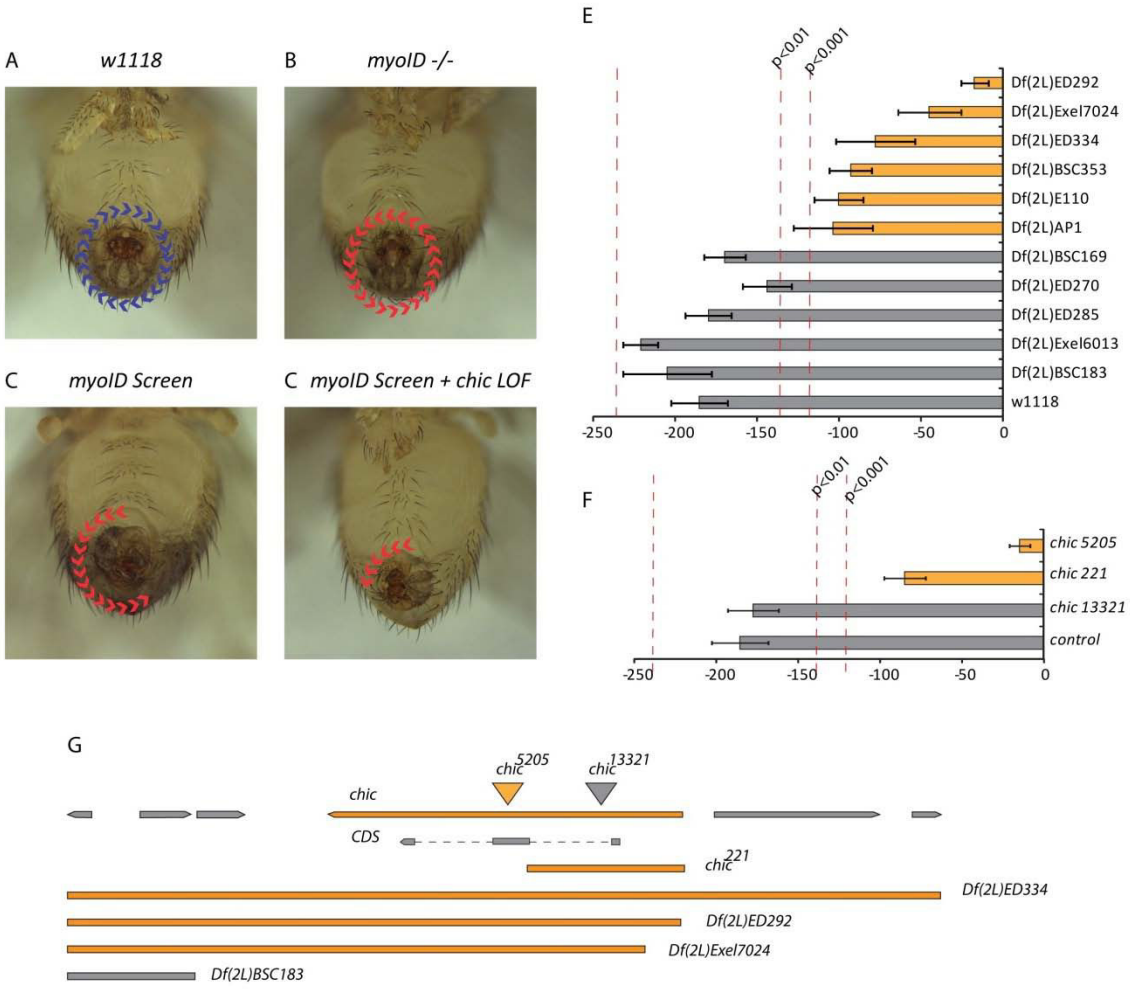

Figure 37. Genome wide screen unveils the role of *chic* in LR patterning.

A) Control male terminalia rotates +360° or clockwise. B) *myoID* mutant terminalia rotates -360° or counterclockwise. C) The tester line designed for the screen is a strong *myoID* loss of function dominant condition that results in -180 rotation of the terminalia. D) The tester line in combination with *chic* loss of function results in -80° rotation. E) Graphic of the average rotation degree of the tester line in combination with deficiencies that uncover *chic,* colored in yellow, flanking deficiencies, colored in gray. Error bars represent the SEM, n=30-40 flies, red lines represent *p*-values for T-student test. F) Graphic of the avererage rotation degree of the tester line in combination with *chic* alleles. Error bars represent the SEM, n=30-40 flies, red lines represent *p*-values for T-student test. G) Genome map of *chic* locus, interacting deficiencies are colored in yellow and non interacting deficiencies in black; the null alleles $chic^{221}$ and $chic^{5205}$ phenocopied the interaction, colored in yellow, while the $chic^{13321}$ hipomorphic allele did not.

encodes the actin binding protein Profilin (Figure 37G). Same wise deficiencies that flank *chic* locus, do not phenocopy the interaction phenotype (Figure 37E). Indeed, null mutations for *chic* modify the tester line dominant phenotype in the same way as the original deficiencies, and a P-element inserted in *chic* locus that does not alter its function (Schnorr et al., 2001), does not phenocopy the interaction (Figure 37). All of these data together suggest that chic interacts genetically with *myoID*.

Over expression of *chickadee* rescues *myoID* loss of function phenotype

Since null mutations for chic modify the tester line dominant phenotype into an impaired rotation defect; we hypothesized Chic could be involved in the cell movements occurring during terminalia rotation; we then predicted that the over expression of chic would have the opposite effect. Overexpression of Chic in an otherwise wild type background has no effect, using *ptc-gal4*, *AbdB^{LDL}-Gal4* or *myoID-Gal4;* however the over expression of Chic in the tester line genetic background modified the phenotype towards a complete sinistral loop (Figure 38B). Thus the chic loss of function condition impaired rotation while the over expression condition enhanced it. The effect observed upon *chic* overexpression is specific because the same manipulation with other cytoskeleton known regulators in the tester line background had no effect on terminallia looping.

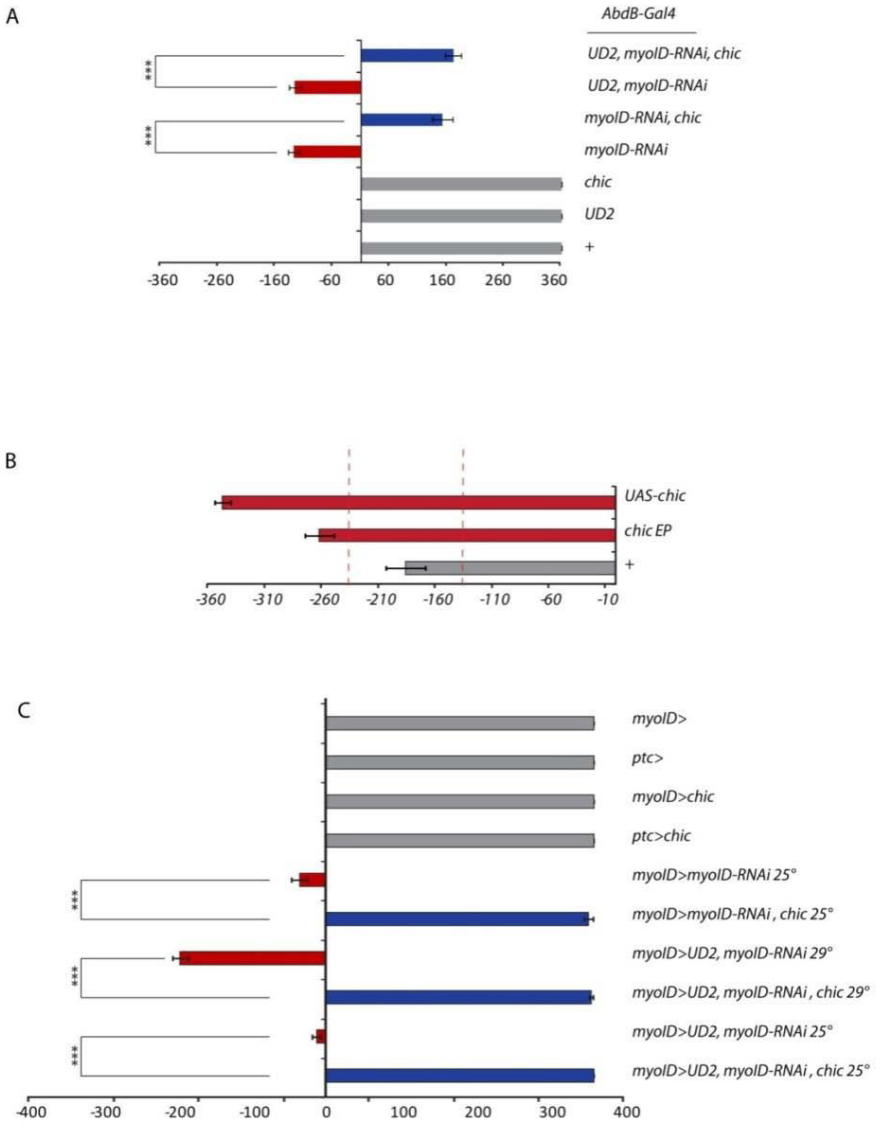

Figure 38. *Chic* overexpression rescues *myoID* depletion.

A) Depletion of *myoID* by *Abdb-Gal4* resulted in an incomplete sinistral rotation, -100°, (red) which could be rescued to a dextral one by the overexpression of *chic,* +160° (blue). Adding one copy of *UAS-Dicer2* did not affect chic mediated rescue of *myoID-RNAi* phenotype. Overexpression of Chic alone did not affect terminalia rotation nor did the control Gal4 lines (grey). Error bars represent the SEM, n=30-40 flies, *** represent *p*-value <0.0001 for T-student test. B) Depletion of *myoID* by *ptc-Gal4* also resulted in an incomplete sinistral rotation, -185° (grey); however coexpression of *chic* by two different lines (see Materials and methods for detailed explanation) resulted in completely sinistral rotation –360° (red). Error bars represent the SEM, n=30-40 flies, red lines represent *p*-values of 0.001 for T-student test. C) Depletion of *myoID* by *myoID-Gal4* also results in an incomplete sinistral rotation (red) that can be rescued to a complete dextral rotation by coexpression of *chic* (blue). Increase of temperature of adding *UAS-Dicer2* did not affect the chic mediated rescue. Overexpression of chic alone with ptc-Gal4 or myoID-Gal4 did not affect terminalia rotation (grey) Error bars represent the SEM, n=30-40 flies, *** represent *p*-value <0.0001 for T-student test.

We then speculate that Chic might be part of the force mechanism responsible for rotation rather than the direction choice of the movement. We thus tried to over express Chic in a weaker MyoID loss of function condition. We used a *MyoID-gal4, UAS-myoID*^{RNAi} background line which has a similar sinistral but weaker phenotype as the tester line; in this condition the over expression of chic modified the rotation towards a complete dextral rotation, in other words it completely rescued *myoID* phenotype. It is noteworthy that without *chic* over expression, *MyoID-gal4, UAS-myoIDRNAi* never develops a dextral terminallia (Figure 38C). Finally to double-check our results we did the same experiment using a different Gal4 line, we used the A8 specific Abd-B-LDL-Gal4. Consistently, overexpression of *chic* is also able to rescue *myoID* depletion sinistral phenotype (Figure 38A).

Chickadee-RNAi depletion leads to a No-rotation phenotype

Null mutations at the *chicadee* locus are lethal, and hypomorphic combinations that result in viable flies have no obvious terminallia looping phenotype. Therefore we used RNAi technology to study the loss of function phenotype of Chic in terminalia rotation. There are two available RNAi lines, *UAS-chicRNAi#102759* and *UAS-chicRNAi#HMS00550* they target different sequences of chic transcript. Both RNAi lines in combination with ptc-Gal4 or myoID-Gal4 resulted in larval lethality. Thus, we analyzed the depletion in the A8 segment using AbdB-Gal4. This line, in combination

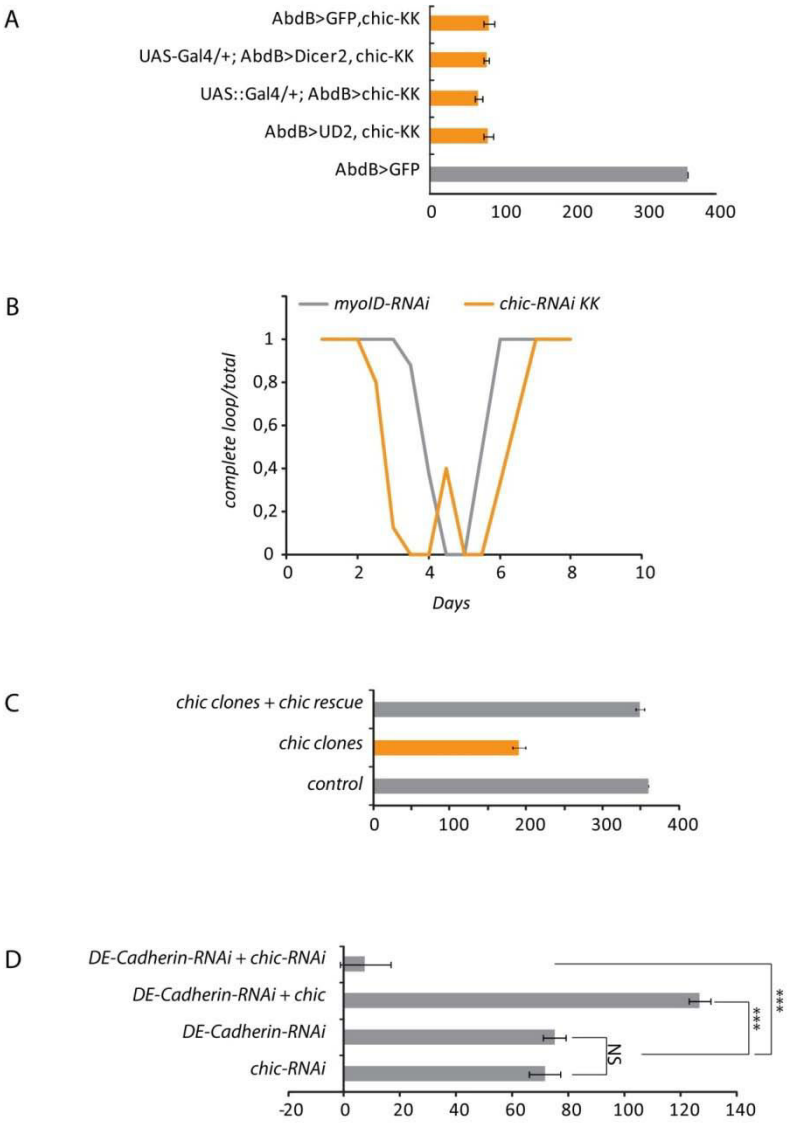

Figure 39. *chic* loss of function phenotypes

A) Knockdown using *UAS-chicRNAi*#102759 resulted in a severe blockage of terminalia rotation, 80° (yellow). This phenotype does not increase with the addition of *Dicer2* or *UAS-Gal4.*AbdB-Gal4 did not affect terminalia rotation (gray) Error bars represent the SEM, n=30-40 flies, *** represent *p*-value <0.0001 for T-student test. B) Graphic of phenotype ratio obtained by the temporal expression of *UAS-chicRNAi*#102759 at different developmental times. *UAS-myoIDRNAi* was done in parallel to compare the temporal requirements of *chic* and *myoID. MyoID* had one clear peak of activity, while *chic* had two clear peaks, one before and one after *myoID. C)* Clones of $chic^{5205}$ null allelle specifically at the A8 segment also resulted in a blockage of terminalia looping (yellow), which could be rescued by chic overexpression. Error bars represent the SEM, n=30-40 flies, *** represent *p*-value <0.0001 for T-student test. D) Depletion of Chic in the A8 phenocopied DE-Cadherin depletion. Further, DE-Cadherin depletion phenotype was enhanced by depletion of Chic and conversely DE-Cadherin depletion phenotype was rescued by *chic* overexpression. Error bars represent the SEM, n=30-40 flies, *** represent *p*-value <0.0001 for T-student test.

with UAS-chicRNAi#102759 results in strong blockage of terminalia rotation. This phenotype does not increase by adding one copy of *UAS-dicer2* or of *UAS-Gal4* (Figure 39A). Surprisingly, *AbdB-Gal4* in combination with *UAS-chicRNAi#HMS00550* resulted in lethality during the pupal period, so we restricted the expression of the RNAi hairpin using a Tub-gal80ts. Indeed, flies with this combination resulted in a similar non rotation phenotype, thus confirming the specificity of our RNAi lines.

Chic in the A8 is efficiently depleted

Chic is widely expressed gene (Robinson et al., 2013), which is expected from a pleiotropic gene that controls actin dynamics. In the genital disc Chic proteins is detected homogeneously throughout the disc (Figure 40A). Depletion of Chic in the A8 disc using *Abdb-Gal4* and *UAS-chicRNAi#102759* effectively eliminates the protein in the A8 segment but not in the rest of the disc (Figure 40C).

Chic RNAi phenotype cannot be rescued by Chic over expression

To confirm our RNAi phenotype specificity, we then tried to rescue by over expressing *chic* coding sequence. However both RNAi constructs target the coding sequence and thus the end phenotype is the same as the depletion alone. We then change our strategy towards a modified genomic version of *chic* that is not targeted by

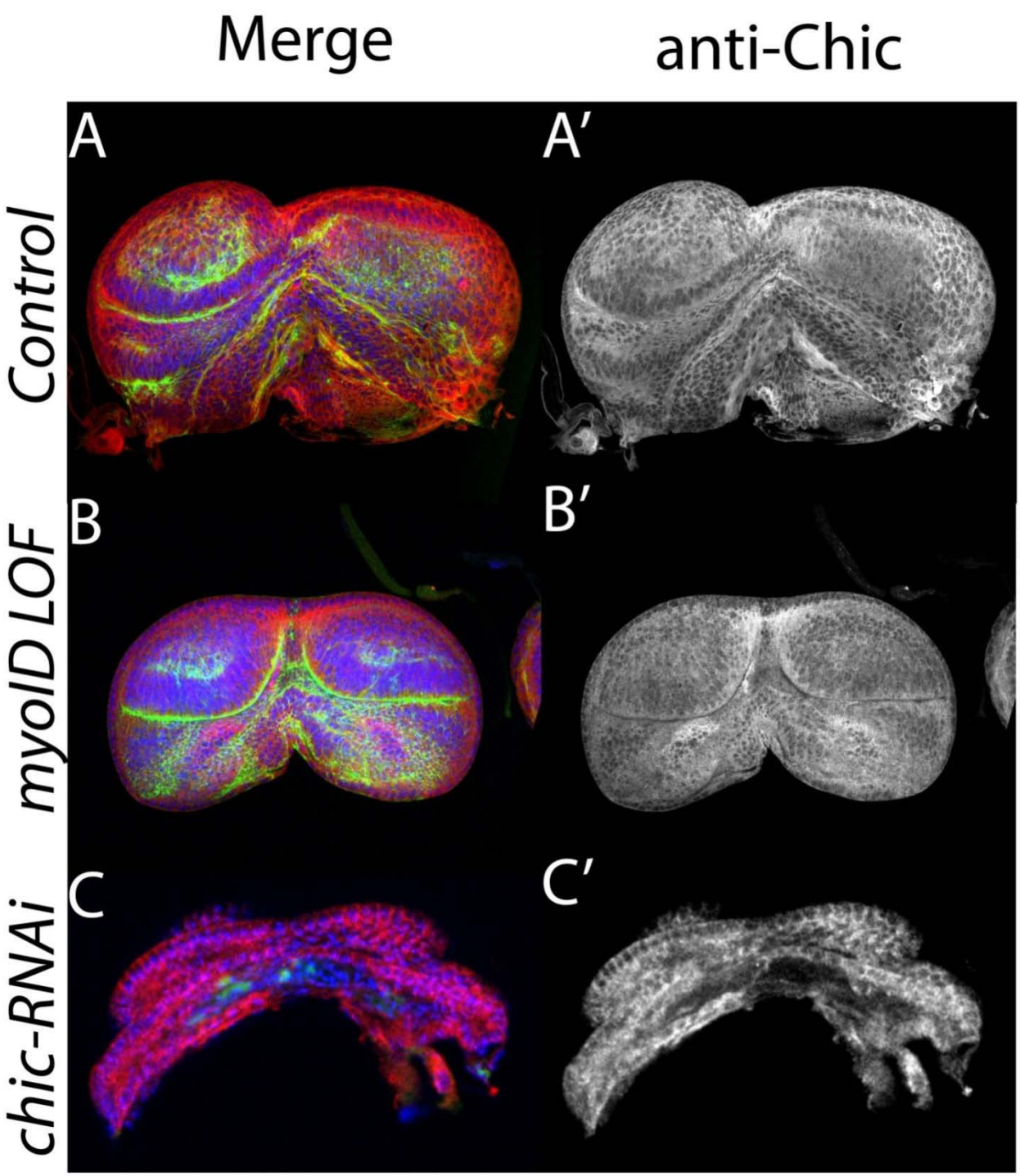

Figure 40. Chic is homogeneously distributed in the genital disc

A) Control genital disc stained for actin (green) and Chic (red) B) Chic staining (red) is not affected upon myoID loss of function. C) Disrupted Chic staining upon expression of UAS-chicRNAi*#102759* in GFP positive cells (green).

the RNAi constructs. In order to do so, we isolated the chic locus from *D.pseudoobscura* a closely related Drosophila specie whose sequence is not targeted by *chic-RNAi* lines but in which Chic function is likely conserved. This strategy has been used to rescue RNAi phenotypes (Langer et al., 2010; Kondo et al., 2009). We constructed two insertions of $chic^{pseudoobscura}$ genomic constructs in chromosomes 2 and 3 respectively. However and despite our efforts *chic-RNAi* phenotype could not be rescued by FlyFos containing chic.

Since our RNAi rescue experiments were discouraging, we tried to rescue a classical mutant for chic with normal *UAS-chic* overexpression construct. For this, we used *chic-Gal4* line which is an insertion into *chic* promoter resulting in a loss of unction mutation of *chic* that also induces expression of the *Gal4* exogene specifically in the *chic* expression pattern. While *chic-Gal4* is embryonic lethal in homozygous conditions or in combination with a deficiency uncovering the chic locus; when in the presence of the *UAS-chic* transgene late stage pupa are normally obtained which develop normally but arrest as a pharate adult and die. This partial lethality rescue, suggest that *UAS-Chic* is indeed capable of rescuing chic mutations and so it induces functional Chic protein.

In order to confirm our *chic-RNAi* terminalia looping phenotypes in a different way, we then induced mitotic clones in the A8 segment of the genital disc in order to generate a A8 segment with around half of the cells completely devoid of Chic protein (See materials and methods section). The induction of clones, containing the null mutation $chic^{p5205}$, lead to a strong blockage of terminalia rotation (Figure 39C); thus confirming the RNAi phenotype. Furthermore, this loss of function condition could be completely

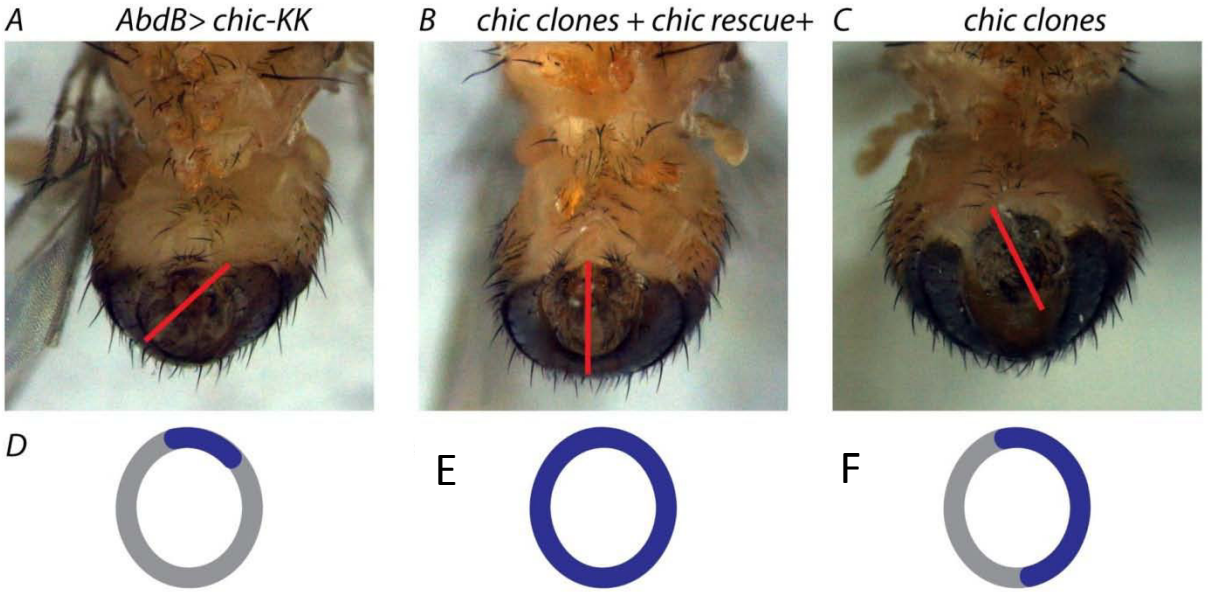

Figure 41. Terminalia rotation defects of Chic depletion in A8

A) RNAi mediated depletion of Chic in the A8 segment blocks terminalia looping, the genotype is *AbdB-Gal4* UAS-chicRNAi*#102759. B)* The phenotype of chic clones can be fully rescued by chic overexpression, the genotype is *w; chic^{p5205}, FRT40A/FRT40a; AbdB-Gal4, UAS-flp/UAS-chic. C)* Flies with clones of chic null mutants specifically in the A8 segment showed impaired terminalia looping, the genotype is *w; chic^{p5205}, FRT40A/FRT40a; AbdB-Gal4, UAS-flp. D)* Graphic representation of average rotation in chic depletion in blue compared to the control in gray, genotype as in A. E) Graphic representation of average rotation as in B. F) Graphic representation of average rotation as in C

rescued by the addition of *UAS-chic* transgene; thus confirming the role of Chic in terminalia rotation (Figure 39C and 41).

Temporal requirement

MyoID activity in directing dextral terminalia rotation is required for 3 hours before pupariation (Speder et al., 2006). To test whether Chic and MyoID have synchronous functions in the A8 segment, we used the temperature-dependent TARGET gene expression system (McGuire et al., 2004) to knockdown the expression of *chic* in the A8 segment at different developmental times. This method has been used to map the temporal activities of MyoIC and DE-Cadherin relative to MyoID activity. MyoIC ativity is perfectly synchronized with MyoID, while DE-Cadherin activity is required hours before MyoID peak (Petzoldt et al., 2012).

The minimal time at which Chic depletion resulted in terminalia rotation defects was 3 hours, which seems reminiscent of MyoID activity. However Chic activity did not completely overlap with MyoID, rather it seem to peak once before MyoID peak and again after (Figure 39B).

Chic and DE-Cadherin

Adherent junctions are adhesive cell-cell contacts and signaling platforms, localizing apically in epithelial cells (Miyoshi and Takai, 2008). Their core component is the dimeric Ca2+-dependent transmembrane protein E-Cadherin, establishing cell adhesion through extracellular domain binding of homodimers at the apical surfaces of adjacent cells (Niessen and Gottardi, 2008).

Since the depletion of Chic and DE-Cadherin using AbdB-Ga4 result in very similar phenotypes, with similar activity peaks just before MyoID activity and both bind to MyoID, we sought these two proteins might work together in establishing dextral terminalia rotation. This interaction is not new, in fact is has proposed for several other models. In cultured cells profilin (Pfn1) depletion leads to E-Cadherin delocalization (Zou et al., 2007), Pfn1 overexpression promotes adherent junction formation through R-Cadherin (Zou et al., 2009), and the control that Pfn1 imposes on AJ is mediated by Rho1 and its effector Dia1 (Bonacci et al., 2012). In Drosophila, E-cadherin, F-actin and APC2 failed to localize properly in chic mutant testes, which leads to a loss of stem cells phenotype that could be partially rescued by overexpression of APC2, a known regulator of AJ (Shields, 2014). Similarly, DE-Cadherin has been shown to strongly influence MyoID function. MyoID binds to DE-Cadherin in A8 segment, if this binding is blocked MyoID fail to control dextral rotation.

We then hypothesized that Chic and De-Cadherin might function together in terminalia rotation. Consistently, the depletion of both DE-Cadherin and Chic in the A8 results is a stronger phenotype that if depleting either one alone. Furthermore, the

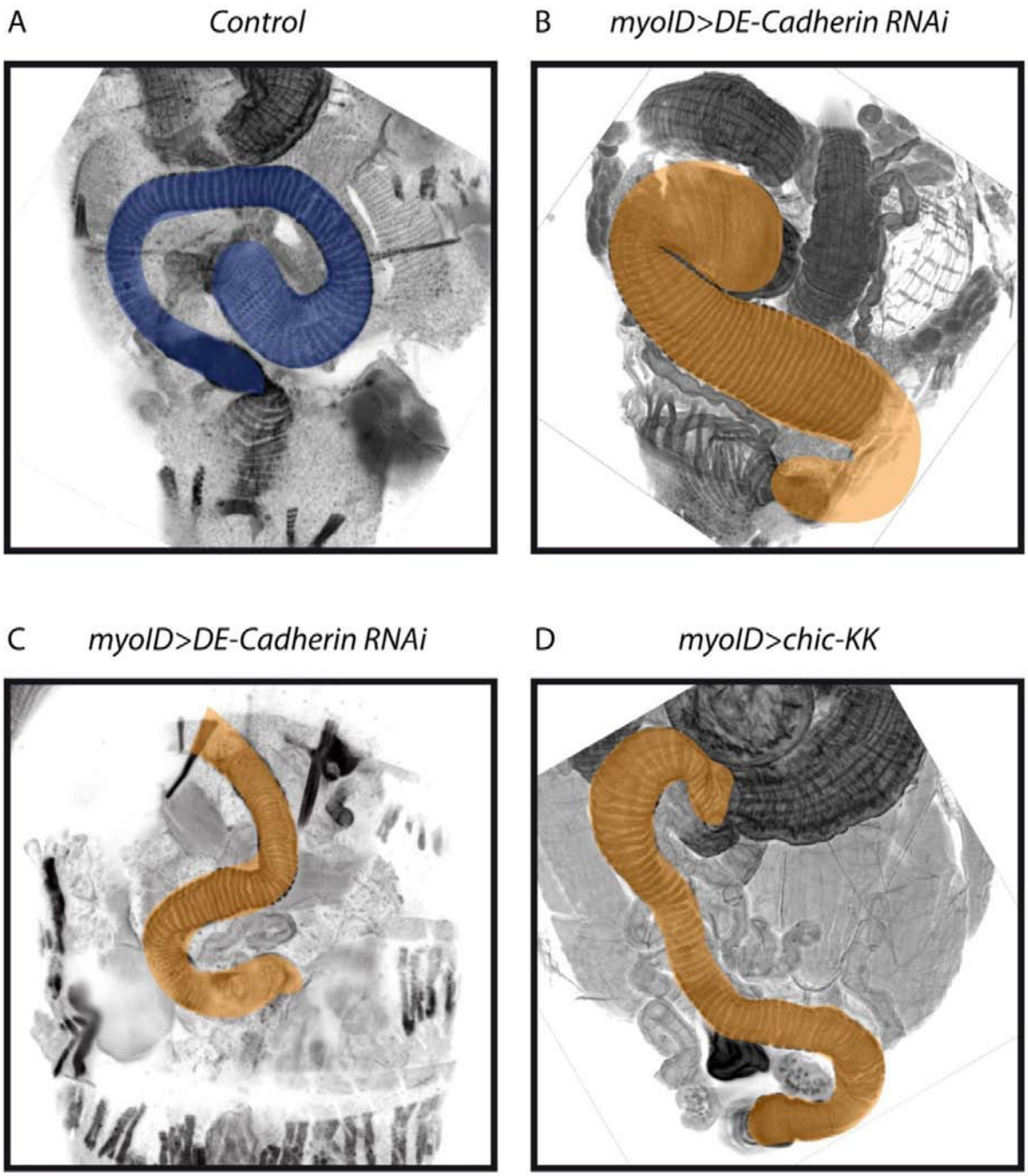

Figure 42. Chic and Cadherin are required in the Hindgut organizer for proper dextral looping

A) In control flies, the AHG is clearly looped dextrally. B) Depletion of DE-Cadherin in the transient H1 cells result in a mislooped AHG, C) Depletion of DE-Cadherin in the transient H1 cells restricted to 12 hours during L3 stage. D) Depletion of Chic in the transient H1 cells restricted to 12 hours during L3 stage

overexpression of *chic* slightly ameliorates the terminalia rotation phenotype induce by DE-Cadherin depletion (Figure 39D). These results suggest that Chic and DE-Cadherin might be functionally coupled in the terminalia looping process.

Chic and DE-Cadherin function in H1 cells to control Adult Hindgut looping

As stated before, the looping of the terminalia is not the only L/R organ in Drosophila; there are at least two that occur during metamorphosis and in which their L/R organizer are known. The dextral looping of the Adult hindgut is controlled by MyoID activity in its specific L/R organizer: the H1 cells. The overall mechanism that conveys the original MyoID-generated asymmetries in the adult hindgut is controlled by the Ft/Ds pathway in coordination with the Fz-planar cell polarity cascade. Neither the Ft/Ds nor the Fz-PCP pathways have a clear role in transmitting dextral information in the terminalia. However, the original L/R asymmetries are generated by MyoID in both tissues, thus the adult hindgut loop represents an attractive model to study the core L/R module, which should play a role in all MyoID dependant L/R tissues.

In other to explore the possibility that Chic would be involved in adult hindgut looping, we depleted its expression specifically in the H1 cells, the L/R organizer for the AHG. RNAi depletion of Chic, using either *myoID-Gal4* or *byn-Gal4* results in larval lethality likely for pleiotropic effectsnot taking place in the H1 cells. To avoid this problem we

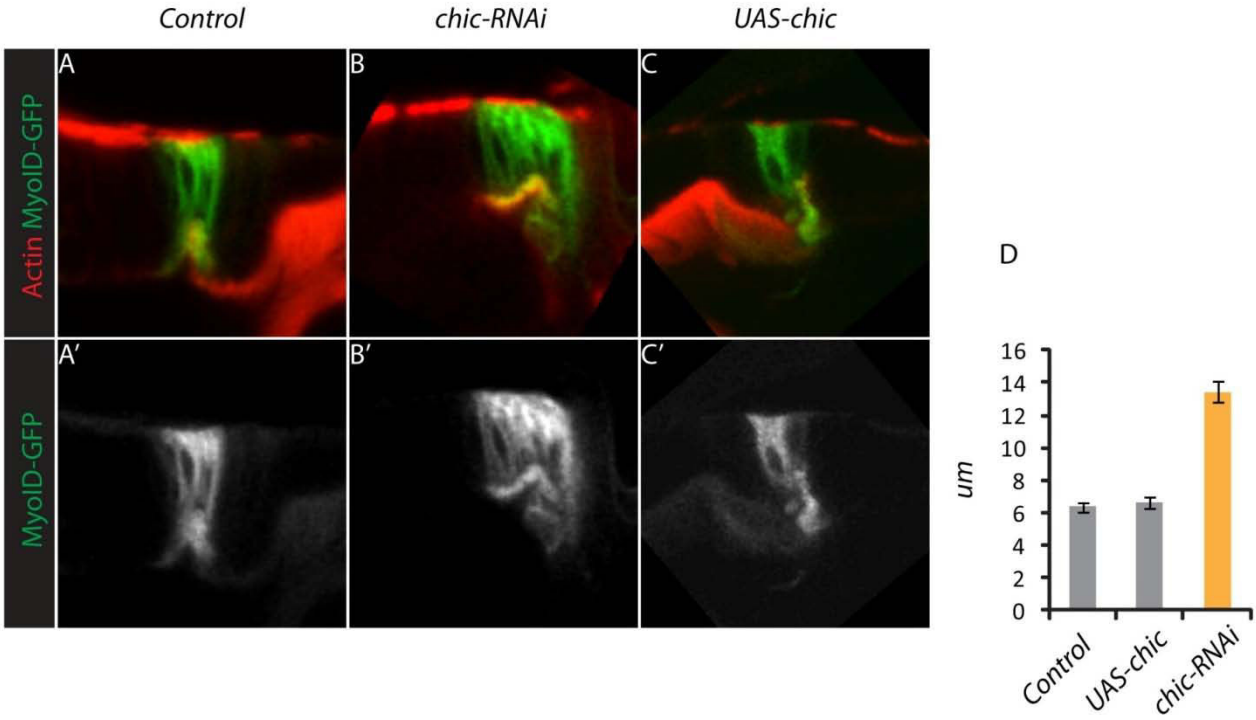

Figure 43. MyoID localization is not Chic dependant

A) MyoID-GFP in H1 cells is distributed along the A-P axis. B) MyoID-GFP distribution in H1 cells upon Chic depletion is not affected, however the H1 domain seems enlarged. C) MyoID-GFP distribution in H1 cells upon Chic overexpression is not affected. D) Graphic of average H1 domain width. Error bars represent the SEM, n=5-8.

specifically depleted Chic in H1 cells during a restricted time window, using the *TubGal80^{TS}* construct. In this condition, viable flies were obtained; the confocal analysis of the AHG loop revealed a completely penetrant mislooped phenotype, we interpreted this phenotype as a loss of L/R polarity (Figure 42D compared to A). We then wondered if depletion of DE-Cadherin in H1 cells would have a similar effect. RNAi depletion of *DE-Cadherin* using MyoID-Gal4 yields some adult escapers, we then analyzed the AHG loop of these escapers. The AHG in this condition is clearly mislooped (Figure 42B) but as a side effect they are also severely thicker. To test if ths was a consequence of the loss of polarity consequence of the depletion of De-Cadherin in H1 cells or if it was a consequence of the continous depletion of DE-Cadhering in adult stages, we restricted DE-Cadherin depletion to L3 stages, using the TubGal80TS construct. In this condition a completely penetrant mislooped phenotype is observed without the thickening of the AHG (Figure 42C). Therefore we conclude that both De-Cadherin and Chic are required specifically in H1 cells to generate or transmit dextral information. We speculate that the function in H1 cells of these proteins is likely conserved with that of the A8 terminalia L/R organizer.

General Discussion

V General Discussion

The AHG as a model to study L/R patterning

The main objective of this thesis study was to establish the adult hindgut (AHG) as a model for understanding the molecular and cellular basis underlying L/R patterning in Drosophila. This was particularly interesting because first it directly questions the hypothesis of the existence of several organizing centers in Drosophila during one specific developmental stage. Though, the existence of several organizing centers was somehow expected due to the independent nature of the adult asymmetric organs with respect to the embryonic ones; this study is the first one to clearly demonstrate that several independent organizers occur at similar developmental times. Therefore the identification of H1 cells as the AHG organizers is crucial for the understanding of Drosophila L/R establishment. Second, before the study of L/R asymmetry in Drosophila was mainly focused on two asymmetric organs the embryonic gut and the adult terminallia rotation and the genetic comparison between these two was used as an argument for constructing a "core" L/R module. This for example was the case for Abd-B the Hox-bearing transcription factor which was originally discovered to affect *myoID* transcription in the terminallia rotation process during a genome-wide deficiency screen. Then Abd-B effect on *myoID* transcription was further expanded to the embryonic gut.

Similarly, the role of the adherent junction component DE-cadherin in L/R determination and its interaction with MyoID had been documented for both the terminallia roation and the embryonic gut. Thus the integration of a new model for L/R asymmetry in Drosophila serves as a model for similar comparisons.

Most likely, the initial L/R asymmetry breaking event occurs at the cellular level in a given population of cells, termed the organizer, which in turn propagate this original L/R bias into a coordinated L/R movement. In the AHG the organizer lays in the H1 cells, a transient structure, easily recognized by the expression of *wg* and *myoID.* The main advantage of this model is its simplicity; the H1 cells break the symmetry and then transmit this breaking information into the H2 cells, the proper AHG primordium. This whole process happens during a 10 hour period, the propagation of L/R bias can be then observed in H2 cells right after this short period of time. Furthermore, the L/R information is maintained for at least 50 hours until a final dextral loop appears in the AHG. This models in thus useful as it has all the theoretical steps for L/R patterning and they can be independently assessed. For example the specific special and temporal inactivation of a component in can be easily achieved using the Gal4/UAS system in combination with the temperature dependant repressor Gal80ts. Similarly the effects of a mutation can be assessed at different time-point tu understand its role; a general misloop phenotype can be thus divided into H2 cell early (10H) mispolarization, as is the case for myoID, Ds and Ft.

The main question of how the initial symmetry breaking event happens can be

applied to the AHG organizer, as it can for any other symmetry breaking event. Though at present this question is not close to being answered we have some insights that may help the planning of future experiments.

In the adult hindgut it is clear that the initial symmetry breaking event happens in H1 cells and is controlled by the activity of MyoID. In other tissues (the embryonic gut and the genital disc) it has been shown that the motor domain of MyoID is the only domain responsible for the L/R activity of MyoID; likely this is also true for the H1 cells. In the genital disc MyoID localize to the adherent junctions where it has been shown to bind DE-Cadherin, while in H1 cells MyoID seems to be equally distributed along the membrane based on the results presented in this thesis. The group of Yohanns Beillaiche has assessed MyoID localization in the developing notum of Drosophila with similar results (Bosveld and Beillaiche personal communication). Despite the homogeneous distribution of MyoID in H1 cells, the association with DE-Cadherin seems to also play a role in the AHG dextral looping; as depletion of DE-Cadherin led to L/R defects. MyoID localization was originally assessed through antibody staining in the embryonic gut and the genital disc; though this antibody is no longer available, we managed to solve this issue by creating a GFP tagged version of MyoID expressed and normal physiological levels which is able to rescue the *myoID* mutant phenotype. Therefore, the difference in the localization pattern might just be a reflex ion of the different strategies, being likely the GFP tagged method more sensitive. The MyoID::GFP tagged version might be useful for doing in vivo recordings of myoID activity during the time period in which is required in H1 cells.

We have also developed an ex-vivo culture approach that recapitulates most of the initial steps of L/R propagation. Thought this sytem recapitulates H2 cells early polarization and the initial steps of H1 cells detachment, the system does not allow further exporation as the tissue in culture suffers a development arrest, somehow around 8-10 HAPF. This approach despite its limitations appears elegant to study MyoID function through live imaging; the obvious experiment would be to follow myoID localization/dynamics using our newly generated MyoID-GFP expressed at physiological levels. Whether to expect MyoID to move around in a particular direction or to be progressively localized one side of the cell, this assay might be usefull to answer to this question. However, it is not a simple experiment to do, H1 cells are highly dynamic especially at the moment when they detach from the H2 cells; therefore analyzing the dynamics of MyoID in an already dynamic cell population might be difficult.

Still understanding the dynamics of MyoID in the organizer is a critical step into understanding L/R symmetry breaking. Cultured mammalian cells had been shown to exhibit stereotypical L/R asymmetric patterns when cultured into a special medium. This has never been shown using *Drosophila* cells. However, it could be possible to dissociate H1 cells and culture them while analyzing MyoID localization. Drosophila cells have a particularly useful screening center devoted to automatically detect phenotypic patterns and/or protein localization while specifically knock-down the expression of genes. Therefore, setting up an assay to reveal cellular asymmetries in Drosophila cells might be a powerful approach. However this system is not completely flawless, the S2 cells (or S2R+ cells) which are commonly use in Drosophila cell culture assays do not look like an

epithelia in culture while all the cell types that have been used for L/R assays in mammalian systems do.

Ft/Ds in L/R patterning

We show a clear functional link betweenboth PCP pathways and L/R MyoID pathway in Drosophila AHG patterning. This link has already been reported several times in higher vertebrates, to name a few: the inversing mutant in a distant homolog of diego, both *Vang* and *Pk* mutants display clear L/R defects in mouse and the human L/R defective condition Bardet-Biedl syndrome has been related to the *bbs4* gene which when mutated leads to PCP defects in mouse. However our results are of importance to the field because i) this is the first time that a link between the PCP pathways and L/R asymmetry is drawn in an invertebrate species pointing out the conservative role of this link and ii) our results point out a crucial role of the global pathway, more specifically of Ds atypical cadherin in L/R asymmetry; which is the first report, to my knowledge, that the role of the global pathway has been linked to L/R establishment.

The involvement of both the core and the global PCP pathways in the adult hindgut loop suggests that they are involved in both the propagation and maintenance of the initial dextral bias. There is currenty some controversy about whether the global PCP and the core PCP proteins function in the same pathway, in two separate pathways or both. The most accepted view is that the global pathway indirectly cues the core-PCP pathway. Though, at this point we have no evidence that clearly states that the core

pathway activity lays downstream of the Ft/Ds pathway as it has been proposed for several other models. It is likely that this is the case for the following reasons: i) the defects obtain by depletion of the core PCP components are always less frequent than the depletion of the Ft/DS components; ii) only Ds protein has a clear role in H1 cells; and ii) depletion of Ft or Ds in H2 cells result in cell disorientation 10hrs APF, while this is not the case for components of the PCP pathway. The critical experiments to do would be to perform epistatic analysis; for example, the overexpression of Ds in H1 cells result in a mislooped phenotype but whether or not this is dependent of the core-PCP pathway is not know, therefore it would be crucial to analyze flies overexpressing Ds in H1 cells and mutant for the core-PCP pathway in H2 cells. His is of course genetically complicated but following the recent advances in drosophila transgenic recourses it might be achievable; for example using both the Gal4 and the LexA systems.

One key observation in the study of the core PCP pathway is the fact that some of their components are transiently localized to one side of the cell (typically proximal/distal sides); I was not able to observe such localization by any of the core PCP pathway components, likely because the known sided localization must occur at a transient period during pupal development, where the AHG is practically unreachable by normal dissection.

On the Ft/Ds side, it has been shown that both Dachous and Fat are slightly localized towards one side of the cell membrane and that localization leads to the strong accumulation of the atypical myosin Dachs (Ambegaonkar et al., 2012; Brittle et al.,

2012 ; Bosveld et al., 2012). Ds localization was assessed by the knock-in allele Ds::GFP, the HA-tagged form and the overexpression of a GFP tagged form of Ds. In any of these was an accumulation of Ds obvious, somehow consistent with the weak accumulation of Ds in other tissues. However, more precise microscopy techniques should be able to resolve this issue. On the other hand, Dachs whch is strongly localized and is usually easier to see than Ds was also analyzed. There are several tools used to analyze the localization of Dachs: an antibody published by the Strutt group, an V5-tagged overexpression form and a Citrine-tagged form. Dach localization was assessed by the overexpression of the V5- and citrine-Tagged versions In the case of the citrine-tagged version a clear membrane accumulation was evident in the posterior membrane of H2 cells; though at this point we have not been able to resolve whether this is L/R asymmetric feature or not.

Chic and the underlying actin cytoskeleton

We have uncovered through the use of the powerful genetic system of D*rosophila* a new role of Chic/Profilin in controlling the directional dextral movement of the terminalia; we have also shown that this role is achieved in concert with MyoID, the known dextral determinant in flies, and DE-Cadherin; and finally that the Chic/Profilin role in L/R patterning is conserved among tissues. However, at present we lack information to propose a clear model for Chic function; new data from Michel Ostap's

Lab have shown that some type 1 myosins, including *Drosophila* MyoID are able to impose a chiral direction over sliding actin filaments when anchored to a phospholipid membrane (Pyrpassopoulos et al., 2012). This results is most telling, they strongly suggest that the simplest L/R asymmetry complex is composed only of actin filaments and myosin. Though at present we lack information to conclude whether or not this asymmetric sliding capability of myoID is the functional information that breaks asymmetry in flies; this assay still can be used to infer the activity of MyoID cofactors. To my knowledge there is currently no way of setting up a similar experiment in flies, as it would require to look at individual actin filaments inside a cell. However, the in vitro assay can be applied to understand the relationship between components that have been isolated through genetic screen and in which an exact molecular explanation is missing. Such is the case of Chic/Profilin; initially isolated through a genetic screen, has been shown to be needed along with MyoID for proper L/R function, and forms a complex in vivo with MyoID but the exact mechanism of action has remain completely elusive.

At present we know very little about Chic function in actin dynamics and almost nothing of its function in L/R asymmetry establishment. While classic loss-of-function experiments are hard to analyze due to the fact that Chic is a general component on actin dynamics and thus affecting its function leads to a general cytoskeleton problem. The in vitro approach might be suitable for understanding at a molecular level the role of Chic and MyoID.

The strongest evidence that we have regarding the functional link between Chic and MyoID in L/R patterning is that the overexpression of Chic can, in some specific conditions, rescue MyoID loss of function phenotype. To my knowledge this is the only gene to which this particular function has been reported. Again, the *in-vitro* actin gliding assay might provide useful information. At this point our lab has set-up collaboration with Michael Ostap's group to understand the molecular basis of Chic-MyoId function. We know that Chic is dispensable for MyoId asymmetric gliding of actin filaments in-vitro, because the original assay did not include any Profilin homolog in the mix, however it would be important to know whether the addition of Chic would affect the actin motility in this particular assay, as it has been reported in other actin polymerization assays (Jégou et al., 2011).

The sinistral factor

To this date the most convincing evidences of the existence of a sinistral factor in *Drosophila* are i) the specific nature of *myoID* loss of function phenotype, in which a complete inversion of the L/R axis is observed as opposed to a randomization off the axis or a symmetrical state and ii) the fact that Abd-B, the upstream activator factor of *myoID,* when depleted in the organizer leads to a symmetric state that can be rescued by *myoID* forced expression.

Those two key observations have lead to the proposal that Abd-B controls the expression of both *myoID* and the yet elusive sinistral factor (Coutelis et al., 2013). This particular conclusion is based upon the assumption that when Abd-B is missing in the L/R organizer the only two genes whose expression is affected are *myoID* and the sinitral factor. Otherwise, how would it be possible to restore dextral looping in Abd-B depletion upon *myoID* forced expression?

While this reasoning appears logic, most efforts to isolate the sinistral factor have not been successful, I though useful to discuss some examples that show that the nature of the sinistral factor might be more complex than estimated.

During our deficiency genome-wide screen (See Chapter: Genome wide deficiency based interaction screen) we identified a specific region in Chromosome 2 able to completely rescue *myoID* loss of function, therefore acting as a putative sinistral factor. While this deficiency uncovered only 5 genes, none of them was clearly able to explain the interacting phenotype of the deficiency by itself. Thus raising the question of what exactly is behind this deficiency that makes it rescue *myoID* loss of function phenotype? Of course, at present we have no answer to this question. However a key observation is that none of the proteins encoded in these genes have structural similarity with MyoID; which is expected from a sinistral factor that functions in a similar fashion to MyoID.

When these observations were done, we lacked a method for generating precise deletions, which if now available through the CRISPR/Cas9 method. We also lacked a

way of visualizing the expression of these genes which is also now available through the Flylight and Viena-Tile projects. These two recent and powerful tools might provide enough insights into the nature of this particular region involved so strongly in L/R patterning.

Another example that questions the simplicity of the sinistral factor model is the fact that while *myoID* has a similar function in the adult hingut and the terminalia, and while Abd-B controls its expression in both tissues, the specific regions where Abd-B binds in *myoID* locus are unique in the genome. This is surprising as the expectation was that the regulatory regions in both MyoID and the sinistral factor had co-evolveed, thus resulting in similar sequences controlling the expression of MyoID and the sinistral factor.

Finally, the "symmetric" phenotype induced by the loss of most genes that have been related to *myoID* and thus to L/R asymmetry in *Drosophila* are explained by the hypothesis, not yet tested, that they also affect the sinistral pathway. Such is the case of DE-Cadherin, of Abd-B and of Dachsous. Therefore, the sinistral factor should act very similar to MyoID. All Drosophila myosins have been tested for L/R phenotypes but none has been identified as the sinitral factor (Petzoldt et al., 2012). Since the sinistral factor is thus not a myosin, how is it able to function in such a similar way as MyoID? Of course, this question has not a clear answer at present and only the identification of such factor will be able to shed light into this mechanism.

As a summary, while the existence of a sinistral factor is almost certain, the

nature of this factor is where the surprise will be. Likely it is not related structurally to MyoID, but it should act upstream of the same components as MyoID (Cadherin, Dachsous). It is under the control of Abd-B yet the regulatory regions are likely not similar to those of *myoID.* Could it be that the sinistral factor lies in front of our eyes and yet it has been so hard to see?

Mammalian cells in culture, in a particular way of culture, are able to orient themselves in a chiral L/R asymmetric way. Strikingly, while most cells exhibit a dextral chirality some have a sinistral one; and the overall dextral chirality of those cells can be reverted by adding drugs that disturb the actin cytoskeleton (Wan et al., 2011). This experiment demonstrates the intrinsic chiral property of the actin cytoskeleton. Of course such experiment is hard to do in vivo as disturbing the actin cytoskeleton would have much more dramatic effects that would cover from sight any L/R phenotype. However these experiments strongly suggest the chiral nature of the actin cytoskeleton, at least for mammalian cultured cells, raising the possibility that the actin cytoskeleton lays at the base of L/R asymmetric breaking event.

The evolution of L/R asymmetry

Another advantage of the AHG as a model for L/R is the fact that it has recently appeared during the course of *Drosophila* evolution (around 50 million years ago). This

established a temporal framework in which all the necessary components for L/R asymmetry appeared for a specific organ. We have shown that MyoID is necessary in a row of transient cells (termed H1) for the correct dextral orientation of the hindgut primordium (named H2 cells); we have also shown that the propagation/mainteinance of this dextral orientation is originally transmitted through the atypical cadherin Dachsous, further propagated by the Dachsous/Fat patchway and finally maintained by the core Fz-PCP pathway (see Results chapter). Therefore, 50 million years ago all these components assembled into a new L/R organizing center which provided a dextral looping.

As it has been previously hypothesized, evolution functions on the rearrangement of pre-existing components (Werner et al., 2010). At present is hard to completely understand how the AHG dextral loop came to existence. The most probable scenario would be that the essential components for L/R patterning in other tissues (i.e the terminalia looping) were reused to form the adult hindgut organizer. There are at least two possible ancestral conditions: i) the absence of expression of L/R components in the AHG pimordium or ii) the complete lack of H1 cells. Since MyoID is specifically detected in H1 cells either ancestral condition would lead to the absence of MyoID in non-looped species. Thus, if the appearance of adult hingut looping correlated with the appearance of H1 cells it would also correlate with the gain of *myoID* expression. This is not particularly true for the PCP components as they are mostly functional in H2 cells for correct AHG dextral looping. Thus the questions: were the PCP components present in the AHG primordium before the appearance of dextral looping? If so, what was their

function? We did not detect any other obvious phenotype in the AHG after the inactivationof the PCP components, however this does not completely rule out the possibility that they have another yet elusive function in this organ.

The identification of a particular cis-regulatory region in *myoID* locus provides a good explanation on how the AHG looped came to existence: the appearance of a novel cis-regulatory element in the *myoID* locus evolved the adult hindgut dextral loop, without modifying the other dextral organs (i.e. the terminalia looping). Similar events in which the appearance (or loss) of a cis-regulatory element in a gene correlates with the appearance of a specific trait have been reported, in particular for the interspecies variation of wing and body pigmentation in *Drosophila* genus (Gruber et al., 2012; Kalay and Wittkopp, 2010; Wittkopp, 2010; Jeong et al., 2008; Prud'homme et al., 2006; Werner et al., 2010; Williams et al., 2008). Therefore, cis-regulatory element variation might be a common principle in animal evolution that might be proven true also for the evolution of L/R structures.

L/R patterning in insect evolution is particularly diverse, while most likely most insect orders have a dextrally coiled embryonic gut, the terminallia dextral looping is a particularity of a group of flies which do not include mosquitoes (Reviewed in Suzanne et al., 2010), the testes dextral coiling is present in the closest relatives to *Drosophila melanogaster* but is not in the *Drosophila pseudoobscura* group. It would be interesting to understand if cis-regulatory elements in *myoID* locus underlie the diversity of L/R structures in insects. Recently the complete genome sequence of many (>40) insects

from different orders became publicly available facilitating the exploration on the evolution of *myoID* sequence.

Our results on a cis-regulatory element in *myoID* underlying AHG looping shows for the first time the evolutionary advantage of having several L/R organizers, as opposed to vertebrates which rely on only one. Having several organizers liberate the evolutionary constrains of L/R pattering by letting each L/R organ bare its own evolutionary pressures. Briefly, whatever the evolutionary pressure that caused the fixation of the AHG dextral loop did not affected the L/R patterning at the terminalia. This particularity of *Drosophila* (which might be true also for other insects) has likely contributed to the diversification of L/R asymmetric structures.

VI Figure index

Figure 1. Examples of L/R asymmetric traits in the animal kingdom

Figure 2. The apicobasal polarity in epithelial cells

Figure 3. Planar Cell Polarity in the Drosophila wing epithelium

Figure 4. Schematics of polarization mechanisms in the wing

Figure 5. Properties of the core planar polarity proteins in Drosophila wing development.

Figure 6. Fat and Dachsous interactions in the Drosophila wing

Figure 7. Illustrative views ofc Fat and Dachsous atypical cadherins

Figure 8. Structure and development of the alimentary tract of the fly

Figure 9. Comparison between larval and adult hindguts

Figure 10. Overview of the UAS/GAL4 system in Drosophila

Figure 11. Overview of the transgenic RNAi mediated depletion system in Drosophila

Figure 12. Overview of the FRT/FLP mediated clone induction system in Drosophila

Figure 13. Evolution of the AHG looping direction in Drosophila

Figure 14. Putative AHG Cis-Regulatory Module revealed by conservation scores

Figure 15. Abd-B in myoID regulation

Figure 16. Abd-B downregulation affects myoID expression

Figure 17. Generation of enhancer specific CRISP mutants in myoID locus

Figure 18. Genomic map of Crisp Mutants and regions specific for Sophophora (looped) flies

Figure 19. Subdivision of the AHG based on Gal4 expression patterns

Figure 20. AHG precursors detection using linage tracing and selective Gal4 lines

Figure 21. The rectal junction precursors

Figure 22 . The anterior ileum precursors

Figure 23. The stem-cell region precursors

Figure 24. The relation between growth and looping in the AHG

Figure 25. The looping moment revealed by time serial sections

Figure 26. Depletion of Abd-B or Byn in the imaginal ring strongly impairs AHG formation

Figure 27. Depletion of Abd-B but not Byn in H2 cells results in absence of terminallia structures

Figure 28. Abd-B depletion leads to byn down regulation

Figure 29. Abd-B and byn are highly enriched genes in the hindgut

Figure 30. Effects on bynVT-Gal4 expression upon increased and decreased Abd-B level

Figure 31. Localization of putative Abd-B BS at the byn locus

Figure 32. Markers of proper AHG development in culture

Figure 33. H2 dextral polarization revealed by time-lapse confocal microscopy

Figure 34. Examples of asymmetry revealed by tagged centrosomes

Figure 35. Multiple Cnn-positive structures uppon Cnn-GFP overexpression

Figure 36. General strategy for deficiency-based genome wide screen

Figure 37. Genome wide screen unveils the role of chic in LR patterning

Figure 38. Chic overexpression rescues myoID depletion

Figure 39. chic loss of function phenotypes

Figure 40. Chic is homogeneously distributed in the genital disc

Figure 41. Terminalia rotation defects of Chic depletion in A8

Figure 42. Chic and Cadherin are required in the Hindgut organizer for proper dextral looping

Figure 43. MyoID localization is not Chic dependant

VII General References

Adams, D.S., Robinson, K.R., Fukumoto, T., Yuan, S., Albertson, R.C., Yelick, P., Kuo, L., McSweeney, M., and Levin, M. (2006). Early, H+-V-ATPase-dependent proton flux is necessary for consistent left-right patterning of non-mammalian vertebrates. Development 133, 1657–1671.

Adler, P.N. (2002). Planar Signaling and Morphogenesis in Drosophila. Developmental Cell 2, 525–535.

Adler, P.N. (2012). The frizzled/stan pathway and planar cell polarity in the Drosophila wing. Curr. Top. Dev. Biol. 101, 1–31.

Adler, P.N., Charlton, J., and Liu, J. (1998). Mutations in the cadherin superfamily member gene dachsous cause a tissue polarity phenotype by altering frizzled signaling. Development 125, 959–968.

Aigouy, B., Farhadifar, R., Staple, D.B., Sagner, A., Röper, J.-C., Jülicher, F., and Eaton, S. (2010). Cell Flow Reorients the Axis of Planar Polarity in the Wing Epithelium of Drosophila. Cell 142, 773–786.

Ambegaonkar, A.A., Pan, G., Mani, M., Feng, Y., and Irvine, K.D. (2012). Propagation of Dachsous-Fat Planar Cell Polarity. Current Biology 22, 1302–1308.

De Anda, F.C., Pollarolo, G., Da Silva, J.S., Camoletto, P.G., Feiguin, F., and Dotti, C.G.

(2005). Centrosome localization determines neuronal polarity. Nature 436, 704–708.

Andersen, D.S., Colombani, J., and Léopold, P. (2013). Coordination of organ growth: principles and outstanding questions from the world of insects. Trends Cell Biol. 23, 336–344.

Antic, D., Stubbs, J.L., Suyama, K., Kintner, C., Scott, M.P., and Axelrod, J.D. (2010). Planar cell polarity enables posterior localization of nodal cilia and left-right axis determination during mouse and Xenopus embryogenesis. PLoS One 5, e8999.

Asami, T., Gittenberger, E., and Falkner, G. (2008). Whole-body enantiomorphy and maternal inheritance of chiral reversal in the pond snail Lymnaea stagnalis. J. Hered. 99, 552–557.

Axelrod, J.D. (2009). Progress and challenges in understanding planar cell polarity signaling. Semin Cell Dev Biol 20, 964–971.

Ayukawa, T., Akiyama, M., Mummery-Widmer, J.L., Stoeger, T., Sasaki, J., Knoblich, J.A., Senoo, H., Sasaki, T., and Yamazaki, M. (2014). Dachsous-Dependent Asymmetric Localization of Spiny-Legs Determines Planar Cell Polarity Orientation in Drosophila. Cell Rep.

Bach, E.A., Ekas, L.A., Ayala-Camargo, A., Flaherty, M.S., Lee, H., Perrimon, N., and Baeg, G.-H. (2007). GFP reporters detect the activation of the Drosophila JAK/STAT pathway in vivo. Gene Expression Patterns 7, 323–331.

Bard, F., Casano, L., Mallabiabarrena, A., Wallace, E., Saito, K., Kitayama, H., Guizzunti, G.,

Hu, Y., Wendler, F., DasGupta, R., et al. (2006). Functional genomics reveals genes involved in protein secretion and Golgi organization. Nature 439, 604–607.

Barrangou, R., Fremaux, C., Deveau, H., Richards, M., Boyaval, P., Moineau, S., Romero, D.A., and Horvath, P. (2007). CRISPR provides acquired resistance against viruses in prokaryotes. Science 315, 1709–1712.

Basto, R., Lau, J., Vinogradova, T., Gardiol, A., Woods, C.G., Khodjakov, A., and Raff, J.W. (2006). Flies without centrioles. Cell 125, 1375–1386.

Bastock, R., Strutt, H., and Strutt, D. (2003). Strabismus is asymmetrically localised and binds to Prickle and Dishevelled during Drosophila planar polarity patterning. Development 130, 3007–3014.

Beumer, K.J., and Carroll, D. (2014). Targeted genome engineering techniques in Drosophila. Methods 68, 29–37.

Blum, M., Schweickert, A., Vick, P., Wright, C.V.E., and Danilchik, M.V. (2014). Symmetry breakage in the vertebrate embryo: When does it happen and how does it work? Dev. Biol.

Bohni, R., Riesgo-Escovar, J., Oldham, S., Brogiolo, W., Stocker, H., Andruss, B.F., Beckingham, K., and Hafen, E. (1999). Autonomous control of cell and organ size by CHICO, a Drosophila homolog of vertebrate IRS1-4. Cell 97, 865–875.

Bonacci, T.M., Hirsch, D.S., Shen, Y., Dokmanovic, M., and Wu, W.J. (2012). Small GTPase Rho regulates R-cadherin through Dia1/profilin-1. Cellular Signalling 24, 2102–2110.

Bosveld, F., Bonnet, I., Guirao, B., Tlili, S., Wang, Z., Petitalot, A., Marchand, R., Bardet, P.L., Marcq, P., Graner, F., et al. (2012). Mechanical control of morphogenesis by Fat/Dachsous/Four-jointed planar cell polarity pathway. Science 336, 724–727.

Böttcher, R., Hollmann, M., Merk, K., Nitschko, V., Obermaier, C., Philippou-Massier, J., Wieland, I., Gaul, U., and Förstemann, K. (2014). Efficient chromosomal gene modification with CRISPR/cas9 and PCR-based homologous recombination donors in cultured Drosophila cells. Nucleic Acids Res. 42, e89.

Brand, A.H., and Perrimon, N. (1993). Targeted gene expression as a means of altering cell fates and generating dominant phenotypes. Development 118, 401–415.

Brittle, A., Thomas, C., and Strutt, D. (2012). Planar Polarity Specification through Asymmetric Subcellular Localization of Fat and Dachsous. Current Biology 22, 907–914.

Brittle, A.L., Repiso, A., Casal, J., Lawrence, P.A., and Strutt, D. (2010). Four-jointed modulates growth and planar polarity by reducing the affinity of dachsous for fat. Curr. Biol. 20, 803–810.

Brock, A.R., Wang, Y., Berger, S., Renkawitz-Pohl, R., Han, V.C., Wu, Y., and Galko, M.J. (2012). Transcriptional regulation of Profilin during wound closure in Drosophila larvae. J Cell Sci 125, 5667–5676.

Brodsky, M.H., and Wolfe, S. (2014). Fly Factor Survey.

Bryant, D.M., and Mostov, K.E. (2008). From cells to organs: building polarized tissue. Nat. Rev. Mol. Cell Biol. 9, 887–901.

Buchon, N., Osman, D., David, F.P.A., Fang, H.Y., Boquete, J.-P., Deplancke, B., and Lemaitre, B. (2013). Morphological and molecular characterization of adult midgut compartmentalization in Drosophila. Cell Rep 3, 1725–1738.

Di Cara, F., and King-Jones, K. (2013). How clocks and hormones act in concert to control the timing of insect development. Curr. Top. Dev. Biol. 105, 1–36.

Casal, J., Lawrence, P.A., and Struhl, G. (2006). Two separate molecular systems, Dachsous/Fat and Starry night/Frizzled, act independently to confer planar cell polarity. Development 133, 4561–4572.

Chen, W.-S., Antic, D., Matis, M., Logan, C.Y., Povelones, M., Anderson, G.A., Nusse, R., and Axelrod, J.D. (2008). Asymmetric Homotypic Interactions of the Atypical Cadherin Flamingo Mediate Intercellular Polarity Signaling. Cell 133, 1093–1105.

Chew, S.K., Chen, P., Link, N., Galindo, K.A., Pogue, K., and Abrams, J.M. (2009). Genome-wide silencing in Drosophila captures conserved apoptotic effectors. Nature 460, 123–127.

Chintapalli, V.R., Wang, J., Herzyk, P., Davies, S.A., and Dow, J.A.T. (2013). Data-mining the FlyAtlas online resource to identify core functional motifs across transporting epithelia. BMC Genomics 14, 518.

Christensen, R.G., Enuameh, M.S., Noyes, M.B., Brodsky, M.H., Wolfe, S.A., and Stormo, G.D. (2012). Recognition models to predict DNA-binding specificities of homeodomain proteins. Bioinformatics 28, i84–89.

Coast, G. (2007). The endocrine control of salt balance in insects. Gen. Comp. Endocrinol. 152, 332–338.

Cognigni, P., Bailey, A.P., and Miguel-Aliaga, I. (2011). Enteric Neurons and Systemic Signals Couple Nutritional and Reproductive Status with Intestinal Homeostasis. Cell Metabolism 13, 92–104.

Cohen, E. (2013). Chapter One - Water Homeostasis and Osmoregulation as Targets in the Control of Insect Pests. In Advances in Insect Physiology, Ephraim Cohen, ed. (Academic Press), pp. 1–61.

Courtemanche, N., Lee, J.Y., Pollard, T.D., and Greene, E.C. (2013). Tension modulates actin filament polymerization mediated by formin and profilin. PNAS 110, 9752–9757.

Coutelis, J.B., Petzoldt, A.G., Spéder, P., Suzanne, M., and Noselli, S. (2008). Left-right asymmetry in Drosophila. Semin. Cell Dev. Biol. 19, 252–262.

Coutelis, J.B., Geminard, C., Speder, P., Suzanne, M., Petzoldt, A.G., and Noselli, S. (2013). Drosophila left/right asymmetry establishment is controlled by the Hox gene abdominal-B. Dev Cell 24, 89–97.

Cui, C., Little, C.D., and Rongish, B.J. (2009). Rotation of organizer tissue contributes to left-right asymmetry. Anat Rec (Hoboken) 292, 557–561.

D'Brot, A., Chen, P., Vaishnav, M., Yuan, S., Akey, C.W., and Abrams, J.M. (2013). Tango7 directs cellular remodeling by the Drosophila apoptosome. Genes Dev. 27, 1650–1655.

Das, G., Reynolds-Kenneally, J., and Mlodzik, M. (2002). The atypical cadherin Flamingo links Frizzled and Notch signaling in planar polarity establishment in the Drosophila eye. Dev. Cell 2, 655–666.

Dongen, S.V. (2006). Fluctuating asymmetry and developmental instability in evolutionary biology: past, present and future. J. Evol. Biol. 19, 1727–1743.

Donoughe, S., and DiNardo, S. (2011). dachsous and frizzled contribute separately to planar polarity in the Drosophila ventral epidermis. Development 138, 2751–2759.

Drosophila 12 Genomes Consortium, Clark, A.G., Eisen, M.B., Smith, D.R., Bergman, C.M., Oliver, B., Markow, T.A., Kaufman, T.C., Kellis, M., Gelbart, W., et al. (2007). Evolution of genes and genomes on the Drosophila phylogeny. Nature 450, 203–218.

Eaton, S., and Jülicher, F. (2011). Cell flow and tissue polarity patterns. Curr. Opin. Genet. Dev. 21, 747–752.

Ejsmont, R.K., Sarov, M., Winkler, S., Lipinski, K.A., and Tomancak, P. (2009a). A toolkit for high-throughput, cross-species gene engineering in Drosophila. Nat. Methods 6, 435–437.

Ejsmont, R.K., Sarov, M., Winkler, S., Lipinski, K.A., and Tomancak, P. (2009b). A toolkit for high-throughput, cross-species gene engineering in Drosophila. Nat. Methods 6, 435–437.

Evans, C.J., Olson, J.M., Ngo, K.T., Kim, E., Lee, N.E., Kuoy, E., Patananan, A.N., Sitz, D., Tran, P., Do, M.-T., et al. (2009b). G-TRACE: rapid Gal4-based cell lineage analysis in

Drosophila. Nat. Methods 6, 603–605.

Fox, D.T., and Spradling, A.C. (2009). The Drosophila hindgut lacks constitutively active adult stem cells but proliferates in response to tissue damage. Cell Stem Cell 5, 290–297.

Fox, D.T., Gall, J.G., and Spradling, A.C. (2010). Error-prone polyploid mitosis during normal Drosophila development. Genes Dev. 24, 2294–2302.

Gao, J., Hu, Y., Toda, M.J., Katoh, T., and Tamura, K. (2011). Phylogenetic relationships between Sophophora and Lordiphosa, with proposition of a hypothesis on the vicariant divergences of tropical lineages between the Old and New Worlds in the family Drosophilidae. Mol. Phylogenet. Evol. 60, 98–107.

Géminard, C., González-Morales, N., Coutelis, J.-B., and Noselli, S. (2014). The myosin ID pathway and left-right asymmetry in Drosophila. Genesis 52, 471–480.

Gerlach, H. (2013). Chirality: A Relational Geometric-Physical Property. Chirality 25, 684–685.

Goodrich, L.V., and Strutt, D. (2011). Principles of planar polarity in animal. Development 138, 1877–1892.

Grande, C. (2010). Left-right asymmetries in Spiralia. Integr. Comp. Biol. 50, 744–755.

Gratz, S.J., Cummings, A.M., Nguyen, J.N., Hamm, D.C., Donohue, L.K., Harrison, M.M., Wildonger, J., and O'Connor-Giles, K.M. (2013). Genome engineering of Drosophila with the CRISPR RNA-guided Cas9 nuclease. Genetics 194, 1029–1035.

Gray, R.S., Roszko, I., and Solnica-Krezel, L. (2011). Planar cell polarity: coordinating morphogenetic cell behaviors with embryonic polarity. Dev. Cell 21, 120–133.

Gros, J., Feistel, K., Viebahn, C., Blum, M., and Tabin, C.J. (2009). Cell movements at Hensen's node establish left/right asymmetric gene expression in the chick. Science 324, 941–944.

Gruber, J.D., Vogel, K., Kalay, G., and Wittkopp, P.J. (2012). Contrasting properties of gene-specific regulatory, coding, and copy number mutations in Saccharomyces cerevisiae: frequency, effects, and dominance. PLoS Genet. 8, e1002497.

Gupta, B.L., and Berridge, M.J. (1966). Fine structural organization of the rectum in the blowfly, Calliphora erythrocephala (Meig.) with special reference to connective tissue, tracheae and neurosecretory innervation in the rectal papillae. J. Morphol. 120, 23–81.

Hadjieconomou, D., Rotkopf, S., Alexandre, C., Bell, D.M., Dickson, B.J., and Salecker, I. (2011). Flybow: genetic multicolor cell labeling for neural circuit analysis in Drosophila melanogaster. Nat. Methods 8, 260–266.

Hartenstein, V. (1995). Atlas of Drosophila Development (Cold Spring Harbor Laboratory Press).

Harumoto, T., Ito, M., Shimada, Y., Kobayashi, T.J., Ueda, H.R., Lu, B., and Uemura, T. (2010a). Atypical cadherins Dachsous and Fat control dynamics of noncentrosomal microtubules in planar cell polarity. Dev. Cell 19, 389–401.

Harumoto, T., Ito, M., Shimada, Y., Kobayashi, T.J., Ueda, H.R., Lu, B., and Uemura, T.

(2010b). Atypical Cadherins Dachsous and Fat Control Dynamics of Noncentrosomal Microtubules in Planar Cell Polarity. Developmental Cell 19, 389–401.

Hogan, J., Valentine, M., Cox, C., Doyle, K., and Collier, S. (2011). Two frizzled planar cell polarity signals in the Drosophila wing are differentially organized by the Fat/Dachsous pathway. PLoS Genet 7, e1001305.

Hopkins, C.R. (1967). The fine-structural changes observed in the rectal papillae of the mosquito Aedes aegypti, L. and their relation to epithelial transport of water and inorganic ions. J R Microsc Soc 86, 235–252.

Hozumi, S., Maeda, R., Taniguchi, K., Kanai, M., Shirakabe, S., Sasamura, T., Speder, P., Noselli, S., Aigaki, T., Murakami, R., et al. (2006). An unconventional myosin in Drosophila reverses the default handedness in visceral organs. Nature 440, 798–802.

Huet, F., Lu, J.T., Myrick, K.V., Baugh, L.R., Crosby, M.A., and Gelbart, W.M. (2002). A deletion-generator compound element allows deletion saturation analysis for genomewide phenotypic annotation. Proc. Natl. Acad. Sci. U.S.A. 99, 9948–9953.

Ishikawa, H.O., Takeuchi, H., Haltiwanger, R.S., and Irvine, K.D. (2008). Four-jointed Is a Golgi Kinase That Phosphorylates a Subset of Cadherin Domains. Science 321, 401–404.

Jasper, H., Benes, V., Schwager, C., Sauer, S., Clauder-Münster, S., Ansorge, W., and Bohmann, D. (2001). The genomic response of the Drosophila embryo to JNK signaling. Dev. Cell 1, 579–586.

Jégou, A., Niedermayer, T., Orbán, J., Didry, D., Lipowsky, R., Carlier, M.-F., and

Romet-Lemonne, G. (2011). Individual actin filaments in a microfluidic flow reveal the mechanism of ATP hydrolysis and give insight into the properties of profilin. PLoS Biol. 9, e1001161.

Jeong, S., Rebeiz, M., Andolfatto, P., Werner, T., True, J., and Carroll, S.B. (2008). The evolution of gene regulation underlies a morphological difference between two Drosophila sister species. Cell 132, 783–793.

Jinek, M., Chylinski, K., Fonfara, I., Hauer, M., Doudna, J.A., and Charpentier, E. (2012). A programmable dual-RNA-guided DNA endonuclease in adaptive bacterial immunity. Science 337, 816–821.

Jory, A., Estella, C., Giorgianni, M.W., Slattery, M., Laverty, T.R., Rubin, G.M., and Mann, R.S. (2012). A Survey of 6,300 Genomic Fragments for cis-Regulatory Activity in the Imaginal Discs of Drosophila melanogaster. Cell Reports 2, 1014–1024.

Kalay, G., and Wittkopp, P.J. (2010). Nomadic enhancers: tissue-specific cis-regulatory elements of yellow have divergent genomic positions among Drosophila species. PLoS Genet. 6, e1001222.

Kharchenko, P.V., Alekseyenko, A.A., Schwartz, Y.B., Minoda, A., Riddle, N.C., Ernst, J., Sabo, P.J., Larschan, E., Gorchakov, A.A., Gu, T., et al. (2011). Comprehensive analysis of the chromatin landscape in Drosophila melanogaster. Nature 471, 480–485.

Kondo, S., Booker, M., and Perrimon, N. (2009). Cross-species RNAi rescue platform in Drosophila melanogaster. Genetics 183, 1165–1173.

Krasnow, R.E., Wong, L.L., and Adler, P.N. (1995). Dishevelled is a component of the frizzled signaling pathway in Drosophila. Development 121, 4095–4102.

Langer, C.C.H., Ejsmont, R.K., Schönbauer, C., Schnorrer, F., and Tomancak, P. (2010). In vivo RNAi rescue in Drosophila melanogaster with genomic transgenes from Drosophila pseudoobscura. PLoS ONE 5, e8928.

Lawrence, P.A., and Casal, J. (2013). The mechanisms of planar cell polarity, growth and the Hippo pathway: some known unknowns. Dev. Biol. 377, 1–8.

Lawrence, P.A., Casal, J., and Struhl, G. (2002). Towards a model of the organisation of planar polarity and pattern in the Drosophila abdomen. Development 129, 2749–2760.

Lawrence, P.A., Struhl, G., and Casal, J. (2007). Planar cell polarity: one or two pathways? Nat. Rev. Genet. 8, 555–563.

Lemaitre, B., and Miguel-Aliaga, I. (2013). The Digestive Tract of Drosophila melanogaster. Annual Review of Genetics 47, 377–404.

Lengyel, J.A., and Iwaki, D.D. (2002). It takes guts: the Drosophila hindgut as a model system for organogenesis. Dev. Biol. 243, 1–19.

Lenhart, K.F., Holtzman, N.G., Williams, J.R., and Burdine, R.D. (2013). Integration of nodal and BMP signals in the heart requires FoxH1 to create left-right differences in cell migration rates that direct cardiac asymmetry. PLoS Genet. 9, e1003109.

Levin, M., Thorlin, T., Robinson, K.R., Nogi, T., and Mercola, M. (2002). Asymmetries in

H+/K+-ATPase and cell membrane potentials comprise a very early step in left-right patterning. Cell 111, 77–89.

Lewis, J., and Davies, A. (2002). Planar cell polarity in the inner ear: How do hair cells acquire their oriented structure? Journal of Neurobiology 53, 190–201.

Van der Linde, K., Houle, D., Spicer, G.S., and Steppan, S.J. (2010). A supermatrix-based molecular phylogeny of the family Drosophilidae. Genet Res (Camb) 92, 25–38.

Ludwig, M.Z., Bergman, C., Patel, N.H., and Kreitman, M. (2000). Evidence for stabilizing selection in a eukaryotic enhancer element. Nature 403, 564–567.

Ma, D., Yang, C.H., McNeill, H., Simon, M.A., and Axelrod, J.D. (2003). Fidelity in planar cell polarity signalling. Nature 421, 543–547.

Mallo, M., and Alonso, C.R. (2013). The regulation of Hox gene expression during animal. Development 140, 3951–3963.

Manning, L., Heckscher, E.S., Purice, M.D., Roberts, J., Bennett, A.L., Kroll, J.R., Pollard, J.L., Strader, M.E., Lupton, J.R., Dyukareva, A.V., et al. (2012). A Resource for Manipulating Gene Expression and Analyzing cis-Regulatory Modules in the Drosophila CNS. Cell Reports 2, 1002–1013.

Mao, Y., Rauskolb, C., Cho, E., Hu, W.-L., Hayter, H., Minihan, G., Katz, F.N., and Irvine, K.D. (2006). Dachs: an unconventional myosin that functions downstream of Fat to regulate growth, affinity and gene expression in Drosophila. Development 133, 2539–2551.

Marianes, A., and Spradling, A.C. (2013). Physiological and stem cell compartmentalization within the Drosophila midgut. eLife 2, e00886–e00886.

Matakatsu, H., and Blair, S.S. (2004). Interactions between Fat and Dachsous and the regulation of planar cell polarity in the Drosophila wing. Development 131, 3785–3794.

Matakatsu, H., and Blair, S.S. (2006). Separating the adhesive and signaling functions of the Fat and Dachsous protocadherins. Development 133, 2315–2324.

Matis, M., and Axelrod, J.D. (2013). Regulation of PCP by the Fat signaling pathway. Genes Dev. 27, 2207–2220.

McGuire, S.E., Le, P.T., Osborn, A.J., Matsumoto, K., and Davis, R.L. (2003). Spatiotemporal rescue of memory dysfunction in Drosophila. Science 302, 1765–1768.

McGuire, S.E., Mao, Z., and Davis, R.L. (2004). Spatiotemporal gene expression targeting with the TARGET and gene-switch systems in Drosophila. Sci. STKE 2004, pl6.

Meyer, L.R., Zweig, A.S., Hinrichs, A.S., Karolchik, D., Kuhn, R.M., Wong, M., Sloan, C.A., Rosenbloom, K.R., Roe, G., Rhead, B., et al. (2013). The UCSC Genome Browser database: extensions and updates 2013. Nucleic Acids Res 41, D64–9.

Mislow, K. (1999). Molecular Chirality. In Topics in Stereochemistry, S.E. Denmark, ed. (John Wiley & Sons, Inc.), pp. 1–82.

Miyoshi, J., and Takai, Y. (2008). Structural and functional associations of apical junctions with cytoskeleton. Biochim. Biophys. Acta 1778, 670–691.

Mooseker, M.S., and Cheney, R.E. (1995). Unconventional myosins. Annu Rev Cell Dev Biol 11, 633–675.

Morgan, D., Turnpenny, L., Goodship, J., Dai, W., Majumder, K., Matthews, L., Gardner, A., Schuster, G., Vien, L., Harrison, W., et al. (1998). Inversin, a novel gene in the vertebrate left-right axis pathway, is partially deleted in the inv mouse. Nat. Genet. 20, 149–156.

Morgan, N.S., Heintzelman, M.B., and Mooseker, M.S. (1995). Characterization of myosin-IA and myosin-IB, two unconventional myosins associated with the Drosophila brush border cytoskeleton. Dev Biol 172, 51–71.

Murakami, R., and Shiotsuki, Y. (2001). Ultrastructure of the hindgut of Drosophila larvae, with special reference to the domains identified by specific gene expression patterns. J Morphol 248, 144–150.

Murakami, R., Shigenaga, A., Matsumoto, 1Akira, Yamaoka, I., and Tanimura, T. (1994). Novel tissue units of regional differentiation in the gut epithelium of Drosopbila, as revealed by P-element-mediated detection of enhancer. Roux's Arch Dev Biol 203, 243–249.

Myat, M.M. (2005). Making tubes in the Drosophila embryo. Dev. Dyn. 232, 617–632.

Myrick, K.V., Huet, F., Mohr, S.E., Alvarez-García, I., Lu, J.T., Smith, M.A., Crosby, M.A., and Gelbart, W.M. (2009). Large-scale functional annotation and expanded implementations of the P{wHy} hybrid transposon in the Drosophila melanogaster genome. Genetics 182, 653–660.

Nakamura, T., and Hamada, H. (2012). Left-right patterning: conserved and divergent mechanisms. Development 139, 3257–3262.

Nambiar, R., McConnell, R.E., and Tyska, M.J. (2009). Control of cell membrane tension by myosin-I. Proc Natl Acad Sci U S A 106, 11972–11977.

Namigai, E.K.O., Kenny, N.J., and Shimeld, S.M. (2014). Right across the tree of life: The evolution of left–right asymmetry in the Bilateria. Genesis 52, 458–470.

De Navas, L., Foronda, D., Suzanne, M., and Sánchez-Herrero, E. (2006). A simple and efficient method to identify replacements of P-lacZ by P-Gal4 lines allows obtaining Gal4 insertions in the bithorax complex of Drosophila. Mech. Dev. 123, 860–867.

Nègre, N., Brown, C.D., Ma, L., Bristow, C.A., Miller, S.W., Wagner, U., Kheradpour, P., Eaton, M.L., Loriaux, P., Sealfon, R., et al. (2011). A cis-regulatory map of the Drosophila genome. Nature 471, 527–531.

Niessen, C.M., and Gottardi, C.J. (2008). Molecular components of the adherens junction. Biochim. Biophys. Acta 1778, 562–571.

Noyes, M.B., Christensen, R.G., Wakabayashi, A., Stormo, G.D., Brodsky, M.H., and Wolfe, S.A. (2008). Analysis of homeodomain specificities allows the family-wide prediction of preferred recognition sites. Cell 133, 1277–1289.

Nübler-Jung, K. (1987). Insect epidermis: disturbance of supracellular tissue polarity does not prevent the expression of cell polarity. Roux's Arch Dev Biol 196, 286–289.

Obbard, D.J., Maclennan, J., Kim, K.W., Rambaut, A., O'Grady, P.M., and Jiggins, F.M. (2012). Estimating divergence dates and substitution rates in the Drosophila phylogeny. Mol Biol Evol 29, 3459–3473.

Okumura, T., Utsuno, H., Kuroda, J., Gittenberger, E., Asami, T., and Matsuno, K. (2008). The development and evolution of left-right asymmetry in invertebrates: lessons from Drosophila and snails. Dev. Dyn. 237, 3497–3515.

Oldham, S., Stocker, H., Laffargue, M., Wittwer, F., Wymann, M., and Hafen, E. (2002). The Drosophila insulin/IGF receptor controls growth and size by modulating PtdInsP[[3]] levels. Development 129, 4103–4109.

Olofsson, J., Sharp, K.A., Matis, M., Cho, B., and Axelrod, J.D. (2014). Prickle/spiny-legs isoforms control the polarity of the apical microtubule network in planar cell polarity. Development 141, 2866–2874.

Papagiannouli, F., Schardt, L., Grajcarek, J., Ha, N., and Lohmann, I. (2014). The Hox gene Abd-B controls stem cell niche function in the Drosophila testis. Dev. Cell 28, 189–202.

Peacock, A.J., and Anstee, J.H. (1977). Anatomical and ultrastructural study of the rectum of Jamaicana Flava (Caudell). Micron (1969) 8, 9–18.

Peeters, H., and Devriendt, K. (2006). Human laterality disorders. Eur J Med Genet 49, 349–362.

Peng, Y., and Axelrod, J.D. (2012). Asymmetric protein localization in planar cell polarity: mechanisms, puzzles, and challenges. Curr Top Dev Biol 101, 33–53.

Petzoldt, A.G., Coutelis, J.B., Geminard, C., Speder, P., Suzanne, M., Cerezo, D., and Noselli, S. (2012). DE-Cadherin regulates unconventional Myosin ID and Myosin IC in Drosophila left-right asymmetry establishment. Development 139, 1874–1884.

Pfeiffer, B.D., Jenett, A., Hammonds, A.S., Ngo, T.-T.B., Misra, S., Murphy, C., Scully, A., Carlson, J.W., Wan, K.H., Laverty, T.R., et al. (2008). Tools for neuroanatomy and neurogenetics in Drosophila. Proc. Natl. Acad. Sci. U.S.A. 105, 9715–9720.

Pohl, C. (2011). Left-right patterning in the C. elegans embryo. Commun Integr Biol 4, 34–40.

Pollock, J.N. (1982). Training manual for tsetse control personnel. Volume I. Tsetse biology, systematics and distribution; techniques. x+280 pp.

Port, F., Chen, H.-M., Lee, T., and Bullock, S.L. (2014). Optimized CRISPR/Cas tools for efficient germline and somatic genome engineering in Drosophila. Proc. Natl. Acad. Sci. U.S.A.

Prelog, V. (1982). Basic Principles of the CIP-System and Proposals for a Revision. Angewandte Chemie-International Edition - ANGEW CHEM INT ED 21, 567–583.

Prud'homme, B., Gompel, N., Rokas, A., Kassner, V.A., Williams, T.M., Yeh, S.-D., True, J.R., and Carroll, S.B. (2006). Repeated morphological evolution through cis-regulatory changes in a pleiotropic gene. Nature 440, 1050–1053.

Pyrpassopoulos, S., Feeser, E.A., Mazerik, J.N., Tyska, M.J., and Ostap, E.M. (2012). Membrane-bound myo1c powers asymmetric motility of actin filaments. Curr Biol 22,

1688–1692.

Raya, A., and Izpisua Belmonte, J.C. (2006). Left-right asymmetry in the vertebrate embryo: from early information to higher-level integration. Nat Rev Genet 7, 283–293.

Ren, X., Sun, J., Housden, B.E., Hu, Y., Roesel, C., Lin, S., Liu, L.-P., Yang, Z., Mao, D., Sun, L., et al. (2013). Optimized gene editing technology for Drosophila melanogaster using germ line-specific Cas9. Proc. Natl. Acad. Sci. U.S.A. 110, 19012–19017.

Repiso, A., Saavedra, P., Casal, J., and Lawrence, P.A. (2010). Planar cell polarity: the orientation of larval denticles in Drosophila appears to depend on gradients of Dachsous and Fat. Development 137, 3411–3415.

Robertson, C.W. (1936). The metamorphosis of Drosophila melanogaster, including an accurately timed account of the principal morphological changes. Journal of Morphology 59, 351–399.

Robinson, S.W., Herzyk, P., Dow, J.A.T., and Leader, D.P. (2013). FlyAtlas: database of gene expression in the tissues of Drosophila melanogaster. Nucleic Acids Res. 41, D744–750.

Rogulja, D., Rauskolb, C., and Irvine, K.D. (2008). Morphogen control of wing growth through the Fat signaling pathway. Dev. Cell 15, 309–321.

Sagner, A., Merkel, M., Aigouy, B., Gaebel, J., Brankatschk, M., Jülicher, F., and Eaton, S. (2012). Establishment of Global Patterns of Planar Polarity during Growth of the Drosophila Wing Epithelium. Current Biology 22, 1296–1301.

Sambrook, J. (2001). Molecular Cloning: A Laboratory Manual, Third Edition (Cold Spring Harbor, N.Y: Cold Spring Harbor Laboratory Press).

Schnorr, J.D., Holdcraft, R., Chevalier, B., and Berg, C.A. (2001). Ras1 interacts with multiple new signaling and cytoskeletal loci in Drosophila eggshell patterning and morphogenesis. Genetics 159, 609–622.

Segalen, M., and Bellaïche, Y. (2009). Cell division orientation and planar cell polarity pathways. Seminars in Cell & Developmental Biology 20, 972–977.

Seisenbacher, G., Hafen, E., and Stocker, H. (2011). MK2-dependent p38b signalling protects Drosophila hindgut enterocytes against JNK-induced apoptosis under chronic stress. PLoS Genet. 7, e1002168.

Sharma, P., and McNeill, H. (2013). Regulation of long-range planar cell polarity by Fat-Dachsous signaling. Development 140, 3869–3881.

Shields, A.R., Spence, A.C., Yamashita, Y.M., Davies, E.L., and Fuller, M.T. (2014). The actin-binding protein profilin is required for germline stem cell maintenance and germ cell enclosure by somatic cyst cells. Development 141, 73–82.

Shimada, Y., Yonemura, S., Ohkura, H., Strutt, D., and Uemura, T. (2006). Polarized Transport of Frizzled along the Planar Microtubule Arrays in Drosophila Wing Epithelium. Developmental Cell 10, 209–222.

Shingleton, A.W., Das, J., Vinicius, L., and Stern, D.L. (2005). The Temporal Requirements for Insulin Signaling During Development in Drosophila. PLoS Biol 3, e289.

Siepel, A., Bejerano, G., Pedersen, J.S., Hinrichs, A.S., Hou, M., Rosenbloom, K., Clawson, H., Spieth, J., Hillier, L.W., Richards, S., et al. (2005). Evolutionarily conserved elements in vertebrate, insect, worm, and yeast genomes. Genome Res 15, 1034–1050.

Simon, M.A. (2004). Planar cell polarity in the Drosophila eye is directed by graded Four-jointed and Dachsous expression. Development 131, 6175–6184.

Simon, M.A., Xu, A., Ishikawa, H.O., and Irvine, K.D. (2010a). Modulation of fat:dachsous binding by the cadherin domain kinase four-jointed. Curr. Biol. 20, 811–817.

Simon, M.A., Xu, A., Ishikawa, H.O., and Irvine, K.D. (2010b). Modulation of Fat:Dachsous Binding by the Cadherin Domain Kinase Four-Jointed. Current Biology 20, 811–817.

Singer, J.B., Harbecke, R., Kusch, T., Reuter, R., and Lengyel, J.A. (1996). Drosophila brachyenteron regulates gene activity and morphogenesis in the gut. Development 122, 3707–3718.

Singh, J., and Mlodzik, M. (2012). Planar cell polarity signaling: coordination of cellular orientation across tissues. Wiley Interdiscip Rev Dev Biol 1, 479–499.

Song, H., Hu, J., Chen, W., Elliott, G., Andre, P., Gao, B., and Yang, Y. (2010). Planar cell polarity breaks bilateral symmetry by controlling ciliary positioning. Nature 466, 378–382.

Speder, P., Adam, G., and Noselli, S. (2006). Type ID unconventional myosin controls left-right asymmetry in Drosophila. Nature 440, 803–807.

St Johnston, D. (2002). The art and design of genetic screens: Drosophila melanogaster. Nat Rev Genet 3, 176–188.

Strutt, H., and Strutt, D. (2002). Nonautonomous planar polarity patterning in Drosophila: dishevelled-independent functions of frizzled. Dev Cell 3, 851–863.

Strutt, H., and Strutt, D. (2008). Differential stability of flamingo protein complexes underlies the establishment of planar polarity. Curr. Biol. 18, 1555–1564.

Strutt, H., and Strutt, D. (2009). Asymmetric localisation of planar polarity proteins: Mechanisms and consequences. Seminars in Cell & Developmental Biology 20, 957–963.

Strutt, H., Mundy, J., Hofstra, K., and Strutt, D. (2004). Cleavage and secretion is not required for Four-jointed function in Drosophila patterning. Development 131, 881–890.

Suzanne, M., Petzoldt, A.G., Speder, P., Coutelis, J.B., Steller, H., and Noselli, S. (2010). Coupling of apoptosis and L/R patterning controls stepwise organ looping. Curr Biol 20, 1773–1778.

Takashima, S., Mkrtchyan, M., Younossi-Hartenstein, A., Merriam, J.R., and Hartenstein, V. (2008). The behaviour of Drosophila adult hindgut stem cells is controlled by Wnt and Hh signalling. Nature 454, 651–655.

Takashima, S., Younossi-Hartenstein, A., Ortiz, P.A., and Hartenstein, V. (2011). A novel tissue in an established model system: the Drosophila pupal midgut. Dev. Genes Evol. 221, 69–81.

Takashima, S., Paul, M., Aghajanian, P., Younossi-Hartenstein, A., and Hartenstein, V. (2013). Migration of Drosophila intestinal stem cells across organ boundaries. Development 140, 1903–1911.

Taniguchi, K., Hozumi, S., Maeda, R., Okumura, T., and Matsuno, K. (2007). Roles of type I myosins in Drosophila handedness. Fly (Austin) 1, 287–290.

Taniguchi, K., Maeda, R., Ando, T., Okumura, T., Nakazawa, N., Hatori, R., Nakamura, M., Hozumi, S., Fujiwara, H., and Matsuno, K. (2011). Chirality in planar cell shape contributes to left-right asymmetric epithelial morphogenesis. Science 333, 339–341.

Thomas, C., and Strutt, D. (2012). The roles of the cadherins Fat and Dachsous in planar polarity specification in Drosophila. Dev. Dyn. 241, 27–39.

Thompson, M.T. (2012). Alimentary Canal of the Mosquito; (General Books LLC).

Tree, D.R.P., Shulman, J.M., Rousset, R., Scott, M.P., Gubb, D., and Axelrod, J.D. (2002). Prickle mediates feedback amplification to generate asymmetric planar cell polarity signaling. Cell 109, 371–381.

Vandenberg, L.N., and Levin, M. (2013). A unified model for left-right asymmetry? Comparison and synthesis of molecular models of embryonic laterality. Dev. Biol. 379, 1–15.

Viktorinova, I., and Dahmann, C. (2013). Microtubule polarity predicts direction of egg chamber rotation in Drosophila. Curr Biol 23, 1472–1477.

Vinson, C.R., and Adler, P.N. (1987). Directional non-cell autonomy and the transmission of polarity information by the frizzled gene of Drosophila. Nature 329, 549–551.

Wallingford, J.B. (2012). Planar cell polarity and the developmental control of cell behavior in vertebrate embryos. Annu. Rev. Cell Dev. Biol. 28, 627–653.

Werner, T., Koshikawa, S., Williams, T.M., and Carroll, S.B. (2010). Generation of a novel wing colour pattern by the Wingless morphogen. Nature 464, 1143–1148.

Williams, T.M., Selegue, J.E., Werner, T., Gompel, N., Kopp, A., and Carroll, S.B. (2008). The regulation and evolution of a genetic switch controlling sexually dimorphic traits in Drosophila. Cell 134, 610–623.

Wittkopp, P.J. (2010). Variable transcription factor binding: a mechanism of evolutionary change. PLoS Biol. 8, e1000342.

Wolff, T., and Rubin, G.M. (1998). Strabismus, a novel gene that regulates tissue polarity and cell fate decisions in Drosophila. Development 125, 1149–1159.

Wong, L.L., and Adler, P.N. (1993). Tissue polarity genes of Drosophila regulate the subcellular location for prehair initiation in pupal wing cells. J Cell Biol 123, 209–221.

Wood, W.B. (1998). Handed asymmetry in nematodes. Semin. Cell Dev. Biol. 9, 53–60.

Wu, J., and Mlodzik, M. (2008). The Frizzled Extracellular Domain Is a Ligand for Van Gogh/Stbm during Nonautonomous Planar Cell Polarity Signaling. Developmental Cell 15, 462–469.

Xie, T. (2009). Stem cell in the adult Drosophila hindgut: just a sleeping beauty. Cell Stem Cell 5, 227–228.

Xu, J., Keymeulen, A.V., Wakida, N.M., Carlton, P., Berns, M.W., and Bourne, H.R. (2007). Polarity reveals intrinsic cell chirality. PNAS 104, 9296–9300.

Yang, Y. (2012). Planar cell polarity during development. Preface. Curr. Top. Dev. Biol. 101, xi–xiii.

Yang, C., Axelrod, J.D., and Simon, M.A. (2002). Regulation of Frizzled by Fat-like Cadherins during Planar Polarity Signaling in the Drosophila Compound Eye. Cell 108, 675–688.

Yoshiba, S., and Hamada, H. (2014). Roles of cilia, fluid flow, and Ca2+ signaling in breaking of left-right symmetry. Trends Genet. 30, 10–17.

Zeidler, M.P., Perrimon, N., and Strutt, D.I. (1999). The four-jointed gene is required in the Drosophila eye for ommatidial polarity specification. Curr. Biol. 9, 1363–1372.

Zeidler, M.P., Perrimon, N., and Strutt, D.I. (2000). Multiple Roles for four-jointed in Planar Polarity and Limb Patterning. Developmental Biology 228, 181–196.

Zou, C., Huang, W., Ying, G., and Wu, Q. (2007a). Sequence analysis and expression mapping of the rat clustered protocadherin gene repertoires. Neuroscience 144, 579–603.

Zou, L., Jaramillo, M., Whaley, D., Wells, A., Panchapakesa, V., Das, T., and Roy, P. (2007b).

Profilin-1 is a negative regulator of mammary carcinoma aggressiveness. British Journal of Cancer 97, 1361–1371.

Zou, L., Hazan, R., and Roy, P. (2009). Profilin-1 overexpression restores adherens junctions in MDA-MB-231 breast cancer cells in R-cadherin-dependent manner. Cell Motility and the Cytoskeleton 66, 1048–1056.

VIII Acknoledgements

I would like to thank Stéphane Noselli who provided carefully considered feedback and valuable comments. Special thanks also go to all the members of the laboratory: Charles Géminard, Christian Ghiglione, Patrick Jouandin, Raphaël Rousset, Véronique Van de Bor, Jean-Baptiste Coutelis, Gaëlle Le Breton, Solange Roumengous, Geordie Zimniak, Delphine Cerezo, Caroline Meira-da-Silva and Nadège Parassol-Girard who provided technical help and sincere encouragement. I would also like to express my gratitude to members of the Institute: especially to Francisco (Paco) Martin, Nuria Romero, Giovanni Marchetti and Tamas Matusek for sharp discussions that helped me during the course of this work.

Most importantly, I would like to thank both my family: Martagloria Morales Garza, Ovidio González Gómez, Fernanda González Morales and Ximena Gargari Mondragón both for their moral support and warm encouragements.

IX Supplementary Material

Supplementary Table 1 List of Drosophila stocks used

Supplementary table 2 List of PhastCons

Supplementary Table 3 List of Gal4 lines tested with expressed in the AHG

Supplementary Table 4 List of deficiencies tested in regions 21A-B, 25D-E and 50D

Supplementary Table 1 List of Drosophila stocks used

Stock number	*1st Chromosome*	*2nd Chromosome*	*3rd Chromosome*	Unknown location	Usage	Comments
	w	*chic-flyfosattp40 052096*	*mkrs/tm6b*		chic genomic rescue	
		chic-flyfosattp40 052096			chic genomic rescue	the number corresponds to the number of fosmid clone used
			chic-flyfosattp2 047881		chic genomic rescue	the number corresponds to the number of fosmid clone used
			UAS-Diap1		block apoptosis	
		UAS-Decad-wt	*uas-chic*		Chic -Cad Interaction	
		UAS-Decad-GFP	*uas-chic*		Chic -Cad Interaction	
		UAS-Decad-RNAi	*uas-chic*		Chic -Cad Interaction	
		UAS-Decad-DN	*uas-chic*		Chic -Cad Interaction	
	w		*uas-chic+3'UTR-Flag/tm3*		chic overexpression	
	w	*chic-gal4*	*uas-chic*		*chic rescue*	*rescue from embryinic lethality to late pupa*
			uas-chic, chic-trip		Chic RNAi rescue	does not rescue
		chic-kk, uas-decad-DN			Chic-Cad interaction	
	w	*chic-kk, DECAD-RNAi*			Chic-Cad interaction	

	w		*uas-diap1, uas-chic*		Chic-JNK interaction	
		uas-p35	*uas-chic*		Chic-JNK interaction	
			uas-chic, uas-bsk-dn		Chic-JNK interaction	
			uas-hep4e, uas-chic		Chic-JNK interaction	
			uas-chic, uas-puc2a		Chic-JNK interaction	
	w		*uasMyoIC,uaschic*		Chic-MyoIC interaction	
		chic-kk	*mid-RNAi 2x*		Chic-MyoID	
		myoID k2	*uas-chic*		Chic-MyoID	
			mid RNAi 2x UAS chic		Chic-MyoID interaction	
S1	*w*	*chicp5202, MyoID-RFPSTOP*			Chic-MyoID interaction	
S2	*w*	*chicp5202, MyoID-RFPSTOP*			Chic-MyoID interaction	
	w	*chic5202, myoIDK2*			Chic-MyoID interaction	
	yw hsFLP122	act<cd2,y>d:citrine A2			dachs YFP clones	
	Ud2	*PTC gal 4 mid k1*	*mid RNAi 2x*		*deficiency screen*	
		PTC gal 4 mid k1	*mid RNAi 2x*		*deficiency screen*	
9182	*w*	*def2L25*			Deficiency Screen	
24626	*w*	*df2lED50001/cyo*			Deficiency Screen	
6153	*w*	*df(2l)21/cyo*			Deficiency Screen	
		ptc-gal4, myoID K1			Deficiency Screen	
	yw hsFLP122	if/CYO	Ubi:GFP attB-P(acman-HA:DS), FRT80 /TM	B	Ds reporter	endogenous ds HA tagged
	w	ds-EGFP-loxP w+loxp, frt40/S-T			Ds reporter	GFP tagged endogenous ds
UamuraLab				Ubi::fmi-3xGFP	flamingo reporter	I never detected any GFP pattern
		myoID gal 4	*tubGal80TS UAS GFP*		Gal4	
			dpp-gal4/tm6b		Gal4	

			ptc-gal4, R80		*Gal4*	
				drm-gal4,GFP	*Gal4*	
			48ygal4, mcd8GFP		*Gal4*	
	30557		*en-Gal4 UASmcd8RFP*		*Gal4*	
		w	*myoID-gal4,UD2*	*dr/tm3*	*Gal4*	
		yw		*ac69-Gal4/TM2*	Gal4	
			myoID-gal4, UD2		Gal4	
			ptc-GAl4, UASmcd8GFP		Gal4	
			myoID-Gal4, uas-myrRFP/CYO		Gal4	
			Su(H)GBE-gal4/CYO		Gal4	
			Su(H)GBE-gal4, UASmcd8GFP/CYO		GAl4	
13aMel		*w*		*arm-Gal4/tm6b*	*Gal4*	
	914	*w,twi-gal4*			Gal4	
				byn-Gal4, UAS-PHGFP, UASGalt-RFP/Tm6b	Gal4	hindgut RFP golgi and membrane green
				byn-Gal4, UD2/Tm6b	Gal4 and Dicer2	
			sp/cyo	*byn-Gal4, UD2/Tm6b*	Gal4 and Dicer2	
			chic-gal47313, uasmcd8GFP/cyo		Gal4 chic with GFP	
				byn-Gal4, UAS-PHGFP/Tm6b dfd-YFP	Gal4 hindgut and GFP	line used for quantifications
	47466				Gal4 hindgut screen	
	49931				Gal4 hindgut screen	
	48461				Gal4 hindgut screen	
	48278				Gal4 hindgut screen	
	47381				Gal4 hindgut screen	

47253				Gal4 hindgut screen
45926				Gal4 hindgut screen
45919				Gal4 hindgut screen
47620				Gal4 hindgut screen
49320				Gal4 hindgut screen
46732				Gal4 hindgut screen
46714				Gal4 hindgut screen
38687				Gal4 hindgut screen
48011				Gal4 hindgut screen
40680				Gal4 hindgut screen
47826				Gal4 hindgut screen
40648				Gal4 hindgut screen
45586				Gal4 hindgut screen
45341				Gal4 hindgut screen
29398			bynVT-Gal4 attp	Gal4 hindgut screen
201648			VT025776-junction	Gal4 hindgut screen
	yw		*uas:luciferace attp2*	Gal4 reporter
	yw	*uas-hid 14/cyo*		induce apoptosis
		uas-hid 4		induce apoptosis
	UASDRONC/FM7			induce apoptosis
		TubP:Gal80ts,	*UAS-FLP, Ubi-p63E(FRT.STOP)Stinger*	lineage tracing
		TubP:Gal80ts,	*UAS-FLP, Ubi-p63E(FRT.STOP)Stinger, UAS:nRFP*	lineage tracing
			UAS-FLP, Ubi-p63E(FRT.STOP)Stinger	lineage tracing
28281			*UAS-FLP, Ubi-p63E(FRT.STOP)Stinger, UAS:nRFP*	lineage tracing

29037	*uas-Baz-GFP*				membrane apical GFP	
			UAS-PH(PLCgamma)-GFP		membrane GFP	marks pip2, clean membrane pattern in imaginal ring
27392	*w*		*UASmcd8-chRFP*		membrane RFP	
288		ds38k/Cyo			mutant	
11394		ds05142/CYO			mutant	
5298	dsh 1				mutant	
9454	dsh A3				mutant	
5297	dsh 6/ Fm7a				mutant	
	w	ds UAC71, frt40/ CYO GFP	p(Act<stop>ds-EGFP/TM6b		mutant and rescue ds	
	w	ds UAC71Sm6b			mutant ds	
6370		fj lacW9-11 / Cyo			mutant Fj and lacZ enhancer trap	
140296		*myoId-pBac (dsRed-stop), frt40a*			mutant myoID	
	w	ds UAC71, frt40/ CYO GFP	p(Act<stop>dsS>Ax3-EGFP/TM6b		mutante and rescue ds	
	w		*myoID-dvir J17 attp2*		*myoID genomic from d,virilis*	
	w	*myoID k2*	*myoID-flyfos/tm6b*		*myoID mutant and rescue for d,pseudoobscura*	
		myoID lacZ			myoID reporter	
707			*UAS-LacZnuclear*		Overexpress LacZ	
28874			*uas-rac1wt*		Overexpressio Rac1	
28872				uas-rho1 wt	Overexpressio rho1	
7334			*uas-rho1 wt*		Overexpressio rho1	
			UAS myoID 34/tm3		overexpression	

			UAS-Decad wt/tm3		Overexpression	
28873				uas-cdc42-wt	Overexpression cdc42	
			uas-chic-venus 7/tm3		overexpression chic Venus tagged	
			uas-chic-venus 6		overexpression chic Venus tagged	
			uas-chic-venus 3/tm3		overexpression chic Venus tagged	
		uas-chic-venus 4			overexpression chic Venus tagged	localizes properly, does not rescue chic mutations
S, Blair	w		UAS-ds		Overexpression ds	
S, Blair	w		UAS-dsΔICD		Overexpression ds truncated	
S, Blair	w		UAS-dsΔECD		Overexpression ds truncated	
S, Blair	w		uas-fat		Overexpression fat	
S, Blair	w		UAS-fatΔECD		Overexpression fat truncated	
S, Blair	w		UAS-fatΔICD		Overexpression fat truncated	
			uas:MyoID/tm3		Overexpression MyoID	
30099			wts EP/tm6b		overexpression warts	
28813		uas-yki-gfp			overexpression yorkie	
28816				uas-yki-V5	overexpression yorkie	
28816				uas-yki-s168a-gfp	overexpression yorkie modified	
28836				uas-yki-s168a-GFP	overexpression yorkie modified	
28818				uas-yki-S1689-V5	overexpression yorkie modified	

		spCyo	*UAS myoID RNAi 2x*		RNAi
			UAS myoID RNAi 2x		RNAi
		Decad-RNAi (HV)			RNAi
27727		*rho1-trip*			RNAi
28021		*cdc42-trip*			RNAi
35756		*cdc42-trip*			RNAi
34910		*rac1-trip*			RNAi
28985		*rac1-trip*			RNAi
	w	*chic-KK*	*mkrs/tm6b*		*RNAi*
28009				fj-TRIP	RNAi
34323				fj-TRIP	RNAi
28008				ds-TRIP	RNAi
14350				ds-GD	RNAi
32964				ds-TRIP	RNAi
29566				ft-Trip	RNAi
34970				ft-Trip	RNAi
6774			fj-GD		RNAi
6774		fj-GD			RNAi
27664				d-TRIP	RNAi
108863				Ft-KK	RNAi
1665			fmi-GD		RNAi
31736		diego-GD			RNAi
36219		ds-GD			RNAi
43075		fz-GD			RNAi
31734			diego-GD		RNAi
43077				fz-GD	RNAi
7376		stmb-GD			RNAi
51382				fmi-GD	RNAi
108410				diego-KK	RNAi
35040				diego-TRIP	RNAi

35050				stan-TRIP	RNAi
26066				stan-TRIP	RNAi
32413				pk-Trip	RNAi
100819				stmb-kk	RNAi
105493				fz-kk	RNAi
31307				dsh-trip	RNAi
31306				dsh-trip	RNAi
31306				dsh-trip	RNAi
11099				pk-GD	RNAi
101525				dsh-kk	RNAi
34354				vang-trip	RNAi
27661				hippo-trip	RNAi
27662				wts-trip	RNAi
34064				wts-TRIP	RNAi
33614				hippo-trip	RNAi
51939				drip-gd	RNAi
106911				drip-KK	RNAi
101764				otp-kk	RNAi
34329				tll-trip	RNAi
101534				byn-kk	RNAi
43909				byn-GD	RNAi
	w		*10x-stat92-gfp*		Stat reporter
		10x-stat92-gfp			Stat reporter
28291			UAS:D-V5-His		Tagged Dachs
30910	*w*	*UAS-RFP-KDEL*			tagged ER
30907	*w*		*UAS-RFP-Golgi (galt)/tm6b*		tagged golgi
	yw		*uas:chic, uas:luciferace attp2*		test Gal4 activity after chic overexpression
oregonR					wlid type stock

w1118	wlid type stock

Supplementary table 2 List of PhastCons

Name	chromosome	chromStart	chromEnd	score
lod=32	chr2L	10491867	10491887	322
lod=20	chr2L	10491888	10491898	259
lod=37	chr2L	10491908	10491931	342
lod=82	chr2L	10491950	10492001	448
lod=36	chr2L	10492015	10492030	338
lod=65	chr2L	10492058	10492110	417
lod=42	chr2L	10492191	10492215	359
lod=21	chr2L	10492295	10492304	266
lod=79	chr2L	10492337	10492393	443
lod=131	chr2L	10492396	10492505	511
lod=126	chr2L	10492550	10492611	506
lod=42	chr2L	10492622	10492654	359
lod=103	chr2L	10492661	10492720	479
lod=20	chr2L	10492783	10492791	259
lod=191	chr2L	10492812	10492945	561
lod=11	chr2L	10492948	10492953	179
lod=13	chr2L	10492965	10492971	202
lod=123	chr2L	10492991	10493073	503
lod=123	chr2L	10493086	10493168	503
lod=12	chr2L	10493173	10493178	191
lod=68	chr2L	10493212	10493250	423
lod=84	chr2L	10493260	10493334	451
lod=56	chr2L	10493341	10493364	397
lod=142	chr2L	10493374	10493457	522
lod=139	chr2L	10493461	10493556	519
lod=456	chr2L	10493560	10493781	678
lod=132	chr2L	10493785	10493859	512
lod=64	chr2L	10493860	10493883	415
lod=135	chr2L	10493893	10493976	515
lod=443	chr2L	10493977	10494197	674
lod=203	chr2L	10494285	10494369	570
lod=202	chr2L	10494423	10494488	569
lod=101	chr2L	10494492	10494533	476
lod=40	chr2L	10494537	10494578	352
lod=223	chr2L	10494582	10494718	582
lod=17	chr2L	10494720	10494734	238
lod=24	chr2L	10494737	10494761	284
lod=43	chr2L	10494779	10494813	362

lod=98	chr2L	10494873	10494947	472
lod=66	chr2L	10494967	10495029	419
lod=22	chr2L	10495033	10495062	272
lod=42	chr2L	10495072	10495107	359
lod=10	chr2L	10495149	10495154	166
lod=82	chr2L	10495204	10495263	448
lod=16	chr2L	10495754	10495785	229
lod=11	chr2L	10495838	10495857	179
lod=15	chr2L	10495899	10495919	221
lod=12	chr2L	10495998	10496007	191
lod=10	chr2L	10496313	10496319	166
lod=30	chr2L	10496429	10496486	314
lod=11	chr2L	10496525	10496531	179
lod=55	chr2L	10496537	10496565	395
lod=73	chr2L	10496626	10496658	433
lod=286	chr2L	10496662	10496787	616
lod=144	chr2L	10496788	10496851	524
lod=15	chr2L	10497100	10497108	221
lod=43	chr2L	10497115	10497149	362
lod=14	chr2L	10497166	10497175	212
lod=61	chr2L	10497192	10497252	409
lod=41	chr2L	10497253	10497284	355
lod=23	chr2L	10497306	10497315	278
lod=20	chr2L	10497318	10497331	259
lod=26	chr2L	10497360	10497383	294
lod=17	chr2L	10497415	10497435	238
lod=35	chr2L	10497439	10497459	334
lod=29	chr2L	10497516	10497545	309
lod=47	chr2L	10497847	10497872	374
lod=597	chr2L	10497879	10498158	714
lod=22	chr2L	10498182	10498200	272
lod=29	chr2L	10498203	10498224	309
lod=39	chr2L	10498279	10498331	349
lod=20	chr2L	10498442	10498455	259
lod=71	chr2L	10498457	10498508	429
lod=13	chr2L	10499071	10499080	202
lod=21	chr2L	10499132	10499142	266
lod=24	chr2L	10499154	10499203	284
lod=34	chr2L	10499225	10499263	330
lod=77	chr2L	10499288	10499349	440
lod=139	chr2L	10499363	10499446	519
lod=19	chr2L	10499507	10499532	252
lod=33	chr2L	10499550	10499565	326
lod=43	chr2L	10499590	10499626	362
lod=71	chr2L	10499660	10499702	429
lod=26	chr2L	10499728	10499743	294

lod=12	chr2L	10499777	10499787	191
lod=67	chr2L	10499844	10499879	421
lod=33	chr2L	10499892	10499952	326
lod=15	chr2L	10500502	10500536	221
lod=29	chr2L	10500569	10500594	309
lod=10	chr2L	10500663	10500670	166
lod=22	chr2L	10500695	10500704	272
lod=15	chr2L	10500774	10500779	221
lod=17	chr2L	10500782	10500789	238
lod=28	chr2L	10500800	10500819	304
lod=16	chr2L	10500850	10500857	229
lod=31	chr2L	10500899	10500930	318
lod=14	chr2L	10500953	10500969	212
lod=71	chr2L	10500975	10501032	429
lod=46	chr2L	10501058	10501088	371
lod=25	chr2L	10501377	10501401	289
lod=15	chr2L	10501422	10501454	221
lod=26	chr2L	10501474	10501495	294
lod=116	chr2L	10501568	10501655	495
lod=46	chr2L	10501689	10501724	371
lod=88	chr2L	10501758	10501813	458
lod=48	chr2L	10501826	10501860	377
lod=15	chr2L	10501901	10501915	221
lod=40	chr2L	10501979	10502009	352
lod=27	chr2L	10502013	10502031	300
lod=20	chr2L	10502048	10502064	259
lod=43	chr2L	10502112	10502145	362
lod=95	chr2L	10502161	10502214	468
lod=17	chr2L	10502230	10502244	238
lod=13	chr2L	10502302	10502334	202
lod=20	chr2L	10502396	10502421	259
lod=46	chr2L	10502430	10502492	371
lod=19	chr2L	10502536	10502552	252
lod=54	chr2L	10502836	10502897	392
lod=52	chr2L	10502918	10502974	387
lod=12	chr2L	10502978	10502986	191
lod=14	chr2L	10503049	10503089	212
lod=20	chr2L	10503304	10503333	259
lod=12	chr2L	10503352	10503363	191
lod=35	chr2L	10503387	10503404	334
lod=24	chr2L	10503437	10503461	284
lod=17	chr2L	10503468	10503515	238
lod=88	chr2L	10503544	10503666	458
lod=21	chr2L	10503745	10503760	266
lod=124	chr2L	10503766	10503861	504
lod=67	chr2L	10503873	10503917	421

lod=13	chr2L	10503984	10503999	202
lod=17	chr2L	10504060	10504077	238
lod=42	chr2L	10504088	10504102	359
lod=20	chr2L	10504131	10504143	259
lod=78	chr2L	10504163	10504209	442
lod=14	chr2L	10504224	10504235	212
lod=42	chr2L	10504262	10504292	359
lod=18	chr2L	10504308	10504329	245
lod=24	chr2L	10504342	10504363	284
lod=22	chr2L	10504391	10504405	272
lod=15	chr2L	10504663	10504672	221
lod=44	chr2L	10504827	10504898	365
lod=31	chr2L	10504937	10504985	318
lod=17	chr2L	10505003	10505017	238
lod=26	chr2L	10505031	10505056	294
lod=53	chr2L	10505062	10505109	390
lod=66	chr2L	10505462	10505553	419
lod=61	chr2L	10505594	10505666	409
lod=16	chr2L	10505693	10505713	229
lod=25	chr2L	10505920	10505927	289
lod=66	chr2L	10505934	10505957	419
lod=128	chr2L	10505961	10506018	508
lod=33	chr2L	10506099	10506117	326
lod=12	chr2L	10506127	10506137	191
lod=23	chr2L	10506178	10506190	278
lod=71	chr2L	10506199	10506256	429
lod=81	chr2L	10506301	10506459	447
lod=23	chr2L	10506473	10506537	278

Supplementary Table 3 List of Gal4 lines tested with expressed in the AHG

			Larva	Adult						
Stock number	Name	gene	Imaginal Ring	Stem-Cells	Pylorus	Iluem anterior	Ileum posteior	Rectal junction		Papilla	Sheath
38687	R49E02	E2f	yes			yes					
40648	R93C07	CG31418	no (only larval pylorus)								
40680	R94C12	en				yes	yes	yes	yes	yes	
45341	R48H08	beat-IIIc									
45586	R32C11	stg			yes			yes	yes		yes
45919	R86H07	CG14020									
45926	R88B08	inv	yes								
46714	R56F05	CTPsyn	yes								
46732	R82G11	sba	yes		yes		yes	yes	yes	yes	yes
47253	R94C10	en								yes	
47381	R56G11	dally						yes			
47466	R15D02	rut					yes	yes	yes		yes
47620	R50D03	E2f		yes							
47826	R88C04	inv		yes	yes						
48011	R94D09	en				scattered	yes			yes	
48278	R10H12	bi								yes	
48461	R11E08	bi						yes		base	
49320	R25E10	Adf1					yes	yes	yes	weak	
49931	R36C06	al								yes	
201648	VT025776	Rh50						yes	x		
205774	bynVT-Gal4	byn	yes		yes	yes	yes	yes	yes	yes	yes

Supplementary Table 4 List of deficiencies tested in regions 21A-B, 25D-E and 50D

Region 21A-B					
Name	SF	SP	NR	DP	DF
w1118	0	84	16	0	0
Df(2L)net62	0	93	7	0	0
Df(2L)Exel6001	0	84	16	0	0
Df(2L)ED929	3	94	3	0	0
Df(2L)ED5878	24	73	3	0	0
Df(2L)net-PM86A	0	0	0	0	100
Df(2L)PM51	0	0	0	0	100
Df(2L)PM44	0	0	0	5	95
Df(2L)net-PMC	0	0	3	13	83
Df(2L)net-PMF	0	0	0	39	61
Df(2L)PM59	0	0	0	47	53
Df(2L)PM1	0	0	10	42	48
Df(2L)net18	0	0	30	56	15
Df(2L)PM82	0	2	33	60	5
Df(2L)net-PM47C	0	0	6	88	6
Df(2L)TE21A	3	24	15	53	6
Df(2L)net-PM29A	0	0	26	74	0
Df(2L)PM73	0	0	58	42	0
Df(2L)PM4	0	8	92	0	0
Df(2L)net14	0	3	94	3	0
Df(2L)PMA	0	0	100	0	0
Df(2L)PMD	0	2	95	2	0
Df(2L)PMG	0	17	83	0	0
Df(2L)PM11	0	6	94	0	0
Df(2L)PM45	0	3	94	3	0

Df(2L)ED50001	0	0	100	0	0
l(2)gl4	27	70	3	0	0

Region 25D-E					
Name	SF	SP	NR	DP	DF
w1118	0	84	16	0	0
Df(2L)ED292	0	10	56	0	5
Df(2L)Exel7024	6	15	56	12	12
Df(2L)ED334	13	16	68	3	0
Df(2L)2802	10	90	0	0	0
Df(2L)Exel6013	3	97	0	0	0
Df(2L)ED270	3	80	18	0	0
Df(2L)ED284	3	77	21	0	0
Df(2L)E110	0	77	23	0	0
Df(2L)ED285	3	94	3	0	0
Df(2L)ED347	3	97	0	0	0
Df(2L)BSC169	3	92	6	0	0
Df(2L)BSC168	0	94	6	0	0
Df(2L)ED279	50	47	3	0	0
UAS-chic; pin	88	12	0	0	0
UAS-chic; Cyo	91	6	3	0	0

Region 50D					
Name	SF	SP	NR	DP	DF
control	0	84	16	0	0
Tango 7 GSV7	55	45	0	0	0
Df(2R)Exel7130	71	29	0	0	0
Df(2R)Exel7131	13	83	3	0	0
Df(2R)BSC134	0	84	16	0	0

Df(2R)BSC401	3	97	0	0	0
Df(2R)50C-101	3	97	0	0	0